Investigation of internal feedback in hearing aids

Friis, Lars

Publication date:
2009

Document Version
Publisher's PDF, also known as Version of record

Investigation of internal feedback in hearing aids

Ph.D. thesis by

Lars Friis

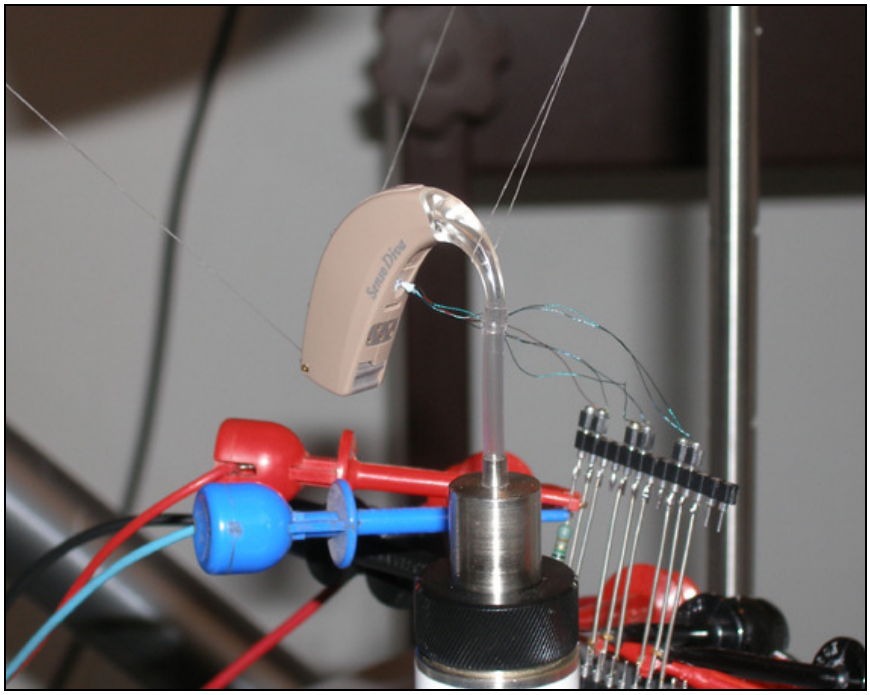

In coorporation with:

Widex A/S

Acoustic Technology, DTU Elektro, Technical University of Denmark

2008

Table of contents

Preface

This thesis is being submitted to the Technical University of Denmark as partial and final fulfillment of the requirements for the degree of Doctor of Philosophy in Electronics and Communications.

The work described in the thesis was completed between July 1, 2005 and June 30, 2008 and it is the result of an industrial Ph.D.-project in cooperation between the author, Widex A/S and Acoustic Technology, DTU Elektro, Technical University of Denmark. The project was supervised by Associate Professor Mogens Ohlrich and Associate Professor Finn Jacobsen from Acoustic Technology at Technical University of Denmark in conjunction with Lars Bækgaard Jensen and Morten Pihl Linkenkær from Widex A/S.

Without the help of many people this thesis would never have come into existence. Most of all I would like to thank my main supervisor Mogens Ohlrich for numerous challenging and constructive discussions. Moreover, I sincerely appreciate his great enthusiasm about the project and uncompromising thoroughness. Thanks also go to my other supervisors for good advice and firm belief in the project.

I wish to thank Widex A/S for starting the project and for practical advice and access to equipment. Special thanks go to Søren Christensen for competent help with development of experimental setups and solutions to practical problems. I also wish to thank my colleagues at Widex A/S in the construction department for their firm belief in my competence and the concept of the project.

Finally, I am very grateful to my lovely wife Reni, who has given me invaluable moral support, contributed with many hours of proofreading and patiently listened to my endless monologues about fuzzy structures.

Lars Friis

Summary: Investigation of internal feedback in hearing aids

There are many aesthetics and structural design requirements to modern hearing aids and their size has been reduced considerably during the last decades. This has led to designs where the receiver (loudspeaker) and microphones are placed closely together. As a consequence, problems with vibroacoustic transmission from the receiver to the microphones often occur during the use of hearing aids. This transmission causes feedback at certain critical gain levels where it produces a loud uncomfortable squealing. Consequently feedback often constitutes the limiting factor for the maximum obtainable gain in the hearing aid and it therefore represents a critical design problem.

Feedback in hearing aids is usually divided into *external* and *internal* feedback. External feedback is caused by the leakage of sound from the ear canal whereas internal feedback is due to transmission of sound and vibrations internally in the hearing aid. As a result of reducing the size of hearing aids, manufacturers have experienced an increase in internal feedback problems. The main objective of the present thesis is therefore to examine the vibroacoustic mechanisms responsible for *internal* feedback in hearing aids. This is approached by the development of a full vibroacoustic 3D-model of a so-called "behind the ear" hearing aid manufactured by Widex A/S. The 3D-model is developed using finite element analysis and it is capable of simulating the so-called "open-loop" transfer functions. These open-loop transfer functions relate the microphone output voltages and the receiver driving voltage when the receiver and microphones are electrically disconnected.

The main scientific part of the thesis consists in the study and extension of a relatively recent method. This method is the "Theory of fuzzy structures" and it is intended for predicting the vibrations of a deterministic "master" structure with one or more attached complex "fuzzy" substructures with partly unknown dynamic properties. An important part of the theory regarding the modeling of fuzzy substructures attached to the master through a continuous interface is thoroughly examined and reformulated in a more simple form. Such fuzzy substructures are modeled by including spatial memory in the fuzzy boundary impedance. The main effect of an attached fuzzy substructure is the introduction of high damping in the vibration response of the master structure, but, it is shown that spatial memory reduces this damping. The method of including spatial memory is hereafter extended such that it also comprises modeling of fuzzy structures with a *two-dimensional* interface. Furthermore, a novel experimental method for estimating the fuzzy parameters of complex substructures is developed by the author. Using this method the damping of the structural fuzzy is estimated and the fuzzy parameters are subsequently derived. The developed method is finally utilized for estimating the fuzzy parameters of certain internals in the considered hearing aid. The estimated fuzzy parameters are experimentally validated and they reveal a high spatial memory in the fuzzy boundary impedance.

Different methods are used for determining the properties of the remainder components in the hearing aid. The determined properties include the stiffnesses of the rubber suspensions, vibration forces of the receiver and the vibration sensitivity of the microphones. Moreover, the sound pressure in the tube system from the receiver to the ear canal is simulated and validated experimentally. All the determined properties including the fuzzy parameters are incorporated into the full 3D-model. Simulated results for the open-loop transfer functions show good agreement with measurements on the hearing aid considered. By analyzing the simulations results, it is revealed that feedback is caused by local pressure generated by the vibrations of the shell close to the microphone inlets. These vibrations are mainly caused by the reaction forces from the high pressure in the tube system of the hearing aid.

Resumé: Undersøgelse af intern feedback i høreapparater

Der stilles mange æstetiske og konstruktionsmæssige krav til moderne høreapparater, og især deres størrelse er blevet reduceret i løbet af de sidste årtier. Dette har ført til konstruktioner, hvor højtaleren og mikrofonerne sidder meget tæt på hinanden. Under brug af høreapparater opstår der derfor ofte problemer med vibroakustisk tilbagekobling fra højtaleren til mikrofonerne. Denne tilbagekobling forårsager feedback ved kraftige forstærkninger af lyden, og der genereres herved en høj og ubehagelig hyletone. Dette betyder, at feedback ofte sætter grænsen for, hvor meget forstærkning, der kan opnås i høreapparater. Feedback udgør derfor et kritisk konstruktionsproblem.

Feedback i høreapparater opdeles normalt i *ekstern* feedback og *intern* feedback. Ekstern feedback skyldes lækage af lyd fra øregangen, mens intern feedback forårsages af transmission af lyd og vibrationer internt i høreapparatet. Som konsekvens af at høreapparater er blevet mindre, har høreapparatproducenter i de seneste år oplevet en stigning af problemer pga. intern feedback. Målsætningen med denne afhandling er derfor at kortlægge de vibroakustiske mekanismer, som forårsager *intern* feedback i høreapparater. Dette opnås ved udvikling af en fuld vibroakustisk 3D-model af et såkaldt "bag-øret"-apparat, der produceres af Widex A/S. 3D-modellen er baseret på finite element analyse, og den er i stand til at simulere de såkaldte "open-loop"-overføringsfunktioner. Disse overføringsfunktioner beskriver sammenhængen mellem spænding genereret af mikrofonerne og drivspænding på højtaleren, når den elektriske forbindelse mellem mikrofoner og højtaler er afbrudt.

Den videnskabelige del af afhandlingen består hovedsagelig i undersøgelse og udvidelse af en relativ ny metode. Denne metode hedder "Theory of fuzzy structures", og den er beregnet til at modellere vibrationerne i en deterministisk hovedstruktur (master struktur), der har en eller flere tilkoblede komplekse eller "fuzzy" substrukturer med delvist ukendte dynamiske egenskaber. En vigtig del af teorien analyseres og forsimples i afhandlingen. Denne del omhandler modellering af fuzzy substrukturer, som er koblet til deres hovedstruktur gennem en kontinuer grænseflade. Den rumlige kobling i substrukturerne medtages ved at indføre "rumlig hukommelse" i deres overfladeimpedans. Det vises, at indflydelsen af en tilkoblet fuzzy substruktur hovedsagelig er tilføjelse af høj dæmpning i hovedstrukturens frekvensrespons, men også at den rumlige hukommelse reducerer denne dæmpning. Metoden udvides herefter til at omfatte modellering af fuzzy strukturer, som har en 2-dimensionel kontinuer grænseflade. Tilmed udvikles en simpel eksperimentel metode til estimering af komplekse substrukturers fuzzy parametre. Ved brug af denne metode estimeres først den tilførte dæmpning, og derefter udledes de tilhørende fuzzy parametre. Endelig benyttes metoden til bestemmelse af fuzzy parametre for bestemte komponenter i det betragtede høreapparat. Disse fuzzy parametre valideres ved brug af vibrationsmålinger, og det afsløres, at der er høj rumlig hukommelse i komponenternes overfladeimpedans.

Forskellige metoder bruges til bestemmelse af egenskaberne for de resterende komponenter i høreapparatet. Disse egenskaber omfatter bl.a. stivhederne af de bløde gummiophæng, højtalerens vibrationskræfter og mikrofonernes vibrationsfølsomhed. Desuden simuleres lydtrykket i rørsystemet fra højtaleren til øregangen og disse simuleringer valideres eksperimentelt. Alle de bestemte egenskaber, såvel som de bestemte fuzzy parametre, inkorporeres i 3D-modellen af det betragtede høreapparat. Simulerede open-loop-overføringsfunktioner viser god overensstemmelse med målinger på det betragtede høreapparat. Ved analyse af simuleringsresultaterne afsløres det, at feedback skyldes lokalt tryk tæt på mikrofonernes indgang, som er genereret af skallens vibrationer. Disse vibrationer forårsages hovedsageligt af reaktionskræfter fra det høje lydtryk i høreapparatets rørsystem.

PART I:

INTRODUCTION

1 Introduction to the thesis

1.1 Feedback

There are many aesthetics and structural design requirements to modern hearing aids. Especially the size of hearing aids has been reduced during the last decades and, naturally, this has led to designs where the loudspeaker and microphones are placed very close to one another. As a consequence, problems with vibroacoustic transmission from the loudspeaker to the microphones often occur during the use of hearing aids. Sound and vibrations generated by the loudspeaker, which also is called the *receiver*, is picked up by the microphones and an unwanted sound loop is formed. This phenomenon is called feedback and occurs at certain critical gain levels in the hearing aid where it produces a very loud and uncomfortable squealing. Feedback often constitutes the limiting factor for the maximum obtainable gain in the hearing aid and it therefore represents a critical design problem.

Feedback in hearing aids can be divided into two types of problems and these are; *external feedback* and *internal feedback* (see Dillon, 2001). External feedback is caused by the leakage of sound from the ear canal mainly through the vent in the earmould. The purpose of this vent is to reduce the occlusion effect (see Dillon, 2001), but, at the same time it represents an unwanted sound source close to the microphones. For many years external feedback has been the predominant problem and this subject has therefore received considerable attention in the open literature. In recent years, however, hearing aid manufacturers have experienced an increase in feedback problems due to internal transmission of sound and vibrations. The main reasons are that hearing aids have become considerably smaller and at the same time also more powerful. Hearing devices designed for severely hearing-impaired persons are now able to amplify the incoming sound by up to about 80 dB. To realize such extreme gain levels it is necessary to produce custom-made earmoulds without a vent. As these fit perfectly in the ear and ear canal of the user, the leakage of sound becomes negligibly small and the internal feedback thus becomes the gain-limiting factor.

1.2 Objective and scientific contribution

The main objective of this thesis is to examine the general and fundamental vibro-acoustic mechanisms responsible for *internal feedback* in hearing aids. This is approached by developing a mathematical/physical model of the transmission of sound and vibrations from the receiver to the microphones. More specifically, the model aims to describe the transfer function relating the input driving voltage of the receiver to the output voltage from the microphones when the receiver and microphones are electrically disconnected. Such a frequency dependent function is a so-called "open-loop" transfer function (see Dillon, 2001). The present thesis considers a specific hearing aid series that is manufactured by Widex A/S. This series has been and still is particularly troublesome regarding internal feedback.

The main scientific contribution of the thesis consists of the study and extension of a relatively recent method for predicting the vibrations of built-up structures with partly unknown dynamic properties of attached components. This method, which represents an alternative to conventional methods of vibration analysis, is called the "Theory of fuzzy structures" (see Soize, 1986; Chabas et al., 1986; Soize et al., 1986). Part of the developments made by the author, are presented in two papers published in the Journal of the Acoustical Society of America. An experimental method for estimating the so-called "fuzzy parameters" defining a fuzzy structure is presented in the thesis. This method is developed by the author and it is utilized in the modeling of the hearing aid considered. To the best of the author's knowledge, no applications of the theory of fuzzy structures to real-life practical problems have been reported in the open literature. Finally, the thesis presents a number of prediction methods for determining the acoustical and dynamical properties of miniature components. Some of these methods are well-known, but, the specific application to miniature components is unusual and their implementation thus represents significant new insight.

1.3 State of the art

The issue of modeling vibrations and acoustics in hearing aids has only received little attention in the open literature. With the main purpose of examining the external feedback paths, Egolf published a series of papers from 1977 to 1989 concerning the modeling of the acoustics in a hearing aid. This included the acoustics in the tube system comprising the receiver, transmission tubes and the ear canal in conjunction with the properties of the microphones. Furthermore, Killion (1975) presented a method for measuring the vibration sensitivity of hearing aid microphones.

Literature concerning the dynamic and acoustic behavior of the receiver and microphones are mainly found in the form of more or less complete technical reports supplied by the manufacturers (see Warren, 2001; Lopresti, 2003; Bukhard, 1965; Knowles electronics, 1969 and 1981). In the author's opinion literature linking all these single topics is lacking in the open literature.

The lack of well-founded knowledge about the internal feedback phenomenon in hearing aids has somehow given rise to mystification about its causes. In research and development groups some believe that sound pressure is built up inside the hearing aid and in one way or another leaked to the outside air close to the microphone inlets. Others think that strong vibrations are picked up by the vibration sensitivities of the microphones and thus generating electrical error output. And yet again, some blame imperfections in the construction and assembly of the hearing aid, such as imprecise mounting of the components or poor fitting of the tubes in the acoustic tube system.

In real life, solutions for reducing feedback are often based on practical experience and trial-and-error procedures. So far, the main practical precaution for minimizing internal feedback is resiliently mounting of the receiver and microphones in soft rubber suspensions. Moreover, feedback canceling algorithms are a standard part of the digital processing in modern hearing aids and such algorithms are still subject to ongoing research. Despite of this, feedback is still a predominant problem. It is therefore the author's intention and hope that this thesis will contribute with scientifically well-founded knowledge about the internal feedback phenomenon. Hopefully this knowledge will result in clear and practical design rules for minimizing the internal feedback problem.

1.4 Structure of the thesis

The remainder of part I of the thesis presents an introduction to the construction and principles of the considered hearing aid series. The complexity of modeling vibrations and acoustics in hearing aids is hereafter demonstrated by a simple model of the vibratory part of a hearing aid. This model is presented in the form of a conference paper (paper I) presented by the author at the 13th International Congress of Sound and Vibration, 1996 (ICSV13). Finally, the last section of part I provides an overview of the methods used for modeling the various hearing aid components.

Part II concerns the theoretical aspects and the practical use of the theory of fuzzy structures. First, the reader is introduced to the method. Second, the method development of the theory of fuzzy structures is presented and highlights are discussed. Hereafter an important part of the theory is studied thoroughly and extended in two journal papers. Results from these papers are further discussed in the thesis. Subsequently the reader is introduced to an experimental method for

estimating fuzzy parameters that is applied to certain parts of the hearing aid. Results for the fuzzy parameters are presented, discussed and finally experimentally validated.

Methods for modeling other miniature components are outlined and applied in part III. The miniature components concerned are the receiver, microphones, resilient suspensions and the acoustic tube system in the hearing aid. After this, all modeling results are collected in Part IV where the full vibroacoustic 3D-model is presented. Simulation results from the developed model are first validated through open-loop measurements of a number of nominally identical hearing aids and then analyzed and discussed. Lastly conclusions on the results and knowledge obtained in the thesis are presented.

2 Modeling of the considered hearing aid

2.1 Presentation of the considered hearing aid

Full modeling of the vibrations and acoustics of a hearing aid is a complicated and elaborate task. The author has therefore chosen to focus on only *one* specific hearing aid model produced by Widex A/S. This hearing aid model belongs to the category of so-called BTE hearing aids (Behind The Ear hearing aids), which is placed behind the user's ear as shown in fig. 2.1. Moreover, the considered model is a so-called "power hearing aid", which is capable of amplifying the sound by up to about 65 dB at certain frequencies. Naturally, such powerful hearing aids are intended for users with severe hearing loss. Higher amplification is only achieved by the so-called "high-power hearing aids" that normally are slightly larger in size than the power hearing aids.

Figure 2.1 BTE hearing aid placed behind the user's ear.

The hearing aid in question is shown in fig. 2.2 in a configuration with the top half-shell removed. Overall the hearing aid is only about 40 mm long and weighs about 3.5 g. As seen in fig. 2.2, the two microphones are mounted in rubber suspensions with their inlets just below the microphone cover. Sound is picked up by both of these microphones and transformed into electrical signals. These signals are sent to the processor where they are digitalized, processed and amplified. Among other tasks, the processing includes determination of the direction of the sound by using the time difference between the two signals. Depending on the specific hearing aid type the processor

contains different sound processing programs that are targeted for typical everyday situations. After processing and amplification, the altered electric signal is fed to the receiver that produces an improved version of the sound, which has been customized for the user. As shown in figs. 2.1 and 2.2 the sound is let from the receiver through a tube of steel, then through the ear hook and finally through a plastic tube to the earmould placed in the user's ear. This relatively long tube system, which has a length of almost 80 mm, represents a very significant acoustic load on the receiver. The interaction of the receiver and this system governs the final sound product at the eardrum of the user. The membrane of the receiver, which is placed parallel to the large surface of the magnetic shield, is vibrating strongly during operation. In an attempt to isolate this excitation from the rest of the hearing aid, the receiver is mounted in a resilient rubber suspension. This suspension is only in contact with the magnetic screen in positions close to the steel pipe. The purpose of the screen is to shield the so-called telecoil and receiver magnetically from each other as well as enclosing the receiver acoustically.

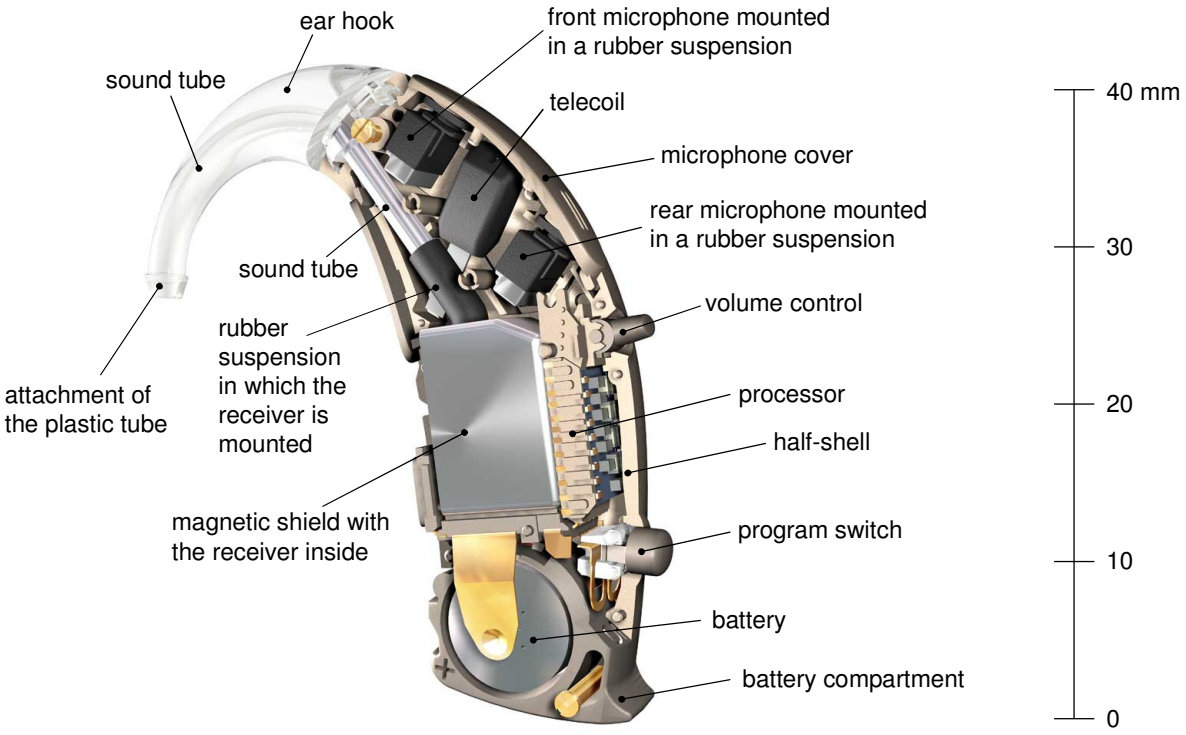

Figure 2.2 The structure of the BTE hearing aid considered.

2.2 Complexity of modeling sound and vibrations in hearing aids

As shown in fig. 2.2, a hearing aid consists of a variety of different components and modeling of the acoustic and dynamic behavior of all these components is quite complicated. For illustration purposes the vibratory part of the vibroacoustic transmission from the receiver to the microphones was examined through a simplified vibration model including only simple elements such as lumped masses, springs and beams connected to one another. This model is presented in the succeeding congress paper presented on the 13th International Congress of Sound and Vibration, 2006 (ICSV13). The paper gives a good introduction to the challenges of modeling sound and vibrations in hearing aids and it demonstrates that the interaction between the various components results in a complicated vibration pattern with many resonances in the important frequency range from 100 Hz to 10.000 Hz. The effect of mounting the receiver in rubber suspensions of different stifnesses is also examined in paper I.

2.2.1 Paper I:

Two-dimensional model of the vibro-acoustic feedback in a hearing aid

ICSV13 - Vienna
The Thirteenth International Congress on Sound and Vibration
Vienna, Austria, July 2-6, 2006

TWO-DIMENSIONAL MODEL OF THE VIBRO-ACOUSTIC FEEDBACK IN A HEARING AID

Lars Friis*[1], Mogens Ohlrich[2]

[1]Widex A/S, Ny Vestergårdsvej 25, DK-3500 Værløse, Denmark, and
Acoustic Technology, Ørsted•DTU, Technical University of Denmark
Building 352, DK-2800 Kgs. Lyngby, Denmark
[2]Acoustic Technology, Ørsted•DTU, Technical University of Denmark,
Building 352, DK-2800 Kgs. Lyngby, Denmark
l.friis@widex.com

Abstract

In this paper we investigate the vibration patterns of a "behind the ear" hearing aid model. Due to the minimal structural design of hearing aids, problems with vibro-acoustic transmission from the loudspeaker to the microphones often arise. Vibrations and sound pressure are picked up by the microphones and an unwanted electrical/vibro-acoustical loop is formed. This phenomenon is also known as feedback. The vibratory part of the vibro-acoustic transmission from the loudspeaker to the hearing aid shells is examined for a simple mathematical vibration model of the hearing aid. This simple model includes the main parts of the hearing aid such as the loudspeaker, hook, shells, battery and resilient connections. By employing mobility synthesis, these components are modelled as lumped masses, springs and beam components, which are connected to one another. Results from the vibration model reveal a complicated pattern of resonances governed by the various components and their interaction with one another. Furthermore, the vibration isolation effect of the loudspeaker suspension is investigated.

INTRODUCTION

There are many aesthetics and structural design requirements to modern hearing aids. These have resulted in designs where the loudspeaker and microphones are placed very close to one another. As a consequence of this, problems with vibro-acoustic transmission from the loudspeaker to the microphones often arise. Vibrations and sound pressure are "picked up" by the microphones and an unwanted electrical/vibro-acoustical loop is formed. The phenomenon is called feedback and occurs at certain critical gain levels in the hearing aid where it produces an uncomfortable howling sound.

This paper investigates the vibratory part of the vibro-acoustic transmission from the loudspeaker to the shells in a so-called "behind the ear" hearing aid. This is placed behind the user's ear with the curved *hook* around the upper part of the ear. It has two microphones that monitor the sound pressure and converts this into an electrical signal, which is amplified in the hearing aid and is fed to the loudspeaker. The sound pressure from the loudspeaker is led through a canal in the hook and into a soft plastic tube, which is firmly connected to a moulded ear plug. In order to obtain good vibration isolation, the loudspeaker and the microphones are mounted resiliently in soft rubber suspensions. More general information about hearing aids is found in Reference 1.

A full three-dimensional analysis of the vibration transmission is very difficult due to the interactions between structural components of complex shapes and because of mechanical properties and connections that are often uncertain. However, a fundamental understanding of certain overall transmission phenomena may be obtained from studies of less complicated models. Herein we consider only a two-dimensional hearing aid model, consisting of masses, springs and beam components. In a first attempt wide simple beams are chosen to represent approximately modal behaviour and certain elastic properties similar to those of the complex shells. The simple mechanical model considered in this paper is based on the hearing aid shown in Figure 1.

The simple vibration model considered includes the main parts of the hearing aid such as the loudspeaker, resilient suspensions, hook, shells, and battery. By employing mobility synthesis [2], these components are modelled as lumped masses and springs, and elastic beam components, which are connected to one another. Altogether the model has a total weight of about three grams.

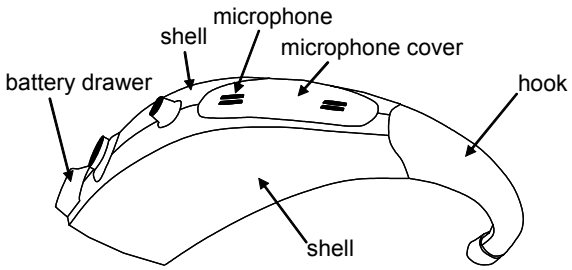

Figure 1 – "Behind the ear" hearing aid.

Examples of the use of mobility synthesis can be found in Ref. [2] where the method is described in details. Moreover, Gardonio [3] has examined a multi-degree-of-freedom system consisting of a source and receiver separated by vibration isolating mounts by using mobility synthesis.

HEARING AID MODEL AND OUTLINE OF THEORY

Figure 2 shows sketches of the "behind the ear" hearing aid and a two-dimensional model of masses, springs, and beams. The vibration response of this system is governed by three motion degrees-of-freedom, comprising velocities v_x, v_y, and υ_z in the *x*-direction, *y*-direction, and the rotational direction around *z*, respectively. Components are denoted by a capital letter, and the junctions where the components

are connected are denoted with a number in a circle. Furthermore, springs are denoted by a capital S with a number as subscript and each spring represents a stiffness in all three motion coordinates.

Component A represents the loudspeaker which is the vibration source of the hearing aid. The driving mechanism and loudspeaker membrane are primarily vibrating in the *y*-direction and the loudspeaker is modelled as a mass which is driven by a harmonic force $F_{exc,y}e^{i\omega t}$ in this direction at its centre of gravity. The air pipe, B, is modelled as an equivalent Bernoulli-Euler beam, which is connected to the loudspeaker through one part of the loudspeaker suspension represented by spring S_1. Sound pressure from the loudspeaker is let through the air pipe and into the hook C, which is modelled as a beam with varying cross-section as shown in Figure 2. The hook is coupled to the air pipe and to the upper and lower shells D and E through the somewhat indefinable connection springs S_2, S_3 and S_6. These shells are represented by two simple beams with approximately the same dimensions as the actual shells. In the left-most end, the two shells are connected to one another through connection spring S_9. Vibration isolation of the loudspeaker from the shells is obtained by the loudspeaker suspension represented by springs S_4 and S_7. Finally the battery G, which is modelled as a mass, is held into place by two springs S_5 and S_8 connected to the upper and lower shell, respectively.

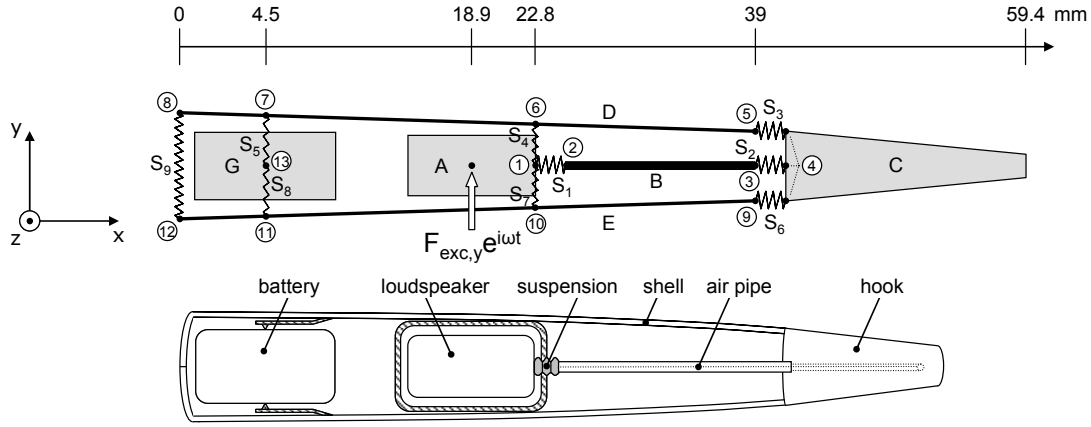

Figure 2 – Vertical section of hearing aid and model consisting of masses, springs and beam components.

Weight, dimensions and elastic properties of each component are given in Table 1-3.

Table 1 – Properties of beam components.

Symbol	Component	E-module [MPa]	Weight [g]	Loss factor	Length [mm]	Height [mm]	Width [mm]
B	Air pipe	210	0.104	0.003	14.0	1.76	0.582
C	Hook	1.9	0.262	0.061	20.4	4.9-2.3	8.1-2.3
D, E	Shells	2.3	0.575	0.05	39.0	1.3	10.8

Table 2 - Mass properties.

Symbol	Component	Weight [g]	Length x [mm]	Length y [mm]
A	Loudspeaker	0.770	8.15	4.45
G	Battery	0.812	7.8	5.3

Table 3 - Properties of resilient elements.

Symbol	Component	Stiffness			Loss factor
		s_x [N/m]	s_y [N/m]	s_z [Nm]	
S1	Loudspeaker suspension	180	180	$7.47 \cdot 10^{-4}$	0.1
S2, S3, S6, S9	Contact springs	∞	∞	3.33	0.01
S4, S7	Loudspeaker suspension	180	180	$7.47 \cdot 10^{-4}$	0.1
S5, S8	Battery springs	∞	2475	∞	0.001

The vibration model is developed by using mobility synthesis and each component is described in terms of its complex velocities and forces symbolized by the column vectors $\overline{v}_i$ and $\overline{F}_j$, respectively. By assuming harmonic motion at angular frequency ω, the complex velocities $\overline{v}_i$ at position i generated by the forces $\overline{F}_j$ at position j can be related through a 3×3 mobility matrix $\overline{\overline{Y}}_{ij}$ as $\overline{v}_i e^{i\omega t} = \overline{\overline{Y}}_{ij} \overline{F}_j e^{i\omega t}$. With the time dependence suppressed this is given by

$$\begin{bmatrix} v_x \\ v_y \\ \upsilon_{z'} \end{bmatrix}_i = \begin{bmatrix} Y_{xx} & Y_{xy} & Y_{xz'} \\ Y_{yx} & Y_{yy} & Y_{yz'} \\ Y_{z'x} & Y_{z'y} & Y_{z'z'} \end{bmatrix}_{ij} \begin{bmatrix} F_x \\ F_y \\ M_{z'} \end{bmatrix}_j . \tag{1}$$

Here subscript *x*, *y*, and *z'* refers to the *x*-direction, *y*-direction and the rotational direction around *z*, respectively. By superposition of velocity contributions from forces in all positions the total complex velocities of each component can be described. The mobilities of the masses, mass-less springs and beams can all be found in [2] and the dynamic properties of the non-uniform hook, is obtained by using transmission theory according to Reference [4].

Now, the loudspeaker is excited at its centre by the harmonic force $F_{y,exc} e^{i\omega t}$, and this results in a mixed force and moment excitation at junction 1. The excitation vector, $\overline{F}_{exc}$, acting at junction 1 is thus given as

$$\overline{F}_{exc} = \begin{bmatrix} F_{x,exc} \\ F_{y,exc} \\ M_{z',exc} \end{bmatrix} = \begin{bmatrix} 0 \\ F_{y,exc} \\ -(l_{A,x}/2) F_{y,exc} \end{bmatrix}, \tag{2}$$

where $l_{A,x}$ is the length of the loudspeaker in the x-direction. In the following the harmonic responses for each component are derived by using mobility synthesis. Continuity in all junctions is already included in the equations. Further, it is assumed that velocities in the left end of the hook, denoted junction 4, are the same at all three spring connections. Spring forces are defined as positive when the springs are compressed. Altogether, the equations of motion include 13 unknown velocity vectors and 9 unknown spring force vectors. In these equations the first subscript of the mobilities refers to the component, whereas the second and the third subscript refer to the position of the velocity vector and the force vector, respectively. The derived harmonic responses for the components or positions in Figure 2 are:

Loudspeaker: $$\bar{v}_1 = \bar{\bar{Y}}_A(\bar{F}_{exc} - \bar{F}_{S_1} - \bar{F}_{S_4} + \bar{F}_{S_7}) \quad (3)$$

Pipe: $$\bar{v}_2 = \bar{\bar{Y}}_{B,2,2}\bar{F}_{S_1} - \bar{\bar{Y}}_{B,2,3}\bar{F}_{S_2} \qquad \bar{v}_3 = \bar{\bar{Y}}_{B,3,2}\bar{F}_{S_1} - \bar{\bar{Y}}_{B,3,3}\bar{F}_{S_2} \quad (4\text{-}5)$$

Hook: $$\bar{v}_4 = \bar{\bar{Y}}_C(\bar{F}_{S_2} + \bar{F}_{S_3} + \bar{F}_{S_6}) \quad (6)$$

Upper shell: $$\bar{v}_5 = -\bar{\bar{Y}}_{D,5,5}\bar{F}_{S_3} + \bar{\bar{Y}}_{D,5,6}\bar{F}_{S_4} + \bar{\bar{Y}}_{D,5,7}\bar{F}_{S_5} + \bar{\bar{Y}}_{D,5,8}\bar{F}_{S_9} \quad (7)$$

$$\bar{v}_6 = -\bar{\bar{Y}}_{D,6,5}\bar{F}_{S_3} + \bar{\bar{Y}}_{D,6,6}\bar{F}_{S_4} + \bar{\bar{Y}}_{D,6,7}\bar{F}_{S_5} + \bar{\bar{Y}}_{D,6,8}\bar{F}_{S_9} \quad (8)$$

$$\bar{v}_7 = -\bar{\bar{Y}}_{D,7,5}\bar{F}_{S_3} + \bar{\bar{Y}}_{D,7,6}\bar{F}_{S_4} + \bar{\bar{Y}}_{D,7,7}\bar{F}_{S_5} + \bar{\bar{Y}}_{D,7,8}\bar{F}_{S_9} \quad (9)$$

$$\bar{v}_8 = -\bar{\bar{Y}}_{D,8,5}\bar{F}_{S_3} + \bar{\bar{Y}}_{D,8,6}\bar{F}_{S_4} + \bar{\bar{Y}}_{D,8,7}\bar{F}_{S_5} + \bar{\bar{Y}}_{D,8,8}\bar{F}_{S_9} \quad (10)$$

Lower shell: $$\bar{v}_9 = -\bar{\bar{Y}}_{E,9,9}\bar{F}_{S_6} - \bar{\bar{Y}}_{E,9,10}\bar{F}_{S_7} - \bar{\bar{Y}}_{E,9,11}\bar{F}_{S_8} - \bar{\bar{Y}}_{E,9,12}\bar{F}_{S_9} \quad (11)$$

$$\bar{v}_{10} = -\bar{\bar{Y}}_{E,10,9}\bar{F}_{S_6} - \bar{\bar{Y}}_{E,10,10}\bar{F}_{S_7} - \bar{\bar{Y}}_{E,10,11}\bar{F}_{S_8} - \bar{\bar{Y}}_{E,10,12}\bar{F}_{S_9} \quad (12)$$

$$\bar{v}_{11} = -\bar{\bar{Y}}_{E,11,9}\bar{F}_{S_6} - \bar{\bar{Y}}_{E,11,10}\bar{F}_{S_7} - \bar{\bar{Y}}_{E,11,11}\bar{F}_{S_8} - \bar{\bar{Y}}_{E,11,12}\bar{F}_{S_9} \quad (13)$$

$$\bar{v}_{12} = -\bar{\bar{Y}}_{E,12,9}\bar{F}_{S_6} - \bar{\bar{Y}}_{E,12,10}\bar{F}_{S_7} - \bar{\bar{Y}}_{E,12,11}\bar{F}_{S_8} - \bar{\bar{Y}}_{E,12,12}\bar{F}_{S_9} \quad (14)$$

Battery: $$\bar{v}_{13} = \bar{\bar{Y}}_G(\bar{F}_{S_8} - \bar{F}_{S_5}) \quad (15)$$

Springs: $$\bar{v}_1 - \bar{v}_2 = \bar{\bar{Y}}_{S_1}\bar{F}_{S_1} \qquad \bar{v}_3 - \bar{v}_4 = \bar{\bar{Y}}_{S_2}\bar{F}_{S_2} \qquad \bar{v}_5 - \bar{v}_4 = \bar{\bar{Y}}_{S_3}\bar{F}_{S_3} \quad (16\text{-}18)$$

$$\bar{v}_1 - \bar{v}_6 = \bar{\bar{Y}}_{S_4}\bar{F}_{S_4} \qquad \bar{v}_{13} - \bar{v}_7 = \bar{\bar{Y}}_{S_5}\bar{F}_{S_5} \qquad \bar{v}_9 - \bar{v}_4 = \bar{\bar{Y}}_{S_6}\bar{F}_{S_6} \quad (19\text{-}21)$$

$$\bar{v}_{10} - \bar{v}_1 = \bar{\bar{Y}}_{S_7}\bar{F}_{S_7} \qquad \bar{v}_{11} - \bar{v}_{13} = \bar{\bar{Y}}_{S_8}\bar{F}_{S_8} \qquad \bar{v}_{12} - \bar{v}_8 = \bar{\bar{Y}}_{S_9}\bar{F}_{S_9}\,. \quad (22\text{-}24)$$

It should be kept in mind that all the unknown vectors include three motion coordinates and the matrix equations (3)-(24) therefore comprise of a system of 66 equations with 66 unknown velocities and spring forces. Now, if all terms in the equations involving velocities and spring forces are collected on the left-hand side of the equality signs, and thus isolating the terms involving the excitation forces $\bar{F}_{exc}$ on the right-hnd side, then the system of equations can be expressed as one matrix equation as

$$\bar{\bar{H}}_X \bar{X} = \bar{\bar{H}}_F \bar{F}_{exc} \quad \Leftrightarrow \quad \begin{bmatrix} & 66 \text{ x } 66 & \end{bmatrix}\begin{bmatrix} 66 \end{bmatrix} = \begin{bmatrix} 66 \text{ x } 3 \end{bmatrix}\begin{bmatrix} 3 \end{bmatrix}, \quad (25)$$

where $\overline{X}$ is a column vector with 66 elements containing all velocities and spring forces, $\overline{\overline{H}}_X$ is a 66×66 element matrix containing the terms in front of the velocities (zeros and ones) and the terms in front of the spring forces (mobilities), and $\overline{\overline{H}}_F$ is a 66×3 element matrix containing the terms in front of the excitation forces (mobilities). Finally, the system of equations can be solved numerically for $\overline{X}$ for one frequency at a time by multiplying with the inverted matrix $\overline{\overline{H}}_X^{-1}$ on both sides of eq. (25), which yields

$$\overline{X} = \overline{\overline{H}}_X^{-1} \overline{\overline{H}}_F \overline{F}_{exc} . \tag{26}$$

Damping in the beam components and in the springs are included by introducing complex bending stiffness and complex spring constants, respectively, with corresponding damping loss factors. Furthermore, the loss factor of the hook, and the stiffness of the loudspeaker mounts have been determined experimentally. Other spring stiffnesses have been estimated theoretically.

NUMERICAL RESULTS

In the following numerical results from the vibration model are presented. In this preliminary study only two types of motion coordinates have been used. These are the velocities in the *y*-direction and in the rotational direction around *z*. The vibration of the hearing aid is here characterized in terms of the squared velocity ratio $< v^2 > / |v_{free}|^2$ where $< v^2 >$ is the spatially averaged mean-square velocity of the shells and $|v_{free}|^2$ is the squared magnitude of the free velocity of the loudspeaker in the *y*-direction. This free velocity is a convenient reference since it can be determined experimentally. The loudspeaker is modeled as a pure mass M_A and when this is excited by $F_{y,exc}$ its free velocity becomes

$$v_{free} = \frac{F_{y,exc}}{i\omega M_A} . \tag{27}$$

Figure 3 shows the normalized mean-square velocity of the shells for three different values of the spring stiffnesses of S_2, S_3, and S_6. It is seen that several resonances occur within the frequency range considered. And although the complex system vibrates as a whole, it is possible to identify the main cause of most of these resonances by performing a parameter study. For the dimensions and elastic properties chosen each resonance peak can be assigned to an individual component mode as indicated in Figure 3. The occurrence of the two lowest resonances at 58 Hz and 264 Hz are primarily controlled by the soft loudspeaker suspension e.g. springs

S_1, S_4, and S_7, because the hearing aid vibrates as a two-degree-of-freedom mass-spring-mass system with the loudspeaker as one mass, the suspension as the spring and the rest of the hearing aid as the second mass. In the frequency range above the mass-spring-mass modes the suspension works efficiently as a vibration isolator. The overall decrease in vibration level of the shells is about 40 dB per decade.

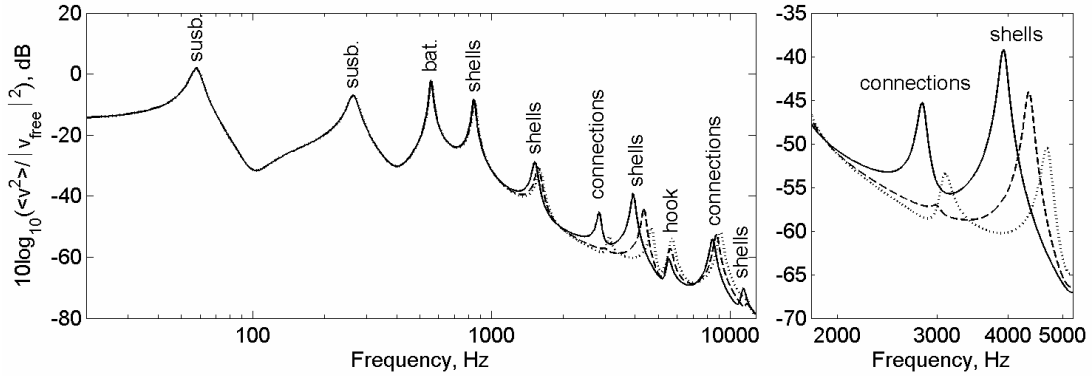

Figure 3. Frequency variation of normalized mean-square velocity of shells. For different values of stiffness $s_{z'}$ of the contact springs S_2, S_3, and S_6: ——, $s_{z'}$=3.33 Nm; – – –, $s_{z'}$=6.66 Nm; ·····, $s_{z'}$=10.0 Nm.

Especially the shells produce many resonances in the frequency range from 840 Hz to 11.4 kHz but also the resiliently connected battery, the hook and the more or less rigid connections (S_2, S_3, and S_6) may contribute to feedback problems. The connections in particular are difficult to describe dynamically and in order to investigate how sensitive the model is to small changes the mean-square velocity of the shells has been plotted for three different cases of the connection springs. Focusing on the frequency range from about 2000 Hz to 5000 Hz it is seen from the "zoom" in Figure 3 that a doubling of the connection spring stiffness from $s_z = 3.33$ Nm to 6.66 Nm causes the resonance peak at 2823 Hz with a vibration level of -45.3 dB to almost vanish. Further, by increasing the stiffnesses to 10.0 Nm, the resonance peak moves up to 3102 Hz and becomes significant with a vibration level of -53.4 dB. Additionally, a large drop of more than 10 dB in vibration level of the resonant peaks caused by the shells can be observed. This parameter study reveals that small changes may remove or produce troublesome resonance peaks.

Figure 4 shows the normalized mean-square velocity of the shells for four different values of the loudspeaker suspension stiffnesses S_4 and S_7. Also shown in Figure 4 is a case where the loudspeaker is rigidly connected to the shells. Vibration at this condition forms the basic or reference for evaluating the isolation effectiveness of the resilient suspensions. Naturally, when the stiffness of the springs S_4 and S_7 is increased then the previously mentioned two mass-spring-mass modes moves towards higher frequencies. The frequency range where the suspension works as a vibration isolator is accordingly moved upwards and gives a poorer isolation in the whole frequency range. An increase of the stiffness values of three and ten times thus result in an increase of the overall vibration level of about 9 and 20 dB, respectively.

Especially in the frequency range from about 400 Hz to 1000 Hz the vibration isolation is very poor due to modes caused primarily by the battery and the shells. Nevertheless, at 10 kHz the vibration level is significantly lower than the reference even in the poorest performing case.

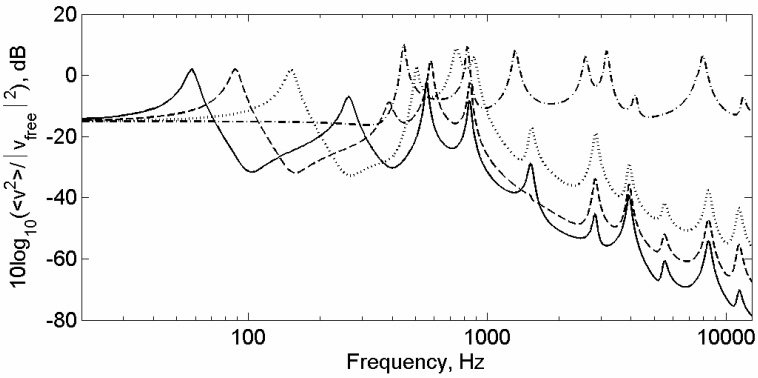

Figure 4. Frequency variation of the normalized mean-square velocity of the shells for different values of springs stiffnesses S_4 and S_7: ——, nominal values as in Table 1.3 ; – – –, three times larger; ·····, ten times larger; – · –, infinitely stiff.

CONCLUSIONS

The vibration patterns of a so-called "behind the ear" hearing aid has been examined through a simple mathematical vibration model developed by using mobility synthesis. In a first attempt wide, simple beams were chosen to represent approximately the dynamic characteristics of the complex shells. For this choice of components it was revealed that several structural resonances occur in the frequency range from 58 Hz and up to 10 kHz and these are caused by the loudspeaker suspension and individual component modes. Further, it was shown that little changes in the structural parameters may have a large effect on the vibrations of the simulated shells. Finally, the effect of the loudspeaker suspension was investigated, and this showed that appreciable vibration isolation is obtained in the frequency range above 1000 Hz.

[1] Crocker M. J., "Encyclopedia of Acoustics", Volume four, John Wiley & Sons, Inc. (1997).
[2] Bishop R. E. D. and Johnson D. C., "The Mechanics of Vibration", Cambridge University Press, Cambridge (1960).
[3] Gardonio P., Elliott S. J., Pinningston R. J., "Active isolation of structural vibration on a multi-degree-of-freedom system. Part I: The dynamics of the system", Journal of Sound and Vibration, **207**, 61-93 (1997).
[4] Rocke R. D., "Transmission matrices and lumped parameter models for continuous systems", Research report from Dynamics Laboratory, California Institute of Technology, Pasadena, California (1966).

2.3 Overview of modeling methods

Unfortunately the simple dynamical model presented in the congress paper is unable to reveal the specific mechanisms responsible for internal feedback as these involve both vibrations and acoustics in three dimensions. The overall goal of the present work is therefore to develop a total 3D-model of the considered hearing aid describing both the vibrations and acoustics and their mutual interaction.

The 3D-model, which is presented in Part IV of this thesis, describes the vibrations and acoustics of the hearing aid in the frequency domain and it assumes stationary harmonic oscillation. Moreover, it only applies for small signals and does not take any nonlinear effects into account. For the sake of simplicity the hearing aid is considered to be ”free in space” and thus not placed behind the ear of a user. Also, it should be noted that the frequency range of interest regarding feedback is from 100 Hz to 10 kHz.

Figure 2.3 gives an overview of the developed and the various implemented methods used for modeling the considered hearing aid. Also shown are methods for determining the acoustic and dynamic properties of the components in the hearing aid.

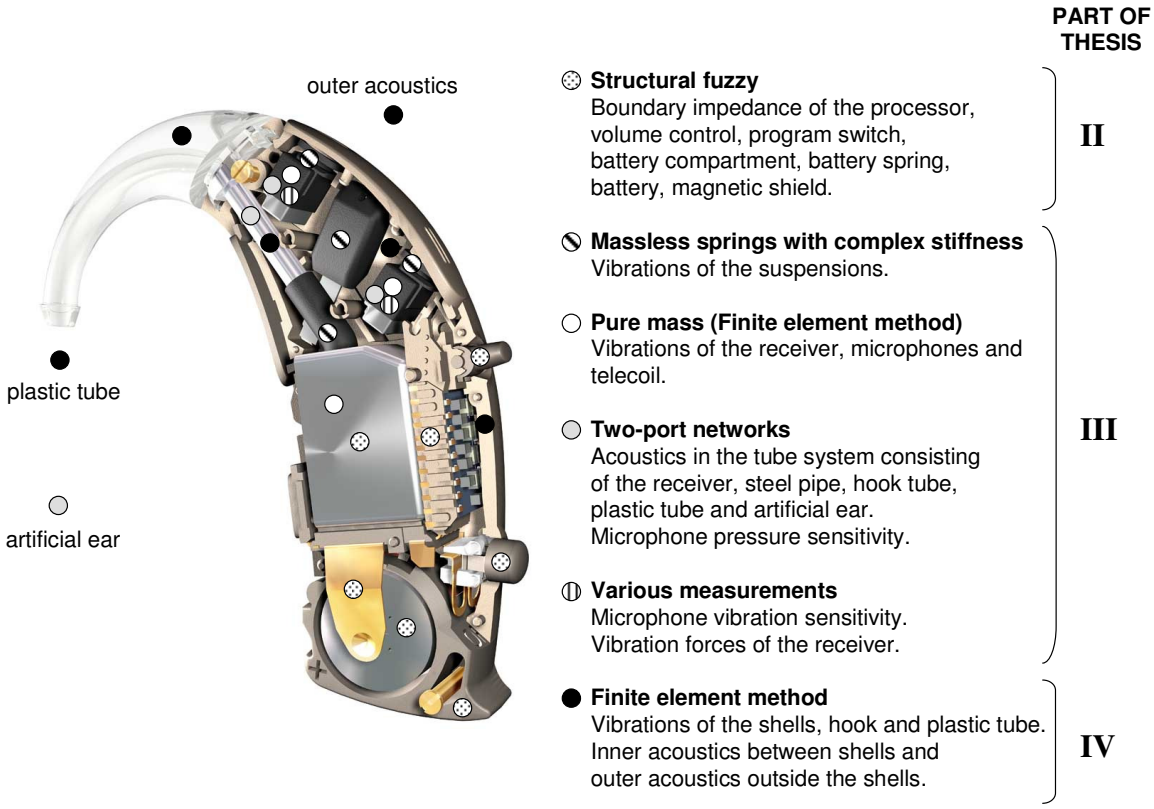

Figure 2.3 Overview of methods used for modeling the considered hearing aid .

Because of the mentioned uncertainties of the dynamic coupling properties of many of the components it has been chosen to utilize the theory of fuzzy structures. This method represents an alternative to traditional methods of vibration analysis as it is capable of modeling the vibrations of complex structures with uncertain properties. These complex structures that are more or less compliantly attached have many degrees of freedom. As shown in the fig. 2.3, the so-called "structural fuzzy" comprises a number of components in the lower part of the hearing aid that are attached to the covering shell and to each other in a rather indefinable and uncertain way. It is characteristic for these components that only their influence on mainly the shell needs to be determined. Their specific vibrations during operation are not known and, as such, the components are regarded as a "black box".

In order to examine the mechanisms causing feedback, determination of the specific acoustical and mechanical properties of the receiver and microphones are very important. These properties have mainly been obtained by employing two-port networks. Also the acoustic tube system carrying the sound from the receiver to the ear canal has been modeled using these two-port networks. In this system the eardrum and ear canal of the user have been replaced with a so-called "artificial ear" or a "coupler" representing an average human ear. Further, to model the vibrations of the receiver and the microphones, stiffness properties of the rubber suspensions have been determined. This has been achieved through experiments involving specially designed setups for miniature components. Also the vibration forces of the receiver and the vibration sensitivity of the microphones have been determined experimentally by using such miniature arrangements.

The dynamics of the remainder components such as the shell, tubes, hook as well as the inner and outer acoustics on each side of the shell have been modeled using the finite element analysis (see Cook *et al.*, 2002). All the determined acoustical and dynamical properties have been prepared for implementation in the full 3D-model of the hearing aid. As mentioned this model is presented in part IV of the thesis where simulation results are also validated experimentally.

PART II:

MODELING OF FUZZY STRUCTURES

3 Introduction

The present part of the thesis first offers a short introduction to the “Theory of fuzzy structures”. Hereafter follows a presentation of the method development of this theory where the most important discussions and results are highlighted. This is succeeded by a thorough study and method extension of a specific part of the theory concerning fuzzy structures attached to the master through a continuous boundary. New derivations, physical interpretations and results are presented in paper II and III. Finally, an experimental method for determining the fuzzy parameters is proposed. This method, developed by the author, is applied to the hearing aid device in question. Results from simulations are assessed experimentally.

The theory of fuzzy structures is a relatively new topic that was introduced in 1986 by Christian Soize at ONERA in France (see Soize, 1986; Chabas *et al.*, 1986; Soize *et al.*, 1986). This theory is an alternative to conventional methods of vibration analysis such as mobility synthesis (see Bishop and Johnson, 1960), Finite element analysis (see Cook *et al.*, 2002) etc. As opposed to these conventional methods, the theory of fuzzy structures is intended for modeling the vibrations of a deterministic main structure with one or more attached complex substructures having *imprecisely* known properties. These substructures are called “fuzzy substructures” and the main structure is denoted the “master structure”. Excitation of the fuzzy occurs only through the vibrations of the master. So to speak, the structural fuzzy is regarded as a “black box” and its specific motion displacements are not known. The main effect of the attached structural fuzzy is the introduction of strong damping in the frequency response of the master structure.

Figure 3.1 shows examples of complicated systems that can be modeled using the theory of fuzzy structures. These systems are typical engineering constructions of both small and large size that basically consist of an outer shell and a number complicated internal substructures. The well-defined outer shell is considered to be the master structure and it is modeled by using conventional methods of vibration analysis. In contrast, the dynamic properties of the internal substructures are only partly known and their dynamics and influence therefore have to be modeled by using an alternative method. The theory of fuzzy structures represents such a promising alternative method. For a more detailed introduction to the theory of fuzzy structures, the reader is referred to the first part of paper II.

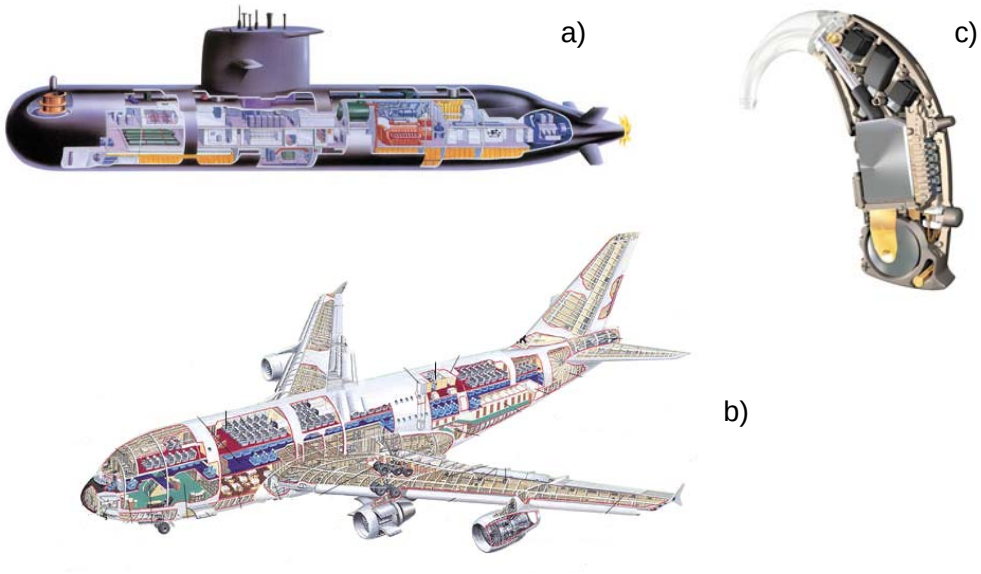

Figure 3.1. Examples of complicated systems consisting of a well-defined outer shell-like structure (the master) and a collection of complicated and resonant internal structures (fuzzy substructures). Shown are (a) a submarine, (b) an airplane and (c) a hearing aid.

4 Method development

4.1 The dynamic neutralizer

For many years it has been commonly known from experiments that vibrations of a complicated system consisting of a main structure and a large number of small attached resonant substructures often appears to be more damped than structural losses in the main structure itself can account for. Already in 1928 Ormondroyd and Den Hartog revealed that a “dynamic absorber” could produce a considerable reduction in vibration level, however, only in a relatively narrow frequency band around its natural frequency. To be most effective such an auxiliary system is usually attached to the main structure at points where forcing occurs. Energy from the main structure is “drained” from the master structure into the auxiliary system vibrating strongly. Therefore, the term “dynamic neutralizer” has been adopted (see White and Walker, 1982). The bandwidth of influence can be slightly increased by a tuning that involves small adjustments of both stiffness and damping of the resilient part of the device. For a more recent and detailed treatment of this subject see the monograph by Mead (1999).

4.2 Structural fuzzy of type I and type II

It took almost sixty years before Soize and co-workers suggested that attached resonant substructures in effect behave like a multitude of different dynamic neutralizers. Since these dynamic neutralizers have different natural frequencies they introduce a high damping in the main structure over a broader frequency range. The first part of the theory of fuzzy structures was presented in 1986 (see Soize, 1986; Chabas e*t al.*, 1986; Soize *et al.*, 1986) and concerns structural fuzzy modeled as a multitude of attached dynamic neutralizers. This kind of fuzzy was denoted “type I fuzzy” and it was intended for modeling complex structures attached to the master through a point or a small local area with dimensions that are small relative to the master’s wavelength (see Cremer *et al.*, 1988). The structural fuzzy was represented by a probabilistic boundary impedance

acting on the so-called master. Several years after the presentation of type I fuzzy, Soize briefly introduced “type II fuzzy” (see Soize, 1993) that is intended for modeling the effects of complex structures attached to the master structure through a continuous boundary. This type therefore includes spatial coupling between different positions in the fuzzy. Some years later Soize (1998) and Soize and Bjaoui (2000) further extended and validated the method theoretically on a model of a master plate with a number of attached complex structures representing a real-life complex engineering structure.

4.3 Interpretation of Soize’s theory

In order to account for model uncertainties Soize’s theory of fuzzy structures involves probabilistic concepts and high-level mathematics. The methodology is carefully conceived and many aspects are taken into account. Furthermore, the theory was originally prepared for numerical modeling using the finite element method and was therefore formulated using a special terminology. Unfortunately this formulation makes rather difficult reading for most vibration researchers and engineers and to some extent this has overshadowed the important conclusions of the theory. Several researches have pointed out that the main results of the theory can be explained without using the full methodology. In particular it has been shown that some important results can be understood without the use of probabilistic concepts. Xu and Igusa (1992), Pierce *et al.* (1995) and Strasberg *et al.* (1996) introduced more simple and deterministic methods for predicting the smoothed average response of the master. These methods revealed that the fuzzy damping effect is practically independent of the structural losses in the fuzzy. And it was shown that the damping mainly depends on the resonating mass per unit natural frequency and that the dynamic properties of the fuzzy are governed by this fuzzy parameter. During the mid-nineties many of the main theoretical aspects were discussed and further exemplified. Ruckman and Feit (1995) published a tutorial on Soize’s method. Sparrow *et al.* (1994) and Russell (1995) investigated Soize’s fuzzy oscillators in great detail. Furthermore, Lyon (1995) compared the theory of fuzzy structures with the statistical energy analysis (SEA), and he stated that the fuzzy results also can be obtained by using SEA. Nevertheless, he also concluded that the theory of fuzzy structures was a new approach capable of providing valuable details of certain structural interaction phenomena. Moreover, Langley and Bremner (1999) presented a hybrid SEA method for modeling complex dynamic

systems, by partitioning the involved degrees of freedom into a “global set” and “local set”. To some extent, this method resembles the theory of fuzzy structures.

4.4 The fuzzy damping effect

From around the mid-nineties and up till now one of the most debated topics of the fuzzy theory has been the nature of the fuzzy damping effect. Langley (1997) investigated whether an undamped oscillator is capable of dissipating energy. He concluded that energy is not dissipated but “absorbed” since such an oscillator never reaches steady state vibration. Moreover, in a series of papers Weaver (1996, 1997a, 1997b, 1998, 2001) and Carcaterra and Akay (2004, 2007) examined the transient dynamic behavior of structural fuzzy consisting of both a finite and an infinite number of oscillators. It was concluded that the steady state results provided by Pierce *et al.* (1995) and Strasberg *et al.* (1996) are correct also for transient excitation when the fuzzy consists of infinitely many oscillators. In the case of a finite number of oscillators, however, it was revealed that the damping effect generally is *apparent* and only occurs for early and moderate time histories. At later time histories, the energy from the fuzzy returns to the master, resulting in a series of exponentially decaying pulses in the impulse response. It was further shown that the return time of the energy is short for a limited number of oscillators and long for a high number of oscillators. For the special case of a very long return time and relatively high loss factors in the structural fuzzy, the energy may dissipate before the energy returns to the master. The same damping effect as in the case of infinitely many oscillators is therefore obtained. For steady state vibration, Strasberg (1997) showed that the dissipation is real as vibratory power continuously is transferred from the master to the structural fuzzy and converted into heat.

Another addressed subject during this period was the development of design criteria for maximizing the fuzzy damping effect. Already in 1993 Igusa and Xu addressed this subject. Above all Maidanik (1995), Maidanik and Dickey (1996) and Maidanik and Becker (1998a, 1998b, 1999a, 1999b) published a series of papers that in great detail investigated the actual damping effect obtained for different distributions of resonating mass per unit frequency. From new definitions of different types of loss factors concerning the damping, design criteria for maximum effect were set up. Other authors have also contributed with investigations regarding design criteria for maximum damping. This includes Koc *et al.* (2005), Akay *et al.* (2005) and Carcaterra and Akay (2007).

In 1997 Strasberg addressed the central question of when a complex substructure can be regarded as structural fuzzy. He suggested that the term “structural fuzzy” only should be used when there is modal overlap of the oscillator resonances (see Strasberg *et al.*, 1996). Maidanik (2001) and Maidanik *et al.* (2006) also investigated the modal overlap and offered a criteria for replacing a sum with an integral. This criterion is important when replacing the impedance of a finite number of oscillators with that of an infinite number of oscillators.

4.5 Different local connections

As the fundamental ideas of Soize’s theory became clearer, new investigations were initiated concerning the oscillator type, spatial distribution and direction of local oscillator attachments. Rochat and Sparrow (1995) investigated the damping effect of simple oscillators on compressional and shear waves. Strasberg (1996), Garrelick (1997) and Mencik and Berry (2005) addressed the problem of modeling one or more locally attached continuous structures as fuzzy substructures. Moreover, Drexel and Ginsberg (2001) examined the damping induced in a simple cantilever beam by a finite number of spatially distributed oscillators. Also Maidanik and Becker (2003a, 2003b) studied the induced damping resulting from a multitude of oscillators having more than one degree-of-freedom.

4.6 Experimental work and fuzzy parameters

The theoretical work published on the theory of fuzzy structures is extensive. But, to the best of the author’s knowledge no real-life applications of the theory have been reported in the open literature. One of the main reasons for this is presumably the lack of straightforward methods for estimating the fuzzy parameters. One method was presented by Soize in 1998 and this was applied to a prototype complex structure and later validated by Soize and Bjaoui (2000). This method estimates the fuzzy parameters by solving a constrained optimization problem, where it is assumed that the system mean energies can be estimated with an SEA model. In other words the technique requires that the internal damping as well as the modal density of the fuzzy can be estimated from the fuzzy design. But, how to perform such estimations is not clearly specified. Moreover, Pierce

(1997) demonstrated the relationship between the distribution of resonating mass per unit natural frequency and the frequency dependent impedance matrix of the fuzzy. This method naturally infers that measurement of the fuzzy impedance matrix is feasible. Such experimental task, however, is not straightforward.

A few experimental investigations on laboratory-designed fuzzy structures are reported in the open literature. This includes Nagem (1996) who compared simulations and measurements of the vibration response of a beam with many attached oscillators. Additionally, Brennan (1997) investigated the characteristics of a wideband vibration neutralizer consisting of a mass as the master structure and centre-driven beams as neutralizers. More recently, Koc *et al.* (2005) and Carcaterra *et al.* (2005) performed experimental investigations on beams with a finite number of oscillators tuned for maximum damping effect.

5 Modeling of structural fuzzy with continuous boundary

5.1 Introduction

With the exception of the papers published by Soize (1993, 1998) and Soize and Bjaoui (2000) all the mentioned literature concerns structural fuzzy attached to the master through a local point-like boundary. However, many real-life engineering structures consist of complex substructures attached to the master through a continuous boundary. One example is the attachment of the internals of a hearing aid in the form of the processor, magnetic screen, battery, battery compartment etc. All in all these internals comprise a complex structure, which is in contact with approximately half of the inner surface area of the hearing aid shell. These components are not rigidly attached but more or less compliantly mounted between the two half-shells. Moreover, the contact between the individual components is likewise more or less compliant and not well-defined.

The method of modeling structural fuzzy with continuous boundary (see Soize, 1993) was only briefly presented 1993 and in the author's opinion this method is not easily applied to real-life problems in its present form. Paper II therefore offers a derivation of the fuzzy boundary impedance in conjunction with new physical interpretations concerning the spatial coupling. Moreover, Soize's elaborate formulation is simplified and extended, and the smoothed fuzzy boundary impedance including spatial memory is formulated from simple mathematics and without the use of probabilistic concepts.

Paper III extends Soize's method such that it allows modeling of fuzzy substructures with a two-dimensional continuous boundary. Additionally, Paper III presents a simple method for determining the so-called "equivalent coupling factor", a quantity that determines the rate of spatial coupling. The validity of this developed method is demonstrated by numerical simulations of the vibration response of a master plate structure with fuzzy attachments.

5.2 Paper II:

Vibration modeling of structural fuzzy with continuous boundary

Vibration modeling of structural fuzzy with continuous boundary

Lars Friis[a)]
Acoustic Technology, Ørsted DTU, Technical University of Denmark, Building 352, DK-2800 Kgs. Lyngby, and Widex A/S, Ny Vestergaardsvej 25, DK-3500 Vaerloese, Denmark

Mogens Ohlrich[b)]
Acoustic Technology, Ørsted DTU, Technical University of Denmark, Building 352, DK-2800 Kgs. Lyngby, Denmark

(Received 29 June 2007; revised 5 November 2007; accepted 20 November 2007)

From experiments it is well known that the vibration response of a main structure with many attached substructures often shows more damping than structural losses in the components can account for. In practice, these substructures, which are not attached in an entirely rigid manner, behave like a multitude of different sprung masses each strongly resisting any motion of the main structure (master) at their base antiresonance. The "theory of structural fuzzy" is intended for modeling such high damping. In the present article the theory of fuzzy structures is briefly outlined and a method of modeling fuzzy substructures examined. This is done by new derivations and physical interpretations are provided. Further, the method is extended and simplified by introducing a simple deterministic approach to determine the boundary impedance of the structural fuzzy. By using this new approach, the damping effect of the fuzzy with spatial memory is demonstrated by numerical simulations of a main beam structure with fuzzy attachments. It is shown that the introduction of spatial memory reduces the damping effect of the fuzzy and in certain cases the damping effect may even be eliminated completely. © *2008 Acoustical Society of America.*
[DOI: 10.1121/1.2823498]

PACS number(s): 43.40.At, 43.40.Tm [DF] Pages: 718–728

I. INTRODUCTION

It is commonly known from experiments that vibrations of a complicated system consisting of a main structure and a large number of small attached resonant substructures often appears to be more damped than the main structure's damping properties would imply. Already in 1928 Ormondroyd and Den Hartog[1] revealed that a "dynamic absorber" could produce a considerable reduction in vibration level, however, only in a relatively narrow frequency band around its natural frequency. To be effective such an auxiliary system is usually attached at the forcing point of the main structure. And the auxiliary system is predominantly a reflecting device controlled by its stiffness and mass, although its bandwidth of influence can be slightly increased by a tuning, which involves small adjustments of both stiffness and damping of the device. Therefore, the term "dynamic neutralizer" has been adopted.[2] For a more recent and detailed treatment of this subject the reader is referred to the monograph by Mead.[3] It took almost 60 years before Soize[4] and Chabas *et al.*[5] suggested that attached resonant substructures, in effect, behave like a multitude of dynamic neutralizers with different natural frequencies that introduce a high damping in the main structure over a broader frequency range.

Many complicated engineering systems consist basically of an outer shell- or a box-like *master* structure and a complicated *internal* structure. Examples of such structures varying from small to large sizes are electromechanical hearing aids, machines, aircraft, and ship hulls. The outer master structure is often well defined and its vibration can be predicted using conventional methods of vibrational analysis. In contrast, the dynamic properties of the internals may only be partly known and therefore their dynamics and influence have to be modeled by using an alternative method such as that offered by "fuzzy structure theory."[4–9] This theory is intended for an overall and simple prediction of the vibration of the master structure, and the theory considers the internal parts as a single or several independent "fuzzy substructures," which are known in some statistical sense only.

In some systems the fuzzy substructures are attached to the master through a continuous boundary or junction. This could, for example, be line-coupled machinery in a ship hull or passenger seats and luggage compartments attached to the main structure of an airplane. The continuous connection boundary implies that spatial coupling within the fuzzy has to be considered, and it is only in special cases that this coupling can be neglected.

Often the motion of the continuous junctions is varying significantly with position due to the spatial variation of vibration in the master structure, and spatial coupling forces in the fuzzy have to be accounted for. The present article addresses this problem of including spatial coupling in the modeling of structural fuzzy.

With frequency or vibration wavelength as a parameter, Fig. 1 shows three scenarios, each with three different cases

[a)]Electronic mail: lf@oersted.dtu.dk
[b)]Electronic mail: mo@oersted.dtu.dk

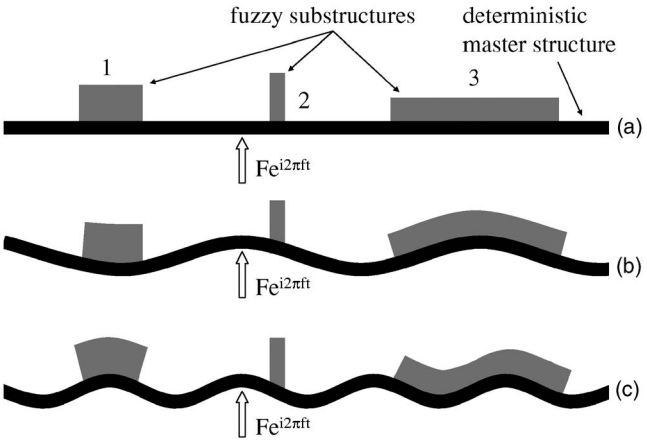

FIG. 1. Three different fuzzy substructures attached to a master structure undergoing harmonic vibration: (a) low frequency rigid body motion, (b) low frequency wave motion, and (c) mid-frequency wave motion.

of fuzzy substructures attached to a master. It is assumed that a time harmonic force of amplitude F and angular frequency $\omega=2\pi f$ excites the master and generates vibration in the whole system. At very low frequencies the master structure vibrates as a rigid body in translational motion [see Fig. 1(a)], and the junction displacement at the boundary of the fuzzy substructures is almost constant. This implies that the spatial coupling within each substructure has no significant effect on the response of the system as a whole. Now, increasing the excitation frequency introduces elastic motion in the master structure and hence at the interface with the fuzzy. When the vibration wavelength of the master becomes comparable with the dimensions of the fuzzy connection area then the spatial coupling begins to take effect. This is the case in Fig. 1(b) where the boundary displacement of substructure 3 is varying whereas those of substructures 1 and 2 are nearly constant. In Fig. 1(c) the frequency has been increased further and the boundary displacements of both substructures 1 and 3 are varying, whereas the boundary displacement of substructure 2 remains close to constant.

Fuzzy structure theory was originally developed by Soize and co-worker and presented in a series of papers[4–7] during a 10-year period starting in 1986. These papers involve probabilistic concepts in order to take the model uncertainties into account. In attempts to explain the main ideas behind the theory, these papers have been subject to numerous simplifications, interpretations, and extensions during the last 20 years.

In particular, Pierce *et al.*[8] and Strasberg and Feit[9] have introduced more simple and deterministic methods in order to predict the average responses of the master. In these methods the main parameter describing the fuzzy is taken to be the distribution of resonating mass per unit frequency. One of the crucial steps in applying fuzzy structure theory is the very estimation of this mass distribution. Both Soize[10,11] and Pierce[12] have addressed this problem throughout the last 10 years.

In 1993 Soize briefly presented a method[6] for including spatial memory in the modeling of structural fuzzy with continuous boundaries. Despite this, elaborating literature has so far mainly been concerned with structural fuzzy *without* spatial coupling effects. However, in order to utilize Soize's innovative theory on structural fuzzy with spatial memory, there is a strong need for a detailed examination of the suggested method in addition to a presentation of necessary supplementary derivations. Moreover, a simple method for implementing the structural fuzzy is still absent in the open literature. The objective of the present article is to extend Soize's theory by using a simplifying approach, which to some extent is based on the methods introduced by Pierce. *et al.*,[8] and Strasberg and Feit.[9] The outline of the present article is as follows. Succeeding a brief outline of the theory of fuzzy structures in Sec. II, the method of including spatial memory is discussed in details and extended in Sec. III; this includes (i) derivation of the boundary impedance of Soize's spatial oscillator, (ii) derivation of the boundary impedance of an infinite number of *identical* spatial oscillators evenly distributed on the fuzzy connection area, and (iii) introduction to Soize's local *equivalent oscillator* and *equivalent coupling factor* and a presentation of new physical interpretations. Further, in Sec. IV we present a new approach for determining the boundary impedance of structural fuzzy with spatial memory. Finally, numerical simulations based on this approach are presented in Sec. V in order to illustrate the damping effects of structural fuzzy, which includes spatial memory.

II. STRUCTURAL FUZZY WITHOUT SPATIAL MEMORY

The purpose of the fuzzy structure theory is to model the overall vibrational response of a master structure, which has an attachment of one or more *resonant* substructures. A fuzzy substructure is considered as being composed of many simple oscillators resonating at different frequencies and being attached to the master at their base. When modeling such a system it is an advantage to separate the fuzzy from its master. Each fuzzy substructure is conveniently represented in terms of its *boundary impedance*.[4,5] Using this approach the modeling of the response of the master with fuzzy attachments can be achieved without exceeding the number of degrees of freedom required for predicting the response of the master structure itself. As mentioned previously, one can neglect the spatial coupling effects in the fuzzy when a fuzzy substructure of multiple resonators is connected to the master over a small length or over a small area of virtually constant motion.

This is illustrated in Fig. 2 showing a fuzzy substructure, which is modeled by N simple oscillators that is attached locally at an area A of the master structure. An expression for the total *boundary* impedance $\underline{z}_{\text{fuzzy}}(f)$ of this substructure can be derived by superposition and by assuming, say, that the nth simple oscillator of the fuzzy is defined by the mass M_n, the undamped resonance frequency $f_{r,n}$ and the loss factor η. By introducing the complex stiffness of the oscillator $\underline{s}_n=s_n(1+i\eta)$, where $s_n=(2\pi f_{r,n})^2 M_n$ is the impedance of the oscillator $\underline{Z}_n=\underline{F}_n/\underline{v}_n$ at the attachment base yields[9]

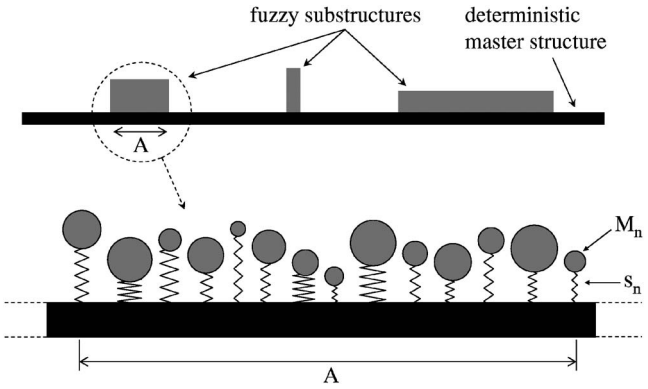

FIG. 2. Master structure exemplifying an attached fuzzy substructure, which is composed of N simple oscillators resonating at different frequencies and without spatial memory.

$$\underline{Z}_n = \frac{\underline{s}_n}{i\omega}\left(1 - \frac{\underline{s}_n}{\underline{s}_n - \omega^2 M_n}\right) = -i2\pi f\left(\frac{f_{r,n}^2}{f^2}\right)(1+i\eta) \times M_n\left(1 - \frac{f_{r,n}^2(1+i\eta)}{f_{r,n}^2(1+i\eta) - f^2}\right). \quad (1)$$

Figure 3 shows the frequency variation of this oscillator impedance in a normalized form for different values of spring damping η. Below and above its resonance frequency the oscillator is, respectively, mass controlled and spring controlled. Further, at resonance of the oscillator, where the impedance is very large and almost purely real, it will strongly oppose any movements of its base. It is this particular feature of the oscillator, which results in the damping effect of the fuzzy substructure.

Generally, the different oscillators of a fuzzy substructure have different masses and natural frequencies and they are attached randomly to the master structure within the considered fuzzy connection area. Also, the total mass of all the oscillators equals the mass of the fuzzy substructure M_{fuzzy} $= \Sigma_{n=1}^{N} M_n$. Below a certain frequency, say $f_{r,\text{lower}}$, the oscillators will all be mass controlled. By increasing the frequency gradually from $f_{r,\text{lower}}$ to an upper limit, say $f_{r,\text{upper}}$, the oscillators will resonate one by one. Now, at each frequency within this "resonant" frequency band $f_{r,\text{lower}} \leqslant f_r \leqslant f_{r,\text{upper}}$ at least one oscillator will be close to its base antiresonance and it will therefore oppose the motion of the master. If the oscillators are attached close to one another within the area A, which has a nearly constant displacement, then the effective boundary impedance of all the oscillators, $\underline{z}_{\text{fuzzy}}(f)$, can be approximated by the sum of each oscillator's impedance $\underline{Z}_n(f)$ divided by the attachment area A:

$$\underline{z}_{\text{fuzzy}}(f) = \frac{1}{A}\sum_{n=1}^{N}\underline{Z}_n(f) = -\frac{i2\pi f}{A}\sum_{n=1}^{N}\left(\frac{f_{r,n}^2}{f^2}\right)(1+i\eta) \times M_n\left(1 - \frac{f_{r,n}^2(1+i\eta)}{f_{r,n}^2(1+i\eta) - f^2}\right). \quad (2)$$

This boundary impedance, however, requires specific knowledge about the properties of each oscillator and it is therefore conveniently replaced by an asymptotic and smoothed version.[8,9] This is obtained by considering infinitely many oscillators resonating within the frequency band of $f_{r,\text{lower}} \leqslant f_r \leqslant f_{r,\text{upper}}$ and having a total mass M_{fuzzy}. This smoothed impedance yields[8,9]

$$\underline{z}_{\text{fuzzy}}(f) = -\frac{i2\pi f}{A}\int_{f_{r,\text{lower}}}^{f_{r,\text{upper}}}\left(\frac{f_r^2}{f^2}\right)(1+i\eta) \times m_{\text{fuzzy}}(f_r)\left(1 - \frac{f_r^2(1+i\eta)}{f_r^2(1+i\eta) - f^2}\right)df_r, \quad (3)$$

where the quantity $m_{\text{fuzzy}}(f_r)df_r$ represents the mass resonating between the frequencies f_r and $f_r + df_r$; this means that the total mass of the fuzzy substructure now is expressed as

$$M_{\text{fuzzy}} = \int_{f_{r,\text{lower}}}^{f_{r,\text{upper}}} m_{\text{fuzzy}}(f_r)df_r. \quad (4)$$

The damping effect of the fuzzy substructure is mainly governed by this frequency dependent resonating mass distribution $m_{\text{fuzzy}}(f_r)$.[8,9] Methods for finding this parameter were suggested by Soize[10,11] and Pierce,[12] and different prototype mass distributions were proposed by Pierce *et al.*[8] and Strasberg and Feit.[9]

As an example of the damping effect of structural fuzzy Fig. 4 shows computed results for the velocity vibration response per unit harmonic force, $\underline{Y} = \underline{v}/\underline{F}$, of a flexurally vibrating master beam, free in space, both without and with an attached substructure represented by 16 different simple oscillators. The resonance frequencies of these oscillators are spaced in geometric progression from 500 to 5000 Hz. Further, the oscillators have identical point masses, weighting in total 10% of the master beam and a spring loss factor of $\eta = 0.05$. It is clearly observed that the attached substructure has a strong effect on the master response; this is seen to be reduced considerable over a broad band of frequencies and by up to 18 dB around 1300 Hz. Further, it is seen that this substructure can be modeled successfully as a smoothed structural fuzzy by using the expression in Eq. (3). An ap-

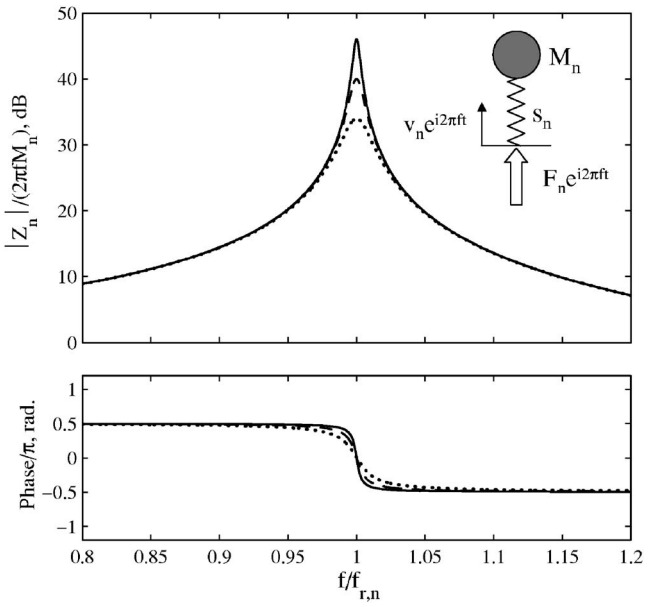

FIG. 3. Frequency variation of normalized impedance, $\underline{Z}_n/(2\pi f M_n)$ for different values of spring damping η: —, 0.005; ---, 0.01; ···, 0.02.

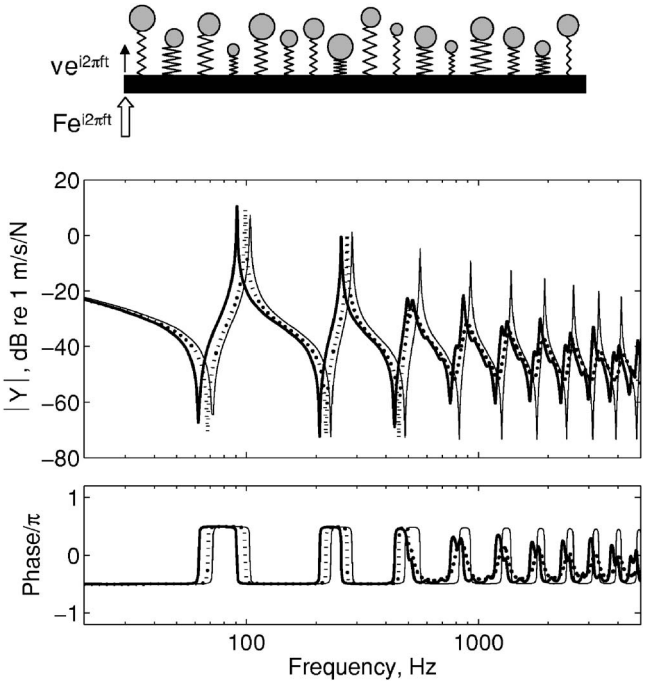

FIG. 4. Vibration velocity response per unit harmonic force, $\underline{Y}=\underline{v}/\underline{F}$, of a master beam free in space. Beam: —, without structural fuzzy; ⋯, with an attached fuzzy substructure represented by 16 simple oscillators, —; with a smoothed layer of structural fuzzy without spatial memory.

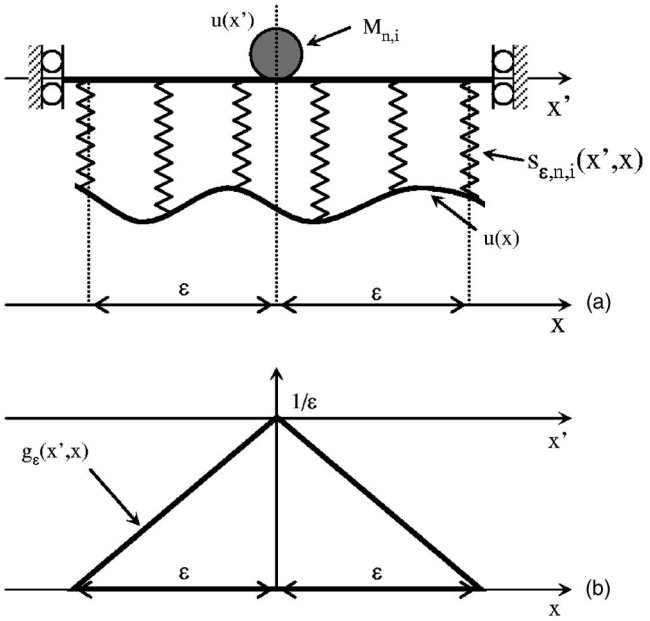

FIG. 5. Fuzzy oscillator with spatial coupling. (a) Oscillator attached to a boundary of motion $\underline{u}(x)$ and (b) stiffness density distribution $g_\varepsilon(x',x)$ of the oscillator spring elements.

proximate condition for using this expression is suggested in Ref. 9 as $\eta > 2\Delta f_{r,n}/f_{r,n}$ where $\Delta f_{r,n}$ is the spacing between adjacent resonance frequencies. In other words this very strict condition requires that $\Delta f_{r,n} < \Delta f_{3\ \mathrm{dB}}/2$ where $\Delta f_{3\ \mathrm{dB}}$ denotes the 3 dB bandwidth of the oscillator at resonance. However, in the present example it applies that the spacing between resonances is $\Delta f_{r,n} \approx 65 \cdot \Delta f_{r,n,3\ \mathrm{dB}}/2$ around 2000 Hz, that is, 65 wider than the suggested requirement. It is therefore evident that acceptable results can be obtained with a much relaxed condition.

III. SOIZE'S STRUCTURAL FUZZY WITH SPATIAL MEMORY

A. Soize's spatial oscillator

Consider a fuzzy substructure connected to the master through a continuous boundary. A fuzzy substructure is generally attached to the master within an area, but for the sake of simplicity we shall here consider a fuzzy attached to the master through a one-dimensional boundary of length L_{fuzzy}. Soize incorporates a spatial memory in the structural fuzzy by introducing a "spatial oscillator" as sketched in Fig. 5(a). A structural fuzzy with spatial memory is composed of N *different sets* ($n \in [1,N]$) of such spatial oscillators. Each of these N sets consists of infinitely many *identical* spatial oscillators spread on the fuzzy connection area—or length. Let us first consider only one spatial oscillator, say the ith ($i \in [1,\infty]$) of the nth set of spatial oscillators of a fuzzy substructure, see Fig. 5(a). This oscillator is defined by the resonance frequency $f_{r,n}$, the lossfactor η and the point mass $M_{n,i}$ located at position x'. Further, the point mass is assumed supported by spring elements of stiffness density $\underline{s}_{\varepsilon,n,i}(x',x)$ that are attached to the master structure at different positions $x \in [x'-\varepsilon, x'+\varepsilon]$. Moreover, the spatial variation of the vibration displacement of the master is shown as $u(x)$ in Fig. 5(a). The actual width 2ε of the distributed springs Soize denotes "the spatial memory" and the stiffness density he defines as[6]

$$\underline{s}_{\varepsilon,n,i}(x',x) = \underline{s}_{n,i} g_\varepsilon(x',x) = (M_{n,i}\omega_{r,n}^2)(1+i\eta) g_\varepsilon(x',x). \quad (5)$$

Here, $\underline{s}_{n,i}$ is the total complex stiffness of the ith oscillator belonging to the nth set, and the quantity $g_\varepsilon(x',x)$ is an even and positive-valued function of area 1. As a one-dimensional spatial memory Soize suggests a simple triangular distribution function $g_\varepsilon(x',x)$ as shown in Fig. 5(b). This is determined as

$$g_\varepsilon(x',x) = \frac{\varepsilon - |x'-x|}{\varepsilon^2} 1_{[x'-\varepsilon,x'+\varepsilon]} \quad (6)$$

where $1_{[x'-\varepsilon,x'+\varepsilon]}$ is a function, which is equal to 1 for $x \in [x'-\varepsilon, x'+\varepsilon]$ and which is 0 elsewhere. As the area under the curve $g_\varepsilon(x',x)$ is 1, the oscillator in Fig. 5(a) has the same natural frequency $f_{r,n}$ as the simple oscillator with mass M_n and stiffness s_n that was considered in Sec. II. From the expression in Eq. (6) it is seen that the distribution $g_\varepsilon(x',x)$ only is dependent on the difference $x'-x$ and therefore it can be written as

$$g_\varepsilon(x'-x) = \frac{\varepsilon - |x'-x|}{\varepsilon^2} 1_{[x'-\varepsilon,x'+\varepsilon]} \quad (7)$$

where it applies that $g_\varepsilon(x'-x) = g_\varepsilon(x-x')$ and further that $\underline{s}_{\varepsilon,n,i}(x'-x) = \underline{s}_{\varepsilon,n,i}(x-x')$.

B. The *n*th set of spatial oscillators

Next, consider the infinitely many identical oscillators belonging to the nth set. Let us assume that the oscillators

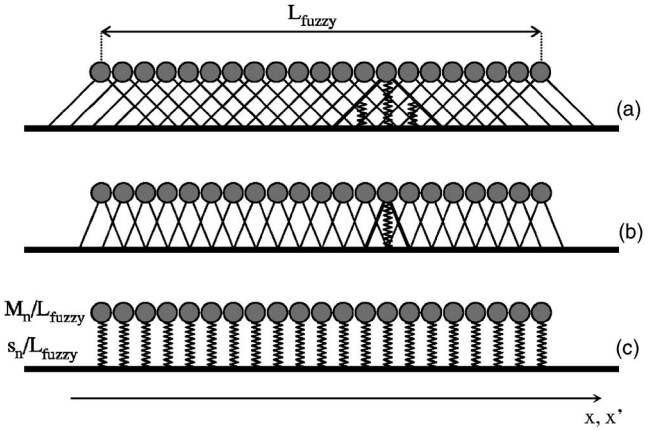

FIG. 6. Structural fuzzy attached to the master; fuzzy with: (a) high spatial memory, (b) small spatial memory, and (c) no spatial memory.

are distributed evenly over the fuzzy boundary, so that each location x' is associated with a point mass $M_{n,i}$. This is illustrated in Fig. 6 where each one of the oscillators representing the one sketched in Fig. 5(a) is depicted as a point mass and the associated triangular stiffness distribution. The point masses can vibrate independently whereas the spring elements overlap spatially at the connection boundary.

These infinitely many *identical* oscillators constitute the nth contribution to the total boundary impedance of the homogeneous fuzzy substructure. The total mass and total stiffness of all the oscillators of the nth set are given as M_n and $\underline{s}_n$, respectively, so that $M_{n,i}=M_n/L_{\text{fuzzy}}$ and $\underline{s}_{n,i}=\underline{s}_n/L_{\text{fuzzy}}$. Figure 6(a) illustrates the case of spatial oscillators with a large width—or a high spatial memory—beacuse the spring elements from the individual oscillators overlap significantly. On the other hand, in Fig. 6(b) the spring elements overlap less because ε is somewhat smaller. Finally, in Fig. 6(c) the spatial memory approaches zero as $\varepsilon \to 0$, and the spatial stiffness density approaches the stiffness of simple discrete springs.

C. Derivation of the boundary impedance of the *n*th set of oscillators

The vibration of the master results in a force at the interface between master and attached fuzzy; this action on the fuzzy we denote the contact force. Now, from the vibration velocity $\underline{v}(x)$ along the fuzzy connection boundary one can express the total contact force $\underline{F}'_{\varepsilon,n}(x_0)$ per unit length at x_0 due to the nth set of oscillators as[6]

$$\underline{F}'_{\varepsilon,n}(x_0) = \int_{L_{\text{fuzzy}}} \underline{z}_{\varepsilon,n}(x_0 - x)\underline{v}(x)dx, \tag{8}$$

where $\underline{z}_{\varepsilon,n}(x_0-x)$ is the boundary impedance associated with the nth set of oscillators. This impedance depends only on the difference (x_0-x), so that $\underline{z}_{\varepsilon,n}(x_0-x)=\underline{z}_{\varepsilon,n}(x-x_0)$ in analogy to the stiffness distribution function in Eq. (7). Although an expression for $\underline{z}_{\varepsilon,n}(x_0-x)$ is shown in Ref. 3, it has not been derived in the open literature. The authors believe that such a derivation is essential in order to appreciate and understand the characteristics of a fuzzy with spatial memory. It is also anticipated that such a derivation will ease the usability of Soize's theory considerably. In view of this, a step by step derivation of $\underline{F}'_{\varepsilon,n}(x_0)$ will be presented in what follows.

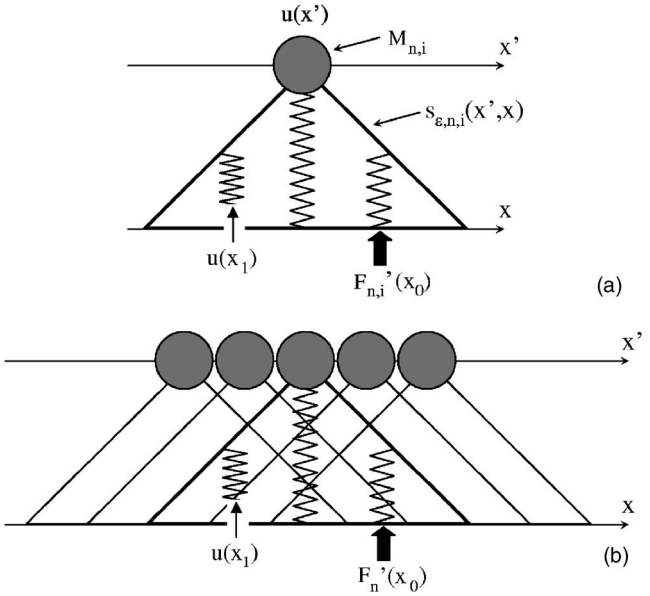

FIG. 7. Derivation of the nth contribution to the fuzzy boundary impedance. (a) Boundary impedance $\underline{z}_{\varepsilon,n,i}(x_0-x_1)$ of the ith oscillator of the nth set of spatial oscillators. (b) Boundary impedance $\underline{z}_{\varepsilon,n}(x_0-x_1)$ of the nth set of spatial oscillators.

Once again, only one spatial oscillator is considered, say, the ith of the nth set of oscillators. This oscillator is sketched in Fig. 7(a). For this particular oscillator we first seek an expression for the boundary impedance $\underline{z}_{\varepsilon,n,i}(x_0-x_1)$ with a spatial contribution over the differential length dx is defined as

$$\underline{F}'_{n,i}(x_0) = \underline{z}_{\varepsilon,n,i}(x_0 - x_1)\underline{v}(x_1)dx|_{\underline{v}(x\notin[x_1,x_1+dx])=0}, \tag{9}$$

where $\underline{F}'_{n,i}(x_0)$ is the force per unit length that excites the connection boundary at x_0 and $\underline{v}(x_1)=i\omega\underline{u}(x_1)$ is the base velocity of the spring element at x_1. Now, the spring element at x_1 is given a displacement $\underline{u}(x_1)$ at its base, whereas all other springs elements are locked such that $\underline{u}(x\neq x_1)=0$, see Fig. 7(a). As the mass $M_{n,i}$ undergoes a displacement $\underline{u}(x')$ the induced spring force $\underline{F}_{S,n,i}(x_1)$ in a differential neighborhood dx around x_1 becomes

$$\underline{F}_{S,n,i}(x_1) = \underline{s}_{\varepsilon,n,i}(x' - x_1)(\underline{u}(x_1) - \underline{u}(x'))dx. \tag{10}$$

Due to the motion of the mass, a reaction force $\underline{F}_{M,n,i}(x')$ influences the spring element and this force is given as

$$\underline{F}_{M,n,i}(x') = -\omega^2 M_{n,i}\underline{u}(x'). \tag{11}$$

Additionally, the motion of the mass also introduces forces in the remaining spring elements, and their total spring force $\underline{F}_{S,n,i}(x\neq x_1)$ can be found as

$$\underline{F}_{S,n,i}(x \neq x_1) = -\underline{s}_{\varepsilon,n,i}(x' - x_1)\underline{u}(x')dx + \int_{L_{\text{fuzzy}}} \underline{s}_{\varepsilon,n,i}(x' - x)\underline{u}(x')dx = -\underline{s}_{\varepsilon,n,i}(x' - x_1)\underline{u}(x')dx + \underline{s}_{n,i}, \tag{12}$$

where $\underline{s}_{n,i}$ is the total stiffness of the spring elements of the oscillator. Because of force equilibrium the sum of the spring

force $\underline{F}_{S,n,i}(x \neq x_1)$ and the reaction force of the mass $\underline{F}_{M,n,i}(x')$ is equal to the spring force $\underline{F}_{S,n,i}(x_1)$ at x_1. Thus, by combination of Eqs. (10)–(12) we get

$$\underline{F}_{S,n,i}(x_1) = \underline{F}_{M,n,i}(x') + \underline{F}_{S,n,i}(x \neq x_1),$$

$$\underline{s}_{\varepsilon,n,i}(x' - x_1)(\underline{u}(x_1) - \underline{u}(x'))dx = (-\underline{s}_{\varepsilon,n,i}(x' - x_1)dx + \underline{s}_{n,i} - \omega^2 M_{n,i})\underline{u}(x'), \tag{13}$$

Rearranging Eq. (13) we find an expression for $\underline{u}(x')$ as a function of $\underline{u}(x_1)$, which yields

$$\underline{u}(x') = \frac{\underline{s}_{\varepsilon,n,i}(x' - x_1)\underline{u}(x_1)dx}{-\omega^2 M_{n,i} + \underline{s}_{n,i}}. \tag{14}$$

Further, the force per unit length $\underline{F}'_{n,i}(x_0)$ at x_0 at the connection boundary is given as

$$\underline{F}'_{n,i}(x_0) = \underline{s}_{\varepsilon,n,i}(x' - x_0)(\underline{u}(x_0)\delta_{x_0,x_1} - \underline{u}(x')), \tag{15}$$

where δ_{x_0,x_1} is the Kronecker delta, that is, $\delta_{x_0,x_1}=1$ when $x_0=x_1$, and otherwise zero. Finally, if Eq. (14) is substituted in Eq. (15) we get the force per unit length $\underline{F}'_{n,i}(x_0)$ exerted onto the fuzzy connection boundary due to its displacement $\underline{u}(x_1)$:

$$\underline{F}'_{n,i}(x_0) = \underline{s}_{\varepsilon,n,i}(x' - x_0)\left(\delta_{x_0,x_1}\underline{u}(x_0) - \frac{\underline{s}_{\varepsilon,n,i}(x' - x_1)\underline{u}(x_1)dx}{-\omega^2 M_{n,i} + \underline{s}_{n,i}}\right) = \underline{s}_{\varepsilon,n,i}(x' - x_0)\left(\delta_{x_0,x_1} - \frac{\underline{s}_{\varepsilon,n,i}(x' - x_1)dx}{-\omega^2 M_{n,i} + \underline{s}_{n,i}}\right)\underline{u}(x_1). \tag{16}$$

According to Eq. (16) $\underline{z}_{\varepsilon,n,i}(x_0 - x_1)dx$ reads

$$\underline{z}_{\varepsilon,n,i}(x_0 - x_1)dx = \frac{\underline{s}_{\varepsilon,n,i}(x' - x_0)}{i2\pi f}\left(\delta_{x_0,x_1} - \frac{\underline{s}_{\varepsilon,n,i}(x' - x_1)dx}{-\omega^2 M_{n,i} + \underline{s}_{n,i}}\right). \tag{17}$$

Now, this is only the impedance of the ith oscillator of the nth set. Assume again that there is an infinite number of *identical* oscillators overlapping one another on the fuzzy connection boundary [see Fig. 7(b)], such that a mass element $M_{n,i}$ is located at each of all positions along the x' axis. Further, each of these oscillators has a total stiffness $\underline{s}_{n,i}$. We now seek an expression for the impedance $\underline{z}_{\varepsilon,n}(x_0 - x_1)$ of the nth set of oscillators. First the oscillators are given the displacement $\underline{u}(x_1)$ at position x_1, whereas all other positions at their spring bases are locked. Then the total force per unit length $\underline{F}'_n(x_0)$ at x_0 is found by integrating the expression in Eq. (16) with respect to x', and this gives

$$\begin{aligned}
\underline{F}'_n(x_0) &= \int_{L_{\text{fuzzy}}} \underline{s}_{\varepsilon,n,i}(x' - x_0)\left(\delta_{x_0,x_1} - \frac{\underline{s}_{\varepsilon,n,i}(x' - x_1)dx}{-\omega^2 M_{n,i} + \underline{s}_{n,i}}\right)\underline{u}(x_1)dx' \\
&= \left(\int_{L_{\text{fuzzy}}} \underline{s}_{\varepsilon,n,i}(x' - x_0)\delta_{x_0,x_1}dx' - \int_{L_{\text{fuzzy}}} \frac{\underline{s}_{\varepsilon,n,i}(x' - x_0)\underline{s}_{\varepsilon,n,i}(x' - x_1)dx}{-\omega^2 M_{n,i} + \underline{s}_{n,i}}\right)\underline{u}(x_1) \\
&= \left(\underline{s}_{n,i}\delta_{x_0,x_1} - \int_{L_{\text{fuzzy}}} \frac{\underline{s}_{n,i}^2 g(x' - x)g(x' - x_0)dx}{-\omega^2 M_{n,i} + \underline{s}_{n,i}}dx'\right)\underline{u}(x_1) \\
&= \left(\underline{s}_{n,i}\delta_{x_0,x_1} - \frac{\underline{s}_{n,i}^2 dx}{-\omega^2 M_{n,i} + \underline{s}_{n,i}}\int_{L_{\text{fuzzy}}} g(x' - x_1)g(x' - x_0)dx'\right)\underline{u}(x_1).
\end{aligned} \tag{18}$$

The integration in the last line of Eq. (18) can be recognized as the convolution product $(g*g)(x_0-x_1)$ and the expression can therefore be simplified to

$$\underline{F}'_n(x_0) = \underline{s}_{n,i}\left(\delta_{x_0,x_1} - \frac{\underline{s}_{n,i}}{-\omega^2 M_{n,i} + \underline{s}_{n,i}}(g * g)(x_0 - x_1)dx\right)\underline{u}(x_1). \tag{19}$$

Finally, by substituting $\underline{s}_{n,i}=\omega_n^2 M_{n,i}(1+i\eta)$ and $\underline{v}(x)=i2\pi f\underline{u}(x)$ in Eq. (19) we have that

$$\underline{F}'_n(x_0) = -i2\pi f\left(\frac{f_{r,n}^2}{f^2}\right)(1 + i\eta)M_{n,i}\left(\delta_{x_0,x_1} - \frac{f_{r,n}^2(1 + i\eta)}{f_{r,n}^2(1 + i\eta) - f^2}(g * g)(x_0 - x_1)dx\right)\underline{v}(x_1). \tag{20}$$

Hence, the total impedance $\underline{z}_{\varepsilon,n}(x_0-x_1)$ of the nth set of oscillators reads

$$\underline{z}_{\varepsilon,n}(x_0 - x_1)dx = -i2\pi f\left(\frac{f_{r,n}^2}{f^2}\right)(1 + i\eta)M_{n,i}\left(\delta_{x_0,x_1} - \frac{f_{r,n}^2(1 + i\eta)}{f_{r,n}^2(1 + i\eta) - f^2}(g * g)(x_0 - x_1)dx\right). \tag{21}$$

A structural fuzzy composed of N sets of infinitely many identical oscillators as described earlier is homogenous, as the boundary impedance only depends on the distance $|x_0-x_1|$. Further, if $\varepsilon \to 0$, then Eq. (21) reduces to the boundary impedance of infinitely many identical simple oscillators as illustrated in Fig. 6(c). Examining the expression in Eq. (21), it is seen that the transfer impedances are proportional to the convolution product $(g*g)(x_0-x_1)$, as the term δ_{x_0,x_1} is zero when $x_0 \neq x$. Figure 8 shows this convolution and it is seen that the transfer impedances extends a distance of 2ε to each side of x. This means that the actual spatial memory is 4ε, and that the transfer impedances are zero for $|x_0-x| \geqslant 2\varepsilon$. Note that the areas below $g(x_0-x)$ and $(g^*g)(x_0-x_1)$ are both equal to 1.

D. Soize's local equivalent oscillator

A numerical implementation of the boundary impedance $\underline{z}_{\varepsilon,n}$ in Eq. (21) is unfortunately rather complicated due to its *nonlocal* nature. This requires for instance the use of a finite

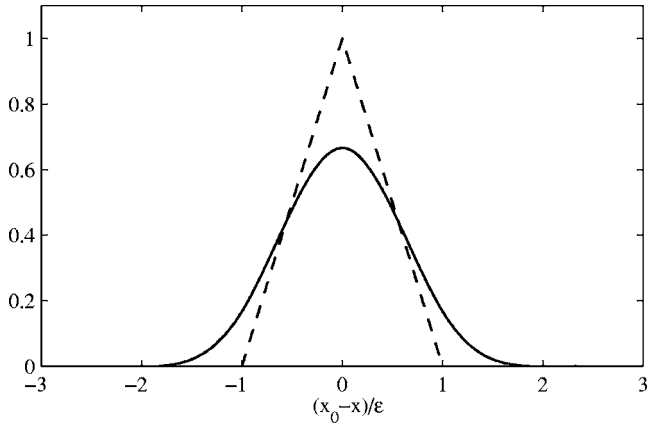

FIG. 8. Examination of the magnitude distribution of the transfer impedance. Functions: ---, $g(x_0-x)/(1/\varepsilon)$; —, $(g^* g)(x_0-x)/(1/\varepsilon)$.

element model with special fuzzy elements. As mentioned earlier, the main purpose of the fuzzy structure theory is to serve as a simple modeling tool. Therefore, Soize introduced the *equivalent local* oscillator. The idea is that the nth set of infinitely many identical equivalent oscillators, can replace the nth set of spatial oscillators. This also implies that the contact force per unit length $\underline{F}'_{\text{equ},n}(x_0)$ introduced by the local equivalent oscillator at x_0 must be equal to the contact force $\underline{F}'_{\varepsilon,n}(x_0)$ given in Eq. (8). This is achieved by introducing the so-called *equivalent coupling factor* α, which transforms all the nonlocal force contributions of the spatial oscillators into equivalent local contributions. As one can imagine, α generally varies with frequency and is both dependent on the length of the spatial memory 2ε and the motion of the master $u(x)$.

Now, let us assume that the nth set of equivalent oscillators consist of an infinite number of *identical* oscillators distributed on the fuzzy connection boundary. Further, each equivalent oscillator has a mass $M_{n,i}$, and masses are located at all positions along the x' axis. For the nth set of equivalent oscillators the boundary impedance $\underline{z}_{\text{equ},n}(x_0)=\underline{F}'_n(x_0)/\underline{v}(x_0)$ is given as[6]

$$\underline{z}_{\text{equ},n}(x_0)=\frac{\underline{s}_{n,i}}{i\omega}\left(1-\frac{\underline{s}_{n,i}}{\underline{s}_{n,i}-\omega^2 M_{n,i}}\alpha\right)=i2\pi f M_{n,i}\times\left(\frac{f_r^2(1+i\eta)(1-(f_r/f)^2(1+i\eta)(1-\alpha))}{f^2-f_r^2(1+i\eta)}\right), \tag{22}$$

where $\alpha\in]0,1]$. If α is chosen properly then the boundary impedance $\underline{z}_{\text{equ},n}(x_0)$ in Eq. (22) can replace successfully the boundary impedance $\underline{z}_{\varepsilon,n}(x_0-x_1)$ of the nth set of spatial oscillators[6] as was given in Eq. (21). The frequency variation of this equivalent impedance $\underline{z}_{\text{equ},n}(x_0)$ is shown in Fig. 9 for different values of α. As indicated in Fig. 9, we now suggest that the equivalent oscillator can be interpreted as a simple oscillator with spring stiffness $\underline{s}_1$ where the mass has been grounded by a second spring with stiffness $\underline{s}_2$. It applies that $\underline{s}_{n,i}=\underline{s}_1+\underline{s}_2$ and the mass of the grounded oscillator is $M_{n,i}$. The relationship between the impedance in Eq. (22) and the impedance of the grounded oscillator $z_{\text{ground},n}$ in Fig. 9 is $\underline{z}_{\text{equ},n}=\underline{z}_{\text{ground},n}/\alpha$ where $\alpha=\underline{s}_1/(\underline{s}_1+\underline{s}_2)$. Note that $\alpha\to 1$ when $\underline{s}_2\to 0$ and $\underline{z}_{\text{equ},n}$ will then approach the impedance of a simple oscillator, Eq. (1). Also, when $\alpha\neq 1$ the oscillator is stiffness controlled at low frequencies. It should be mentioned that the impedance of a set of spatial oscillators results in a stiffness-controlled behaviour of the master at low frequencies. The reason is that the mass-less bar supporting the point mass in Fig. 5(a) is restricted to translational motion and therefore unable to rotate. Any rotation of the master at low frequencies is therefore restricted by the springs.

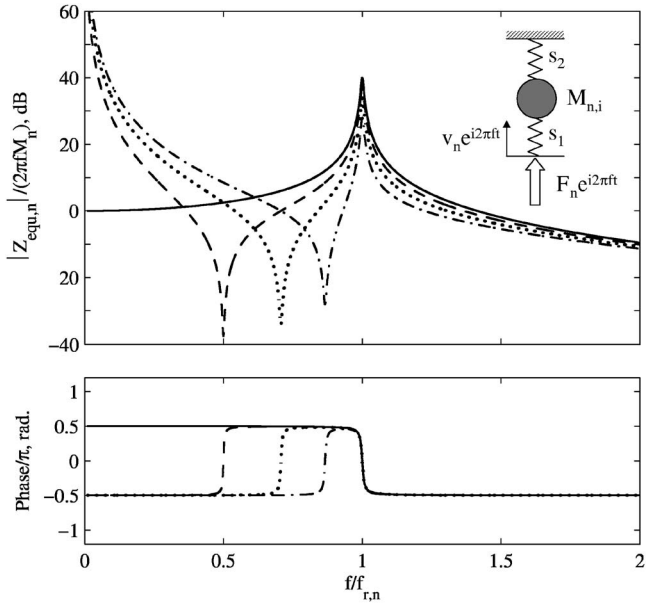

FIG. 9. Frequency variation of normalized impedance, $Z_{\text{equ},n}/(2\pi f M_n)$ for different values of the equivalent coupling factor α: —, 1; ---, 0.75; ···, 0.5; -·-, 0.25.

E. The equivalent coupling factor

Soize states that it is not self-evident that the local *equivalent oscillator* can model correctly a structural fuzzy with spatial memory.[6] And as one can imagine, α has to be chosen carefully. Finding a relationship between ε and α requires matching of boundary forces using the impedances found in Eqs. (21) and (22), frequency by frequency. Such results have been published by Soize[6] and they show α as a function of the spatial memory 2ε for different frequency bands for a simply supported beam. The authors of the present article, however, suggest that α should be determined in a more general way as a function of the ratio ε/λ where λ is the free wavelength in the master, which here is restricted to undergo one-dimensional wave motion only. By transforming Soize's data, it is revealed that a unique relationship between α and ε/λ is found. The transformed data of α as a function of ε/λ are shown in Fig. 10; these results have been fitted with a fourth-order polynomial. It should be noted that the free wavelength is defined only for sinusoidal variations, and for structures with more complicated eigenfunctions, we therefore suggest substituting λ with twice the distance between adjacent nodes.

Finally, it should be mentioned that a general and simple method of predicting α has been the subject of the authors'

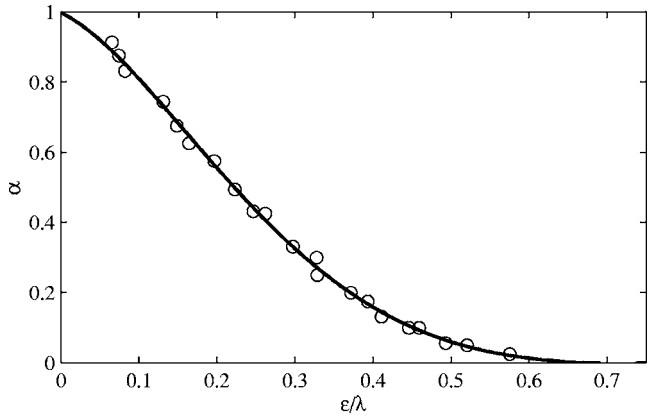

FIG. 10. Variation of the equivalent coupling factor α with ε/λ:(○), data computed from read-off results in Ref. 6; —, polynomial fit.

latest work and will shortly be submitted for publication together with a practical validation of the associated equivalent modelling method.

IV. SMOOTHED EXPRESSION FOR THE BOUNDARY IMPEDANCE OF STRUCTURAL FUZZY WITH SPATIAL MEMORY

The fuzzy structure theory developed by Soize was originally intended for finite element modeling. To determine the damping induced in the master, Soize developed his own methods based on probabilistic concepts in order to account for model uncertainties. A new proposition for a simplified deterministic method for predicting the mean damping induced by structural fuzzy with spatial memory is presented in the following. The purpose of this model is to illustrate the main effects of including spatial memory in the modeling of structural fuzzy.

As a starting point we consider a structural fuzzy consisting of N sets of spatial oscillators with different natural frequencies. The total boundary impedance of the structural fuzzy can be determined as the sum of the impedance contributions from these N sets for which the impedance of the nth set, $n \in [1,N]$, was presented in Eq. (21). The total boundary impedance $\underline{z}_{\text{fuzzy},\varepsilon}(x_0-x_1)$ thus becomes

$$\underline{z}_{\text{fuzzy},\varepsilon}(x_0-x_1) = \sum_{n=1}^{N} \underline{z}_{\varepsilon,n}(x_0-x_1). \tag{23}$$

So far, only Soize has presented a method of predicting the boundary impedance of fuzzy with spatial memory.[6] Now, applying the same approach as in Sec. II a *deterministic* expression for the boundary impedance of the structural fuzzy with spatial memory can be found. Let us approximate the expression in Eq. (23) by infinitely many sets of spatial oscillators resonating between $f_{r,\text{lower}}$ and $f_{r,\text{upper}}$. Hereby the general expression for the total fuzzy boundary impedance attached at area A of the master becomes

$$\underline{z}_{\text{fuzzy},\varepsilon}(x_0-x_1) = \int_{f_{r,\text{lower}}}^{f_{r,\text{upper}}} z_{\varepsilon}(x_0-x_1,f_r)df_r, \tag{24a}$$

or, by inserting the expression from Eq. (21) we get

$$\begin{aligned}\underline{z}_{\text{fuzzy},\varepsilon}(x_0-x_1)dx = &-\frac{i2\pi f}{A}\int_{f_{r,\text{lower}}}^{f_{r,\text{upper}}}\left(\frac{f_r^2}{f^2}\right)(1+i\eta)m_{\text{fuzzy}}(f_r)\\ &\times\left(\delta_{x_0,x_1}-\frac{f_r^2(1+i\eta)}{f_r^2(1+i\eta)-f^2}\right.\\ &\left.\times(g*g)(x_0-x_1)dx\right)df_r,\end{aligned} \tag{24b}$$

where $m_{\text{fuzzy}}(f_r)df_r$ again represents the total mass of the fuzzy resonating between the frequencies f_r and f_r+df_r. Moreover, the same simple approach can be applied to find the equivalent boundary impedance $\underline{z}_{\text{fuzzy,equ}}(x_0)$ if M_n is replaced by $m_{\text{fuzzy}}(f_r)df_r$. A smoothed version of the equivalent boundary impedance then yields

$$\begin{aligned}\underline{z}_{\text{fuzzy,equ}}(x_0-x_1) &= \int_{f_{r,\text{lower}}}^{f_{r,\text{upper}}} z_{\text{equ}}(x_0,f_r)df_r\\ &= -\frac{i2\pi f}{A}\int_{f_{r,\text{lower}}}^{f_{r,\text{upper}}}\left(\frac{f_r^2}{f^2}\right)(1+i\eta)m_{\text{fuzzy}}(f_r)\\ &\quad\times\left(1-\frac{f_r^2(1+i\eta)}{f_r^2(1+i\eta)-f^2}\alpha\right)df_r.\end{aligned} \tag{25}$$

It should be noted that the equivalent coupling factor α generally is a function of frequency. Nevertheless, according to Fig. 10 it is seen that α is constant for a specific value of ε/λ. With the new expression for the boundary impedance of structural fuzzy with spatial memory in Eq. (25) it is therefore possible to model and examine the effects of structural fuzzy with spatial memory in a simple way. For simple cases of mass distributions $m_{\text{fuzzy}}(f_r)$ the integration can be done analytically, whereas the use of more realistic mass distributions will require a numerical integration.

V. BEAM MASTER STRUCTURE WITH STRUCTURAL FUZZY

The influence of structural fuzzy with and without spatial memory will now be illustrated by a numerical example. The finite element method[13] is being used for solving the harmonically forced vibration response of a simply supported Bernoulli–Euler beam, which is considered as the master structure. A fuzzy substructure is attached on the whole length L of the beam, so that $L_{\text{fuzzy}}=L$. The damping loss factor of the beam is 0.005 and the loss factor of the fuzzy oscillator springs is 0.03. The resonating mass per unit frequency, $m_{\text{fuzzy}}(f_r)$, is taken to follow a normal distribution, giving

$$m_{\text{fuzzy}}(f_r) = \frac{M_{\text{fuzzy}}}{\text{std}\sqrt{2\pi}}e^{-(f_{r0}-f_r)^2/(2\cdot\text{std}^2)}, \tag{26}$$

where f_{r0} is the center frequency and std is the standard deviation. This chosen mass distribution is shown in Fig. 11 as a function of the beam's nondimensional frequency Ω being defined as

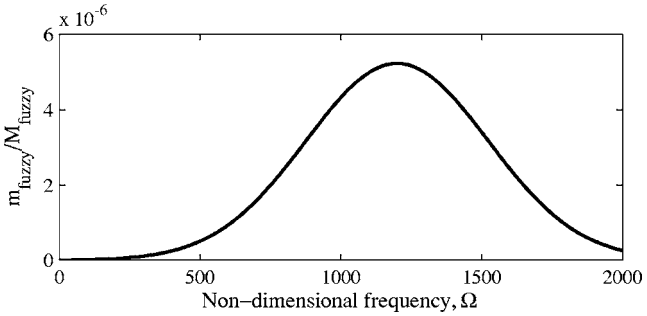

FIG. 11. Normalized resonating mass per unit frequency described by a normal distribution with a centre frequency f_{r0} corresponding to $\Omega=1200$ and a standard deviation *std* of $\Omega=750$.

$$\Omega = 2\pi f \sqrt{\frac{12\rho}{E}}\frac{L^2}{h}, \tag{27}$$

where h is the beam thickness, and ρ and E is the density and Young's modulus of the beam material, respectively. For this distribution the bounding frequencies $f_{r,\text{lower}}$ and $f_{r,\text{upper}}$ correspond to $\Omega=0$ and $\Omega=\infty$, respectively. The center frequency f_{r0} corresponds to $\Omega=1200$ and the standard deviation std is $\Omega=750$. Moreover, the total mass of the fuzzy M_{fuzzy} is taken to be one-twentieth of the beam mass, ρSL, where S is its cross-sectional area.

The boundary impedance of the fuzzy, Eq. (25), is computed by numerical integration; it is assumed that the equivalent coupling factor α is constant with frequency, which means that the ratio ε/λ is constant, whereas ε and λ decrease with frequency at the same rate. Figure 12 shows computed results of the fuzzy boundary impedance $\underline{z}_{\text{fuzzy,equ}}(x_0)$ as a function of the nondimensional frequency for different values of α.

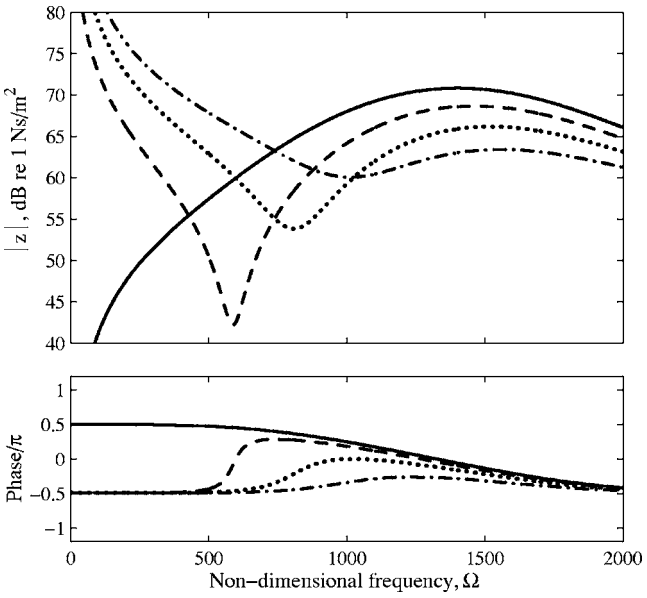

FIG. 12. Amplitude and phase of the fuzzy boundary impedance $\underline{z}_{\text{fuzzy,equ}}$. The total mass of the fuzzy is 1/20 of the master and has a normal-distributed resonating mass per unit frequency. Results are shown for different values of the equivalent coupling factor α: —, 1; ---, 0.75; ⋯, 0.5; -·-, 0.25.

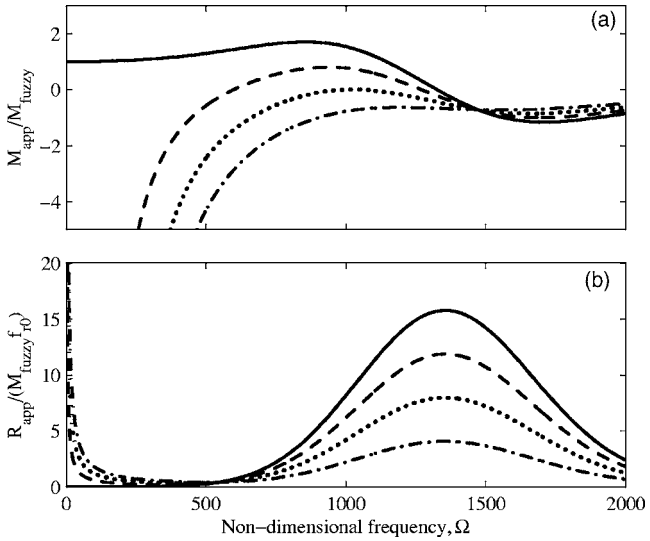

FIG. 13. (a) Normalized apparent mass, $M_{\text{app}}=\text{Im}(\underline{z}_{\text{fuzzy,equ}})/\omega$, and (b) normalized apparent damping, $R_{\text{app}}=\text{Re}(\underline{z}_{\text{fuzzy,equ}})$, of the fuzzy boundary impedance for different values of the α: —, 1; ---, 0.75; ⋯, 0.5; -·-, 0.25.

From these results a number of observations can be made. First, it is clearly seen that the structural fuzzy *without* memory is mass-controlled at frequencies below $\Omega=500$, as the amplitude slope of the boundary impedance is positive and the phase equals $\pi/2$. This is not the case for structural fuzzy *with* memory, which is clearly spring-like with a negative amplitude slope and a phase of $-\pi/2$; this will always be the case when $\alpha<1$. Second, between $\Omega=500$ and $\Omega=2000$ the phase of the fuzzy *without* memory changes smoothly from $\pi/2$ to approximately $-\pi/2$. During this change the real part of the impedance exhibits high values and the fuzzy therefore has a high damping effect. The impedance for $\alpha=0.75$ has a sudden phase change of π after $\Omega=500$ and hereafter it closely follows the phase of the fuzzy for $\alpha=1$. Examining the other two cases of smaller α values, it is found that the phase change is less pronounced and occurs at a higher frequency; therefore the fuzzy never reaches true mass-like behavior. It is also seen that the amplitude of the impedance becomes significantly lower when α is decreased, and this results in a weakening of the effect of the fuzzy. This is clearly observed for frequencies above $\Omega=1000$.

Inspired by Pierce *et al.*[8] the behavior and actual damping effect of the fuzzy is conveniently demonstrated by examining the corresponding apparent mass, $M_{\text{app}}(f)=\text{Im}(\underline{z}_{\text{fuzzy,equ}})/(2\pi f)$, and apparent damping $R_{\text{app}}(f)=\text{Re}(\underline{z}_{\text{fuzzy,equ}})$. Both quantities are shown in normalized form in Fig. 13 for different values of α. Figure 13(a) shows that the apparent mass of the fuzzy *without* memory is equal to the total mass of the fuzzy at $\Omega=0$, and up to around $\Omega=1170$ the apparent mass is higher than the total mass. Further, around $\Omega=1340$ the quantity becomes negative, which indicates a spring-controlled behavior. The three cases of fuzzy *with* memory clearly differ from this behaviour by being mostly spring-like in the whole frequency range. Above, say $\Omega=1350$, the apparent mass is very close in all cases. The apparent damping is plotted in Fig. 13(b), and it is seen that the damping effect of the fuzzy decreases significantly

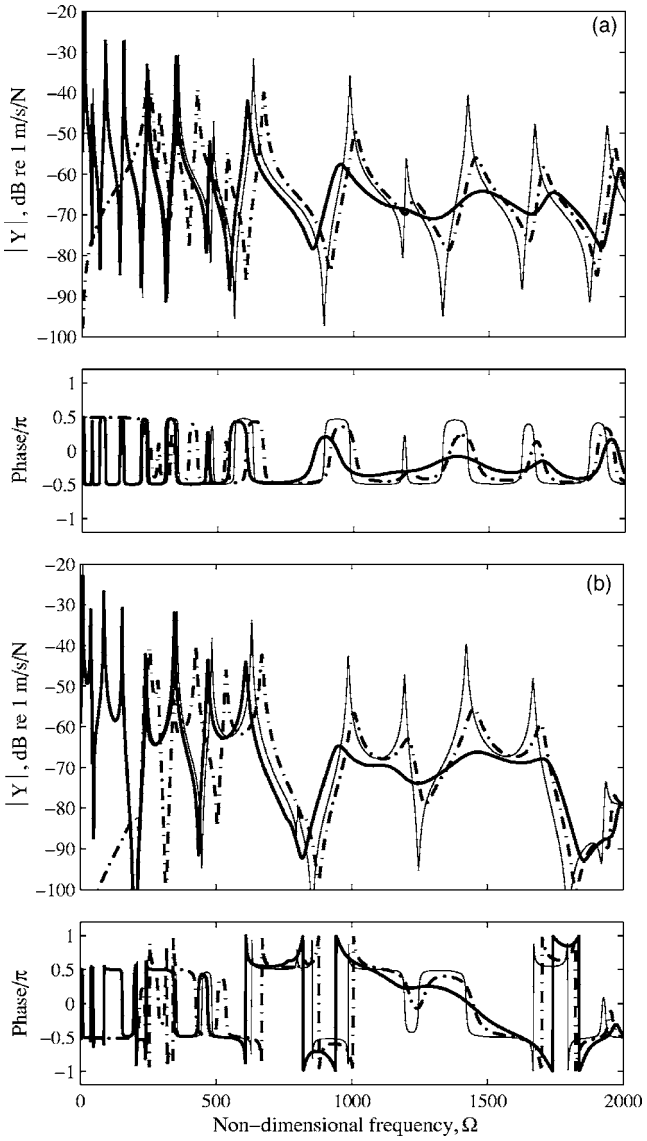

FIG. 14. Vibration velocity response per unit harmonic force, $\underline{Y}(x,x_0)=\underline{v}(x)/\underline{F}(x_0)$, at (a) $x=0.445L$ and (b) $x=0.785L$ of a simply supported beam excited at $x_0=0.445L$. Condition: —, without structural fuzzy and with structural fuzzy for α: —, 1; ---, 0.75; ···, 0.5; -·-, 0.25.

when α is reduced. The reason for this is that a reduction of α corresponds to an increase of ε. Due to the rotational motion in the master, the spring elements in the spatial oscillators counteract one another when $\varepsilon>0$. This also implies that the impedance of the structural fuzzy is reduced significantly, and this results in a lower dissipation induced in the master. For the chosen mass distribution, the maximum damping effect occurs around $\Omega=1360$, which is higher than the center frequency of $\Omega=1200$. At low frequencies below $\Omega=100$ it is seen that the apparent damping becomes very high. This nonphysical behavior is caused by the approximate modeling of the fuzzy boundary impedance, which goes toward infinity at $\Omega=0$.

Finally, Fig. 14 shows results for the vibration velocity response of the simply supported master beam, without and with the fuzzy substructure, which was discussed earlier. The vibration responses at $x=0.445L$ and $x=0.785L$ are given in terms of the beam's mobility $\underline{Y}(x,x_0)=\underline{v}(x)/\underline{F}(x_0)$ for harmonic force excitation at $x_0=0.445L$. Considering both Figs. 14(a) and 13(b) it is seen that the fuzzy *without* spatial memory, $\alpha=1$, introduces a high damping in the master beam. The effect of this stretches over a relatively wide frequency band, which covers at least six flexural modes of the beam. From around $\Omega=950$ to $\Omega=1740$ the damping effect is very pronounced and the vibration velocity of the master is dampened by up to 25 dB. Further, this structural fuzzy, causes the resonances of the beam structure to shift downwards into the region where the fuzzy is mass-like. This is the case in the range from $\Omega=0$ to $\Omega=1340$. Above $\Omega=1340$ the fuzzy becomes spring controlled and the resonances are shifted upwards.

Next, considering the case of structural fuzzy *with* a spatial memory of $\alpha=0.25$, it is evident that the spatial memory significantly decreases the damping effect of the fuzzy. In the main damping region of the fuzzy, the damping effect is reduced by almost 10 dB. This is in good agreement with the apparent damping being reduced by a factor of 3.5 by a decreasing α from 1 to 0.25, see Fig. 13(b). Further, it is seen that the strong spring-like behavior of the fuzzy at low frequencies dominates the response of the structure up to about $\Omega=140$. As the fuzzy is spring-like in the whole frequency range, it only causes the resonance frequencies of the structure to shift upwards. Fig. 14(b) shows the response at a position at some distance from the drive point. The damping effect of the fuzzy both without and with spatial memory is seen to be very similar to what was discussed earlier for the response at the drive point location. This illustrates and confirms that the influence of the structural fuzzy is global, and not specifically associated with the drive point.

VI. SUMMARY AND DISCUSSION

Soize's method of including spatial memory in structural fuzzy has been thoroughly examined and exemplified in the present paper. Additional illustrations and a derivation of the fuzzy boundary impedance have been given in order to explain the ideas governing the method. To simplify the fuzzy modeling, Soize replaces the non-local spatial oscillator with a local equivalent oscillator. In the present article this oscillator has been given a physical interpretation. Further, it has been suggested that the so-called equivalent coupling factor, which transforms the nonlocal boundary impedance into a local impedance, can be determined as a function of the ratio between spatial memory and the free wavelength in the master.

The fuzzy boundary impedance, which includes spatial memory, has been derived deterministically by using a simple smoothing approach. This method assumes that the fuzzy is described in terms of a predefined distribution of resonating mass per unit frequency. The developed method is straightforward and it has been demonstrated that a prediction of the overall vibrations of the master can be made in a simple way.

From numerical simulations of the response of a simply supported beam with structural fuzzy and different amounts of spatial memory, it has been found that the spatial memory

significantly reduces the damping introduced in the master. Further, for the case studied it can be included that the memory in some cases completely eliminates the damping effect of the fuzzy.

Various assumptions have been made in this paper in order to illustrate more clearly the effects of spatial memory in the structural fuzzy. This includes the hypothesis of modeling spatial memory by use of an equivalent spatial oscillator. A validation of this hypothesis and a discussion of its limitations clearly remain to be made. Also, a simple way of determining the equivalent coupling factor is as yet absent in the open literature. However, both of these two topics will be dealt with in a companion paper, which soon will be submitted for publication. Finally, further investigations are still required concerning practical questions of how one can determine the distribution of resonating mass per unit frequency as well as the amount of spatial memory in real-life engineering structures.

[1]J. Ormondroyd and J. P. Den Hartog, "Theory of dynamic vibration absorber," Trans. ASME **50**, APM-241 (1928).

[2]*Noise and Vibration*, edited by R. G. White and J. G. Walker (Ellis Horwood, Chichester, UK, 1982), Chap. 25.

[3]D. F. Mead, *Passive Vibration Control*, (Wiley, Chichester, UK, 1999), Chap. 8.

[4]C. Soize, "Probabilistic structural modeling in linear dynamic analysis of complex mechanical systems, Part I," Rech. Aerosp. (English edition), **5**, 23–48 (1986).

[5]F. Chabas, A. Desanti, and C. Soize, "Probabilistic structural modelling in linear dynamic analysis of complex mechanical systems, part II," Rech. Aerosp. (English edition), **5**, 49–67 (1986).

[6]C. Soize, "A model and numerical method in the medium frequency range for vibroacoustic predictions using the theory of structural fuzzy," J. Acoust. Soc. Am. **94**, 849–865 (1993).

[7]C. Soize, "Vibration damping in low-frequency range due to structural complexity. A model based on the theory of fuzzy structures and model parameters estimation," Comput. Struct. **58**, 901–915 (1995).

[8]A. D. Pierce, V. W. Sparrow, and D. A. Russell, "Fundamental structural-acoustic idealizations for structures with fuzzy internals," J. Vibr. Acoust. **117**, 339–348 (1995).

[9]M. Strasberg and D. Feit, "Vibration damping of large structures induced by attached small resonant structures," J. Acoust. Soc. Am. **99**, 335–344 (1996).

[10]C. Soize, "Estimation of fuzzy substructure model parameters using the mean power flow equation of the fuzzy structure," J. Vibr. Acoust. **120**, 279–286 (1998).

[11]C. Soize, "Estimation of fuzzy structure parameters for continuous junctions," J. Acoust. Soc. Am. **107**, 2011–2020 (2000).

[12]A. D. Pierce, "Resonant-frequency-distribution of internal mass inferred from mechanical impedance matrices, with application to fuzzy structure theory," J. Vibr. Acoust. **119**, 324–333 (1997).

[13]R. Cook, D. S. Malkus, M. F. Plesha, and R. J. Witt, *Concepts and Applications of Finite Element Analysis* (Wiley, New York, 2002).

5.3 Paper III:

Simple vibration modeling of structural fuzzy with continuous boundary by including two-dimensional spatial memory

Simple vibration modeling of structural fuzzy with continuous boundary by including two-dimensional spatial memory

Lars Friis[a)]
Acoustic Technology, Ørsted·DTU, Technical University of Denmark, Building 352, DK-2800 Kgs. Lyngby, Denmark and Widex A/S, Ny Vestergaardsvej 25, DK-3500 Vaerloese, Denmark

Mogens Ohlrich[b)]
Acoustic Technology, Ørsted·DTU, Technical University of Denmark, Building 352, DK-2800 Kgs. Lyngby, Denmark

(Received 6 November 2007; revised 8 April 2008; accepted 28 April 2008)

Many complicated systems of practical interest consist basically of a well-defined outer shell-like *master* structure and a complicated internal structure with uncertain dynamic properties. Using the "fuzzy structure theory" for predicting audible frequency vibration, the internal structure is considered as one or more *fuzzy substructures* that are known in some statistical sense only. Experiments have shown that such fuzzy substructures often introduce a damping in the master which is much higher than the structural losses account for. A special method for modeling fuzzy substructures with a one-dimensional continuous boundary was examined in a companion paper [L. Friis and M. Ohlrich, "Vibration modeling of structural fuzzy with continuous boundary," J. Acoust. Soc. Am. **123**, 718–728 (2008)]. In the present paper, this method is extended, such that it allows modeling of fuzzy substructures with a two-dimensional continuous boundary. Additionally, a simple method for determining the so-called equivalent coupling factor is presented. The validity of this method is demonstrated by numerical simulations of the vibration response of a master plate structure with fuzzy attachments. It is revealed that the method performs very well above a nondimensional frequency of 500 of the master, and it is shown that errors below this frequency are caused mainly by simplifying assumptions concerning the shape of the master vibration displacement. © *2008 Acoustical Society of America.* [DOI: 10.1121/1.2932077]

PACS number(s): 43.40.At, 43.40.Tm [DF] Pages: 192–202

I. INTRODUCTION

For about 20 years, the "theory of fuzzy structures"[1–3] has been known as a suggested alternative method for predicting the vibration of complex systems having many degrees of freedom and uncertain properties. By using this theory, a system is divided into a well-defined *master* structure and one or more complex parts termed as *fuzzy substructures*. It is assumed that the deterministic master, which is typically a shell-like structure, can be modeled by using traditional methods, whereas the fuzzy has imprecisely known properties that are known only in some statistical sense. Examples of real-life fuzzy systems varying from small size to large size are electro-mechanical hearing aids, machines, aircraft, and ship hulls.

Experiments have shown that such fuzzy attachments seemingly introduce high damping in the master structure, due to the dissipation of energy into the many degrees of freedom. The theory of fuzzy structures explains this damping effect, caused by multiple reflections rather than actual damping, by regarding the dynamic behavior of the fuzzy similar to that of a multitude of dynamic neutralizers or absorbers.[4–6] Despite of this relatively simple hypothesis, publications on experimental investigations and practical use of the theory of fuzzy structures have so far been very limited in open literature. This is not only partly due to difficulties in determining the fuzzy parameters but also because of complicating issues such as the incorporation of different motion coordinates and modeling of fuzzy structures connected to the master through a continuous boundary.

The present paper examines and extends a special method of modeling structural fuzzy with a continuous boundary. This method was originally formulated by Soize and briefly presented in a paper from 1993.[3] A successful modeling of structural fuzzy with continuous boundary requires that its stiffness must be taken into account. Soize achieved this by introducing spatial memory in the fuzzy boundary impedance. However, such boundary impedance is nonlocal and, therefore, laborious to implement in numerical methods. A full implementation is, therefore, circumvented by introducing an equivalent coupling factor that converts the distributed impedance to a local form. Soize's method of including spatial memory is clearly innovative; however, in the author's opinion, the main ideas of the method need clarification and physical interpretation.

In a companion paper,[7] Soize's method was thoroughly examined and physical interpretations were offered. Furthermore, the smoothed fuzzy boundary impedance was formulated from simple mathematics without the use of probabilistic concepts. The present paper contributes with an extension of the method to two dimensions and with a simple and

[a)]Electronic mail: lf@oersted.dtu.dk
[b)]Electronic mail: mo@oersted.dtu.dk

 0001-4966/2008/124(1)/192/11/$23.00

general method for determining the equivalent coupling factor. This method is examined through numerical simulations and its limitations are discussed. The companion paper and the present paper represent a continuation of the papers by Pierce *et al.*[8] and Strasberg and Feit[9] but for structural fuzzy with *continuous boundary*.

The theory of fuzzy structures was originally developed by Soize and presented in a series of papers[1–3] from 1986 to 1993. During the last 20 years, the literature has partly focused on interpretation and simplification of Soize's theory that involves probabilistic concepts in order to account for model uncertainties. One milestone was the publications of simple and deterministic methods by Pierce *et al.*[8] and Strasberg and Feit.[9] These papers clarified the main concepts of the theory of fuzzy structures and have provided simple procedures for predicting the smoothed average response of complex systems. Furthermore, it was revealed that the damping induced in the master was governed mainly by the frequency-dependent *resonating mass per unit frequency* of the fuzzy. Several authors have examined the fuzzy damping effect in great detail. This includes Maidanik and Becker[10–12] who unambiguously demonstrated the nature of the damping and set up design rules for complex attachments. The damping caused by different local oscillators was likewise investigated by Maidanik and Becker.[13,14] Moreover, Weaver[15] and Carcaterra and Akay[16] revealed that the fuzzy damping is a transient phenomenon in the case of a finite number of complex attachments. It was shown that the energy returns to the master at later times when excited by a transient. One of the most difficult challenges in applying the theory of fuzzy structures is the determination of the resonating mass per unit frequency. During the last ten years, both Soize[17,18] and Pierce[19] addressed this problem. Another important highlight was the development of a method[3] for including spatial memory in the modeling of structural fuzzy with continuous boundaries. With the exception of a few publications,[7,17,18] succeeding literature has mainly focused on developing methods that regard the structural fuzzy as local fuzzy substructures. Many real-life structures, however, involve fuzzy structures with continuous boundaries, and the authors of the present paper believe that further study in this area is strongly needed in order to clarify some of the main ideas.

In favor of the reader, the method of including spatial memory in structural fuzzy will be briefly outlined in Sec. II below. Hereafter, a general method of determining the equivalent coupling factor is presented for a master structure with one-dimensional wave motion. Next, in Sec. IV, the fuzzy boundary impedance will be derived for structural fuzzy attached to the master through an area. After this, the method of finding the equivalent coupling factor is extended to two-dimensional wave motion in the master structure. Finally, in Sec. V, the method will be validated through numerical simulations and its usability and limitations will be discussed in Section VI.

II. STRUCTURAL FUZZY WITH CONTINUOUS BOUNDARY

A. Introduction

Fuzzy structure theory is intended for predicting the vibration and damping induced in a master structure due to one or more fuzzy substructures. The method is applicable mainly in the midfrequency range, where the master structure has well separated modes and where the fuzzy is highly resonant. Since the fuzzy is more or less compliantly attached to the master, the fuzzy behaves predominantly similar to a large number of "sprung masses" or "dynamic neutralizers" resonating at different frequencies. If these resonance frequencies of the fuzzy are closely spaced, then the fuzzy substructure will minimize and absorb vibration energy from the master over a considerable frequency band. Consequently, by considering the vibration response of the master, it appears as if the master is highly damped.

In the theory of fuzzy structures, each fuzzy substructure is modeled as infinitely many dynamic neutralizers attached to the connection surface. These neutralizers have different masses and their resonance frequencies are closely spaced, and altogether they, therefore, introduce a frequency-dependent damping in the master. Further, it is assumed that the total mass of all the oscillators is equal to the mass of the fuzzy substructure that is to be modeled. A fuzzy substructure is typically separated from the master and conveniently modeled in terms of its boundary impedance $\underline{z}_{\text{fuzzy},\varepsilon}(x_0,y_0;x_1,y_1)$. This boundary impedance expresses the relationship between the force per unit area $\underline{F}''(x_0,y_0)$ induced at (x_0,y_0) due to the velocity $\underline{v}(x_1,y_1)$ of an infinitesimal area element dA at (x_1,y_1), while all other positions are locked, that is,

$$\underline{F}''(x_0,y_0) = \underline{z}_{\text{fuzzy},\varepsilon}(x_0,y_0;x_1,y_1)\underline{v}(x_1,y_1)dA|_{\underline{v}[(x,y)\neq(x_1,y_1)]=0}. \quad (1)$$

B. The spatial oscillator

In many cases, the fuzzy substructure is attached to the master through a continuous boundary. This also implies that the stiffness distribution of the fuzzy has to be taken into account and that the associated transfer terms of the impedance in Eq. (1) can only be neglected in special cases.[7] Consider a fuzzy substructure connected to the master structure through a continuous boundary. Generally, this continuous boundary will be a surface, but for the sake of simplicity, we shall here consider a fuzzy attached to the master through a one-dimensional boundary of length L_{fuzzy}. Soize[3] incorporates the stiffness of such a fuzzy substructure by including a spatial memory in the fuzzy boundary impedance. This is accomplished by introducing a spatial oscillator as sketched in Fig. 1(a). The oscillator is defined by its stiffness width or spatial memory 2ε, the point mass M, the lossfactor η, and the resonance frequency f_r. Furthermore, it has a stiffness density distribution $\underline{s}_\varepsilon(x'-x_1)$ that only depends on $(x'-x_1)$ and which is defined as

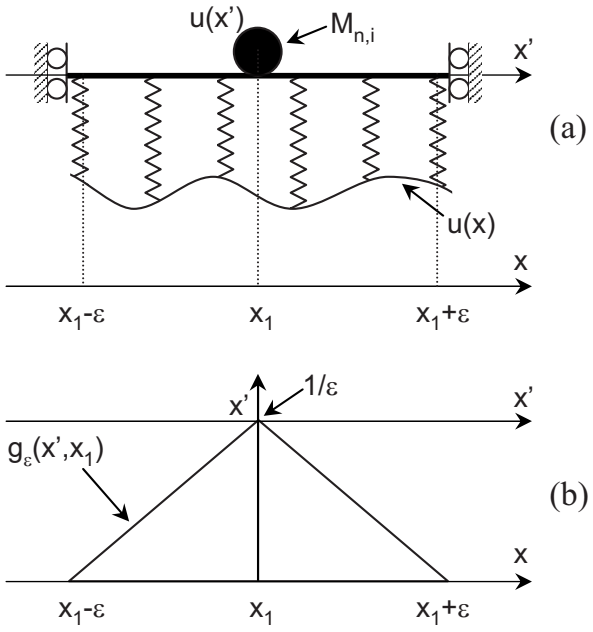

FIG. 1. Fuzzy oscillator with spatial memory. (a) Oscillator attached to a boundary of motion $u(x)$ and (b) stiffness distribution function of the oscillator springs $g_\varepsilon(x'-x_1)$.

$$\underline{s}_\varepsilon(x'-x_1)=\underline{s}g_\varepsilon(x'-x_1)=(M\omega_r^2)(1+i\eta)g_\varepsilon(x'-x_1), \tag{2}$$

where $\omega_r=2\pi f_r$ is the angular resonance frequency and $\underline{s}$ is the complex total stiffness of the oscillator. The distribution function $g_\varepsilon(x'-x_1)$ is an even function with an area of 1. As a one-dimensional spatial memory, Soize suggests[3] that $g_\varepsilon(x'-x_1)$ is a triangular distribution, as shown in Fig. 1(b). This distribution is given as

$$g_\varepsilon(x'-x_1)=g_\varepsilon(x_1-x')=\frac{\varepsilon-|x'-x_1|}{\varepsilon^2}1_{[x_1\in(x'-\varepsilon,x'+\varepsilon)]}, \tag{3}$$

where $1_{[x_1\in(x'-\varepsilon,x'+\varepsilon)]}$ is a function, which is equal to 1 when $x_1\in[x'-\varepsilon,x'+\varepsilon]$ and 0 elsewhere. The spatial oscillator is discussed in more detail in Ref. 7.

C. Sets of infinitely many identical oscillators

Let us consider a fuzzy substructure with spatial memory connected to the master over a length L_{fuzzy}. Such a substructure comprises a *double infinity* of spatial oscillators, as sketched in Fig. 2, where each oscillator is depicted as a point mass and the triangular stiffness distribution shown in Fig. 1(b). First, the oscillators are grouped into sets of infinitely many *identical* oscillators overlapping one another such that each position on L_{fuzzy} is associated with a point mass. Second, the structural fuzzy consists of infinitely many *different* sets, each with its *individual resonance frequency, mass, and spatial memory*.

Now, the nth set $(n\in[1,\infty[)$ of spatial oscillators is shown in Fig. 3(a). This set has a resonance frequency $f_{r,n}$, a total mass of M_n, and a spatial memory of $2\varepsilon_n$. Further, the ith spatial oscillator $(i\in[1,\infty[)$ of this nth set has the natural frequency $f_{r,n,i}=f_{r,n}$, a mass $M_{n,i}=M_n/L_{\text{fuzzy}}$, and a total stiffness $\underline{s}_{n,i}$. The relationship between the force per unit length $F'_{\varepsilon,n}(x_0)$ at x_0 and the velocity $v(x_1)$ at x_1, that is, the boundary impedance of the nth set $\underline{z}_{\varepsilon,n}(x_0-x_1,f_{r,n})$, was derived in Ref. 1. When multiplied by dx_1, this is given as

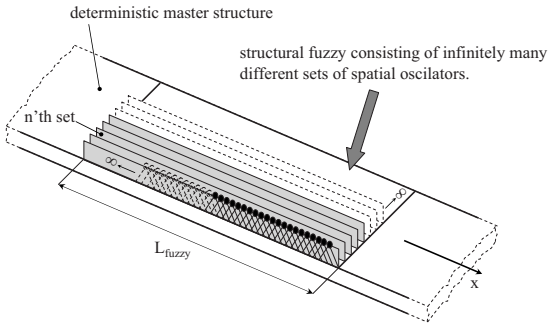

FIG. 2. Master structure undergoing one-dimensional wave motion with a fuzzy substructure attached through a one-dimensional continuous boundary in the x direction. The fuzzy substructure has infinitely many sets of spatial oscillators and the nth set consists of infinitely many identical oscillators with resonance frequency $f_{r,n,i}$, mass $M_{n,i}$, and spatial memory ε_n.

$$\begin{aligned}\underline{z}_{\varepsilon,n}(x_0-x_1,f_{r,n})dx_1&=\frac{\underline{s}_{n,i}}{i\omega}\left[\delta_{x_0,x_1}-\frac{\underline{s}_{n,i}}{\underline{s}_{n,i}-\omega^2M_{n,i}}(g_{\varepsilon_n}*g_{\varepsilon_n})\right.\\&\left.\times(x_0-x_1)dx_1\right]\\&=-i\omega\left(\frac{f_{r,n}^2}{f^2}\right)(1+i\eta)M_{n,i}\\&\times\left[\delta_{x_0,x_1}\right.\\&-\frac{f_{r,n}^2(1+i\eta)}{f_{r,n}^2(1+i\eta)-f^2}(g_{\varepsilon_n}*g_{\varepsilon_n})\\&\left.\times(x_0-x_1)dx_1\right],\end{aligned} \tag{4}$$

where δ_{x_0,x_1} is the Kronecker delta and $*$ means convolution with the argument (x_0-x_1). It is seen that the transfer terms of the boundary impedance in Eq. (4) are proportional to $(g_{\varepsilon_n}*g_{\varepsilon_n})(x_0-x_1)$. This function has been plotted in Fig. 4, and it can be observed that these transfer terms are largest close to x_1 and that the spatial memory in effect reaches $2\varepsilon_n$ on either side of the response point x_1.

The total boundary impedance of the fuzzy substructure can be determined as the sum of all the impedances of all the sets, which yields

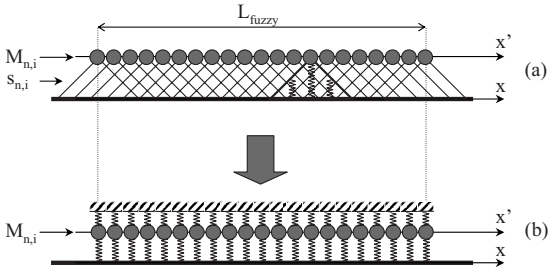

FIG. 3. A set of infinitely many identical oscillators attached to the master: (a) spatial oscillators and (b) equivalent local oscillators.

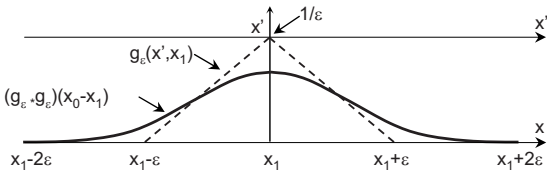

FIG. 4. Fuzzy oscillator with spatial coupling: ---, stiffness distribution function $g_\varepsilon(x'-x_1)$ of the oscillator springs and —, convolution of the stiffness distribution with itself $(g_\varepsilon * g_\varepsilon)(x_0-x_1)$.

$$\underline{z}_{\text{fuzzy},\varepsilon}(x_0-x_1)dx_1=\sum_{n=1}^{\infty}z_{\varepsilon,n}(x_0-x_1,f_{r,n})dx_1. \tag{5}$$

This discrete sum can be replaced by an integral if there is sufficient modal overlap.[20] This is done by replacing $z_{\varepsilon,n}(x_0-x_1,f_{r,n})dx_1$ from Eq. (4) with a continuous distribution denoted by $z_\varepsilon(x_0-x_1,f_r)dx_1df_r$, where f_r is a continuous frequency variable $(f_{r,n}\to f_r)$, and further by assuming that the sets resonate between bounding frequencies $f_{r,\text{lower}}$ and $f_{r,\text{upper}}$. This gives

$$\underline{z}_{\text{fuzzy},\varepsilon}(x_0-x_1)dx_1=\int_{f_{r,\text{lower}}}^{f_{r,\text{upper}}}z_\varepsilon(x_0-x_1,f_r)dx_1df_r. \tag{6}$$

By substituting herein the detailed expression of a continuous version of Eq. (4), the fuzzy boundary impedance becomes

$$\begin{aligned}\underline{z}_{\text{fuzzy},\varepsilon}(x_0-x_1)dx_1&=-\frac{i2\pi f}{L_{\text{fuzzy}}}\int_{f_{r,\text{lower}}}^{f_{r,\text{upper}}}\left(\frac{f_r^2}{f^2}\right)(1+i\eta)m_{\text{fuzzy}}(f_r)\\&\times\left[\delta_{x_0x_1}-\frac{f_r^2(1+i\eta)}{f_r^2(1+i\eta)-f^2}(g_\varepsilon*g_\varepsilon)(x_0-x_1)dx_1\right]df_r,\end{aligned} \tag{7}$$

where $M_{n,i}$ has been replaced by $m_{\text{fuzzy}}(f_r)df_r$ that corresponds to the total mass of the fuzzy substructure resonating in the infinitesimal frequency band between f_r and f_r+df_r.

D. Equivalent local modeling method

A numerical implementation of the boundary impedance given in Eq. (7) is rather complicated due to its *nonlocal* nature and requires, for instance, the use of a finite element model with special fuzzy elements. Unfortunately, this is in contradiction with the idea of the theory of fuzzy structures being a simple modeling tool. However, as indicated in Fig. 3(b), Soize[3] solved this problem by introducing a set of *equivalent local oscillators* that can imitate the boundary forces induced by a set of spatial oscillators. This means that the boundary impedance $\underline{z}_{\text{fuzzy},\varepsilon}$ in Eq. (7) can be replaced with an equivalent boundary impedance $\underline{z}_{\text{fuzzy,equ}}$ that has direct terms only. Figure 3(b) shows that the equivalent local oscillator corresponds to a modified simple oscillator with a spring stiffness $\underline{s}_{1,n,i}$, but where the point mass is grounded via a second spring with stiffness $\underline{s}_{2,n,i}$, such that $\underline{s}_{n,i}=\underline{s}_{1,n,i}+\underline{s}_{2,n,i}$. This means that the equivalent oscillator is springlike at low frequencies because the massless bar that supports the point mass in Fig. 1(a) is unable to rotate; the spatial oscillators, therefore, impose springlike properties on the master at low frequencies.

The relationship between the stiffnesses of the springs for the nth set of equivalent oscillators shown in Fig. 3(b) is given in terms of the *equivalent coupling factor* $\alpha_{n,i}$ and can be expressed as[7]

$$\alpha_{n,i}=\underline{s}_{1,n,i}/(\underline{s}_{1,n,i}+\underline{s}_{2,n,i})=\underline{s}_{1,n,i}/\underline{s}_{n,i}, \tag{8}$$

where $\alpha_{n,i}\in]0,1]$. This parameter $\alpha_{n,i}$ must be determined as a function of the characteristic dimension ε_n of the spatial oscillators, and such a derivation is presented in Sec. III. By introducing $\alpha_{n,i}$, the boundary impedance $\underline{z}_{\text{equ},n}(x_0,f_{r,n})$ of the nth set of equivalent local oscillators becomes[3]

$$\begin{aligned}\underline{z}_{\text{equ},n}(x_0,f_{r,n})&=\frac{\underline{s}_{n,i}}{i\omega}\left(1-\frac{\underline{s}_{n,i}}{\underline{s}_{n,i}-\omega^2M_{n,i}}\alpha_{n,i}\right)\\&=-i\omega\left(\frac{f_{r,n}^2}{f^2}\right)(1+i\eta)M_{n,i}\\&\times\left[1-\frac{f_{r,n}^2(1+i\eta)}{f_{r,n}^2(1+i\eta)-f^2}\alpha_{n,i}\right].\end{aligned} \tag{9}$$

Note that $\alpha_{n,i}\to 1$ when $\underline{s}_{2,n,i}\to 0$ and $\underline{z}_{\text{equ},n}$ will then approach the impedance of a simple oscillator. Further, when $\alpha_{n,i}\to 0$, then $\underline{s}_{1,n,i}\to 0$, which indicates that the structural fuzzy has no effect on the master. Inserting a continuous version of Eq. (9) into Eq. (6) yields the boundary impedance $\underline{z}_{\text{fuzzy,equ}}(x_0)$ of the equivalent fuzzy,

$$\begin{aligned}\underline{z}_{\text{fuzzy,equ}}(x_0)&=-\frac{i2\pi f}{L_{\text{fuzzy}}}\int_{f_{r,\text{lower}}}^{f_{r,\text{upper}}}\left(\frac{f_r^2}{f^2}\right)(1+i\eta)m_{\text{fuzzy}}(f_r)\\&\times\left[1-\frac{f_r^2(1+i\eta)}{f_r^2(1+i\eta)-f^2}\alpha\right]df_r.\end{aligned} \tag{10}$$

This expression also applies for two-dimensional structural fuzzy when the connection *length* L_{fuzzy} is replaced by the connection area A_{fuzzy}. It should be noted that the equivalent coupling factor α generally is a function of frequency. In a companion paper,[7] it was suggested that α can be determined as a function of the ratio ε/λ, where λ is the wavelength of vibration in the master structure, which has one-dimensional wave motion only.

III. METHOD OF DETERMINING THE EQUIVALENT COUPLING FACTOR

A. Matching of boundary forces

Before the suggested equivalent modeling method can be utilized, it is necessary to establish a relationship between the parameters ε and α. This requires that the boundary forces induced by the set of spatial oscillators are matched with the forces induced by the equivalent local oscillators. Results for the equivalent coupling factor α determined in this way were published by Soize[3] but only for a very specific case of a simply supported beam with an attached fuzzy substructure with continuous boundary. His results show the mean value of α as a function of the spatial width ε for only

three coarse frequency bands with a width of 100 Hz going from 350 to 650 Hz. The authors of the present paper, however, seek a simple and general method for finding α. Accordingly, a method for determining α will be presented in the following, again as a function of the ratio $c=\varepsilon/\lambda$. For simple master structures with sinusoidal vibration, the wavelength λ is equal to the free wavelength. For master structures with more complicated eigenfunctions, it is suggested that the term wavelength is replaced by twice the distance between adjacent nodes.

Next, the matching of the boundary forces induced by the nth set of spatial and equivalent oscillators can be expressed as

$$\underline{F}_{\mathrm{equ},n}'(x_0) = \underline{F}_{\varepsilon,n}'(x_0). \tag{11}$$

In terms of velocities and impedances, this becomes

$$\underline{z}_{\mathrm{equ},n}(x_0)\underline{v}(x_0) = \int_{L_{\mathrm{fuzzy}}} \underline{z}_{\varepsilon,n}(x_0 - x_1)\underline{v}(x_1)dx_1. \tag{12}$$

Inserting herein the expressions for the impedances $\underline{z}_{\varepsilon,n}(x_0 - x_1)$ and $\underline{z}_{\mathrm{equ},n}(x_0)$ from Eqs. (4) and (9), respectively, yields

$$\begin{aligned}\underline{s}_{n,i}&\left(1 - \frac{\underline{s}_{n,i}}{\underline{s}_{n,i} - \omega^2 M_{n,i}}\alpha\right)\underline{u}(x_0) \\ &= \underline{s}_{n,i}\left[\underline{u}(x_0) - \int_{L_{\mathrm{fuzzy}}} \frac{\underline{s}_{n,i}}{\underline{s}_{n,i} - \omega^2 M_{n,i}}(g_\varepsilon * g_\varepsilon)\right. \\ &\left.\times(x_0 - x_1)\underline{u}(x_1)dx_1\right].\end{aligned} \tag{13}$$

Next, by rearranging, we obtain an equation that has similar terms on each side of the equality sign,

$$\begin{aligned}\underline{s}_{n,i}&\left[\underline{u}(x_0) - \frac{\underline{s}_{n,i}}{\underline{s}_{n,i} - \omega^2 M_{n,i}}\alpha\underline{u}(x_0)\right] \\ &= \underline{s}_{n,i}\left[\underline{u}(x_0) - \frac{\underline{s}_{n,i}}{\underline{s}_{n,i} - \omega^2 M_{n,i}}\right. \\ &\left.\times\int_{L_{\mathrm{fuzzy}}} (g_\varepsilon * g_\varepsilon)(x_0 - x_1)\underline{u}(x_1)dx_1\right].\end{aligned} \tag{14}$$

By eliminating these terms, Eq. (14) is reduced to

$$\alpha\underline{u}(x_0) = \int_{L_{\mathrm{fuzzy}}} (g_\varepsilon * g_\varepsilon)(x_0 - x_1)\underline{u}(x_1)dx_1, \tag{15}$$

from which an expression for α is obtained,

$$\alpha(x_0) = \frac{\displaystyle\int_{L_{\mathrm{fuzzy}}} (g_\varepsilon * g_\varepsilon)(x_0 - x_1)\underline{u}(x_1)dx_1}{u(x_0)}. \tag{16}$$

B. Approximate expressions for the master's equivalent coupling factor

Determining α from Eq. (16) requires a detailed knowledge about the form of the motion displacement $\underline{u}(x_1)$ of the master. At this point in the analysis, this form has not been identified and it is, therefore, preliminarily approximated by a suitably simple function of x. Moreover, since we are mostly concerned with prediction in the midfrequency range, it is assumed that the wavelength of the master vibration is shorter than the length L of the structure. This also implies that the wave motion in the master is relatively independent of its boundary conditions. Therefore, a sinusoidal function is a good approximation for the one-dimensional vibration of the master, with the exception of the regions very close to the edges. Thus, it is assumed that the displacement $u(x_1)$ of the master can be described as

$$\underline{u}(x_1) = \sin\left(\frac{2\pi}{\lambda}x_1\right), \tag{17}$$

where λ is the free wavelength.[21] Inserting this in Eq. (16) yields α as a function of x_0 and c,

$$\alpha(x_0,c) = \frac{\displaystyle\int_{L_{\mathrm{fuzzy}}} (g_\varepsilon * g_\varepsilon)(x_0 - x_1)\sin\left(\frac{2\pi}{\lambda}x_1\right)dx_1}{\sin\left(\dfrac{2\pi}{\lambda}x_0\right)}. \tag{18}$$

Now, the convolution product inherent in Eq. (18) has only nonzero values when $x_1 \in [(x_0-2\varepsilon),(x_0+2\varepsilon)]$ and it is, therefore, sufficient to solve the integral in this interval provided that x_1 is at least 2ε from the edge of the fuzzy. If this is fulfilled, no truncation errors occur and an analytical solution of Eq. (18) is found by using the symbolic mathematics software MAPLE® (version 10),

$$\alpha(x_0,c) = \alpha(c) = \left[\frac{\sin(\pi c)}{\pi c}\right]^4. \tag{19}$$

This is a surprisingly simple result, which is *independent* of the position x_0 on the master structure because of the homogeneity of the fuzzy. The function $\sin(\pi c)/(\pi c)$ in Eq. (19) is recognized as the sink function. Figure 5 shows α as a function of $c=\varepsilon/\lambda$ for two different regions. In Fig. 5(a), it is seen that $\alpha=1$ when $\varepsilon=0$, which is the case of no spatial memory. Up to about $c=0.8$, α appears to be a uniformly descending function. For values higher than $c=0.8$, α becomes very small and the ordinate is, therefore, extended in Fig. 5(b). Here, the behavior of the sink function is easily recognized, showing soft minima and maxima, and it is revealed that α becomes zero when $c=1,2,3,\ldots$.

For the remaining part of the fuzzy where x_1 is closer than 2ε from the edge of the fuzzy, it is not possible to integrate with respect to x_1 in the whole interval $[(x_0-2\varepsilon),(x_0+2\varepsilon)]$ and the solution for α becomes quite complicated. The simplest way to overcome this problem is to *assume* that α takes on a constant value that can be calculated from Eq. (19). The truncation error introduced because of this assumption naturally depends on the length 2ε. Hence, the larger the values of ε are, the larger the introduced truncation error is.

At this point, two assumptions have been made: First, the vibration of the master is approximated by a sinusoidal function. Errors due to this assumption will only be significant at low frequencies where the free wavelength[21] in the master is large. Second, α is considered to be constant with position. As mentioned, this assumption depends on the

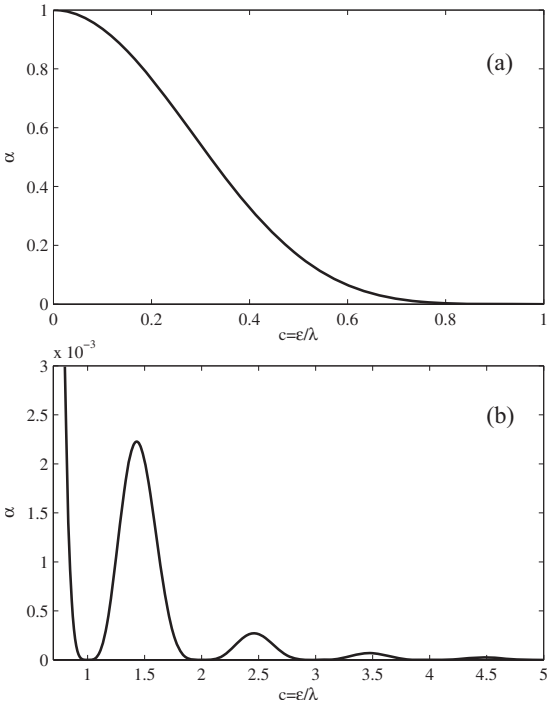

FIG. 5. Variation of the equivalent coupling factor α as a function of the ratio $c=\varepsilon/\lambda$. (a) Values of c from 0 to 1 and (b) from 0.8 to 5.

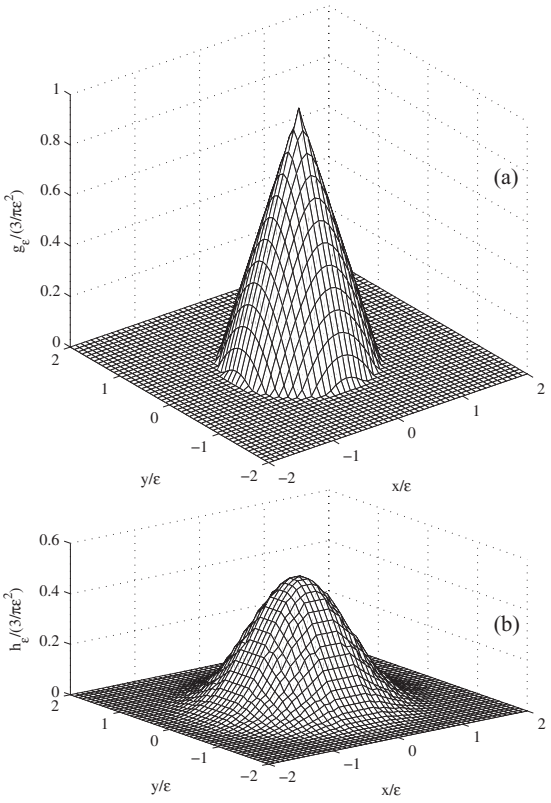

FIG. 6. (a) Normalized stiffness density distribution g_ε of the oscillator springs. (b) Variation of the function h_ε with x and y.

variation of ε with frequency. The significance of these errors in the prediction of α will be examined in Sec. V, where numerical simulations will be presented for a plate master structure with an attached fuzzy substructure with spatial memory.

IV. STRUCTURAL FUZZY WITH TWO-DIMENSIONAL SPATIAL MEMORY

A. Determination of the two-dimensional fuzzy boundary impedance

So far, the method of including spatial memory has been restricted to fuzzy substructures attached to the master structure through a one-dimensional boundary. Most real-life fuzzy structures, however, are attached to their master through a surface that also undergoes two-dimensional vibration. Therefore, the method of including spatial memory in this modeling of fuzzy structures is required and it is, therefore, extended to two dimensions in the following.

To accomplish this, the stiffness distribution function $g_\varepsilon(x'-x_1)$ in Eq. (3) for the spatial oscillator is initially replaced by a two-dimensional version $g_\varepsilon(|r',\theta';r_1,\theta_1|)$, which is a function of the distance $|r',\theta';r_1,\theta_1|$ between two surface points (r',θ') and (r_1,θ_1) described in polar coordinates; it should be noted that the point mass of the spatial oscillator is located at (r',θ'). This two-dimensional stiffness distribution that is shown in Fig. 6(a) in a Cartesian coordinate system represents a cone with a *radius* of ε at its base and a *volume* of 1. Based on these requirements, the distribution can be expressed mathematically as

$$g_\varepsilon(|r',\theta';r_1,\theta_1|) = \frac{\varepsilon - |r',\theta';r_1,\theta_1|}{\frac{1}{3}\pi\varepsilon^3} 1_{[|r',\theta';r_1,\theta_1|\le\varepsilon]}$$
$$= \frac{\varepsilon - \sqrt{r'^2 + r_1^2 - 2r'r_1\cos(\theta'-\theta_1)}}{\frac{1}{3}\pi\varepsilon^3} \times 1_{[|r',\theta';r_1,\theta_1|\le\varepsilon]}, \quad (20)$$

where $1_{[|r',\theta';r_1,\theta_1|\le\varepsilon]}$ is a function that is unity when $|r',\theta';r_1,\theta_1|\le\varepsilon$, and 0 elsewhere. The corresponding stiffness distribution of a two-dimensional spatial oscillator $\underline{s}_{\varepsilon,n,i}(|r',\theta';r_1,\theta_1|)$, thus, becomes

$$\underline{s}_{\varepsilon,n,i}(|r',\theta';r_1,\theta_1|) = \underline{s}_{n,i} g_\varepsilon(|r',\theta';r_1,\theta_1|)$$
$$= (M_{n,i}\omega_{r,n}^2)(1+i\eta) g_\varepsilon(|r',\theta';r_1,\theta_1|), \quad (21)$$

where it applies that $M_{n,i}=M_n/A_{\text{fuzzy}}$ and A_{fuzzy} is the area of the fuzzy connection surface. In the case of a one-dimensional connection boundary, Ref. 7 gives an expression for the force per unit length $\underline{F}_{n,i}'(x_0)$ at x_0 due to the displacement $\underline{u}(x_1)$ at x_1 caused by *only one* spatial oscillator. By replacing this one-dimensional version of g_ε by the new two-dimensional version, we obtain an expression for the relationship between the force per unit area $\underline{F}_{n,i}''(r_0,\theta_0)$ and the displacement $u(r_1,\theta_1)$ that reads

$$\underline{F}_{n,i}''(r_0,\theta_0) = \underline{s}_{\varepsilon,n,i}(|r',\theta';r_1,\theta_1|)\left[\delta_{(r',\theta'),(r_1,\theta_1)} - \frac{\underline{s}_{\varepsilon,n,i}(|r',\theta';r_1,\theta_1|)r_1 dr_1 d\theta_1}{-\omega^2 M_{n,i}+\underline{s}_{n,i}}\right]\underline{u}(r_1,\theta_1), \tag{22}$$

where the infinitesimal area dA_1 is given as $dA_1 = r_1 dr_1 d\theta_1$. Next, to find the force per unit area $\underline{F}_n''(r_0,\theta_0)$ due to a set of infinitely many *identical* spatial oscillators with the base displacement $\underline{u}(r_1,\theta_1)$, Eq. (22) is integrated with respect to (r',θ') over the fuzzy connection surface as

$$\underline{F}_n''(r_0,\theta_0) = \int_{A_{\text{fuzzy}}} \underline{s}_{\varepsilon,n,i}(|r',\theta';r_1,\theta_1|)\left[\delta_{(r',\theta'),(r_1,\theta_1)} - \frac{\underline{s}_{\varepsilon,n,i}(|r',\theta';r_1,\theta_1|)dA_1}{-\omega^2 M_{n,i}+\underline{s}_{n,i}}\right]\underline{u}(r_1,\theta_1)dA'. \tag{23}$$

Finally, this expression can be reduced to

$$\underline{F}_n''(r_0,\theta_0) = \left[\underline{s}_{n,i}\delta_{(r',\theta'),(r_1,\theta_1)} - \frac{\underline{s}_{n,i}^2}{-\omega^2 M_{n,i}+\underline{s}_{n,i}} \times h_\varepsilon(|r_1,\theta_1;r_0,\theta_0|)dA_1\right]\underline{u}(r_1,\theta_1), \tag{24}$$

where the function $h_\varepsilon(|r_1,\theta_1;r_0,\theta_0|)$ is given by

$$\begin{aligned} &h_\varepsilon(|r_1,\theta_1;r_0,\theta_0|) \\ &= \int_{A_{\text{fuzzy}}} g_\varepsilon(|r',\theta';r_1,\theta_1|)g_\varepsilon(|r',\theta';r_0,\theta_0|)dA' \\ &= \int_0^{2\pi}\int_0^{2\varepsilon} g_\varepsilon(|r',\theta';r_1,\theta_1|)g_\varepsilon(|r',\theta';r_0,\theta_0|)r'dr'd\theta'. \end{aligned} \tag{25}$$

It follows that the boundary impedance of the nth set multiplied by dA_1 is given as

$$\begin{aligned} &\underline{z}_{\varepsilon,n}(|r_0,\theta_0;r_1,\theta_1|)dA_1 \\ &= \frac{\underline{s}_{n,i}}{i\omega}\left[\delta_{(r',\theta'),(r_1,\theta_1)} - \frac{\underline{s}_{n,i}}{-\omega^2 M_{n,i}+\underline{s}_{n,i}} \times h_\varepsilon(|r_1,\theta_1;r_0,\theta_0|)dA_1\right], \end{aligned} \tag{26}$$

and by analogy to Eq. (7), the fuzzy boundary impedance becomes

$$\begin{aligned} &\underline{z}_{\text{fuzzy},\varepsilon}(|r_0,\theta_0;r_1,\theta_1|)dA_1 \\ &= -\frac{i2\pi f}{A_{\text{fuzzy}}}\int_{f_{r,\text{lower}}}^{f_{r,\text{upper}}}\left(\frac{f_r^2}{f^2}\right)(1+i\eta)m_{\text{fuzzy}}(f_r) \\ &\quad\times\left[\delta_{(r',\theta'),(r_1,\theta_1)} - \frac{f_r^2(1+i\eta)}{f_r^2(1+i\eta)-f^2} \times h_\varepsilon(|r_1,\theta_1;r_0,\theta_0|)dA_1\right]df_r. \end{aligned} \tag{27}$$

From Eq. (27), it is seen that transfer impedance terms of the fuzzy substructure are proportional to the function $h_\varepsilon(|r_1,\theta_1;r_0,\theta_0|)$. This function can be calculated numerically and the result is shown in Fig. 6(b) for the case $(r_1,\theta_1)=(0,0)$. It is clearly observed that h_ε looks similar to a two-dimensional version of the convolution shown in Fig. 4. Also, it can be seen that h_ε extends to a radius of 2ε relative to (r_1,θ_1) and that the volume under the surface is unity.

B. Determination of the equivalent coupling factor

By analogy to the method in Sec. III, the equivalent coupling factor will now be determined as a function of $c=\varepsilon/\lambda_b$, where λ_b is the vibration wavelength for bending waves. Again, λ_b is suggested to be the free wavelength for simple master structures and twice the distance between adjacent nodes for more complicated master structures. An expression for the equivalent coupling factor is found by extending the expression in Eq. (16) to two dimensions yielding

$$\begin{aligned} \alpha(r_0,\theta_0;c) &= \frac{\int_{A_{\text{fuzzy}}} h_\varepsilon(|r_1,\theta_1;r_0,\theta_0|)\underline{u}(r_1,\theta_1)dA_1}{u(r_0,\theta_0)} \\ &= \frac{\int_0^{2\pi}\int_0^{2\varepsilon} h_\varepsilon(|r_1,\theta_1;r_0,\theta_0|)\underline{u}(r_1,\theta_1)r_1 dr_1 d\theta_1}{\underline{u}(r_0,\theta_0)}. \end{aligned} \tag{28}$$

As for the one-dimensional case, the determination of α requires prior knowledge of the vibration displacements of the master structure. Again this problem is overcome by approximating the displacements by a product of two sinusoidals as

$$\underline{u}(x_1,y_1) = \sin\left(\frac{2\pi}{\lambda_x}x_1\right)\sin\left(\frac{2\pi}{\lambda_y}y_1\right), \tag{29}$$

where λ_x and λ_y are the vibration wavelengths for bending motion in the x and y directions, respectively. By substituting $x_1=r_1\cos(\theta_1)$ and $y_1=r_1\sin(\theta_1)$ in Eq. (29), the displacement is transformed to polar coordinates, giving

$$\underline{u}(r_1,\theta_1) = \sin\left[\frac{2\pi}{\lambda_x}r_1\cos(\theta_1)\right]\sin\left[\frac{2\pi}{\lambda_y}r_1\sin(\theta_1)\right]. \tag{30}$$

Further, the bending wavelength λ_b can be found from the relation between the wave numbers,[21]

$$k_b^2 = k_x^2 + k_y^2 \Leftrightarrow \left(\frac{2\pi}{\lambda_b}\right)^2 = \left(\frac{2\pi}{\lambda_x}\right)^2 + \left(\frac{2\pi}{\lambda_y}\right)^2, \tag{31}$$

which by rearranging becomes

$$\lambda_b = \sqrt{\frac{\lambda_x^2\lambda_y^2}{\lambda_x^2+\lambda_y^2}}. \tag{32}$$

As for the one-dimensional case, it is suggested that λ_b is replaced by the free wavelength for simple master structures and by twice the distance between adjacent nodes for master structures with more complicated eigenfunctions. Again, by only considering positions on the fuzzy connection surface that are at least a distance of 2ε from the edges of the fuzzy,

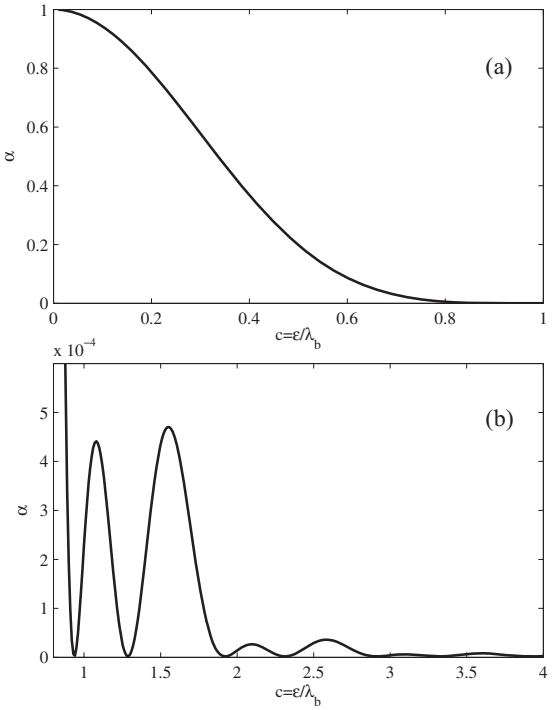

FIG. 7. Variation of the equivalent coupling factor α as a function of $c=\varepsilon/\lambda_b$. (a) Values of c from 0 to 1 and (b) from 0.8 to 4.

an expression for α is found by substituting Eqs. (25) and (30) into Eq. (28). This expression becomes quite complicated and the integrals cannot be solved analytically. Nevertheless, by using numerical integration, α has been determined as a function of $c=\varepsilon/\lambda_b$ and the results are shown in Fig. 7.

First, it should be noted that α does not depend on the forcing position (r_0,θ_0) as long as the response position (r_1,θ_1) is at least a distance of 2ε from the edges of the fuzzy connection surface. Second, it is found that α is insensitive to the specific values of λ_x and λ_y and only depends on λ_b. Figure 7(a) shows that the variation of α resembles the uniformly descending function seen in Fig. 5(a) for values up to $c=0.8$. Again, for values above $c=0.8$, the equivalent coupling factor takes on very small values. Closer inspection of this low value region [see Fig. 7(b)] reveals a different pattern of smooth minima and maxima from that observed in Fig. 5(b). Nevertheless, the equivalent coupling factor still becomes 0 for certain values of c.

V. NUMERCIAL VALIDATION OF EQUIVALENT MODELING METHOD

In a companion paper,[7] it was shown that the spatial memory in the structural fuzzy significantly reduces its damping effect. This finding was achieved by using the equivalent modeling method just described in Sec. II. In the following, the equivalent modeling method will be validated for certain two-dimensional problems by numerical simulations. The finite element method[22] has been used to solve the flexural vibration response of a rectangular plate that is considered as the master; the plate undergoes two-dimensional bending vibration and is assumed to be simply supported along all four edges that have side lengths L_x and L_y, with an

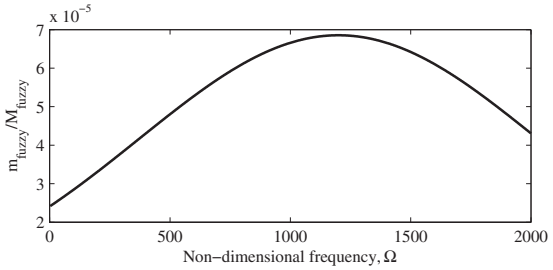

FIG. 8. Normalized resonating mass per unit frequency described by a normal distribution with a centre frequency f_{r0} corresponding to $\Omega=1200$ and a standard deviation std$=0.7f_{r0}$.

aspect ratio given by $L_y=1.3L_x$. A fuzzy substructure is attached to the plate on the whole surface area $A=L_xL_y$, so that $A_{\text{fuzzy}}=A$. The loss factor of the plate is set to 0.005, whereas the loss factor of the fuzzy oscillator springs has been chosen to be 0.03. The resonating mass per unit frequency $m_{\text{fuzzy}}(f_r)$ is a normal distribution given as

$$m_{\text{fuzzy}}(f_r)=\frac{M_{\text{fuzzy}}}{\text{std}\cdot\sqrt{2\pi}}e^{-(f_{r0}-f_r)^2/(2\cdot\text{std}^2)}, \tag{33}$$

where f_{r0} is the center frequency and std is the standard deviation. For this distribution, the bounding frequencies $f_{r,\text{lower}}$ and $f_{r,\text{upper}}$ corresponds to $\Omega=0$ and ∞, respectively. The chosen mass distribution is shown in Fig. 8 as a function of the plate's nondimensional frequency Ω defined as

$$\Omega=\omega\sqrt{\frac{12\rho(1-\nu^2)}{E}}\frac{\sqrt{L_x^2+L_y^2}}{h}, \tag{34}$$

where h is the plate thickness, and ρ, E, and ν are the density, Young's modulus, and Poisson's ratio of the plate, respectively. The center frequency f_{r0} corresponds to $\Omega=1200$ and the standard deviation std$=0.7f_{r0}$. The total mass of the attached fuzzy M_{fuzzy} is one-twentieth of the plate mass, ρAh. Also, the free bending wavelength λ_b in the master plate is found[21]

$$\lambda_b=2\pi\sqrt{\frac{L_x^2+L_y^2}{\Omega}}. \tag{35}$$

For the following response prediction, the boundary impedance of the fuzzy is computed by numerical integration of the integrals in Eqs. (27) and (10), where L_{fuzzy} is replaced by A_{fuzzy} in the latter. Further, $\varepsilon=c\lambda_b$ is assumed to be constant with frequency implying that c and α, respectively, increases and decreases with frequency.

First examined is the effect of a simple fuzzy without spatial memory that is modeled by using Eq. (27) with $\varepsilon=0$. Figure 9 shows results for the vibration velocity response per unit harmonic force of the simply supported master plate, with and without such a fuzzy substructure. Here, the response location (x,y) and excitation position (x_0,y_0) coincide, so the results represent the direct mobility of the system. Since the fuzzy has no spatial memory, it is clearly seen that it has a strong damping effect on the vibration response of the master. This effect mainly occurs from $\Omega=500$ and upwards, where the resonating mass per unit frequency has an appreciable value; that is, it is approximately

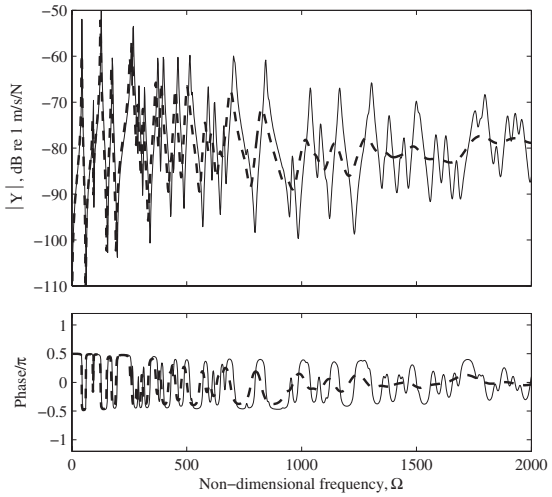

FIG. 9. Vibration velocity response per unit harmonic force of a simply supported plate, $\underline{Y}(x,y;x_0,y_0)=\underline{v}(x,y)/\underline{F}(x_0,y_0)$, at $(x,y)=(x_0,y_0)=(0.175L_x,0.5525L_x)$. Curves: —, without structural fuzzy and ---, with structural fuzzy without spatial memory using Eq. (27) with $\varepsilon=0$.

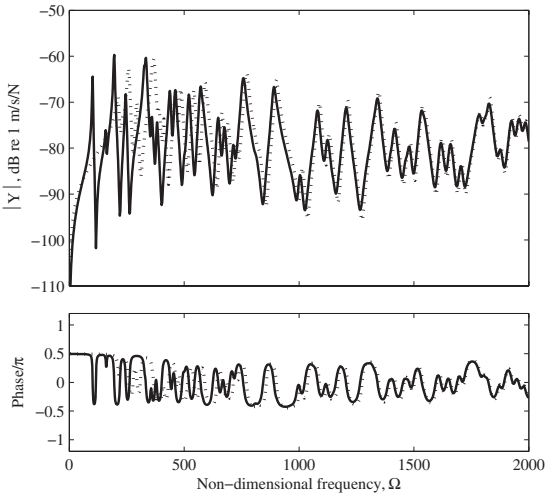

FIG. 11. Vibration velocity response per unit harmonic force of a simply supported plate, $\underline{Y}(x,y;x_0,y_0)=\underline{v}(x,y)/\underline{F}(x_0,y_0)$, at $(x,y)=(x_0,y_0)=(0.175L_x,0.5525L_x)$. Conditions: Structural fuzzy with $\varepsilon=0.2L_x$ and modeled by —, spatial oscillators using Eq. (27) and ⋯⋯, equivalent local oscillators using Eq. (10).

half or more of its maximum value according to the results in Fig. 8. At frequencies above $\Omega=1000$, it is furthermore seen that the direct mobility closely approaches the asymptote of −80 dB for a master plate of infinite size. It should be noted that such high damping effect only occurs at early and moderate times for fuzzy substructures consisting of a finite number of oscillators, which are excited by an impulse, since the "absorbed" energy returns from the fuzzy to the master at later times.[15,16] Drexel and Ginsberg[23] also investigated this damping effect for a master cantilever beam with a finite number of spatially distributed discrete oscillators.

An example of the *transfer* mobility of the plate with and without structural fuzzy is shown in Fig. 10. As in Fig. 9, the vibration velocity response of the master is reduced significantly due to the fuzzy from about $\Omega=500$ and upwards. Also, at high frequencies, the response is strongly reduced and is even less than the transfer mobility of a corresponding infinitely large plate which has a low value of −94 dB at $\Omega=2000$.

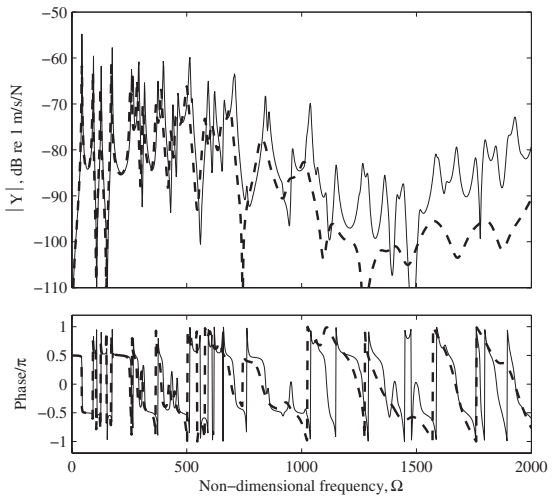

FIG. 10. As in Fig. 9, but for response at $(x,y)=(0.575L_x,1.1375L_x)$ and excitation at $(x_0,y_0)=(0.175L_x,0.5525L_x)$.

Next presented is the validation of the equivalent prediction method. This validation consists in a comparison of simulated responses based on the prediction method using the equivalent local oscillators [Eq. (10)] and the reference method based on spatial oscillators [Eq. (27)]. Consider the simply supported master plate with an attached structural fuzzy that has a constant and *high* spatial memory $\varepsilon=0.2L_x$. By using this value of ε in Eq. (28), the corresponding equivalent coupling factor is found as a function of frequency and substituted in Eq. (10). A comparison of the two predictions is shown in Fig. 11 that displays the vibration responses in terms of the direct mobility. This reveals that there is a very good agreement between the two prediction methods from about $\Omega=500$ and upwards. Significant deviations occur only at low frequencies because of the assumed sinusoidal vibration [Eq. (29)]. Since the plate's edges are simply supported, the sinusoidals are only a really good approximation around the plate's natural frequencies; that is, the frequencies where the conditions $2L/\lambda_x=1,2,3,\ldots$, and $2L/\lambda_y=1,2,3,\ldots$, are both fulfilled. Nevertheless, this error in the estimation of α rapidly reduces with increasing frequency. Evidently, truncation errors that occur at all frequencies due to the constant value of ε do not have a large influence on the prediction based on equivalent oscillators. Moreover, compared to the previous case of no spatial memory (Fig. 9), it is also observed that the spatial memory drastically reduces the damping effect of the fuzzy. In the companion paper,[7] it was shown how the damping effect decreases when α is reduced. The reason for this is that a reduction in α corresponds to an increase in ε. Thus, due to the local angular motion in the master structure, the spring elements in the spatial oscillators counteract one another when $\varepsilon>0$.

The corresponding transfer mobility of the master plate with structural fuzzy of high spatial memory is shown in Fig. 12. Again, the two predictions are seen to be in good agree-

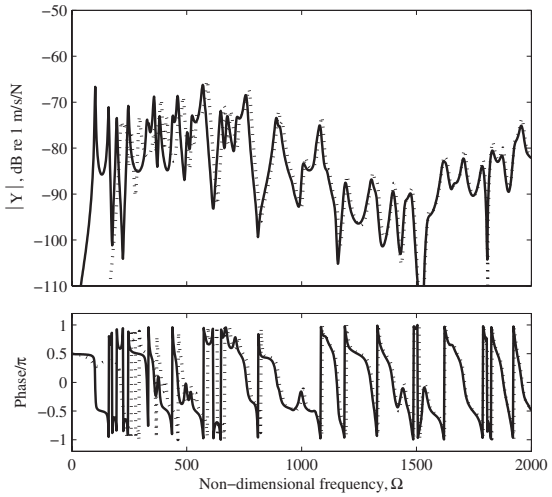

FIG. 12. As in Fig. 11, but for response at $(x,y)=(0.575L_x,1.1375L_x)$ and excitation at $(x_0,y_0)=(0.175L_x,0.5525L_x)$.

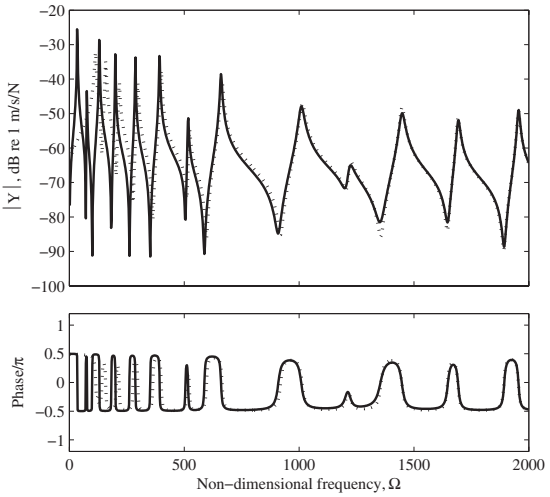

FIG. 13. Vibration velocity response per unit harmonic force of a simply supported beam, $\underline{Y}(x,x_0)=\underline{v}(x)/\underline{F}(x_0)$, at $x=x_0=0.445L$. Conditions: Structural fuzzy with $\varepsilon=0.1L$ modelled by —, spatial oscillators using Eq. (7) and ·····, equivalent local oscillators using Eq. (10).

ment at frequencies from $\Omega=500$ and upwards. Furthermore, the spatial memory in the fuzzy here is also seen to radically reduce the damping effect.

The equivalent method of prediction performs poorly at low frequencies, say, below $\Omega=500$, because the sine-function approximations of the master vibration pattern have to hold for two dimensions. For a one-dimensional master structure, however, this approximation only involves one direction, and the equivalent method is, therefore, expected to perform well also at lower frequencies. To demonstrate this, a beam with one-dimensional wave motion is considered as the master. A fuzzy substructure is attached on the whole length L of the beam, so that $L_{\text{fuzzy}}=L$. The loss factor of the beam is set to 0.005, whereas the loss factor of the fuzzy oscillator springs has been chosen to be 0.03. The resonating mass per unit frequency is again a normal distribution where the center frequency f_{r0} corresponds to $\Omega=1200$ and std $=0.27f_{r0}$. The nondimensional frequency Ω for the beam is defined as

$$\Omega=\omega\sqrt{\frac{12\rho}{E}}\frac{L^2}{h}. \tag{36}$$

In this example, the spatial memory $\varepsilon=0.1L$ and the total mass of the fuzzy M_{fuzzy} is one-twentieth of the beam mass, ρSL, where S is its cross-sectional area. The vibration velocity of the beam in terms of the input mobility is shown in Fig. 13. It is seen that the results of the two types of predictions given by Eqs. (7) and (10) are almost coinciding from $\Omega=250$ and upwards. Thus, as was anticipated, the equivalent method is found to apply at lower frequencies in the one-dimensional case. The results show that the prediction is reliable at least one octave lower in frequency for the two-dimensional case.

VI. SUMMARY AND DISCUSSION

In 1993, Soize[3] introduced a method for modeling structural fuzzy with a continuous boundary. This method was later extended[17] and validated.[18] Moreover, a part of this method was systematically examined and *reformulated* in a more simple form in a companion paper.[7] The main objective of the present paper is to extend the method to two dimensions and to improve its usability.

Structural fuzzy with a continuous boundary can be modeled by including the stiffness of the fuzzy in terms of a spatial memory. Soize implemented such spatial memory by introducing the so-called spatial oscillators. However, to make the implementation of the fuzzy boundary impedance viable, he replaced these nonlocal spatial oscillators with *local equivalent oscillators* that can imitate boundary forces imposed on the master. This approximation required the introduction of the *equivalent coupling factor* that describes the relationship between the width of the spatial oscillators and the stiffness of the local equivalent oscillators. The current paper has presented a simple and general method for determining this factor as a function of a practical parameter given by the ratio between the width of the spatial oscillators and the free structural wavelength in the master structure. By assuming that the vibration pattern of the master structure can be approximated by one or more sinusoidals and that truncation effects at the end of the fuzzy connection boundary can be ignored, an expression for the equivalent coupling factor has been derived. This expression was evaluated analytically for one-dimensional wave motion in the master structure, and it is revealed that the solution is a very simple expression in the form of a sink function to the power of 4.

For instructive reasons, the method of including memory in the structural fuzzy was originally formulated for a structural fuzzy attached to the master through a one-dimensional boundary. In the present paper, this formulation has been extended to two dimensions, so that it applies for structural fuzzy attached to the master through an area. This is achieved by introducing a two-dimensional stiffness distribution for the spatial oscillator. Additionally, an expression for the equivalent coupling factor is derived and computed numerically as a function of a practical parameter, that is, the ratio between spatial memory and the free wavelength of the

vibration in the master. This solution proved to be closely related to the solution for one-dimensional wave motion in the master.

A validation of the equivalent method by using local equivalent oscillators as a replacement for the spatial oscillators has not previously been published in open literature. In the present paper, the validity of the method has, therefore, been tested by comparing numerical simulations of the response of a master plate with attached structural fuzzy. Results, based on the use of spatial oscillators and equivalent oscillators show a very good agreement for frequencies above $\Omega=500$, where Ω is the nondimensional frequency of the master structure. Below this frequency, errors are mainly caused by the assumption of sinusoidal vibration displacement. For a master beam with one-dimensional wave motion and a fuzzy substructure attached on the whole length, it is revealed that good agreement between predictions is already achieved from about $\Omega=250$. The reason is that the assumption of sinusoidal vibration displacement only has to be fulfilled for one dimension.

The present paper has made various assumptions in order to develop a viable method for modelling structural fuzzy with a continuous boundary. First of all, it has been assumed that the size of the spatial memory in the fuzzy is known beforehand. In real-life engineering structures, the spatial memory is often unknown and relatively difficult to measure. Further, the method of determining the equivalent coupling factor only applies for fairly simple master structures, where its vibration pattern can be approximated as one or more sinusoidals in the midfrequency range. Also important is the estimation of the distribution of resonating mass per unit frequency. It is clear that practical methods for determining these fuzzy parameters are still needed.

[1]C. Soize, "Probabilistic structural modeling in linear dynamic analysis of complex mechanical systems, part I," (English edition), Rech. Aerosp. **5**, 23–48 (1986).

[2]F. Chabas, A. Desanti, and C. Soize, "Probabilistic structural modelling in linear dynamic analysis of complex mechanical systems, part II," (English edition), Rech. Aerosp. **5**, 49–67 (1986).

[3]C. Soize, "A model and numerical method in the medium frequency range for vibroacoustic predictions using the theory of structural fuzzy," J. Acoust. Soc. Am. **94**, 849–865 (1993).

[4]J. Ormondroyd and J. P. Den Hartog, "Theory of dynamic vibration absorber," Trans. ASME **50**, APM-241 (1928).

[5]*Noise and Vibration*, edited by R. G. White and J. G. Walker (Ellis Horwood, Chichester, England, 1982), Chap. 25.

[6]D. F. Mead, *Passive Vibration Control* (Wiley, Chichester, England, 1999), Chap. 8.

[7]L. Friis and M. Ohlrich, "Vibration modelling of structural fuzzy with continuous boundary," J. Acoust. Soc. Am. **123**, 718–728 (2008).

[8]A. D. Pierce, V. W. Sparrow, and D. A. Russell, "Fundamental structural-acoustic idealizations for structures with fuzzy internals," J. Vibr. Acoust. **117**, 339–348 (1995).

[9]M. Strasberg and D. Feit, "Vibration damping of large structures induced by attached small resonant structures," J. Acoust. Soc. Am. **99**, 335–344 (1996).

[10]G. Maidanik and K. J. Becker, "Various loss factors of a master harmonic oscillator coupled to a number of satellite harmonic oscillators," J. Acoust. Soc. Am. **103**, 3184–3194 (1998).

[11]G. Maidanik and K. J. Becker, "Characterization of multiple-sprung masses for wideband noise control," J. Acoust. Soc. Am. **106**, 3109–3118 (1999).

[12]G. Maidanik and K. J. Becker, "Criteria for designing multiple-sprung masses for wideband noise control," J. Acoust. Soc. Am. **106**, 3119–3127 (1999).

[13]G. Maidanik and K. J. Becker, "Dependence of the induced loss factor on the coupling forms and coupling strengths: linear analysis," J. Sound Vib. **266**, 15–32 (2003).

[14]G. Maidanik and K. J. Becker, "Induced noise control," J. Sound Vib. **277**, 1041–1058 (2004).

[15]R. L. Weaver, "The effect of an undamped finite degree of freedom "fuzzy" substructure: Numerical solutions and theoretical discussion," J. Acoust. Soc. Am. **100**, 3159–3164 (1996).

[16]A. Carcaterra and A. Akay, "Transient energy exchange between a primary structure and a set of oscillators: Return time and apparent damping," J. Acoust. Soc. Am. **115**, 683–696 (2004).

[17]C. Soize, "Estimation of fuzzy substructure model parameters using the mean power flow equation of the fuzzy structure," J. Vibr. Acoust. **120**, 279–286 (1998).

[18]C. Soize, "Estimation of fuzzy structure parameters for continuous junctions," J. Acoust. Soc. Am. **107**, 2011–2020 (2000).

[19]A. D. Pierce, "Resonant-frequency-distribution of internal mass inferred from mechanical impedance matrices, with application to fuzzy structure theory," J. Vibr. Acoust. **119**, 324–333 (1997).

[20]G. Maidanik, K. J. Becker, and L. J. Maga, "Replacement of a summation by an integration in structural acoustics," J. Sound Vib. **291**, 323–348 (2006).

[21]L. Cremer, M. Heckl, and E. E. Ungar, *Structure-Borne Sound* (Springer-Verlag, Berlin, 1988).

[22]R. Cook, D. S. Malkus, M. F. Plesha, and R. J. Witt, *Concepts and Applications of Finite Element Analysis* (Wiley, New York, 2002).

[23]M. V. Drexel and J. H. Ginsberg, "Modal overlap and dissipation effects of a cantilever beam with multiple attached oscillators," J. Vibr. Acoust. **123**, 181–187 (2001).

5.4 Discussion of the results obtained in paper II and III

In paper III it is shown that modeling of structural fuzzy with two-dimensional spatial memory is possible using equivalent local oscillators above a non-dimensional frequency of $\Omega = 500$ of the master. Sometimes, however, it is desired to model structural fuzzy with spatial memory at lower frequencies. A technique for achieving such modeling is discussed in the following.

Figure 13 in paper II shows the apparent mass and damping for four different values of the equivalent coupling factor α. In fig. 13b it seems as if the apparent damping is directly proportional to α. This proportionality can be utilized for approximating the damping effect at non-dimensional frequencies below 500. An investigation verifying general proportionality between the apparent damping and the equivalent coupling factor is offered in appendix A.

In the case of a fuzzy substructure without spatial memory where $\alpha = 1$, the apparent damping and the resonating mass distribution m_{fuzzy} are related through the simple expression given in Pierce *et. al.* (1995) reading

$$R_{app}(\omega) = \frac{\pi\omega^2}{2} m_{fuzzy}(\omega) . \tag{5.1}$$

Strictly speaking this expression is valid only for lossless fuzzy oscillators. Nevertheless, Pierce demonstrated that it is an excellent approximation for any realistic damping in the structural fuzzy, that is for $\zeta < 0.1$. To transform eq. (5.1) into a function of frequency instead of angular frequency, it is divided with 2π and the frequency dependent apparent damping hereby becomes

$$R_{app}(f) = \pi^2 f^2 m_{fuzzy}(f) . \tag{5.2}$$

From this expression it is revealed that the apparent damping also is proportional to the resonating mass distribution m_{fuzzy}. Due to the proportionality between α and the apparent damping it is easily shown that a general approximate expression for the apparent damping is given as

$$R_{app}(f) = \pi^2 f^2 m_{fuzzy}(f)\alpha(f) . \tag{5.3}$$

This expression reveals that the apparent damping is governed by the *product* of the resonating mass distribution and the equivalent coupling factor.

Consider a fuzzy substructure with the total mass $M_{fuzzy,1}$, resonating mass distribution $m_{fuzzy,1}$ and the equivalent coupling factor α_1 resulting in the apparent damping R_{app}. According to the expression in eq. (5.3), the same apparent damping results from a different fuzzy substructure having the fuzzy parameters $m_{fuzzy,2}$ and α_2 if it applies that

$$m_{fuzzy,2}(f)\alpha_2(f) = m_{fuzzy,1}(f)\alpha_1(f)\,. \tag{5.4}$$

A structural fuzzy having the reduced resonating mass distribution $m_{fuzzy,2}(f) = m_{fuzzy,1}(f)\alpha_1(f)$ and the constant equivalent coupling factor $\alpha_2 = 1$ therefore fulfills this criterion. This is very fortunate as the case of a unity equivalent coupling factor corresponds to a fuzzy substructure without spatial coupling. Such a fuzzy substructure is conveniently modeled by the simple boundary impedance given in eq. (3) in paper II that is applicable at all frequencies.

However, using the reduced resonating mass distribution $m_{fuzzy,2}$ to model a fuzzy substructure with spatial coupling, also results in a reduced total mass $M_{fuzzy,2}$. This is accounted for by modeling the residual mass $M_{fuzzy,res}$ as distributed *pure* mass. The residual mass is determined as

$$M_{fuzzy,res} = M_{fuzzy,1} - M_{fuzzy,2} = \int_{f_{r,lower}}^{f_{r,upper}} m_{fuzzy,1}(f_r)df_r - \int_{f_{r,lower}}^{f_{r,upper}} m_{fuzzy,2}(f_r)df_r\,. \tag{5.5}$$

In addition, for a constant value of α the residual mass yields $M_{fuzzy,res} = \alpha M_{fuzzy}$. By expanding the expression in eq. (3) in paper II with a contribution of distributed pure mass, the boundary impedance of the "reduced-mass" fuzzy substructure $z_{fuzzy,red}(x_0, f)$ finally becomes

$$\underline{z}_{fuzzy,red}(x_0, f) = \\ -\frac{i2\pi f}{A}\int_{f_{r,lower}}^{f_{r,upper}} \left(\frac{f_r^2}{f^2}\right)(1+i\eta)m_{fuzzy,2}(f_r)\left(1-\frac{f_r^2(1+i\eta)}{f_r^2(1+i\eta)-f^2}\right)df_r + \frac{i2\pi f(M_{fuzzy,1}-M_{fuzzy,2})}{A}\,. \tag{5.6}$$

Using this *reduced-mass* impedance, the total mass of the fuzzy is correct whereas the apparent mass becomes somewhat different. This is acceptable though, as the apparent mass load is much less important than the apparent damping when modeling complex structures.

As an example, a structural fuzzy similar to that examined in paper II is considered. For comparison the apparent mass and damping has been computed by using the fuzzy boundary impedances in eq. (3) in paper II and eq. (5.6), respectively. Results are shown in fig. 5.1 for α-

values of 0.75 and 0.25. It is seen that the apparent damping curves calculated by eq. (3) in paper II and eq. (5.6) are practically coinciding. Considering the apparent mass, however, it is clear that the impedances based on eq. (3) in paper II are stiffness-like at low frequencies, whereas the impedances based on eq. (5.6) are mass-like. For the high value of $\alpha = 0.75$ it is seen that the two curves showing apparent mass become close for non-dimensional frequencies above say $\Omega = 1000$. However, this is not the case for the low α-value of 0.25 where the apparent mass based on eq. (5.6) is notably higher. As mentioned, though, the apparent mass is much less significant than the apparent damping when modeling structural fuzzy.

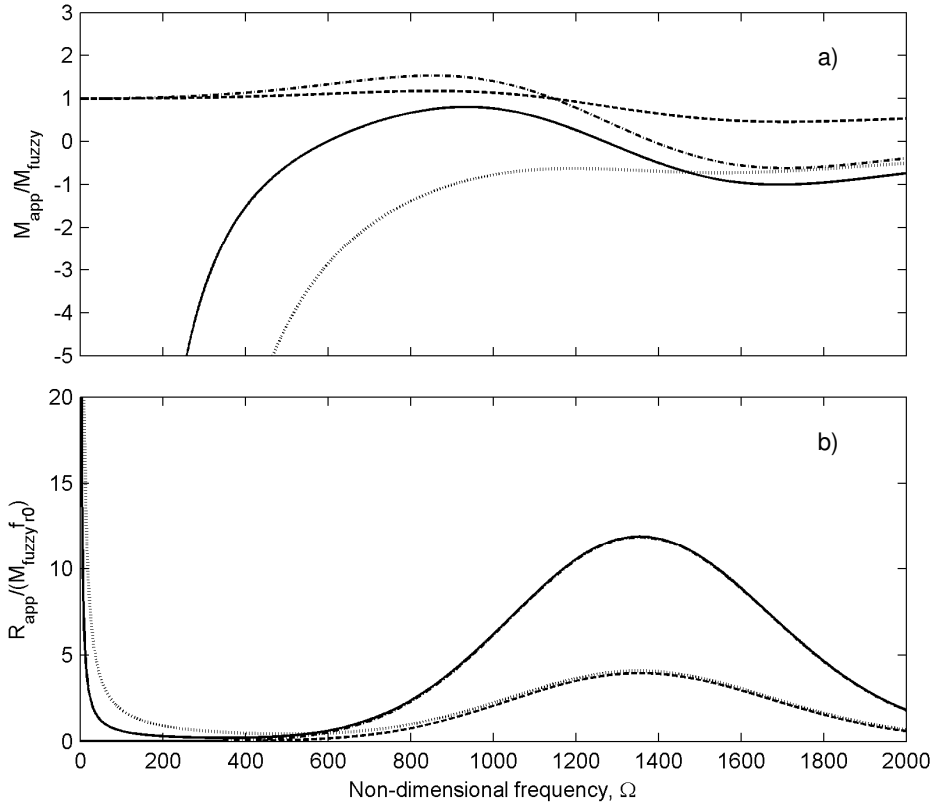

Figure 5.1. (a) Normalized apparent mass and (b) normalized apparent damping of the fuzzy boundary impedance for a structural fuzzy similar to that considered in fig. 11 in paper II. Results based on eq. (3) in paper II for $\alpha = 0.75$ (solid line) and $\alpha = 0.25$ (dotted line); results based on eq. (5.6) for $\alpha = 0.75$ (dashdot line) and $\alpha = 0.25$ (dashed line).

6 Experimental method for estimating fuzzy parameters

6.1 Introduction

In the previous section the theory of fuzzy structures was studied theoretically and extended in two journal papers. The next step is to use the method for modeling the vibrations of a real-life hearing aid. Such practical use, however, requires a functional method for determining the fuzzy parameters, that is, the resonating mass per unit resonance frequency and the equivalent coupling factor.

As mentioned in the section concerning method development the subject of estimating fuzzy parameters has been addressed by Soize (1998) and Soize and Bjaoui (2000). In these papers it is assumed that the modal density and internal damping of the structural fuzzy are measured or estimated from the design. Specifically how to achieve this in practice is not mentioned. In reality estimation of the modal density and internal damping is very difficult when it comes to the internal components of the hearing aid. The method for estimating fuzzy parameters described by Pierce (1997) involves measurement of the fuzzy impedance matrix. However, the fuzzy behaviour of hearing aid internals is partly governed by the indefinable contacts between individual components. If the components are removed from the shell of the hearing aid, they are not interconnected anymore, and it is therefore very difficult to obtain experimental access to the complete complex structure. Hence, an indirect method for estimating the fuzzy parameters is strongly needed.

In the following an indirect but practical method for determining the fuzzy parameters for a real-life complex structure will be presented. The author has developed this novel method with inspiration from Soize (1998). The method, which requires a prototype, is based on in-situ measurements and should be considered as a first attempt to determine the fuzzy parameters of a complex substructure that is considered as homogeneous structural fuzzy. The method requires that the complex substructure is attached to a "dummy master" in the same way it is attached to its actual master. This dummy master may for example be the master itself or the part of the master where the fuzzy is attached. Using this method, an equation for the power equilibrium of the considered system consisting of the dummy master and one or more similar fuzzy substructures is set up. The introduced apparent damping in the master is then estimated from the power equilibrium and the frequency distribution of the resonating mass and the equivalent coupling factor are hereafter extracted by backwards calculation. All quantities in the equation of the power

equilibrium are obtained by measuring the transmitted power during excitation and by measuring the spatially averaged mean-square vibration velocities of the master and the fuzzy connection surfaces, respectively.

After presenting the method for determining fuzzy parameters, it is applied to an example of a realistic but theoretically constructed complex system. Fuzzy response simulations using the estimated fuzzy parameters are hereafter validated with the known responses of the complex system. Finally in section 7 the method is employed to estimate the fuzzy parameters of the hearing aid internals in question.

6.2 Estimation of the apparent damping

In Pierce *et. al.* (1995) it was shown that the vibrations of a system consisting of a master with attached structural fuzzy can be modeled by adding an extra frequency dependent mass term and damping term to the master's equation of motion. The power balance for this system implies that the power P_{exc} supplied by excitation forces is equal to the total losses in the whole system. These losses consist of two contributions that are the power P_{fuzzy} "dissipated" in the structural fuzzy and the structural loss P_{η} in the material of the master. The power balance is therefore

$$P_{exc} = P_{fuzzy} + P_{\eta}. \tag{6.1}$$

Typically P_{fuzzy} is significantly larger than P_{η} at frequencies where the fuzzy oscillators are resonating. Outside this frequency range it applies that $P_{fuzzy} = 0$. If the master is excited by a harmonic point force $F_{exc} = Fe^{i\omega t}$ then the transmitted power becomes (see Cremer *et. al.*, 1988)

$$P_{exc} = \frac{1}{2}\left|F_{exc}\right|^2 \mathrm{Re}(Y_{00}), \tag{6.2}$$

where Y_{00} is the complex direct mobility of the total system. Further, the power dissipated into the structural fuzzy is given in Strasberg and Feit (1996) and is calculated as

$$P_{fuzzy} = \int_{\Omega_{fuzzy}} \frac{R_{app}}{A_{fuzzy}} v_{rms}^2 d\Omega_{fuzzy}, \tag{6.3}$$

where v_{rms} is the rms-value of the master's vibration velocity, R_{app} is the total apparent damping of the fuzzy and A_{fuzzy} is the area of the surface Ω_{fuzzy} where the fuzzy is connected. It should be noted that the ratio (R_{app} / A_{fuzzy}) expresses the damping force per unit area and per unit velocity at the fuzzy connection surface; this frequency-dependent quantity is considered to be the same at all positions due to the homogeneity of the fuzzy. By performing the integration in eq. (6.3) the power P_{fuzzy} becomes a function of the spatially averaged mean-square velocity of the master $\left\langle v_{rms}^2 \right\rangle_{fuzzy}$ where the fuzzy is attached. The dissipated power thus becomes

$$P_{fuzzy} = R_{app} \left\langle v_{rms}^2 \right\rangle_{fuzzy} . \tag{6.4}$$

It is a clear advantage to express P_{fuzzy} as a function of $\left\langle v_{rms}^2 \right\rangle_{fuzzy}$ since this quantity is possible to determine experimentally.

The expression for the time-averaged structural losses in the master structure P_η is found in several text books (see for example Mead, 1999) and is given as

$$P_\eta = \omega \eta E_{pot,\max} , \tag{6.5}$$

where η is the loss factor of the master structure and $E_{pot,\max}$ is its maximum potential. The loss factor can be determined using traditional methods (see Cremer *et al.*, 1988) whereas the maximum potential energy is found by integrating the product of the master's stress σ and strain ε over the surface Ω_{master} as

$$E_{pot,\max} = \int_{\Omega_{master}} \sigma \varepsilon \, d\Omega_{master} . \tag{6.6}$$

Unfortunately the stresses and strains are not easy to measure and $E_{pot,\max}$ is therefore not directly accessible from experiments. However, in the frequency range where the master has some modes the maximum kinetic energy $E_{kin,\max}$ in the master is of the same order of magnitude as the maximum potential energy $E_{pot,\max}$. As demonstrated in the next section it is therefore reasonable to approximate $E_{pot,\max}$ with $E_{kin,\max}$. The maximum kinetic energy is given as (see Cremer *et. al.*, 1988)

$$E_{kin,\max} = \int_{\Omega_{master}} \rho h v_{rms}^2 d\Omega \ , \tag{6.7}$$

where ρ and h is the density and thickness of the master structure, respectively. In cases of ρ and h being nearly constant the maximum kinetic energy becomes

$$E_{kin,\max} = \rho h A_{master} \left\langle v_{rms}^2 \right\rangle_{master} \ , \tag{6.8}$$

where $\left\langle v_{rms}^2 \right\rangle_{master}$ is the spatially averaged mean-square velocity of the master. Fortunately, this velocity is possible to determine experimentally. By assuming that $E_{kin,\max} \approx E_{pot,\max}$ the structural losses in the master P_η becomes

$$\begin{aligned} P_\eta &\approx \omega \eta E_{kin,\max} \\ &\approx \omega \rho h \eta A_{master} \left\langle v_{rms}^2 \right\rangle_{master} . \end{aligned} \tag{6.9}$$

Next, by substituting eq. (6.4) into eq. (6.1) and by rearranging, the sought expression for R_{app} yields

$$R_{app} = \frac{P_{exc} - P_\eta}{\left\langle v_{rms}^2 \right\rangle_{fuzzy}} \ . \tag{6.10}$$

Finally, by inserting eqs (6.2) and (6.9) in eq. (6.10) we obtain an approximate expression for R_{app} in terms of measurable quantities only:

$$R_{app} \approx \frac{\frac{1}{2}\left|F\right|^2 \mathrm{Re}(Y_{00}) - \omega \rho h \eta A_{master} \left\langle v_{rms}^2 \right\rangle_{master}}{\left\langle v_{rms}^2 \right\rangle_{fuzzy}} \ . \tag{6.11}$$

As mentioned earlier, P_{fuzzy} and therefore also P_{exc} is much larger than P_η in the frequency range where the structural fuzzy is resonating and it is therefore *not* necessary to use the *exact* value of P_η to obtain a good estimate for R_{app}. In some cases where η is very small, P_η may even be neglected completely. According to eq. (6.10) neglecting η, results in a minor over-estimation of R_{app}.

6.3 Determination of the resonating mass distribution and the equivalent coupling factor

Let us assume that the apparent damping R_{app} of a fuzzy substructure has been estimated experimentally using eq. (6.11) in a frequency range from 0 Hz up to $f_{\max}$. It is further assumed that the fuzzy substructure has the unknown resonating mass distribution $m_{fuzzy,1}$ and the unknown equivalent coupling factor α_1. Moreover, the total mass of the fuzzy substructure $M_{fuzzy,1}$ is known and it applies that

$$M_{fuzzy,1} = \int_0^{\infty} m_{fuzzy,1}(f)df \ . \tag{6.12}$$

It is now desired to determine the fuzzy parameters of an equivalent structural fuzzy resulting in the same damping R_{app}. According to eq. (5.4) we therefore seek a resonating mass distribution $m_{fuzzy,2}$ and an equivalent coupling factor α_2 for which it applies that $m_{fuzzy,2}\alpha_2 = m_{fuzzy,1}\alpha_1$. This equivalent structural fuzzy is to be modeled using the reduced-mass technique discussed in section 5.4. The equivalent coupling factor is therefore chosen to be $\alpha_2 = 1$ and the resonating mass distribution $m_{fuzzy,2}$ can then be determined by rearranging the expression from eq. (5.3) to

$$m_{fuzzy,2}(f) = \frac{R_{app}(f)}{\pi^2 f^2 \alpha_2} = \frac{R_{app}(f)}{\pi^2 f^2} \ . \tag{6.13}$$

Hereafter, the total resonating mass $M_{fuzzy,2}$ between 0 Hz and $f_{\max}$ is determined as

$$M_{fuzzy,2} = \int_0^{f_{\max}} m_{fuzzy,2}(f)df \ . \tag{6.14}$$

This total resonating mass can take on values in the interval from 0 to $M_{fuzzy,1}$. In the case of $\alpha_1(f) = 1$ we have that $M_{fuzzy,2} = M_{fuzzy,1}$ and that $m_{fuzzy,2} = m_{fuzzy,1}$. On the other hand, if either $\alpha_1(f)$ is less than unity at any frequency or the structural fuzzy is resonating up to a higher

frequency than $f_{\max}$ it applies that $M_{fuzzy,2} < M_{fuzzy,1}$. In such a case, it is necessary to account for the residual mass $M_{fuzzy,res}$ given in eq. (5.5) as $M_{fuzzy,res} = M_{fuzzy,1} - M_{fuzzy,2}$. Hence, the actual fuzzy parameters $m_{fuzzy,1}$ and α_1 are not determined, but instead the influence of the structural fuzzy is modeled with the equivalent fuzzy substructure defined by $m_{fuzzy,2}$ and $\alpha_2 = 1$.

If one wish to model the structural fuzzy using equivalent local oscillators the equivalent coupling factor may be set to a constant value of

$$\alpha_2 = \frac{M_{fuzzy,2}}{M_{fuzzy,1}}. \tag{6.15}$$

Moreover, the corresponding resonating mass distribution $m'_{fuzzy,2}$ is chosen to

$$m'_{fuzzy,2} = m_{fuzzy,2} / \alpha_2, \tag{6.16}$$

such that it applies that

$$M_{fuzzy,1} = \int_0^{f_{\max}} m'_{fuzzy,2}(f)df. \tag{6.17}$$

According to eq. (5.4) a fuzzy substructure with such parameters results in the same apparent damping R_{app} as a fuzzy substructure with the parameters $m_{fuzzy,2}$ and $\alpha_2 = 1$.

It should be kept in mind that the main goal of the theory of fuzzy structures is to model the *influence* of an attached complex structure. We are therefore not interested in the actual behavior of the fuzzy, which is regarded as a "black box". Hence, it is not important if a fuzzy substructure is modeled in terms of its actual fuzzy parameters $m_{fuzzy,1}$ and α_1 or a set of alternative fuzzy parameters $m_{fuzzy,2}$ and α_2.

6.4 Numerical example of the estimation of fuzzy parameters

6.4.1 Two-dimensional master structure with a complex substructure

The presented estimation method will now be examined and validated for a specific example representing a realistic master structure with an attached complex substructure. Considered is a two-dimensional master in form of a freely suspended rectangular plate. A complex structure consisting of fuzzy oscillators is attached to the master through a rectangular area as shown in fig. 6.1a. This complex substructure consists of 609 different simple oscillators. The oscillators are randomly attached to the master structure and there is high modal overlap between the oscillator resonances. Spatial coupling between the oscillators is achieved by imbedding all the oscillator masses in a thin plate as illustrated in fig. 6.1b. The thin plate has a total weight of 10% of the master's weight whereas the oscillators has a total weight of 20% of the master's weight.

The master plate has a constant thickness of 1 mm and side lengths of 60 mm and 27 mm in the *x*- and *y*-direction, respectively corresponding to an area of $A_{master} = 1620$ mm. Moreover, the master plate has a density of $\rho = 1050$ kg/m^3, a Young's modulus of $E = 3 \cdot 10^9$ Pa, a loss factor of $\eta = 0.005$ and a Poisson's ratio of $\nu = 0.33$. The rectangular fuzzy connection surface has side lengths of 28 mm and 20 mm in the *x*- and *y*-direction, respectively. This gives an area of $A_{fuzzy} = 560$ mm^2. The thin plate imbedding the oscillator masses has a thickness of 0.3 mm and it is of the same material as the master.

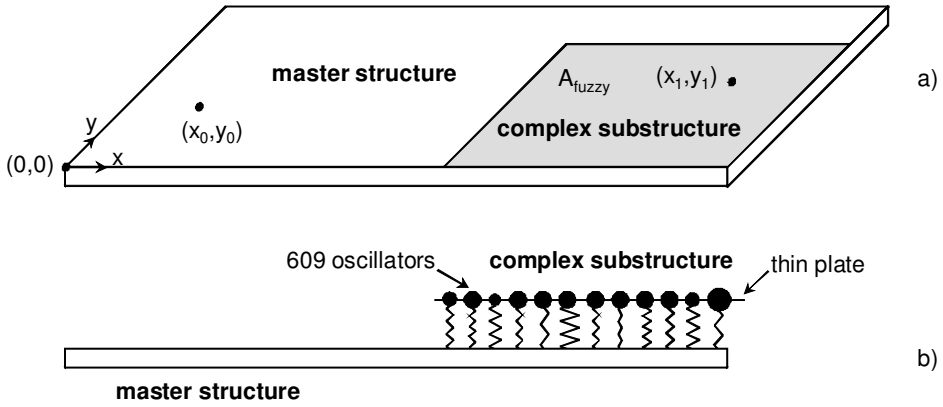

Figure 6.1. Master plate with an attached complex substructure of interconnected oscillators. (a) Master structure and fuzzy connection surface; (b) Construction of the complex substructure.

6.4.2 Vibration response of the master

Using finite element analysis, responses of the master to a unit harmonic point force excitation at $(x_0, y_0) = (13 \text{ mm}, 8 \text{ mm})$ has been computed. Figure 6.2 shows results for the master's direct mobility at $(x_0, y_0) = (13 \text{ mm}, 8 \text{ mm})$ and transfer mobility at $(x_1, y_1) = (50 \text{ mm}, 14 \text{ mm})$ for three cases:

- the master without the complex substructure.
- the master with the attached complex substructure but without spatial coupling.
- the master with the attached complex substructure and with spatial coupling.

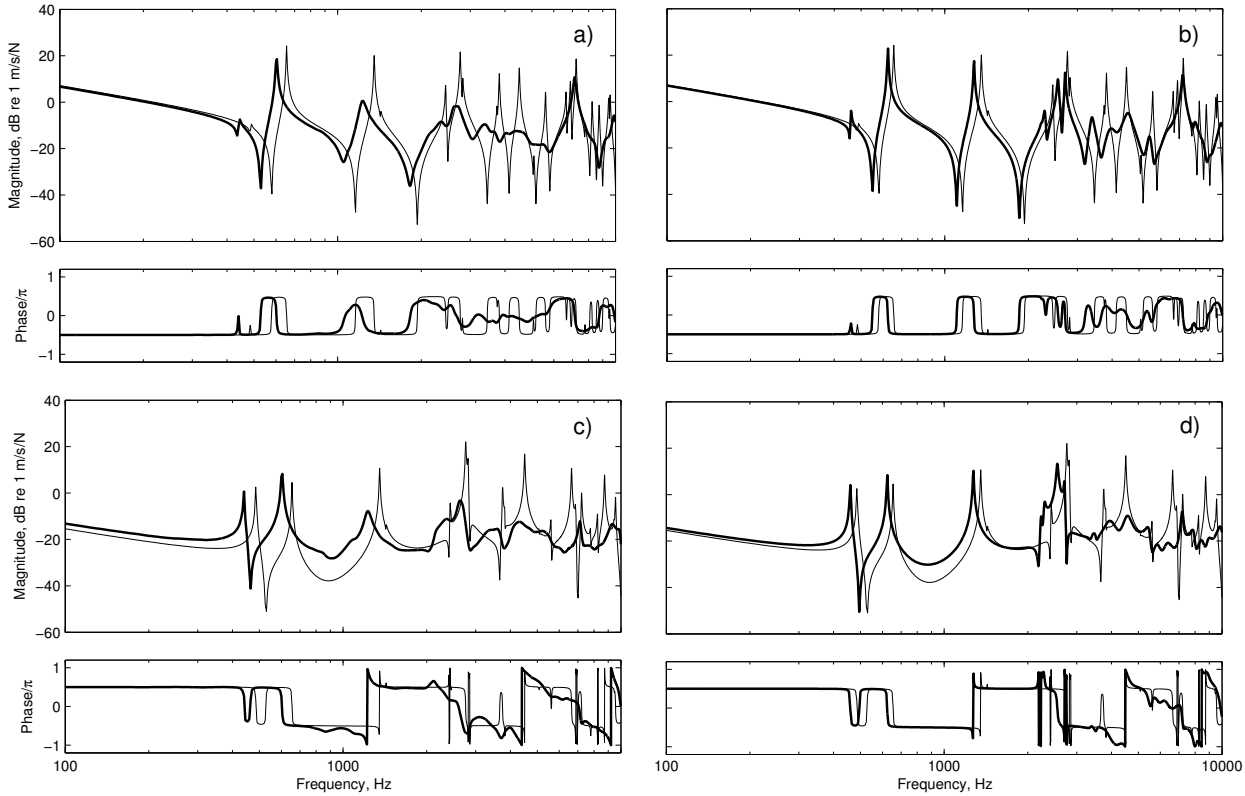

Figure 6.2. Frequency response of the master without the complex substructure (thin solid lines) and with the complex substructure (thick solid lines) to a unit harmonic excitation at (x_0, y_0). The cases shown are: Direct response at (x_0, y_0) (a) without spatial coupling and (b) with spatial coupling; Transfer response at (x_1, y_1) (c) without spatial coupling and (d) with spatial coupling.

From figs. 6.2a and 2b it is clearly seen that the complex substructure introduces a high apparent damping in the response of the master structure from about 1000 Hz and upwards. Especially from 3000 Hz and up to approximately 6000 Hz the damping is strong and the velocity

response is reduced with almost 30 dB. Around 7000 Hz the damping effect has decreased somewhat. Moreover, figs. 6.2c and 2d show that the occurrence of spatial coupling significantly reduces the damping effect of the attached complex structure. Here, strong damping is only achieved from about 2500 Hz and upwards. This limited damping effect is in conjunction with the fuzzy coupling plate being relatively stiff at low frequencies. However, at higher frequencies the plate is considerably more flexible and it is therefore not contributing with a significant coupling effect.

6.4.3 Energies and estimation of fuzzy parameters

In order to apply the described method for estimating the fuzzy parameters, the structural losses in the master have to be estimated. According to eq. (6.9) this requires a study of the potential and kinetic energies of the master. These energies have been computed using the expressions in eqs. (6.6) and (6.7) for cases (ii) and (iii) that include the attached complex substructure. The energies are shown in fig. 6.3 where they have been normalized with their mutual total mechanical energy. It is well-known that the potential and kinetic energies of a vibrating system are equal at system resonances (see Cremer *et al.*, 1988). However, in the present case we only consider a part of the system, being the master. Figure 6.3a shows these energies for the case of no spatial coupling and it is seen that potential and kinetic energies are close to one another above 500 Hz where the first anti-resonance of the master occurs. From fig. 6.3b, it is revealed that this is not entirely the case when spatial coupling is introduced. From 400 Hz to 4000 Hz, the two energies are highly fluctuating and only close to one another in, say, half of this frequency range. By summing the energies in wider frequency bands, however, the differences between the energies are reduced significantly. Furthermore, it should be kept in mind that the structural losses in the master usually are much lower than the transmitted power in the frequency range with fuzzy damping. According to eq. (6.11), exact determination of the structural losses in the master is therefore not necessary for obtaining a good estimation for the apparent damping caused by the structural fuzzy.

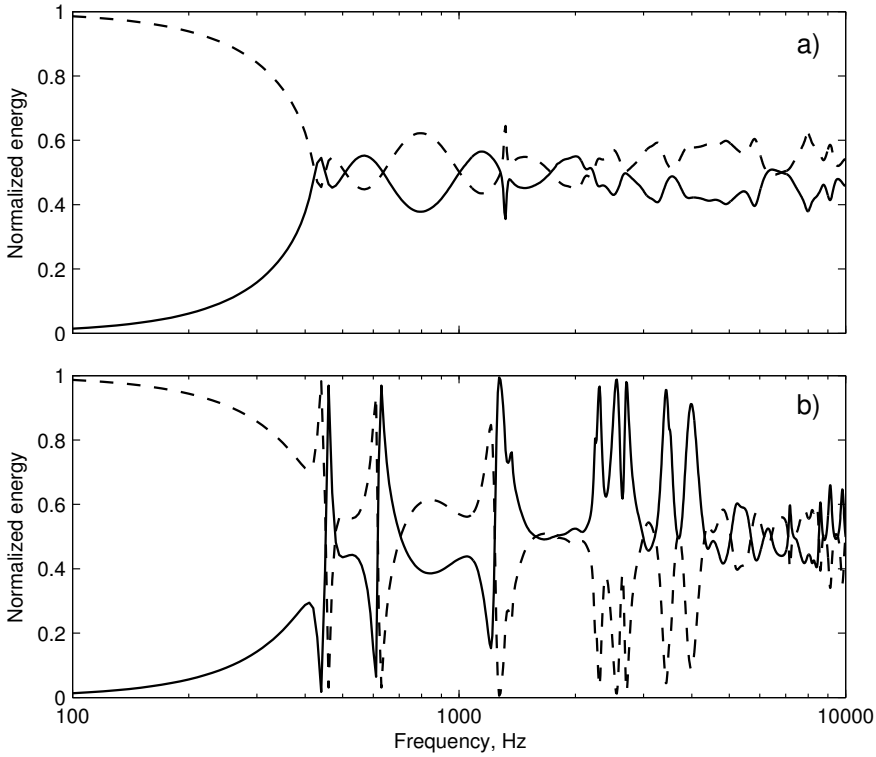

Figure 6.3. Normalized potential (solid line) and kinetic (dashed line) energy of the master with the attached complex substructure (a) without spatial coupling and (b) with spatial coupling.

By using the expression in eq. (6.11) the total apparent damping introduced by the complex structure has been estimated in 1/3-octave bands. It should be noted that the input power, structural losses and mean square velocity of the fuzzy connection boundary first have been synthesized in 1/3-octave bands and then substituted in eq. (6.11). Figure 6.4 shows the results for the apparent damping and the corresponding resonating mass distribution, which is calculated from eq. (6.13).

Again, by considering fig. 6.4a it is clearly observed that the spatial coupling reduces the damping effect of the complex structure in almost all frequency bands. In conjunction with previous statements, significant damping only occurs from about 2500 Hz and upwards where the fuzzy plate is relatively flexible. The two resonating mass distributions shown in fig. 6.4b are accordingly relatively different compared to one another. In the case without spatial coupling, integration of the distribution from 100 Hz to 10000 Hz yields the actual total mass of the fuzzy oscillators. As opposed to this, such an integration for the case with spatial coupling results in a value that is only 0.46 of that of the actual mass. Hence, the resonating mass distribution shown for this case of spatial coupling is *reduced.* According to the results presented in sections 5.4 and 6.3, both the reduced-mass method and the method involving local equivalent oscillators are capable of modeling the damping of the fuzzy substructure.

Let us assume that the reduced resonating mass distribution in fig. 6.4b is denoted $m_{fuzzy,2}$. Using the reduced-mass method, the fuzzy substructure is modeled with the boundary impedance given in eq. (5.6) and the equivalent coupling factor is set to $\alpha_2 = 1$. Moreover, the residual, which is given as $M_{fuzzy,res} = (1-0.46)M_{fuzzy} = 0.54M_{fuzzy}$, is modeled as pure mass. Using the method involving local equivalent oscillators, the fuzzy substructure is modeled with the boundary impedance from eq. (3) in paper II. According to eq. (6.15), the equivalent coupling factor is set to the constant value $\alpha_2 = 0.46$. Furthermore, the resonating mass distribution m_{fuzzy}, which is given in eq. (6.16), becomes $m_{fuzzy} = m_{fuzzy,2} / \alpha_2 = m_{fuzzy,2} / 0.46$.

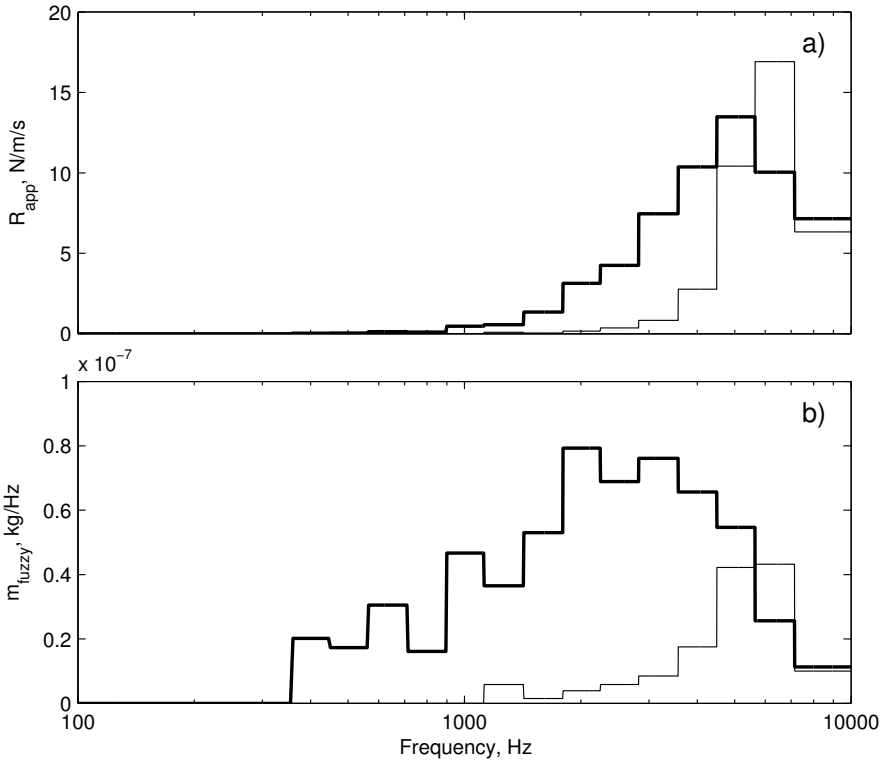

Figure 6.4. Estimations of (a) the total apparent damping and (b) the resonating mass distribution of the complex structure without spatial coupling (thick solid line) and with spatial coupling (thin solid line).

6.4.4 Validation of the estimated fuzzy parameters

To validate the estimated fuzzy parameters the actual response of the master and complex structure is compared to the response of the master with attached structural fuzzy in fig. 6.5. The reduced-mass method has been employed to model the fuzzy substructure. In the case without

spatial coupling, see figs. 6.5a and c, the curves are nearly coinciding in the whole frequency range and the complex structure is therefore modeled successfully as structural fuzzy. The direct mobilities shown in fig. 6.5b for the case with spatial coupling only show minor discrepancies. Also the transfer mobilities in fig. 6.5d, show minor deviations up to about 5000 Hz. Above this frequency, deviations become larger. This is because the complex structure is modeled as *completely homogeneous* fuzzy. However, in real-life engineering structures and in the constructed theoretical example, the complex structures will only be close to homogeneous. Furthermore, adding the fuzzy plate does not improve the homogeneity. It is additionally seen that resonances of the fuzzy responses are slightly shifted down in frequency. This is due to the residual mass $M_{fuzzy,res} = (1-\alpha)M_{fuzzy}$ being modeled as pure mass. In reality some of this mass is resonating, yet without producing damping, and the apparent mass therefore becomes slightly too high as illustrated in fig. 5.1a. Despite of the mentioned deviations, fig. 6.5 clearly illustrates that the *overall* response of the master is modeled successfully using the estimated fuzzy parameters.

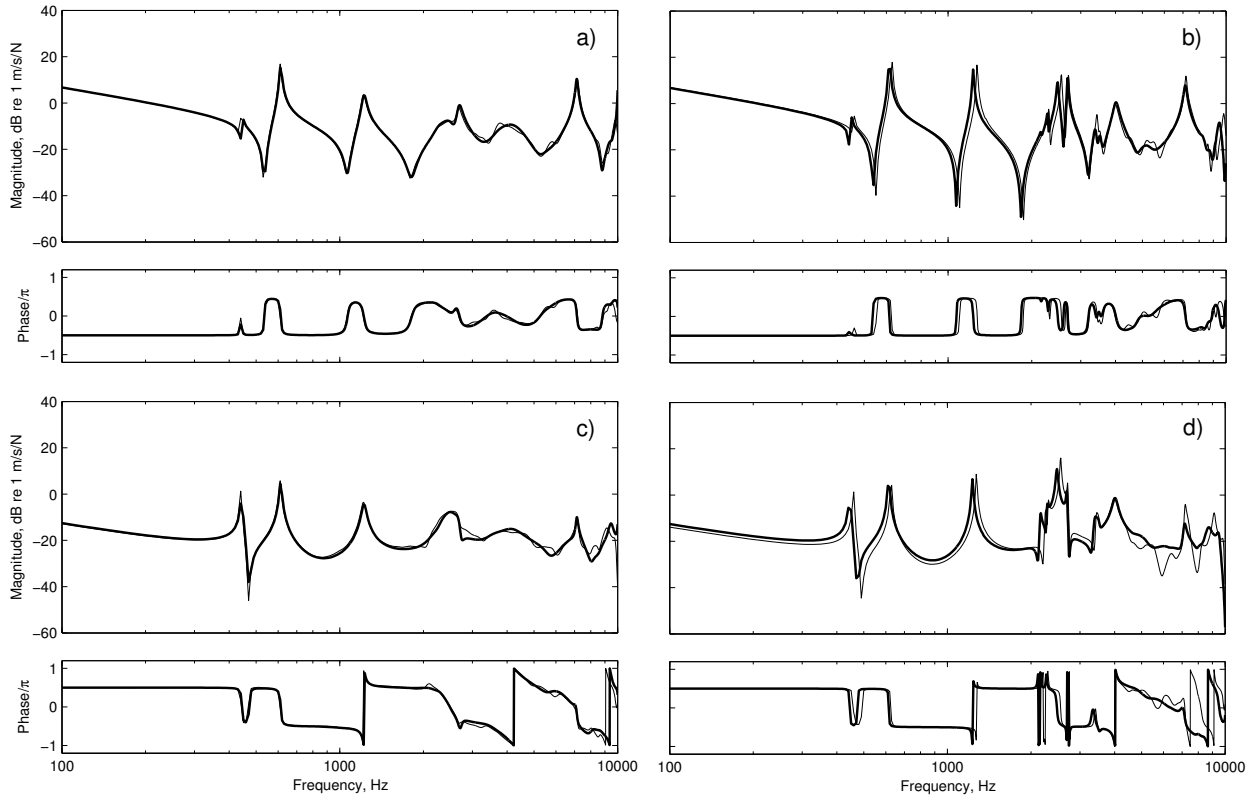

Figure 6.5. The frequency response of the master with the attached complex structure (thin solid lines) and with attached structural fuzzy (thick solid lines) to a unit harmonic excitation at (x_0, y_0) *for the following cases: Response at* (x_0, y_0) *with the complex structure (a) without spatial coupling and (b) with spatial coupling and response at* (x_1, y_1) *with the complex structure (c) without spatial coupling and (d) with spatial coupling.*

7 Experimental estimation of fuzzy parameters

7.1 The complex structure and the setup

In this section the fuzzy parameters are estimated for a number of selected hearing aid components. Figure 7.1 shows the considered internals placed in the half-shell of the hearing aid. As seen in the figure, the components are not rigidly attached to the shell or to each other, not even when the top-half-shell is mounted. The internals shown consist of the processor, program switch, magnetic screen, volume control, battery spring and compartment and the battery itself. Each of these rather delicate components, which in general may vibrate in six motion degrees-of-freedom have *some* resonances in the frequency range up to 10 kHz. Moreover, it is also the many indefinable boundary conditions that cause these components to behave as structural fuzzy. All in all the components form a complex structure with many degrees of freedom and with uncertain dynamic properties and boundary conditions.

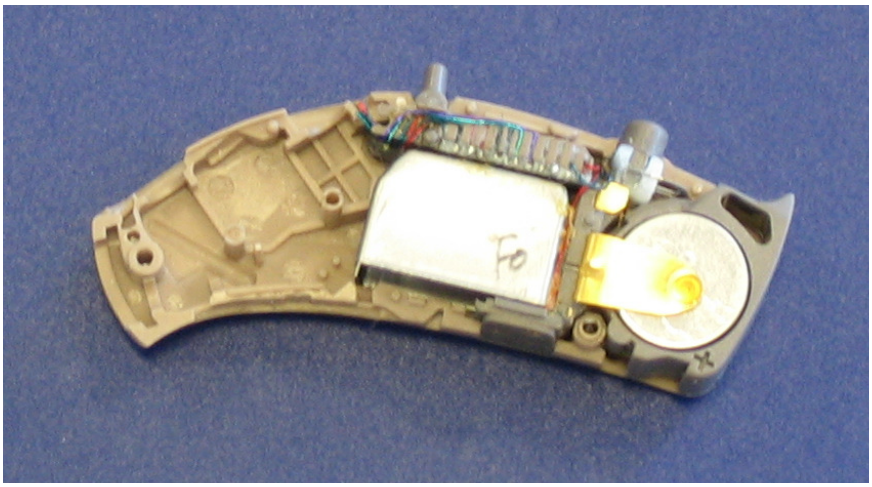

Figure 7.1. Half-shell with attached components constituting a complex substructure.

The experimental setup shown in fig. 7.2 was prepared in order to determine the fuzzy parameters of the complex structure. This setup consists of two complete shells arranged diagonally to a mounting block made of hard plastic. This was firmly mounted to a small force transducer (Brüel and Kjær type 8203) that measured the driving force from the electro-dynamic exciter

(Brüel & Kjær type 4810) shown. Vibrations of the master shells were measured with a laser vibrometer Polytec type OFV-056, and analysis of signals were conducted with a Pulse spectral analyzer from Brüel & Kjær (input output module type 3109 and communication controller module type 7536).

In the following the two shells are considered as the master structure. Furthermore, it is assumed that the structural fuzzy only is attached to its master in the direction perpendicular to the major face of the shell surfaces. Using the setup shown in fig. 7.2 the main vibrations of the shells take place in the direction of the driving force, that is, perpendicular to the large horizontal faces of the shell. It is therefore reasonable to assume that the apparent damping introduced in the master structure is caused by the complex substructure opposing vibrations in this direction only.

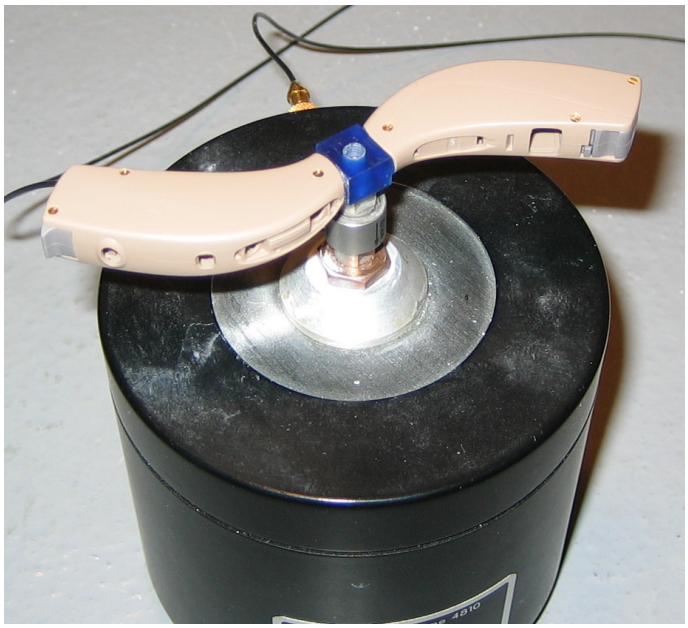

Figure 7.2. Experimental setup showing two complete shells with internals; the shells are attached diagonally to a mounting block that is mounted on a force transducer measuring the driving force produced by the electro-dynamic exciter.

Since the connection between the shells and the mounting block is assumed to be rigid, the elements can be regarded as forming a parallel connection. Furthermore, the block is very compact and it consequently behaves like a pure mass in the considered frequency range. This implies that no energy is dissipated in the mounting block and the same applies to the mass of the force transducer vibrating in phase with the mounting block.

7.2 Estimation of the fuzzy parameters

In the following the fuzzy parameters of the complex substructure will be estimated by using the method described in section 6. Notice that this estimation involves two complex substructures, that is, one in each of the two complete shells. It should be noted, however, that the estimation is independent of any unwanted rotations of the mounting block. The properties of each master and its corresponding complex substructure are given in table 7.1. Young's modulus and the loss factor of the shell material, which is ABS plastic, have been determined experimentally. It is noted that the fuzzy has a larger mass than the master, but, not necessarily all of this mass is resonating in the considered frequency range.

Property	**Value**
Total mass of master	$M_{master} = 1.23$ g
Total mass of the complex structure	$M_{fuzzy} = 2.10$ g
Density of shell material	$\rho = 1050$ kg/m^3
Young's modulus of shell material	E is varying linearly from 3.0 GPa at 100 Hz to 2.6 GPa at 10000 Hz
Structural damping loss factor of shell	$\eta = 0.019$
Average thickness of shell	$t = 0.85$ mm
Area of fuzzy connection surface	$A_{fuzzy} = 548$ mm^2
Area of the master surface	$A_{master} = 1228$ mm^2

Table 7.1. Properties of the master and the corresponding complex substructure.

Measurements have been performed on two nominally identical sets like the one shown in fig. 7.2. Furthermore, three individual measurements have been performed on each set; between each measurement the shells have been handled as during everyday use. More specifically this involves squeezing the shells and shaking the setup. Hence, a number of six measurements and estimations of fuzzy parameters have been carried out.

Figure 7.3 shows the six measurements of the transmitted power per unit squared excitation force (calculated using eq. (6.2)), that is, three measurements for each of the two sets. From fig. 7.3a it is seen that measurement results of the transmitted power for set 1 are close but not exactly the same. This is also the case for the three measurements on set 2 and this indicates that everyday use may change the dynamical properties of the shell and its internals to some degree.

Comparison of the measurements on the two sets reveals that the transmitted power has the same overall pattern. Nevertheless, looking closer, clear discrepancies between the sets are observed.

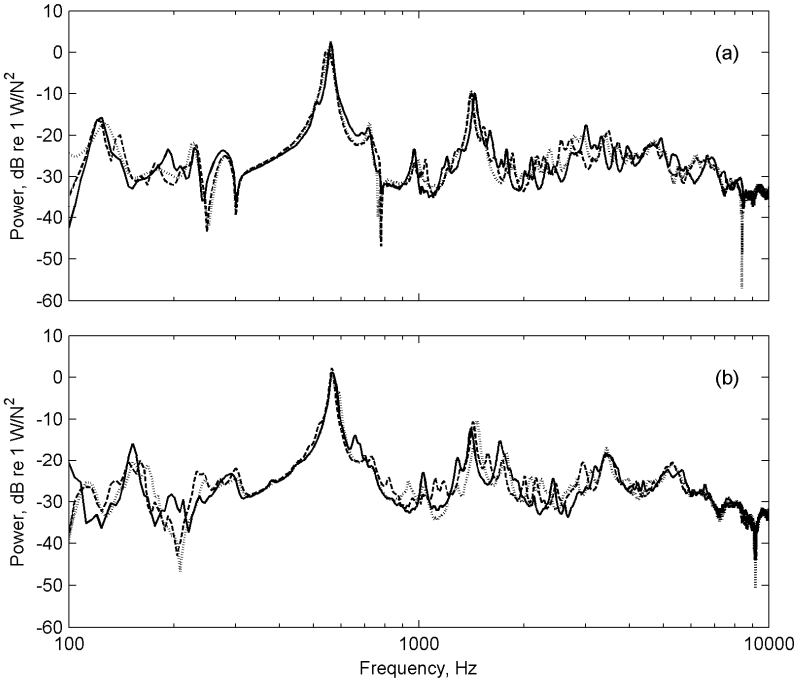

Figure 7.3. Three measurements of the transmitted power per unit squared excitation force for (a) set 1 and (b) set 2.

Six corresponding measurements of the spatially averaged mean-square vibration velocity per unit squared excitation force of the master shells are shown in fig. 7.4. Measurements on both sets are dominated by well-separated resonances occurring from about 550 Hz and upwards. Moreover, from about 2500 Hz the three measurements on each set start to deviate slightly. At frequencies above 1500 Hz, it is observed that the pair of hearing aids of set 2 has more pronounced resonances than those of set 1. Figure 7.5 shows the six measurements of the spatially averaged mean-square vibration velocity per unit squared excitation force of the fuzzy connection surface on the faces of the shells. It is evident that these velocities are almost similar to the ones shown in fig 7.4 for the whole master structure. This is because the internals are connected to more than half of the surface of the master.

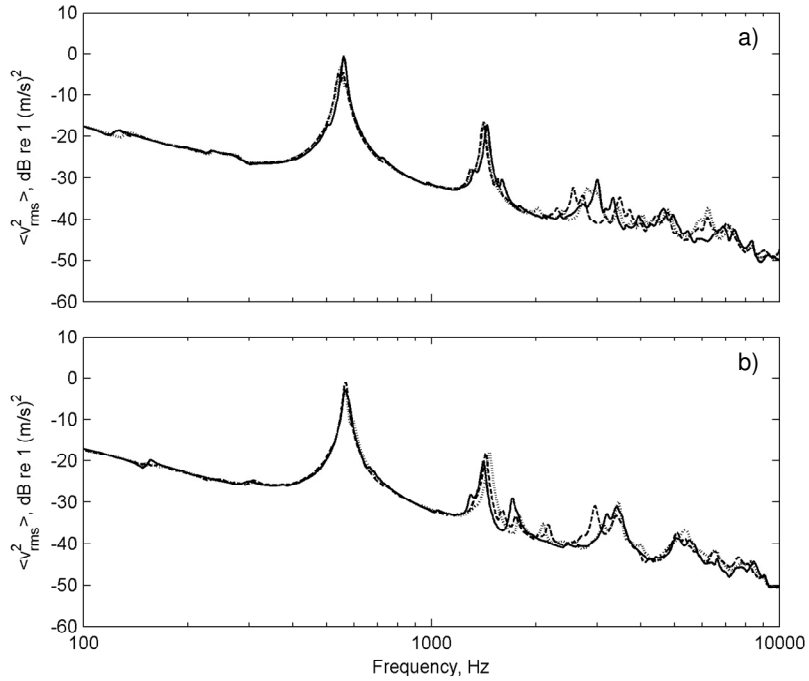

Figure 7.4. Three measurements of the spatially averaged mean-square vibration velocity per unit squared excitation force of the master shells for (a) set 1 and (b) set 2.

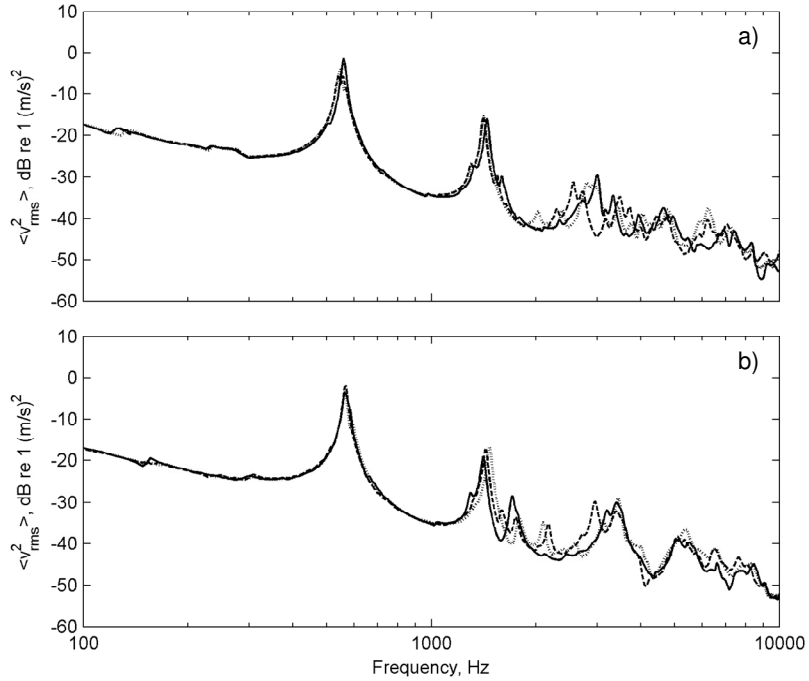

Figure 7.5. Three measurements of the spatially averaged mean-square vibration velocity per unit excitation force of the fuzzy connection surface for (a) set 1 and (b) set 2.

In accordance with the frequency averaging procedure used for determining the fuzzy parameters of the prototype complex substructure in subsection 6.4, each of the measurement results in figs. 7.3 to 7.5 has been synthesized in 1/3-octave bands and put into eq. (6.11) yielding the apparent damping. The resonating mass distribution has thereafter been computed using eq. (6.13). Fig 7.6 shows results for only *one* complex substructure.

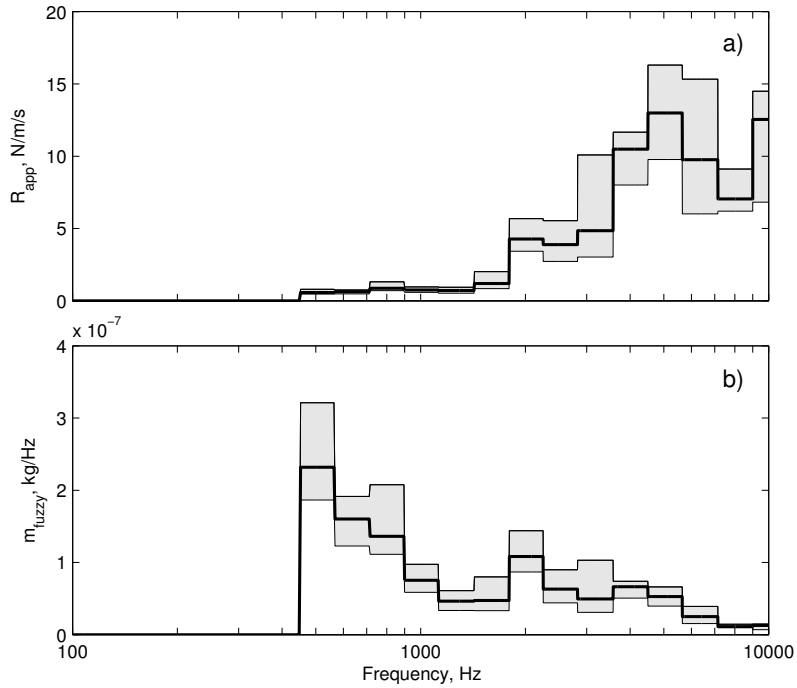

Figure 7.6. Estimations of (a) the total apparent damping and (b) the resonating mass distribution for only one complex substructure. Shown are the mean values (thick solid lines) of six estimations and the interval between the highest and lowest estimations (grey area).

The results are presented as mean values as well as the interval between the highest and lowest estimations. From fig. 7.6a it is seen that the internals introduce a high apparent damping especially from 2000 Hz and upwards. Even though large variations in the apparent damping are observed, the tendencies of the six estimations are in clear agreement. For instance, all estimations show that maximum damping occurs around 5000 Hz. The corresponding resonating mass distributions in fig. 7.6b show high values from 500 Hz to about 900 Hz. Hereafter the values are generally lower as the resonating distribution is proportional to the apparent damping divided by the frequency squared, see eq. (6.13). It has not been possible to estimate the damping effect and thus the resonating mass distribution of the structural fuzzy below 500 Hz. Nevertheless, since the resonating mass distribution takes on high values around 500 Hz one would guess that this also is the case in bands nearby. On the other hand, the anticipated resonating mass distribution below 500 Hz does not result in significant damping of the master. The values resulting from the integration of the mean,

lowest and highest resonating mass distributions are listed in table 7.2 and these reveal that the corresponding total resonating masses are rather low compared to the actual mass of 2.10 g. Hence, the total fuzzy masses are *reduced* masses and the corresponding α-values are therefore obtained from eq. (6.15). These values are likewise given in table 7.2.

Resonating mass distribution	**Total fuzzy mass**	**α-value**
Low	0.32 g	0.15
Mean	0.43 g	0.21
High	0.61 g	0.29

Table 7.2. Results for the estimated resonating mass distributions.

As discussed in subsection 6.3 the reason for the low fuzzy masses is either truncation of the estimation of the mass distribution, spatial coupling or an arbitrary combination of the two.

7.3 Experimental validation of the fuzzy parameters

A finite element model of a full shell was developed in order to validate the estimated parameters. Argyris shell elements (see Argyris *et al.*, 1997 and Allman, 1988) were utilized to model the shell. As seen in fig. 7.7a, many details such as holes and the weak connection between the two half-shells of the hearing aid were included in the model. Results from the finite element analysis were validated by measurements on the setup shown in fig. 7.7b. Basically this is the same setup as shown in fig. 7.2 but without internals. It should be noted that the mounting block and its zero-rotation condition is included in the numerical shell model. Hereafter a fuzzy substructure was simulated using the estimated parameters shown in fig. 7.6 and the reduced mass method discussed in subsection 5.4. With this fuzzy substructure attached to the finite element model of the shell new calculations were made of the shell response. Results including the structural fuzzy were validated by using measurements on the setup from fig. 7.2.

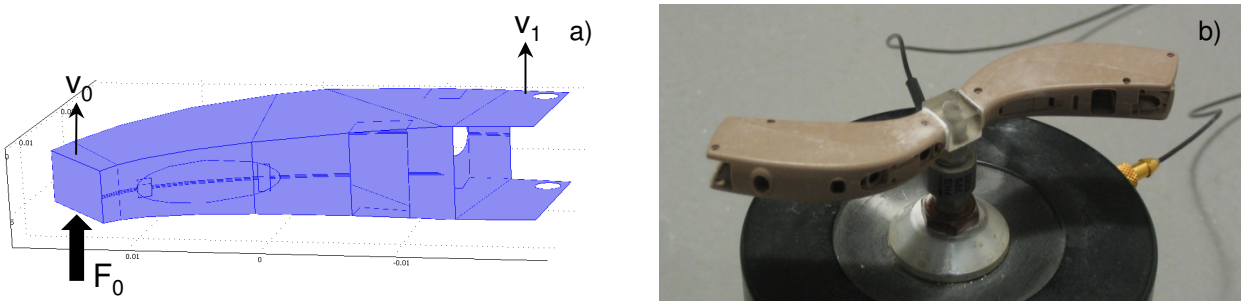

Figure 7.7. (a) Finite element model of the shell and (b) the experimental setup for validating the model (similar to the setup shown in fig. 7.2 but without internals).

Figure 7.8 shows results from these simulations as well as measurements of the direct mobility $Y_{00} = v_0 / F_0$ at the end of the shell. Results for the shell both with and without attached structural fuzzy are plotted. The three measurements on each set are very similar and only one measurement of each set is therefore shown. Dashed gridlines are added on fig. 7.8 at certain frequencies such that simulated and measured results are easily compared. The simulated and measured direct mobilities of the empty shells shown in figs. 7.8a and c exhibit the well-known pattern of mass-like behavior at low frequencies, say, up to about 700 Hz, and a series of alternating anti-resonances and resonances at frequencies above 700 Hz. Moreover, the phase alternates between $-\pi/2$ and $\pi/2$ as it is expected for a direct mobility. There is generally good agreement between the simulations and measurements of the empty shells. Some of the resonances in the simulation are shifted slightly in frequency. The two minor resonance peaks in the band from 5000 Hz to 5500 Hz, however, are shifted somewhat downwards compared to the measurements. It has been checked that the vibration modes corresponding to the resonances are in agreement in the simulations and measurements. From figs. 7.8b and d it is seen that the first resonances are shifted about 350 Hz downwards in frequency when the heavy complex substructure is attached. From about 2000 Hz and upwards where the fuzzy has significant damping effect, both the simulated and measured mobilities are visibly damped. Apart from minor deviations, there is generally good agreement between simulations and measurements. It is furthermore seen that the difference between simulations using the highest and lowest estimation of the fuzzy parameters is very small for the direct mobility.

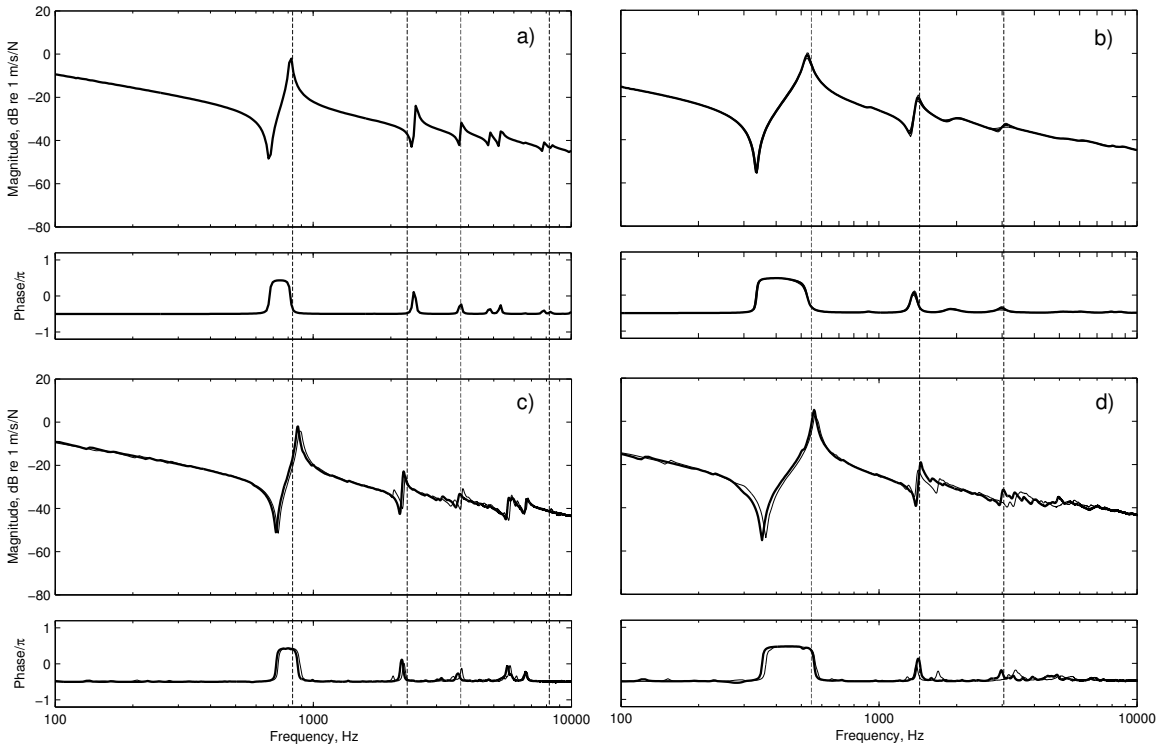

Figure 7.8. Direct mobilities $Y_{00} = v_0 / F_0$ of the shells. Simulated results (a) without structural fuzzy and (b) with structural fuzzy and interval between highest and lowest estimation (grey area); One measurement on set 1 (thick solid line) and set 2 (thin solid line) (c) without internals and (d) with internals.

Similar results are shown in fig. 7.9 for simulated and measured transfer mobilities at position 1, that is, $Y_{10} = v_1 / F_0$. From fig. 7.7a it is seen that the velocity v_1 is measured on the tip flanges of the shells where the vibration velocities are high. The transfer mobilities of the empty shells plotted in figs. 7.9a and c also show the mass-like behavior at frequencies up to 700 Hz. Again above 700 Hz a series of resonances are observed. These resonances are more pronounced than for the direct mobilities due to the very mobile measurement position. Also, there is clearly agreement between simulations and measurements. From fig. 7.9c, however, it is revealed that full symmetry of the experimental setup is not obtained. Since the resonance frequencies of the shell in the left and right side are not completely coinciding, peaks are not as pronounced as in the simulations. Finally, simulation and measurements with structural fuzzy/internals are compared in figs. 7.9b and d. There is clearly an overall agreement between the mobilities, but details are missed. Since this also is the case without the structural fuzzy, discrepancies are not caused by errors in the estimation of the fuzzy parameters but rather in the simplified finite element model of the shell. Moreover, the setup is not ideally diagonal and small rotations of the mounting block are therefore

not avoided completely. Despite of the mentioned discrepancies it can be concluded that measured and simulated responses are in good overall agreement and that the fuzzy modeling succeeds.

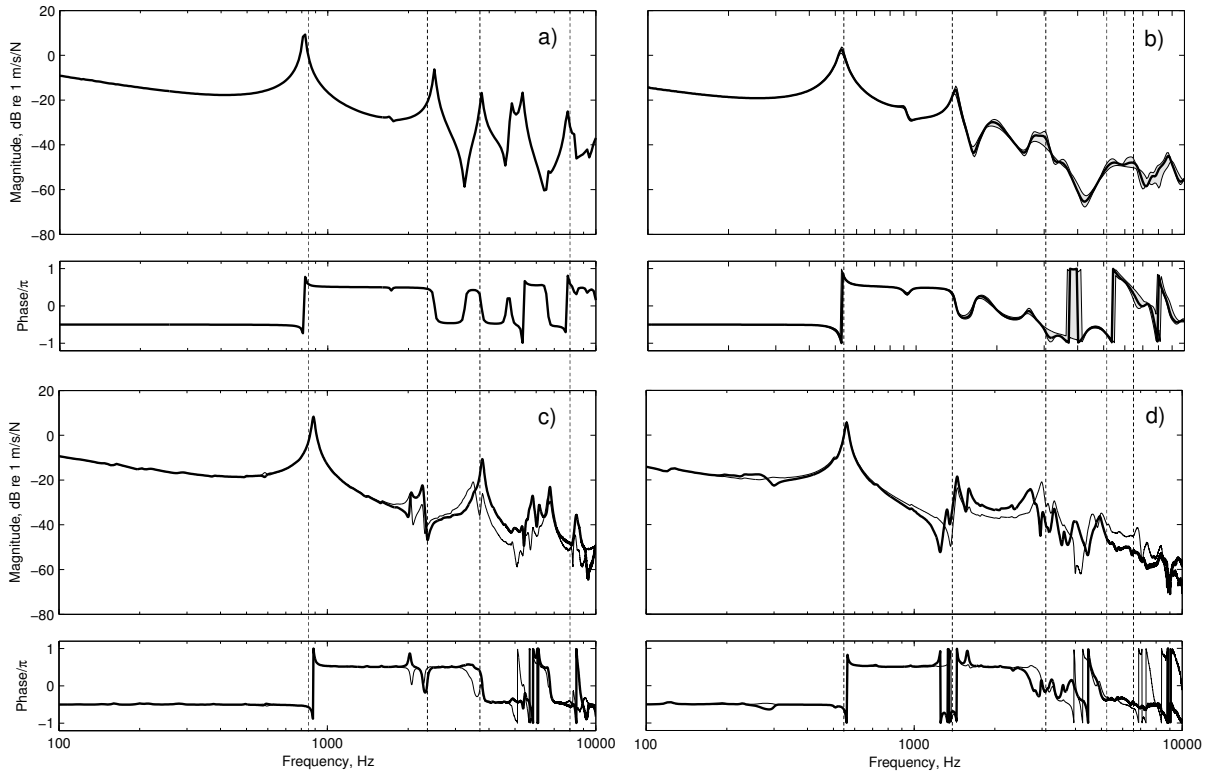

Figure 7.9. Transfer mobilities $Y_{10} = v_1 / F_0$ of the shells. Simulated results (a) without structural fuzzy and (b) with structural fuzzy and interval between highest and lowest estimation (grey area). Shown are measurements on set 1 on the left side (thick solid line) and the right side (thin solid line) (c) without internals and (d) with internals.

PART III:

PROPERTIES OF MINIATURE COMPONENTS

8 Acoustic tube system

8.1 Introduction

A hearing aid provides sound pressure at the eardrum of the hearing impaired user. The sound pressure generated in the tube system is a result of the properties of each participating component such as the "source strength" of the receiver (loudspeaker), acoustic impedances of the tubes as well as the impedance of the eardrum itself. In order to obtain high sound levels at the eardrum, an even higher sound pressure is generated by the receiver. This pressure is not only transmitted to the ear canal but also through the hearing aid in the form of unwanted sound and vibrations. A detailed study of the acoustic system is therefore important to identify the mechanisms responsible for internal feedback.

In this section the acoustic system from the receiver to the eardrum is modeled using transmission theory and more specifically "two-port networks". The two-port network theory as well as methods for determining the properties of the components of the tube system were presented in a series of papers by Egolf and co-workers (see Egolf, 1977; Egolf and Leonard, 1977; Egolf *et al.*, 1978, 1985, 1986, 1988a, 1988b and 1989). Certain parts of the two-port network theory will be outlined briefly in subsections 8.2 and 8.3. After that the properties of the acoustic components of the tube system are discussed. Furthermore, numerical simulations of the sound pressure in the tube system are presented and validated experimentally. Particularly the transfer function from electric voltage driving the loudspeaker to the sound pressure at different positions in the tube system will be studied.

Figure 8.1 shows a sketch of the electro-acoustic tube system from the receiver to the eardrum in the considered hearing aid. Sound pressure is generated by the receiver and it is transmitted to the eardrum through a system consisting of the steel pipe, hook, rubber hose, earmould and finally the user's ear canal.

Using two-port networks, the steel tube, hook and plastic tube are all modeled as straight and narrow tubes where losses due to viscous friction and heat transfer to the walls are accounted for. This particular theory concerning the acoustics in narrow tubes was presented in complete form by Egolf *et al.* (1978, 1985 and 1988b). The ear canal and the eardrum are replaced by the properties of an occluded-ear simulator representing the "average" human ear canal and eardrum. In experiments this ear simulator is used to measure the pressure generated at the eardrum. The ear simulator consists of two parts: The coupler, representing the ear canal, and a microphone accounting for the acoustic impedance of the eardrum. The properties of both coupler and

microphone are found by using electric analog circuits supplied by the respective manufacturers. The properties of the receiver is found by using the "two-load method" (see Egolf, 1977; Egolf and Leonard, 1977; Egolf *et al.*, 1988a), which is a special experimental scheme for determining the properties of electro-acoustic transducers such as receivers and microphones. The geometrical properties as well as the method for determining the two-port parameters of each of the components in the tube system are listed in table 8.1.

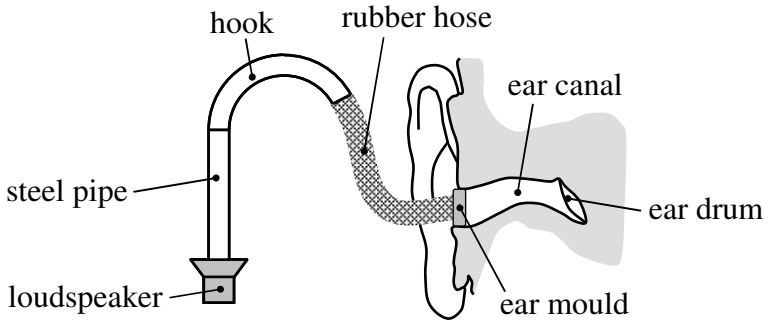

Figure 8.1. Sketch of the tube system from the receiver to the eardrum.

Component	**Details**	**Method used for determining the two-port parameters**
Receiver (R)	Knowles EF 6665	Two-load method
Steel tube (1)	Length $L_1 = 14.0\,\text{mm}$ Radius $r_1 = 0.60\,\text{mm}$	Narrow tube theory
Hook (2)	Length $L_2 = 20.4\,\text{mm}$ Radius $r_2 = 0.81\,\text{mm}$	Narrow tube theory
Rubber tube (3)	Length $L_3 = 25.0\,\text{mm}$ Radius $r_3 = 1.00\,\text{mm}$	Narrow tube theory
Coupler inlet (4)	Length $L_4 = 18.0\,\text{mm}$ Radius $r_4 = 1.50\,\text{mm}$	Narrow tube theory
Coupler (C)	G.R.A.S. IEC 711 Ear Simulator	Electrical analogue circuits from manufacturer
Microphone (M)	G.R.A.S. RA0045	Electrical analogue circuits from manufacturer

Table 8.1. Geometrical properties and method for determining the two-port parameters of each component in the tube system.

8.2 Outline of two-port network theory

The use of transmission theory is a way to account for impedance loading between components in any linear system. Each component is considered as a "black box" where only input and output parameters are known. Using two-port networks the input and output parameters of the *i*'th component are given in terms of the two-element vectors $\{E_{in}\}_i$ and $\{E_{out}\}_i$, which are interrelated through the component's two-by-two transmission matrix $[T]_i$ as

$$\{E_{in}\}_i = [T]_i \{E_{out}\}_i . \tag{8.1}$$

Let us assume that the *i*'th component is a receiver. In expanded form eq. (8.1) therefore yields

$$\begin{Bmatrix} V_{in} \\ I_{in} \end{Bmatrix}_i = \begin{bmatrix} A & B \\ C & D \end{bmatrix}_i \begin{Bmatrix} p_{out} \\ Q_{out} \end{Bmatrix}_i \tag{8.2}$$

where A, B, C and D are the elements of the transmission matrix. Furthermore, V_{in} and I_{in} are the input voltage and current, respectively, and p_{out} and Q_{out} are output sound pressure and volume velocity, respectively. The elements of the transmission matrix are thus defined as

$$A = \left.\frac{V_{in}}{p_{out}}\right|_{Q_{out}=0} \qquad B = \left.\frac{I_{in}}{p_{out}}\right|_{p_{out}=0} \tag{8.3), (8.4}$$

$$C = \left.\frac{V_{in}}{Q_{out}}\right|_{Q_{out}=0} \qquad D = \left.\frac{I_{in}}{Q_{out}}\right|_{p_{out}=0} . \tag{8.5), (8.6}$$

Transmission theory is especially suitable for modeling a series connection of different components like the considered tube system. In such a system the output parameters of one component equals the input parameters of the subsequent component. The transmission matrices therefore only have to be multiplied with one another in order to describe the whole system. Figure 8.2 shows a diagram of the electro-acoustic system modeled with two-port networks.

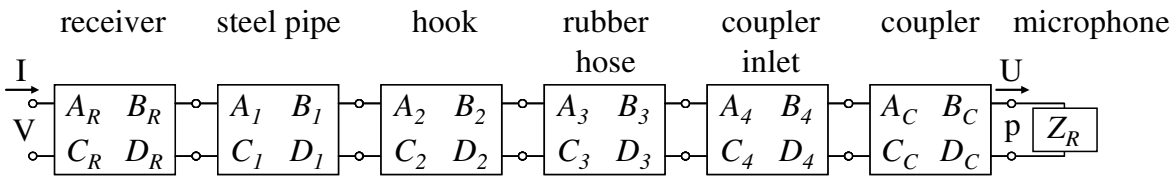

Figure 8.2. Diagram of the electro-acoustic system from the receiver to the eardrum modeled with two-port networks.

The receiver is described with a two-port matrix relating output pressure and volume velocity to input voltage and current. All the components hereafter are purely acoustical and the acoustic impedance of the microphone terminates the whole system. Multiplication of all the transmission matrices yields the total two-by-two element transmission matrix for the whole system as

$$[T]_{total} = \begin{bmatrix} A & B \\ C & D \end{bmatrix}_{total} = \begin{bmatrix} A & B \\ C & D \end{bmatrix}_6 \begin{bmatrix} A & B \\ C & D \end{bmatrix}_5 \begin{bmatrix} A & B \\ C & D \end{bmatrix}_4 \begin{bmatrix} A & B \\ C & D \end{bmatrix}_3 \begin{bmatrix} A & B \\ C & D \end{bmatrix}_2 \begin{bmatrix} A & B \\ C & D \end{bmatrix}_1 . \quad (8.7)$$

From this matrix and the terminating impedance of the eardrum Z_R the transfer function from electrical input voltage on the receiver to the pressure at the eardrum is readily found.

8.3 Determination of two-port parameters

As previously mentioned, the two-port parameters of the receiver are determined by using the experimental two-load method. The principle of this method is to load the receiver with two different acoustical loads with known properties. These acoustical loads may for example be two tubes with different lengths, which are terminated with a known coupler. Driving the receiver with a known voltage and measuring the receiver current and pressure generated in the coupler for the two acoustical load cases, yields four equations with the four two-port parameters as unknowns. If these equations are combined the two-port parameters can be determined. This method was applied to determine the properties of the receiver participating in the considered tube system. The specific physical mechanisms during operation of the receiver, however, are not described by the two-port parameters as only the input and output parameters are related. For more details about the two-load method, the reader is referred to existing literature (see Egolf, 1977; Egolf and Leonard, 1977; Egolf *et al.*, 1988a).

The transmission matrix for narrow tubes with viscous-thermal losses was presented by Egolf and co-workers several years ago (see Egolf *et al.*, 1978, 1985 and 1988b). These papers contain closed form expressions for the two-port parameters. For brevity, however, these are not listed here. Using these two-port parameters the following is assumed:

- Damping is dependent on the walls only and are caused by viscous friction along the tube wall and heat loss to the tube wall.
- The tube wall is rigid.
- The tube wall is isothermal.
- The tube is long enough so that radial end effects are negligible. This implies that $L_n >> a_n$, where L_n is tube length and a_n is the tube diameter.
- The fluid in the tube is continuous.
- The fluid in the tube is excited by small-amplitude perturbations.
- The fluid in the tube is such that $\mu / \rho c a_n << 1$, where μ and ρ is the absolute viscosity and density of the fluid, respectively.
- The excitation angular frequency, ω, is such that it applies that $\mu\omega / \rho c^2 << 1$ and $\omega a_n / c << 1$.
- The acoustic pressure is uniform over the tube cross-section.

The acoustic properties of the coupler and the microphone were determined by employing the electrical analogue circuits supplied by the respective manufacturers. For more information about electrical analogue circuits the reader is referred to the technical report from Knowles by LoPresti (2003).

8.4 Simulation results and experimental validation

Using the determined two-port parameters, the sound pressure was simulated for different positions in the tube system. Figure 8.3 shows simulation results for the sound pressure at the eardrum for the receiver driven by a unity harmonic voltage. Moreover, this pressure is compared to measurements on the acoustic system of four nominally identical hearing aids. The simulation results and the measurements shown in fig. 8.3 show a very good agreement. Even though the simulations only consider straight tubes, the two-port network method performs very well.

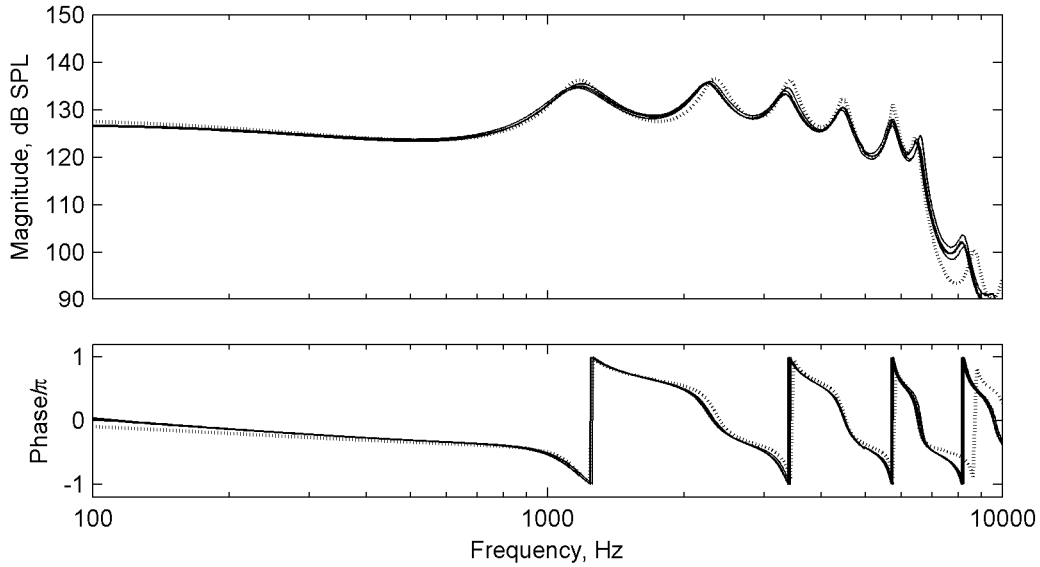

Figure 8.3. Sound pressure level at the eardrum for a unity harmonic voltage driving the receiver. Simulation result (dotted line) and four measurements (solid lines).

In order to analyze the nature of the acoustics in the tube system, fig. 8.4 shows the simulated pressure at the eardrum together with a simulation of the pressure at the outlet of the receiver.

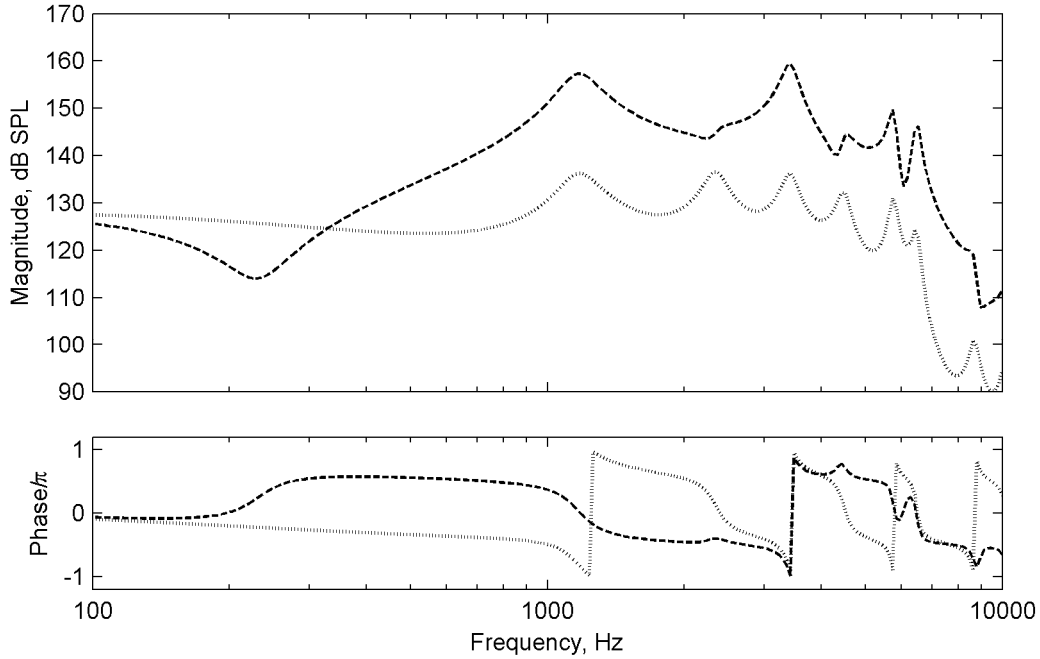

Figure 8.4. Simulations of the sound pressure at the eardrum (dotted line) and at the outlet of the receiver (dashed line) for a unity voltage driving the receiver.

All the peaks of these pressure responses are caused by acoustic resonances governed by the interaction between the receiver and the tubes. The receiver has a relatively small outlet and therefore it generally represents a high acoustic impedance compared to the impedance of the air in the tubes. Moreover, the coupler, or ear canal for that matter, has considerably smaller acoustic impedance than the preceding plastic tube. Acoustically, this implies that the tube system approximately has one end closed and one end open (see Dillon, 2001). Such tube systems have resonances at frequencies f_r where odd multiples of a quarter of the acoustic wavelength λ equals the total length of the system L_{total} . This can be expressed as

$$\frac{n\lambda}{4} = \frac{nc}{4f} = L_{total} \qquad \text{where} \quad n = 1, 3, 5.... \tag{8.8}$$

and where c is the propagation speed of sound in air. As the total length of the system is $L_{total} = 77.4$ mm, these resonances are found to be the cause of the peaks in figs. 8.3 and 8.4 at 1170 Hz, 3421 Hz, 5742 Hz and 6535 Hz where the acoustic wavelengths are $\lambda = 4L_{total}$, $\lambda = \frac{4}{3} L_{total}$, $\lambda = \frac{4}{5} L_{total}$ and $\lambda = \frac{4}{7} L_{total}$, respectively. Since the receiver end of the system is almost closed, the pressure becomes very high at these frequencies. At certain frequencies, where the receiver has mechanical resonance (see Dillon, 2001), the acoustic impedance of the receiver is very low. Both ends of the tube system may therefore be regarded as open. Such systems have resonances at frequencies where multiples of half the acoustic wavelength equals the total length of the tube system:

$$\frac{n\lambda}{2} = \frac{nc}{2f} = L_{total} \qquad \text{where} \quad n = 1, 2, 3.... \tag{8.9}$$

Both criteria are fulfilled at the frequencies 2320 Hz, 4432 Hz and 8625 Hz where the acoustic wavelengths are approximately $\lambda = 2L_{total}$, $\lambda = L_{total}$ and $\frac{1}{2}\lambda = L_{total}$, respectively. The pressure at the receiver outlet is accordingly low at these frequencies. Note that no resonance occurs for $\lambda = \frac{2}{3} L_{total}$ corresponding to $n = 3$. This is due to the receiver having a high impedance at the corresponding frequency given as $f = c / \lambda$.

9 Rubber suspensions

9.1 Dynamic properties of vibration isolators

9.1.1 Introduction

Vibration isolators or suspensions in a hearing aid play an essential role when minimizing internal feedback. These resilient suspensions are used for reducing the vibration transmission from the shell to the microphones and from the receiver to the rest of the hearing aid. In order to evaluate the achieved isolation of the suspensions when placed in the hearing aid, they have to be modeled as a part of a larger numerical model. Such modeling requires that their dynamical properties are determined.

The current section presents an experimental method for determining the dynamic properties of miniature vibration isolators. The method considers the vibration isolators as one or more mass-less springs. These springs are fully described by their complex stiffnesses that can be determined experimentally from vibration measurements. Similar methods considering vibration isolators as one or more springs are already available in literature (see for example Harris and Crede, 1976; Snowdon, 1968). Using these methods the complex stiffnesses are likewise determined experimentally from vibration measurements. To the best of the author's knowledge, however, the specific application of such methods to *miniature* vibration isolators has not received much attention. Such an application involves certain practical problems and solutions to these are of great interest to engineers developing hearing aids. An introduction to the theory of simple mass-isolator systems will be given in the following. This is succeeded by an outline of the employed method for determining the dynamic properties. Finally, this method is applied to the rubber suspensions of the considered hearing aid.

9.1.2 Simple mass-isolator systems

Figure 9.1 shows three examples of mass-isolator systems that are modeled as a mass and one or more springs. In fig. 9.1a the isolator is placed at the vertical axis going through the gravity centre of the mass. Excitation by the complex velocity $v_{1,y}$ in the *y*-direction at the base of the

system therefore only generates the velocity $v_{2,y}$ of the mass. Vibration of the system only involves one motion coordinate and the dynamic properties of the isolator are thus adequately modeled as one spring with the complex stiffness S_{yy}.

In fig. 9.1b the isolator is placed to the left of the vertical axis going through the gravity centre of the mass. This implies that any translational velocity $v_{1,y}$ or rotational velocity $v_{1,z'}$ around the *z*-axis introduced at the system base results in both a translational velocity $v_{2,y}$ and a rotational velocity $v_{2,z'}$ of the mass. Note that a 'dash' on an index, indicates axis of angular velocity and axis of moment in the case of force characterization. This isolator is therefore represented as both a translational and rotational spring having the complex stiffnesses S_{yy} and $S_{z'z'}$, respectively. Strictly speaking, the suspension also has the *cross-stiffnesses* $S_{yz'} = S_{z'y}$ describing the coupling between the two motion coordinates. For simplicity, however, these stiffnesses have been neglected.

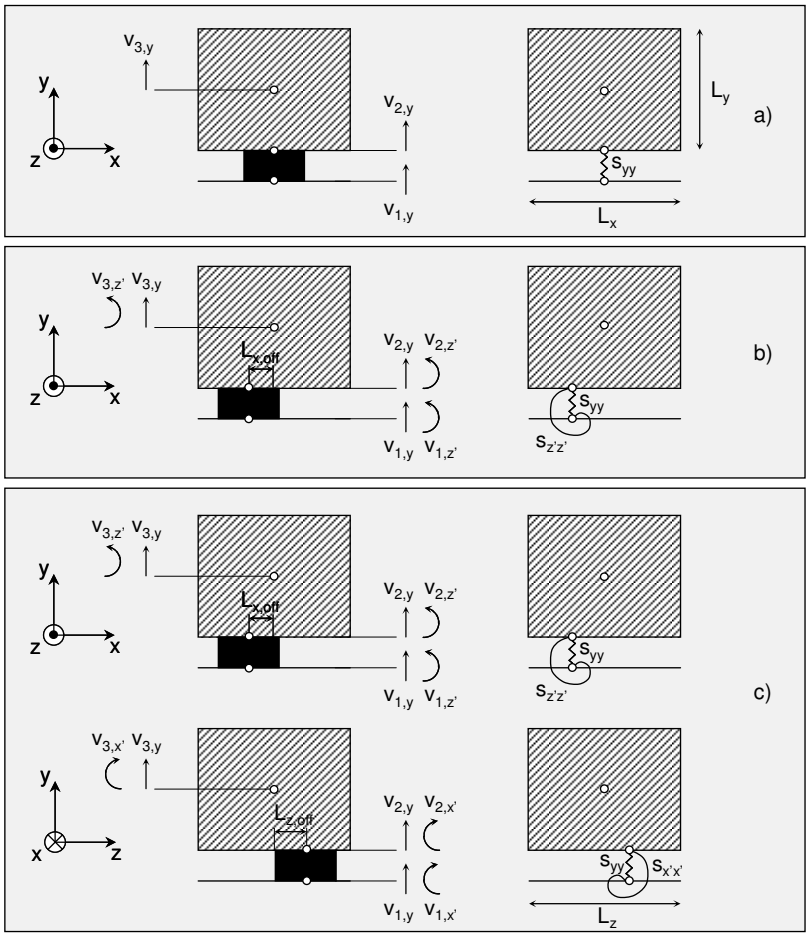

Figure 9.1. Different systems consisting of a mass (shaded areas) and a vibration isolator (black areas). The mass-isolator systems are represented by a pure mass and one or more springs with complex stiffness. Shown are systems involving (a) one (b) two and (c) three motion coordinates.

Finally fig. 9.1c shows a case of a mass-isolator system involving three directions of motion. Two of the directions are the same as in fig. 9.1b whereas the third direction is rotation around the *x*-axis. A third rotational spring with the complex stiffness $S_{x'x'}$ is therefore introduced. Again, the cross-stiffness terms $S_{yz'} = S_{z'y}$, $S_{yx'} = S_{x'y}$ and $S_{z'x'} = S_{x'z'}$ are neglected.

9.1.3 Outline of method for extracting complex stiffnesses

Consider the mass-isolator system shown in fig. 9.1c involving three motion coordinates. Excitation of this system introduces three complex spring forces given by the vector $\{F_S\}$ as

$$\{F_S\} = \begin{bmatrix} F_{S,y} \\ M_{S,z'} \\ M_{S,x'} \end{bmatrix}. \tag{9.1}$$

Here $F_{S,y}$ is the force introduced in the translational spring whereas $M_{S,x'}$ and $M_{S,z'}$ are the moments induced in the springs acting in the rotational *x*- and *z*-directions, respectively. The corresponding velocity vector of the base $\{v_1\}$ and at the mass connection point $\{v_2\}$ are defined as

$$\{v_1\} = \begin{bmatrix} v_{1,y} \\ v_{1,z'} \\ v_{1,x'} \end{bmatrix} \quad \text{and} \quad \{v_2\} = \begin{bmatrix} v_{2,y} \\ v_{2,z'} \\ v_{2,x'} \end{bmatrix} \tag{9.2), (9.3}$$

and they are related to the introduced spring forces as (see Bishop and Johnson, 1960)

$$\{F_S\} = [\mathrm{S}][\{v_1\} - \{v_2\}]/i\omega. \tag{9.4}$$

Here $[\mathrm{S}]$ is the matrix containing the considered stiffnesses reading

$$[S] = \begin{bmatrix} S_{yy} & 0 & 0 \\ 0 & S_{z'z'} & 0 \\ 0 & 0 & S_{x'x'} \end{bmatrix}. \tag{9.5}$$

Equation (9.4) can also be expressed in terms of the mobility matrix of the spring $[Y_S]$ as

$$\{v_1\} - \{v_2\} = [\mathrm{Y_S}]\{F_S\} \tag{9.6}$$

where it applies that

$$[Y_S] = \begin{bmatrix} Y_{S,yy} & 0 & 0 \\ 0 & Y_{S,z'z'} & 0 \\ 0 & 0 & Y_{S,x'x'} \end{bmatrix} = \begin{bmatrix} i\omega/S_{yy} & 0 & 0 \\ 0 & i\omega/S_{z'z'} & 0 \\ 0 & 0 & i\omega/S_{x'x'} \end{bmatrix}. \tag{9.7}$$

Further, due to force equilibrium and continuity the reaction forces acting on the mass are given by the spring force vector $\{F_S\}$ and it therefore applies that

$$\{v_2\} = [Y_{M,22}]\{F_S\}, \tag{9.8}$$

where $[Y_{M,22}]$ is the mobility matrix at the mass connection point reading

$$[Y_{M,22}] = \begin{bmatrix} Y_{M,22,yy} & Y_{M,22,z'y} & Y_{M,22,x'y} \\ Y_{M,22,z'y} & Y_{M,22,z'z'} & 0 \\ Y_{M,22,x'y} & 0 & Y_{M,22,x'x'} \end{bmatrix}. \tag{9.9}$$

Closed form expressions for these mobilities are found in Bishop and Johnson (1960). By isolating $\{F_S\}$ in eq. (9.8) it applies that

$$\{F_S\} = [Y_{M,22}]^{-1}\{v_2\} = [T_{M,22}]\{v_2\} \tag{9.10}$$

where the quantity $[T_{M,22}] = [Y_{M,22}]^{-1}$ has been introduced. Inserting the expression for $\{F_S\}$ into eq. (9.6) the unknown spring forces are eliminated giving

$$\{v_1\} - \{v_2\} = [Y_S][T_{M,22}]\{v_2\}. \tag{9.11}$$

This expression is readily rearranged into

$$\{v_2\} = ([Y_S][T_{M,22}] + [I])^{-1}\{v_1\}, \tag{9.12}$$

representing an expression for the transfer functions from the velocities at the system base, $\{v_1\}$, to the velocities at the connection point on the mass $\{v_2\}$.

Let us assume that the considered mass-isolator system is a model of an experimental arrangement where the measurable harmonic vibration velocities at the base and at the connection point of the mass are given by the two vectors

$$\{v_1\} = \begin{bmatrix} v_{1,y} \\ 0 \\ 0 \end{bmatrix} \quad \text{and} \quad \{v_2\} = \begin{bmatrix} v_{2,y} \\ v_{2,z'} \\ v_{2,x'} \end{bmatrix}, \tag{9.13), (9.14}$$

respectively. Here it is assumed that the base excitation is purely translational.

By inserting these velocity vectors into eq. (9.11) we obtain three equations that each contains one of the stiffnesses. In expanded form the first equation yields

$$\begin{aligned} v_{1,y} - v_{2,y} &= Y_{S,yy}(T_{M,22,yy}v_{2,y} + T_{M,22,z'y}v_{2,z'} + T_{M,22,x'y}v_{2,x'}) \\ &= (i\omega / S_{yy})(T_{M,22,yy}v_{2,y} + T_{M,22,z'y}v_{2,z'} + T_{M,22,x'y}v_{2,x'}) \end{aligned} \tag{9.15}$$

and by rearranging we get an expression for S_{yy} reading

$$S_{yy} = i\omega \frac{T_{M,22,yy}\dfrac{v_{2,y}}{v_{1,y}} + T_{M,22,z'y}\dfrac{v_{2,z'}}{v_{1,y}} + T_{M,22,x'y}\dfrac{v_{2,x'}}{v_{1,y}}}{1 - \dfrac{v_{2,y}}{v_{1,y}}}. \tag{9.16}$$

This expression comprises of known and measurable quantities only. By analogy to eq. (9.14), the corresponding expressions for $S_{z'z'}$ and $S_{x'x'}$ yield

$$S_{z'z'} = i\omega \frac{T_{M,22,z'y}\dfrac{v_{2,y}}{v_{1,y}} + T_{M,22,z'z'}\dfrac{v_{2,z'}}{v_{1,y}}}{-\dfrac{v_{2,z'}}{v_{1,y}}} \tag{9.17}$$

and

$$S_{x'x'} = i\omega \frac{T_{M,22,x'y} \dfrac{v_{2,y}}{v_{1,y}} + T_{M,22,x'x'} \dfrac{v_{2,x'}}{v_{1,y}}}{-\dfrac{v_{2,x'}}{v_{1,y}}}. \tag{9.18}$$

Note that the stiffnesses for the simpler cases (a) and (b) in fig. 9.1, which have less than three motion coordinates, are readily found by removing some of the terms in the expressions in eqs. (9.16) and (9.17).

9.1.4 Dynamic behavior of mass-isolator systems

The dynamic behavior of the mass-isolator systems shown in fig. 9.1 will now be illustrated by three examples with mass and stiffness properties as listed in table 9.1. The mass properties are the same as those of the hearing aid receiver (loudspeaker) in question. It should be noted that the base excitation of the systems is restricted to vibration in the y-direction as specified by the velocity vector $\{v_1\}$ in eq. (9.13).

Mass	
Weight	$m = 0.770$ g
Length in the *x*-direction	$L_x = 7.890$ mm
Length in the *y*-direction	$L_y = 4.090$ mm
Length in the *z*-direction	$L_z = 5.650$ mm
Offset length in the negative *x*-direction from the centre axis	$L_{x,off} = L_x / 2 = 3.945$ mm
Offset length in the positive *z*-direction from the centre axis	$L_{z,off} = 0.986$ mm
Springs	
Translational spring stiffness in the *y*-direction	$S_{yy} = 1 \cdot 10^5$ N/m
Rotational spring stiffness in the *z*-direction	$S_{z'z'} = 1 \cdot 10^{-2}$ Nm
Rotational spring stiffness in the *x*-direction	$S_{x'x'} = 1 \cdot 10^{-1}$ Nm
Loss factor of all springs	$\eta = 0.1$

Table 9.1. Properties of the mass-isolator systems.

The transfer functions of the systems have been simulated numerically using mobility synthesis (see Bishop and Johnson, 1960). Figure 9.2 shows the computed transfer functions from the velocity $v_{1,y}$ at the base to the translational velocity $v_{3,y}$ in the middle of the mass. It is clearly observed that the number of resonances in the different cases is equal to the number of motion coordinates involved. At low frequencies the mass and the base vibrates in phase with equal amplitudes, thus resulting in the transfer functions being 0 dB. The resonance for case (a) in fig. 9.1 occurs around 1800 Hz and for frequencies above 2000 Hz the isolator has an isolating effect. In case (b) a rotational spring around the *z*-axis has been added. This clearly changes the properties of the system. The first resonance, which is primarily rotational, already occurs at 115 Hz. Hereafter the isolator becomes effective and vibration transmission is reduced. At the anti-resonance around 210 Hz vibrations are reduced by almost 30 dB. The second and primarily translational resonance occurs around 3100 Hz, where the isolator looses its isolating effect. Amplification is noted in the band from 2800 Hz to 3800 Hz. Introducing a second rotational spring only alters the transfer function slightly. The main difference is the small peak occurring around 800 Hz. The peak is caused by a primarily rotational resonance involving rotation around the *x*-axis. Since the offset length $L_{z,off}$ in the *z*-direction is rather short, this resonance is correspondingly weak.

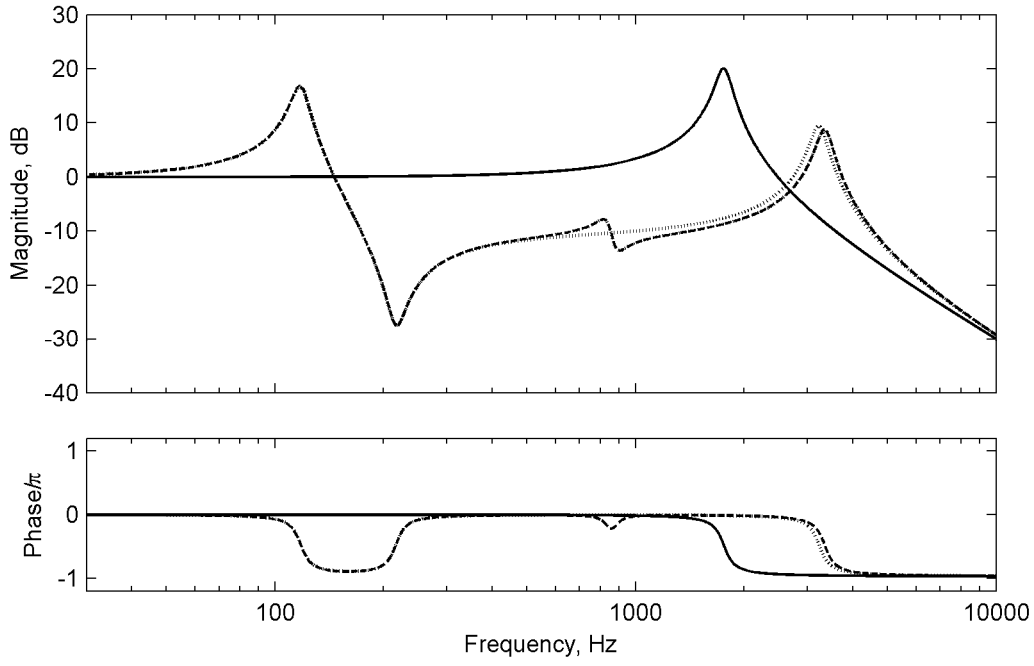

Figure 9.2. Translational transfer functions $v_{3,y} / v_{1,y}$ for the cases shown in fig. 9.1 and with the properties listed in table 9.1. Shown are case (a) (solid line), case (b) (dotted line) and case (c) (dashed line).

Figure 9.3 shows the corresponding transfer functions from the velocity $v_{1,y}$ at the base to the rotational velocities $v_{2z'} = v_{3z'}$ and $v_{2x'} = v_{3x'}$ of the receiver. Naturally the resonances occur at the same frequencies as in fig. 9.2. Not surprisingly, the rotations around the *z*-axis for case (b) and (c) are nearly coinciding. Only the rotational resonance around 800 Hz stand out in case (c). Correspondingly, the rotational velocity around the *x*-axis is small up to around 800 Hz due to the small offset length in the *z*-direction. Above this frequency the *x*-rotation is only about 5 to 10 dB lower than the *z*-rotations.

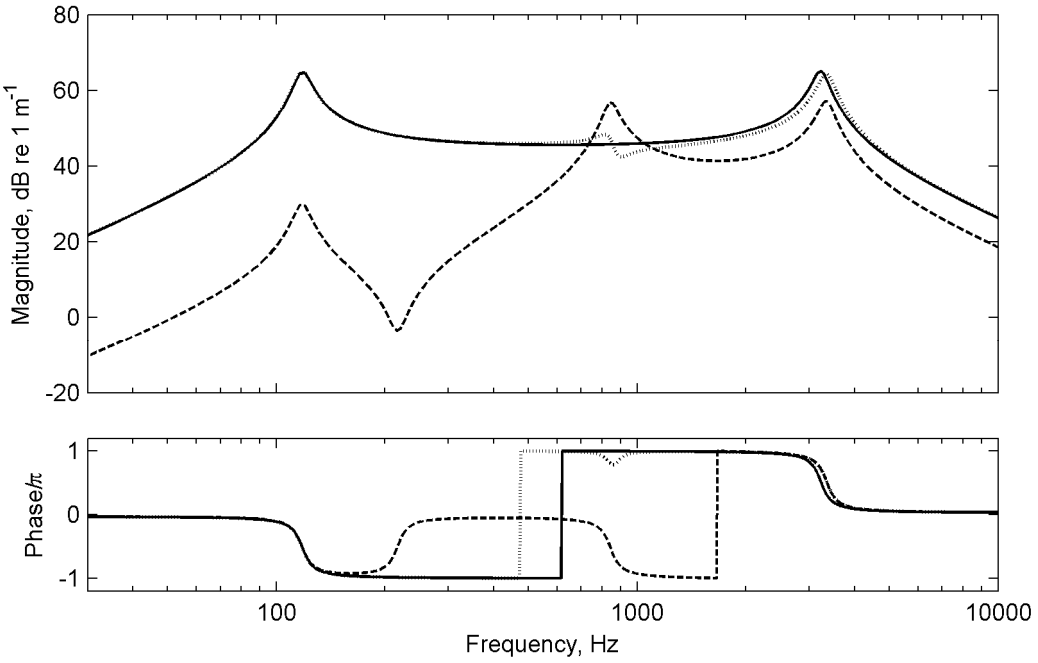

Figure 9.3. Rotational transfer functions for case (b) and (c) shown in fig. 9.1 with the properties listed in table 9.1. Shown are $v_{3,z'} / v_{1,y}$ *(solid line) for case (b) and* $v_{3,z'} / v_{1,y}$ *(dotted line) and* $v_{3,x'} / v_{1,y}$ *(dashed line) for case (c).*

9.2 Experimental results

9.2.1 Experimental setups

Measuring the vibration response of miniature isolators such as the small rubber sleeve suspensions used in a hearing aid requires special setups. A typical dimension, for example, of a microphone with a wrapped rubber isolator is 3.9 mm. Figure 9.4 shows the experimental setups used for determining the properties of the suspensions in the considered hearing aid. Three cases are illustrated (a, b, and c) and regarding the number of motion coordinates these configurations correspond to examples (a), (b), and (c) in fig. 9.1. Corresponding sketches showing the details of these setups are shown in fig. 9.5. Case (a) shows the microphone placed vertically in its thin rubber sleeve suspension. This suspension is mounted in a hard plastic mounting block that has been shaped such that it resembles the attachment in the shell of the hearing aid. In other words the suspension is mounted as if it was placed in the hearing aid.

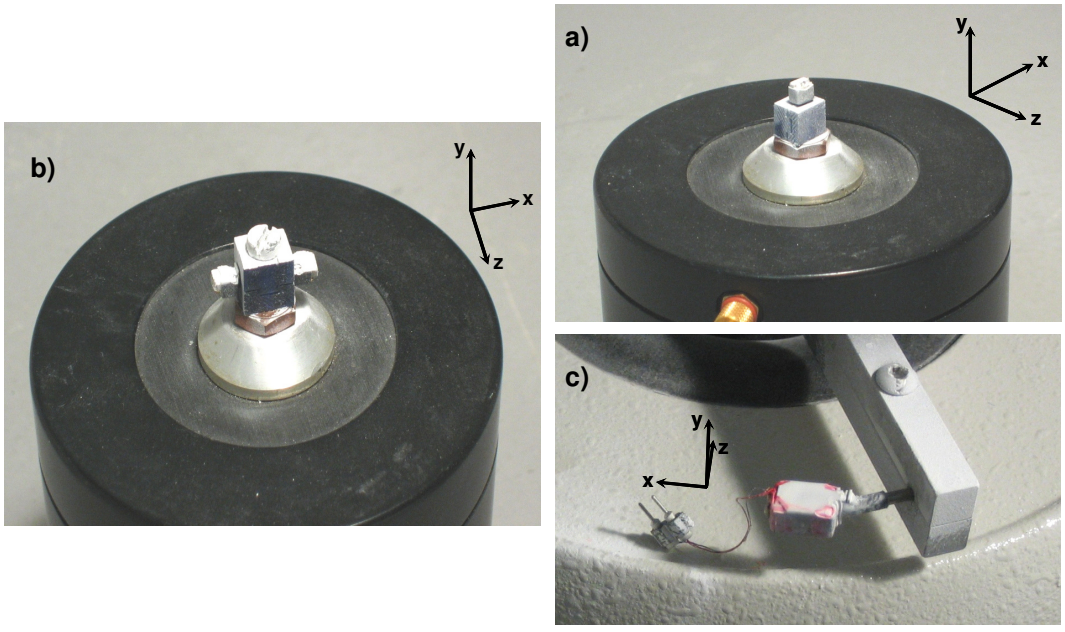

Figure 9.4. Experimental setups for measuring the dynamic properties of hearing aid suspensions. Shown are (a) the microphone with suspension placed vertically, (b) two microphones with suspensions placed horizontally and symmetrically and (c) the receiver with suspension.

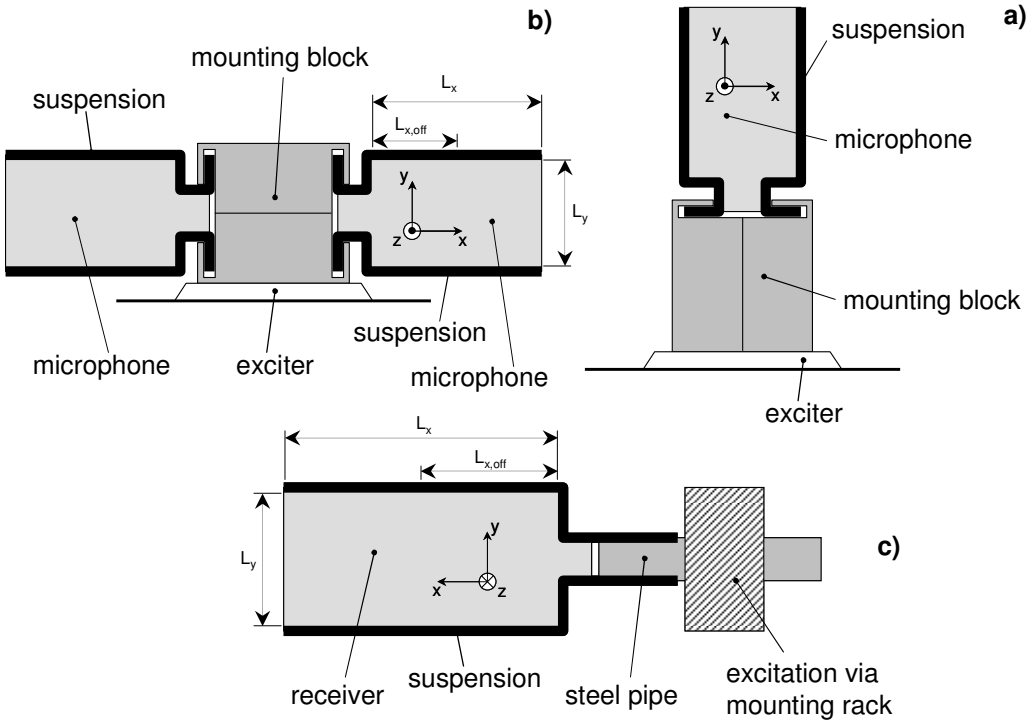

Figure 9.5. Sketches showing the details of the corresponding experimental setups in fig. 9.4 with excitation in the vertical y-direction.

The plastic block is attached rigidly to an electro-dynamic exciter (Brüel & Kjær type 4810) that only excites the system in the *y*-direction. This implies that the vibrations of the mounting block and the microphone only involves translational motion in the *y*-direction. The system therefore corresponds to case (a) in fig. 9.1 where the isolator is considered as a single spring. In case (b) two suspensions and microphones are mounted horizontally and symmetrically. Excitation of the plastic block in the *y*-direction therefore generates translational motion in the *y*-direction as well as the angular motion around the *z*-direction. This system corresponds to case (b) in fig. 9.1 where the suspension is considered as two mass-less springs. Finally, case (c) in fig. 9.4 shows the receiver placed in its suspension. This suspension is mounted to the steel tube as in the hearing aid. Moreover, the steel tube is fixed to a rack which only vibrates in the *y*-direction. This excitation generates vibrations of the receiver in three motion coordinates, being translational motion in the *y*-direction and angular motions around the *z*- and the *x*-axes. Case (c) in fig. 9.1 correspondingly shows such a suspension that is modeled with three springs. It should be noted that the electric cables to microphones and receivers are removed during experiments.

9.2.2 Measured transfer functions

In order to determine the stiffnesses of the suspensions, the vibration velocities of the component mass and the system bases were measured by using a laser vibrometer Polytec type OFV-056. Rotational velocities were measured by measuring in two positions close to one another and dividing by the distance between the two positions. Figure 9.6 shows the transfer functions $v_{3,y} / v_{1,y}$ for case (a) measured on four nominally identical microphone suspensions mounted in an arrangement as in the actual hearing aid considered. As expected the hard plastic block and the microphone vibrate in phase at low frequencies. The resonance of the mass-spring systems occurs around 1000 Hz and the corresponding resonance peaks seem to be heavily damped. Above the frequencies from 1000 Hz to 2000 Hz the suspensions become effective and at 10000 Hz the vibration isolation is about 25 dB in average. Some variance in the resonance frequencies of the suspensions is observed.

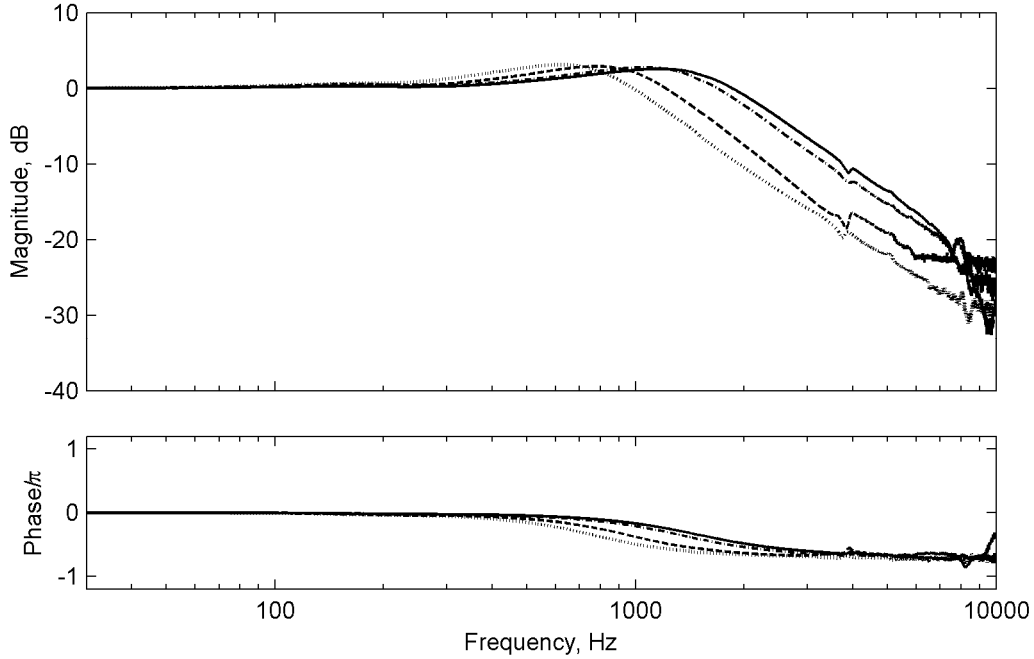

Figure 9.6. Measured transfer function $v_{3,y} / v_{1,y}$ for four nominally identical microphone suspensions of butyl rubber of 36 Shore A participating in the setup shown in fig. 9.4a.

This variance is partly caused by the fact that it is impossible to mount the microphones in their suspensions in the exact same way. Additionally, the suspensions might not be attached in the mounting blocks in the exact same way. These mounting problems, however, are also met when mounting the suspensions and microphones in the hearing aid considered. The variance observed in

fig. 9.6 is therefore representative of the actual variance in the hearing aid. Despite of the variance discussed, the shape of the transfer functions clearly corresponds to the corresponding example case involving one motion coordinate shown in fig. 9.2a.

The transfer functions $v_{3,y} / v_{1,y}$ for case (b) are shown in fig. 9.7 for three suspensions of different types of material. The three materials are butyl rubber, flour silicone rubber, and silicone rubber, all of a Shore 36 A hardness. As expected all three transfer functions have a magnitude level of 0 dB at low frequencies. Moreover, it appears that all three suspensions have their predominantly rotational resonance around 190 Hz, indicating approximately similar stiffness properties. The levels of the resonance peaks, however, are quite different revealing that butyl rubber has the highest value of damping. The group of second resonances occurring in the frequency range from about 2500 Hz to 3500 Hz is predominantly translational and it shows the same damping properties of the three materials as the group of resonances around 190 Hz. Minor resonance peaks are seen from around 650 Hz and 1100 Hz. These peaks most likely occur because of unwanted torsional modes indicating that the setup is not perfectly aligned. Nevertheless, it is concluded that the overall pattern is similar to the corresponding case shown in fig. 9.2. Finally, observing the transfer function of the butyl rubber suspension, which is the material used in the hearing aid considered, it is seen that the vibration isolation effect is almost 15 dB from about 1000 Hz and upwards in frequency.

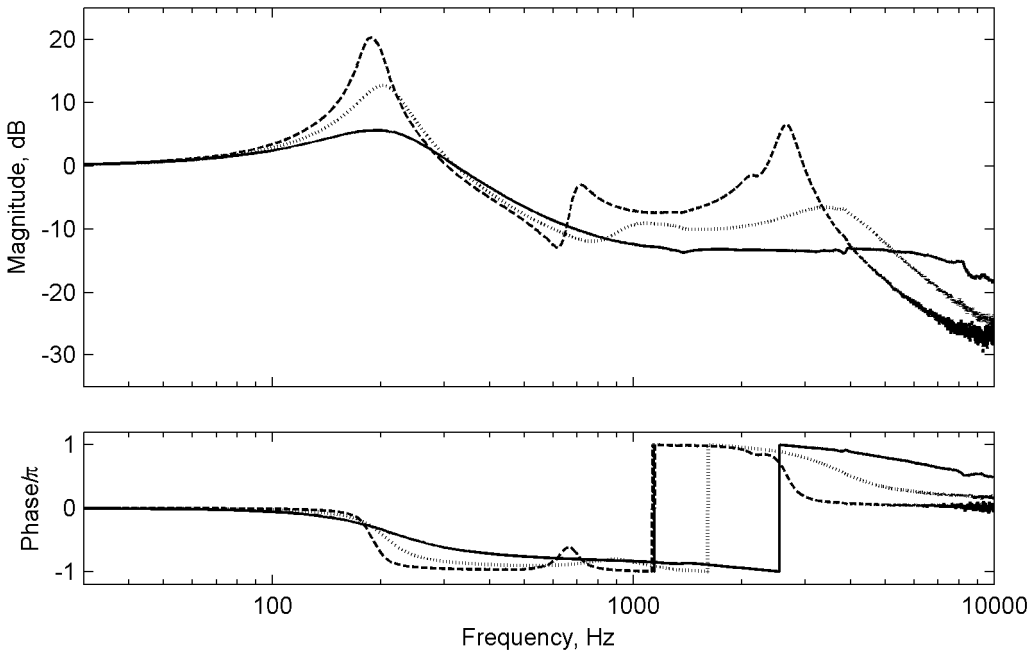

Figure 9.7. Measured transfer functions $v_{3,y} / v_{1,y}$ for the microphone suspensions in the setup shown in fig. 9.4b. Results are shown for the suspension materials butyl rubber (solid line), flour silicone rubber (dotted line) and silicone rubber (dashed line), all of 36 Shore A hardness.

Figure 9.8 shows the transfer functions for the receiver suspension corresponding to the case shown in fig. 9.1c; the suspension is of butyl rubber Shore 50 A hardness. This case involves three complex stiffnesses. Both the transfer functions for the centre point and the connection point of the mass are shown. Due to the high damping of the butyl rubber only two resonances are visible in each of the transfer functions. The first resonance around 100 Hz involves primarily angular motion around the *z*-axis. Moreover, the primarily translational resonance is found around 2800 Hz. The third and very weak resonance, which mainly involves angular motion around the *x*-axis, is not visible. Nonetheless, it occurs at a frequency between 100 Hz and 2800 Hz. As shown in the example in fig. 9.2, this resonance is only weakly excited as the offset length in the *z*-direction is small. Above, say, 4000 Hz minor problems with the setup arise and the mass-spring system is evidently vibrating in other directions than intended. Considering the transfer function for the centre point of the receiver, the isolation effect of the suspension is clearly illustrated. Maximum vibration isolation of 18 dB is achieved around 400 Hz and the isolation effect is more than 12 dB up to 10000 Hz. It should be kept in mind, however, that proper evaluation of the vibration isolation effect of the receiver suspension is characterized by its insertion loss (see Harris and Crede, 1976). Determination of this insertion loss requires that the vibration transmission from the receiver to the hearing aid is calculated with and without using the resilient suspension.

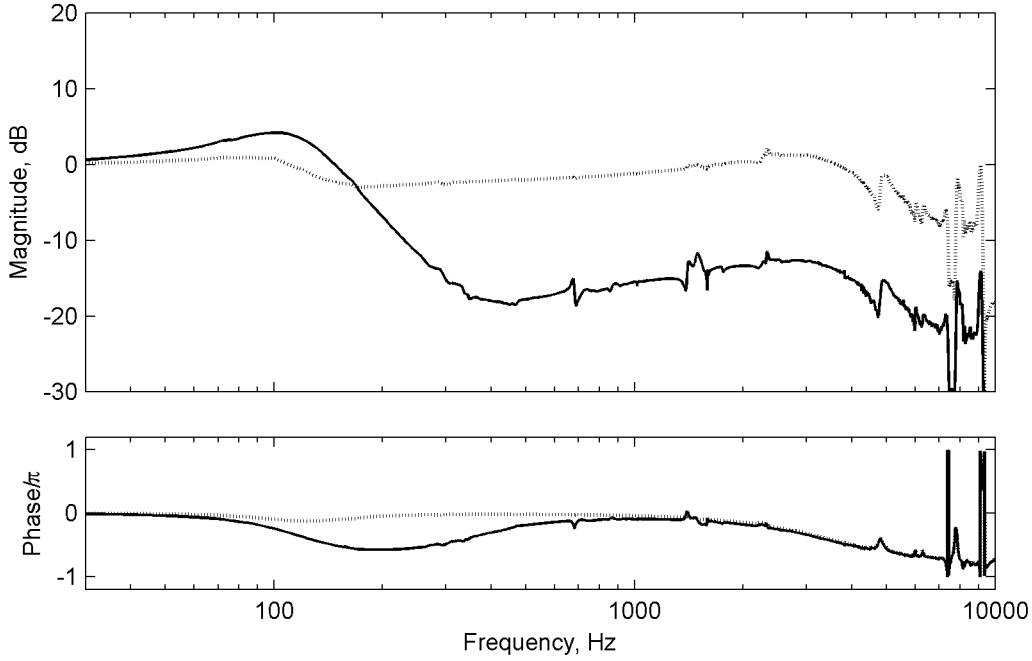

Figure 9.8. Measured transfer functions for the receiver suspension made of butyl rubber 50 Shore A hardness shown in the setup in fig. 9.4c. Shown are the transfer function from the driving point to the centre of the receiver $v_{3,y} / v_{1,y}$ *(solid line) and the driving point to the connection point* $v_{2,y} / v_{1,y}$ *(dotted line).*

Further insight into the properties of the suspensions is gained by examining the rotational transfer functions for cases (b) and (c); such results are plotted in fig. 9.9. First considered is the transfer function for angular motion around the *z*-axis for case (b). The overall shape of this transfer function showing two resonances is clearly in agreement with the corresponding example shown in fig. 9.3. Moreover, the rotational transfer functions for angular motion around the *z*-axis for case (c) likewise show the correct pattern. The transfer function for the angular motion around the x-axis, however, looks somewhat different from the corresponding transfer function shown in fig. 9.3. Nevertheless, if the loss factor and the rotational stiffness around the x-axis properties of the example are changed to $\eta = 1$ and $S_{x'x'} = 1 \cdot 10^{-2}$ Nm, a transfer function closely resembling the one shown in fig. 9.9 is obtained.

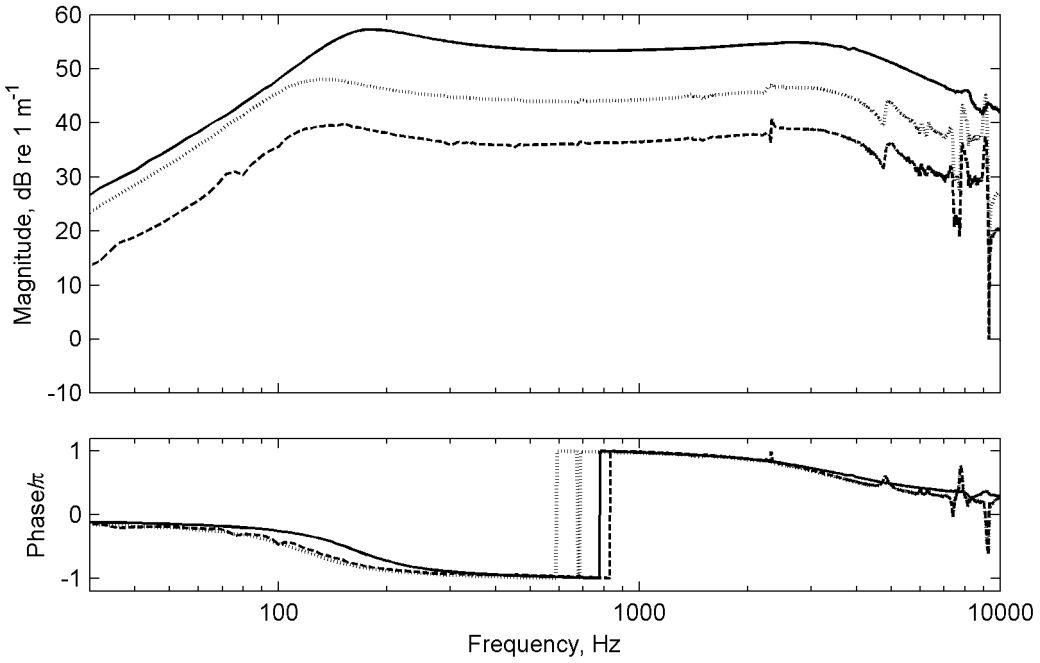

Figure 9.9. Measured rotational transfer functions for the suspensions in butyl rubber. Shown are $v_{3,z'} / v_{1,y}$ *for case (b) (solid line) as well as* $v_{3,z'} / v_{1,y}$ *(dotted line) and* $v_{3,x'} / v_{1,y}$ *(dashed line) for case (c).*

9.2.3 Extracted stiffnesses

The stiffness of the suspensions can be determined from the reported transfer function measurements. Figure 9.10 shows results for four translational stiffnesses of case (a). These stiffnesses are computed using eq. (9.16) and the transfer functions for the four nominally identical microphone suspensions shown in fig. 9.6. Generally the four stiffnesses have the same shape, but, their levels vary up to a factor of 5 in the frequency range from 30 Hz to about 3000 Hz. The reasons for this variance in stiffness as well as transfer function were discussed in subsection 9.2.2. Above 3000 Hz some problems in the determination of the stiffnesses are observed. From fig 9.6 it is seen that the transfer functions are less smooth above 3000 Hz than in the rest of the frequency range considered. These irregularities in the transfer functions are unfortunately enhanced when computing the stiffnesses. The corresponding loss factors are seen to be rather close up to about 2000 Hz. Above this frequency problems also occur in determination of the loss factors. For later use in a numerical model all nominally identical stiffnesses are fitted into one single stiffness curve.

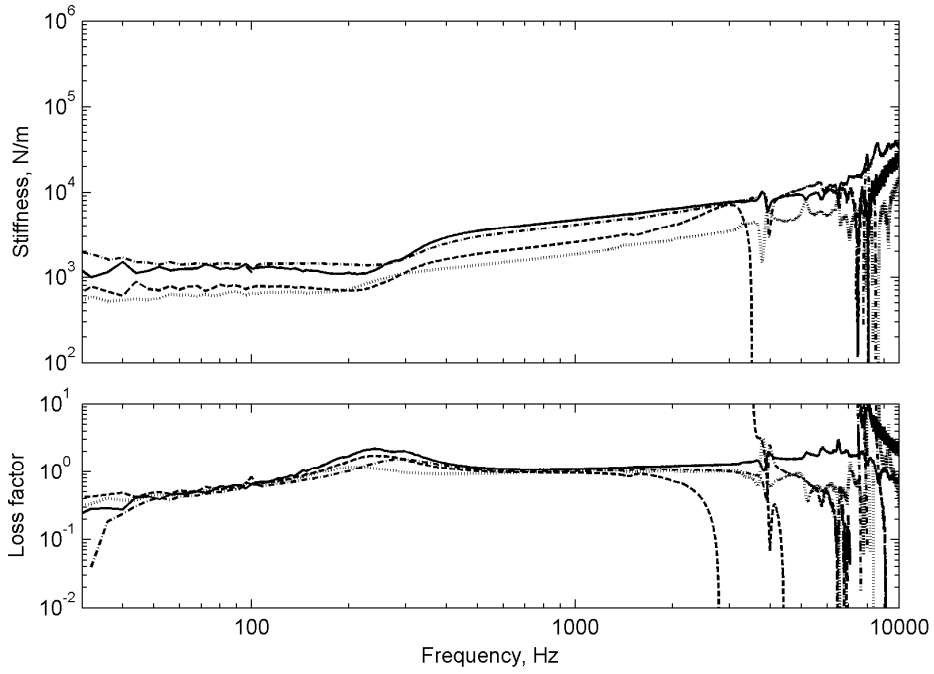

Figure 9.10. Complex stiffnesses S_{yy} in the y-direction for four nominally identical microphone suspensions. The experimental setup shown in fig. 9.4a was utilized.

Figure 9.11 shows the fitted mean translational stiffnesses of the three suspension cases from fig. 9.4 computed using eq. (9.16). It is observed that all three stiffnesses have the characteristic S-shape of rubber materials with high damping (see Snowdon, 1968). This shape is

due to the material's transition from rubber state at low frequencies to the so-called glass-like state at higher frequencies. In the glass-like state the dynamic modulus becomes so large that the characteristic resilience of the material is lost. According to Snowdon (1968) the lossfactor is also dependent on frequency. Normally the lossfactor becomes largest in the transition zone between the two mentioned states. This transition zone approximately occurs at the point where the stiffness function has a curvature of zero. From fig. 9.11 it is seen that the lossfactor is very high in all three cases. Especially in case (a) the loss factor reaches the extremely high value of 2 at 290 Hz.

Finally the corresponding rotational stiffnesses of case (b) and (c) are shown in fig. 9.12. These stiffnesses are all nearly increasing proportionally with frequency and are therefore considerably different from the S-formed stiffnesses shown in fig. 9.11. According to Snowdon (1968) the increase in the stiffness of high-damping rubber materials may be proportional to frequency. Again it is observed that the loss factors reach high values of almost 1.

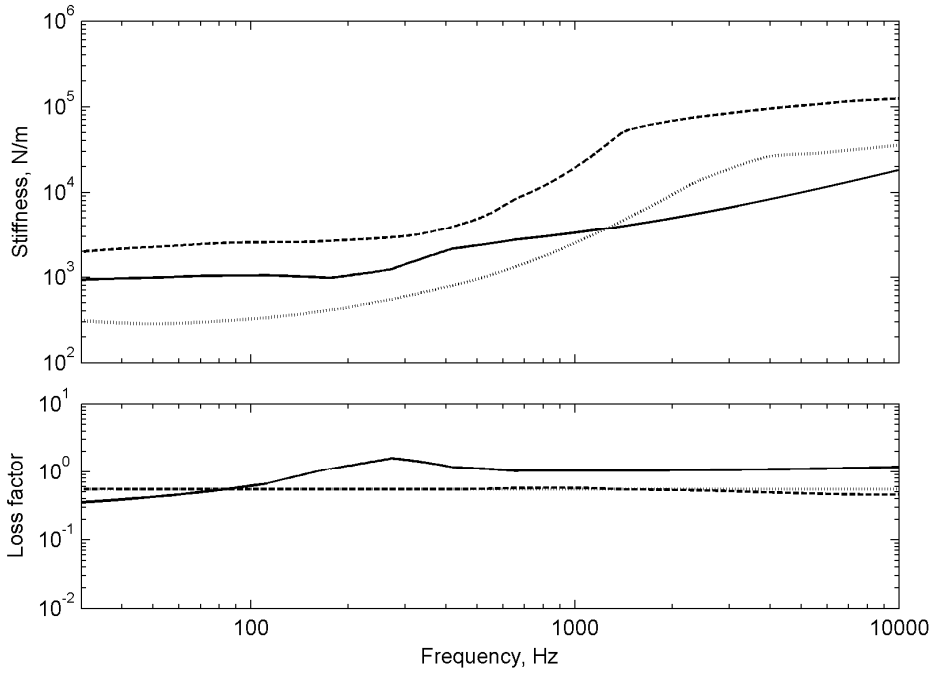

Figure 9.11. Fitted complex stiffnesses S_{yy} in the y-direction for case (a) (solid line), (b) (dotted line) and (c) (dashed line) shown in fig. 9.4.

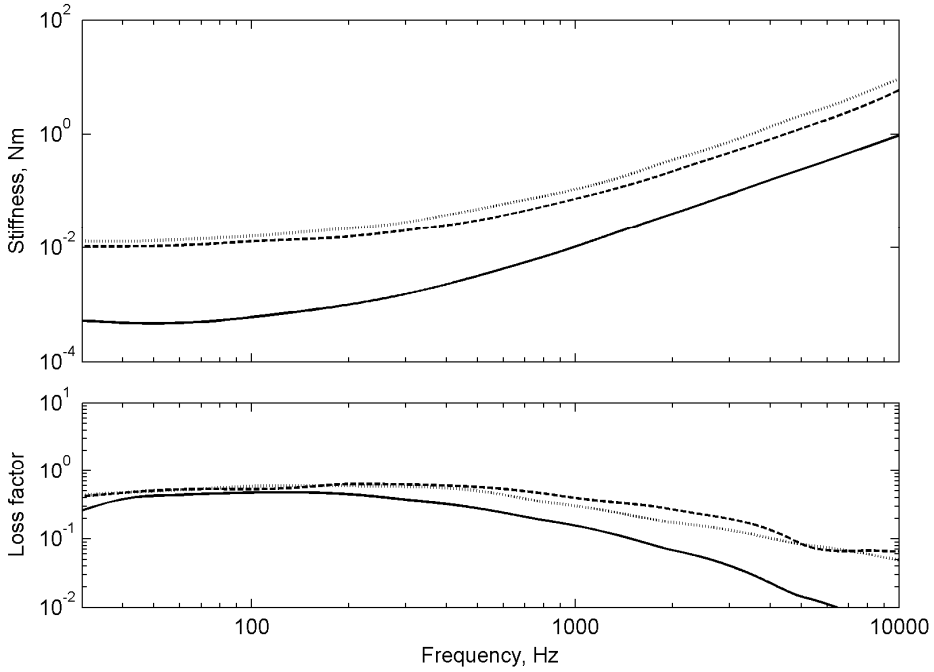

Figure 9.12. Fitted rotational complex stiffnesses. Shown is $S_{z'z'}$ for case (b) (solid line) as well as $S_{z'z'}$ (dotted line) and $S_{x'x'}$ (dashed line) for case (c) shown in fig. 9.4.

Only some of the directions shown in fig. 9.4 have been considered. However, in order to include the suspensions in the full 3D-model all properties of the suspensions must be considered. Fortunately, the dynamic properties in the remaining directions correspond to some of the determined stiffnesses. For the case shown in fig. 9.4b the stiffnesses S_{zz}, $S_{y'y'}$ and $S_{x'x'}$ have not been determined. Due to symmetry of the suspension with regards to the *x*-axis, it can be assumed that $S_{zz} = S_{yy}$ and that $S_{y'y'} = S_{z'z'}$. The torsional spring stiffness $S_{x'x'}$ around the *x*-axis is not so important when evaluating the effect of the suspension and it is therefore assumed that it is very high. Regarding the receiver suspension shown in fig. 9.4c, the stiffnesses S_{zz}, S_{xx} and $S_{y'y'}$ still remains. Also here it can be assumed that $S_{zz} = S_{yy}$ and $S_{y'y'} = S_{z'z'}$ due to symmetry. Again, S_{xx} is assumed to be very high.

9.2.4 Discussion of the results

It was mentioned earlier that the properties of the suspensions are modeled without taking cross-stiffnesses into account. In retrospect, it would have been better to include such cross-stiffnesses even though their influence in practice might be minor. A method for determining these cross-stiffnesses will therefore be discussed in the following.

Considering case (c) in fig. 9.4 and using reciprocity the full stiffness matrix $[S]$ of the receiver suspension is given as

$$[S] = \begin{bmatrix} S_{yy} & S_{yz'} & S_{yx'} \\ S_{yz'} & S_{z'z'} & S_{z'x'} \\ S_{yx'} & S_{zx'} & S_{x'x'} \end{bmatrix}. \tag{9.19}$$

This matrix includes the three cross-stiffnesses $S_{yz'}$, $S_{yx'}$ and $S_{z'x'}$. When exciting the considered system. The velocities in the *y*-direction and the rotational *x*-direction are independent and therefore it applies that $S_{yx'} = 0$. Moreover, the velocities in the rotational *z*-direction and *x*- direction are likewise independent and consequently we also have that $S_{z'x'} = 0$. Neglecting the cross-terms $S_{yx'}$ and $S_{z'x'}$ is therefore valid and only one cross-stiffness, $S_{yx'}$, remains to be determined. An explanation for some of the cross-stiffnesses being zero is also given in Snowdon (1968). Here it is stated that the cross-stiffnesses are zero if the associated coordinate system is placed in the directions of the so-called *principal axes* of the isolator.

The *three* stiffnesses S_{yy}, $S_{z'z'}$ and $S_{x'x'}$ were determined from *three* independent equations formed by eq. (9.9). If the fourth stiffness $S_{yx'}$ is taken into account, we therefore need one more equation to determine this stiffnesses. By analogy to the "two-load" method considered in section 8 (see Egolf, 1977; Egolf and Leonard, 1977; Egolf *et al.*, 1988a), such an extra equation is obtained by replacing the current rather heavy receiver mass with another load. This other load could for example be a light plastic block with the same dimensions as the receiver. In practice the receiver is easily replaced by a plastic block as its suspension is open furthest away from the mounting rack, see fig. 9.5c. The cross-stiffness $S_{yz'}$ has also been neglected in case (b). By analogy to case (c) it is anticipated that this stiffness can also be determined by replacing the microphones with another mass load.

10 Vibration forces of the receiver

10.1 Introduction

The purpose of the receiver (loudspeaker) is to produce a high sound pressure in the acoustic tube system of the hearing aid. This sound pressure is partly governed by the acoustic source strength of the receiver as discussed in section 8. Apart from the acoustic source strength, however, the receiver also has an unwanted *mechanical* source strength. This strength primarily involves forces acting in the direction of the membrane motion and they cause the receiver to vibrate strongly during operation. The exact excitation point of the inner excitation forces of the receiver is not known and it most likely depends on frequency. The vibration forces of the receiver are therefore modelled as *equivalent* vibration forces acting at its centre point. Naturally, these equivalent forces produce the same excitation as the actual excitation mechanisms.

The present section presents an experimental method for determining the equivalent vibration forces acting in the middle of the receiver. This method is developed by the author with inspiration from Laugesen and Ohlrich (1994), Ohlrich (1998), Ohlrich and Friis (2006) and Ohlrich *et al.* (2006). A related study of the free vibrations of a hearing aid receiver using two-port parameters was presented in the technical report from Knowles by Warren (2001). Unfortunately, application of this technique to other hearing aid receivers is not straightforward as it requires deep insight into the receiver's complicated electrical analogue circuits.

10.2 Outline of method for extracting the vibration forces

In the following it is assumed that the excitation forces of the receiver only are dependent on the acoustic system connected to the receiver as well as the receiver driving voltage. If this is not the case, the membrane vibration and thus the acoustical output of the receiver motion is altered by restraining the motion of the receiver or by changing the suspension. From experiments it has been verified that this is not the case.

The setup shown in fig. 4c is utilized for determining the vibration excitation forces of the receiver. For this particular purpose, however, the mounting rack and the pipe is fixed for any

motion and the receiver is driven with a known harmonic voltage U_{rec}. Moreover, the total acoustic system consisting of the steel pipe, hook, plastic tube and coupler is connected to the receiver.

The dynamic properties of the receiver suspension were determined in the previous section. This implies that the total input mobility matrix in the gravity centre of the receiver (in the middle of the receiver) can be determined by regarding the suspension-receiver-system as a mass-spring-system and by the use of mobility synthesis (see Bishop and Johnson, 1960). The mobilities of this matrix involve translational motion in the *y*-direction as well as angular motion around the *z*- and *x*-axes. Hence, the mobility matrix is a three-by-three matrix with nine frequency dependent elements. Let us assume that the mobility matrix is denoted $[Y_{33}]$ and that the three equivalent vibration excitation forces in the gravity centre of the receiver are given by the excitation vector $\{F_{exc}\}$ as

$$\{F_{exc}\} = \begin{bmatrix} F_{y,exc} \\ M_{z',exc} \\ M_{x',exc} \end{bmatrix} \tag{10.1}$$

where $F_{y,exc}$ is the excitation force in the *y*-direction and $M_{z',exc}$ and $M_{x',exc}$ are the excitation moments around the *z*-axis and *x*-axis, respectively. Moreover, the vibration velocities produced in the middle of the receiver are given by the vector $\{v_3\}$ as

$$\{v_3\} = \begin{bmatrix} v_{3,y} \\ v_{3,z'} \\ v_{3,x'} \end{bmatrix} \tag{10.2}$$

where $v_{3,y}$ is the velocity in the y-direction whereas $v_{3,z'}$ and $v_{3,x'}$ are the rotational velocities around the *z*-axis and *x*-axis, respectively. These three velocities can be measured by using a laser vibrometer. The excitation force vector $\{F_{exc}\}$ and velocity vector $\{v_3\}$ are related as

$$\{v_3\} = [Y_{33}]\{F_{exc}\} \tag{10.3}$$

and the force excitation vector is then determined by a matrix inversion of $[Y_{33}]$ yielding

$$\{F_{exc}\} = [Y_{33}]^{-1}\{v_3\} \ . \tag{10.4}$$

The excitation forces of the receiver per unit driving voltage finally becomes

$$\{F_{exc}\} = [Y_{33}]^{-1}\{v_3\}/U_{rec} \ . \tag{10.5}$$

10.3 Experimental results

The excitation forces were computed numerically by using eq. (10.5) and measured data of the vibration velocities in the middle of the receiver. Results for the excitation force in the *y*-direction $F_{y,exc}$ for tests on three nominally identical receivers are shown in fig. 10.1. It is clearly seen that the determined forces are almost coinciding. As expected the maximum excitation force occur around 3400 Hz where the acoustic pressure at the receiver outlet also has its maximum as shown in fig. 8.4. This maximum force reaches the significant level of 3 mN. Not surprisingly the other local maxima occur approximately at frequencies where the acoustic tube system has its resonances.

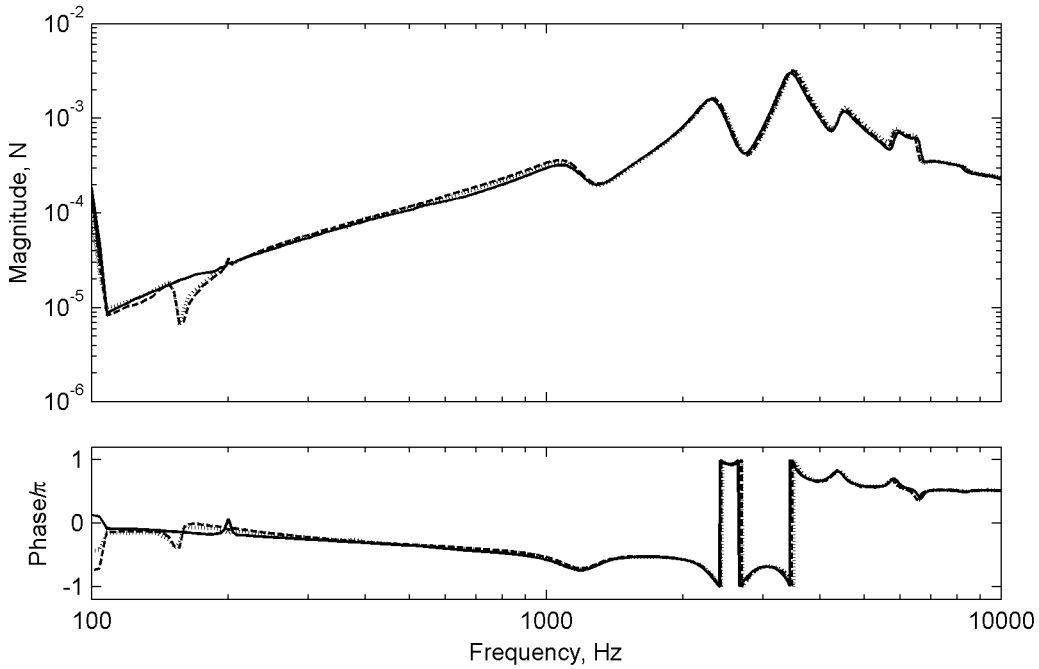

Figure 10.1. Equivalent excitation force $F_{y,exc}$ in the middle of the receivers; results from tests on three receivers.

Results for the corresponding three excitation moments $M_{z',exc}$ around the *z*-axis are shown in fig. 10.2. In order to compare these moments with the forces in fig. 10.1, they have been transformed into force pairs $M_{z',exc} / L_x$ separated by the largest dimension of the receiver being $L_x = 7.890$ mm, see fig. 9.5c. These transformed moments have almost the exact same shape as the forces in fig. 10.1. Their level, however, is considerably lower being 0.35 mN at their maximum around 3400 Hz. This result clearly illustrates that the primary excitation of the receiver occurs in the translational *y*-direction. This was further verified when calculating the three excitation moments $M_{x',exc}$ around the *x*-axis. These moments were very small in magnitude and they are therefore fully negligible. This was expected since the receiver including its membrane and suspension is symmetrical with respect to its local *xy*-plane, see fig. 9.4c or 9.5c.

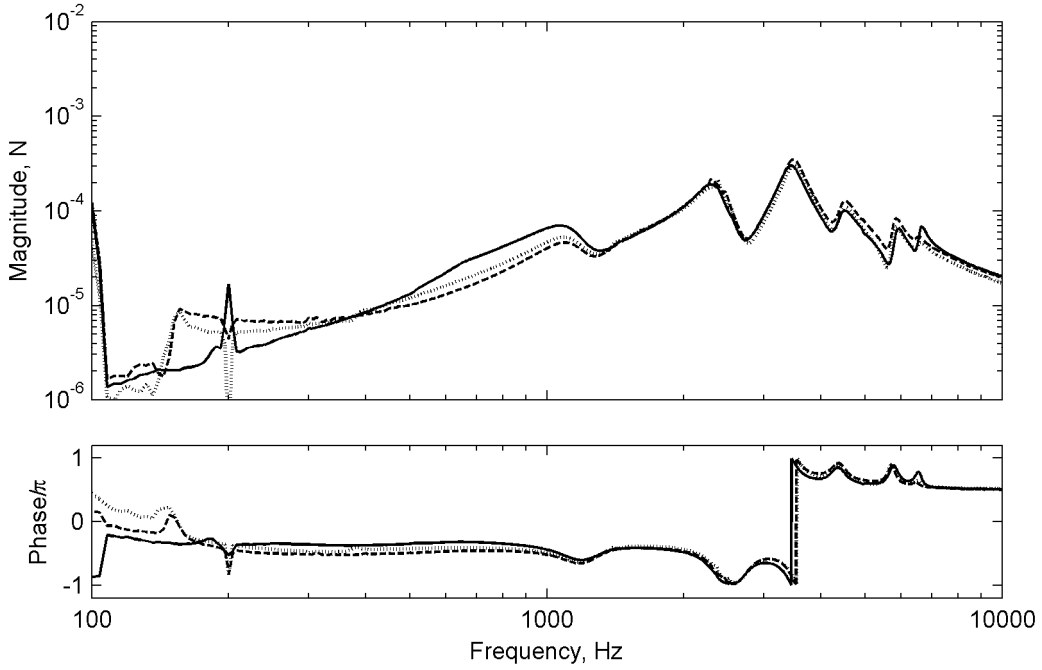

Figure 10.2. Transformed equivalent excitation moments $M_{z',exc} / L_x$ acting in the middle of the receiver; results from tests on three receivers.

11 Microphone sensitivities

11.1 Introduction

To analyze the mechanisms causing internal feedback in hearing aids it is important to determine the pressure sensitivity and the vibration sensitivity of the microphones. If the pressure at the microphone inlets and the vibrations of the microphones are known it is possible to separate the total electrical microphone output into acoustic and mechanical contributions by means of these sensitivities. Figure 11.1 shows the condenser microphone type EM-3346 from Knowles used in the considered hearing aid. Both the pressure and vibration sensitivities of this microphone are determined in this section.

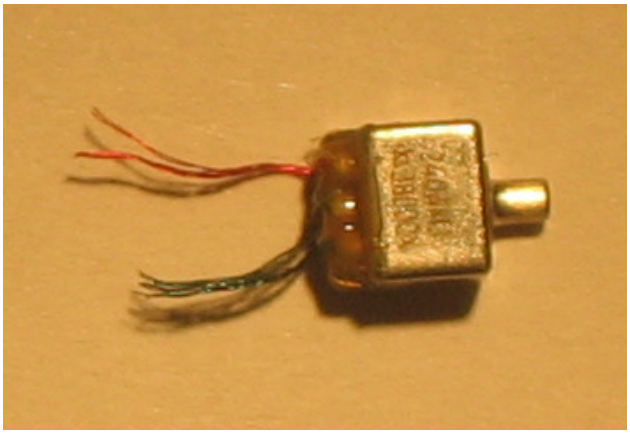

Figure 11.1. Condenser microphone type EM-3346 from Knowles.

11.2 Determination of the pressure sensitivity

The amplitude of the pressure sensitivity is generally displayed on the data sheet published by the manufacturer. If the phase data is needed, however, it is necessary to model the microphone using the two-port network theory considered in section 8. The two-port parameters of the microphone can either be determined experimentally using the two-load method or by employing the electrical analogue circuits published on the manufacturer's homepage (LoPresti, 2003). In this case, the two-port parameters of the microphone have been determined by employing electrical analogue circuits.

Generally the microphones used in hearing aids have very small inlets and the inlets therefore represent a high acoustic input impedance (see Egolf, 1988a). This also implies that the particle velocity u at the inlets is negligibly small and it is consequently assumed that $u = 0$. The transmission matrix of a microphone is given as

$$\begin{Bmatrix} p_{in} \\ Q_{in} \end{Bmatrix} = \begin{bmatrix} A & B \\ C & D \end{bmatrix} \begin{Bmatrix} V_{out} \\ I_{out} \end{Bmatrix} \tag{11.1}$$

where A, B, C and D are the two-port parameters. Moreover, p_{in} and Q_{in} are the input acoustic pressure and volume velocity, respectively, whereas V_{out} and I_{out} are the electrical output voltage and current. Naturally the assumption that $u = 0$ implies that $Q_{in} = 0$. It is therefore also valid to set the two-port parameters C and D to zero.

The pressure sensitivity for the considered microphone has been determined by analogy to the method presented in Egolf (1988a). Figure 11.2 shows the simulated pressure sensitivity. It is observed that the sensitivity varies almost 15 dB in the considered frequency range. Around the frequency 5000 Hz the sensitivity reaches its maximum of nearly -28 dB where there also is a phase change of almost π.

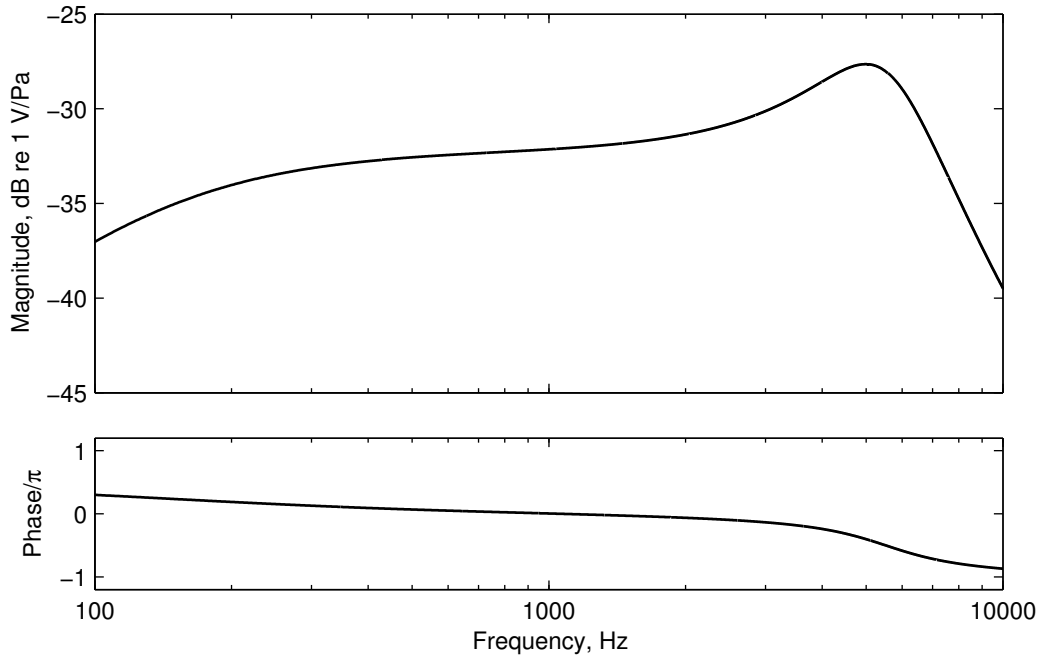

Figure 11.2. Pressure sensitivity of the condenser microphone type EM-3346 from Knowles.

11.3 Determination of the vibration sensitivity

Figure 11.3 shows a sketch of a miniature condenser microphone of type EM from Knowles. This microphone has a very light and pre-stressed membrane, which is located next to a large air filled back volume acting as a spring. When the microphone is set into vibration this air volume is accelerated and creates forces acting on the membrane. The displacements of the membrane hereby produce an unwanted electrical output.

In principle the vibration sensitivity of a microphone can be divided into three directions being the *x*-, *y*- and *z*-directions. It is anticipated, however, that the most critical direction of vibration is the *y*-direction perpendicular to the membrane. The vibration sensitivities in the *x*- and *z*-directions are thus neglected in the present thesis.

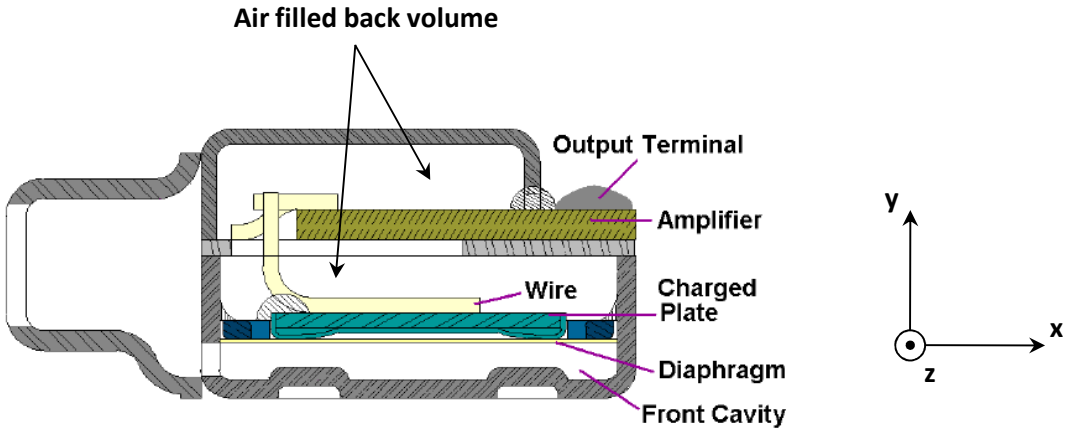

Figure 11.3. Sketch of a miniature condenser microphones of type EM from Knowles (obtained from www.knowles.com).

The vibration sensitivity in the *y*-direction of the EM-3346 microphone is determined by using the experimental method presented in an early paper by Killion (1975). Here the vibration sensitivity is defined as the electrical output produced by the microphone when it has an acceleration of 1 m/s^2 and when the pressure at the inlet is zero. Such conditions can be obtained by using the setup sketched in fig 11.4. A small and rectangular cavity is excited in the *y*-direction by a electro-dynamic exciter. Vertical motion of the top and bottom walls produces a sound field in the cavity where the pressure p at $y = -h/2$ is zero due to symmetry of the cavity. By placing the microphone exactly in the vertical middle at $y = -h/2$, it's electrical output is caused only by the known acceleration in the *y*-direction.

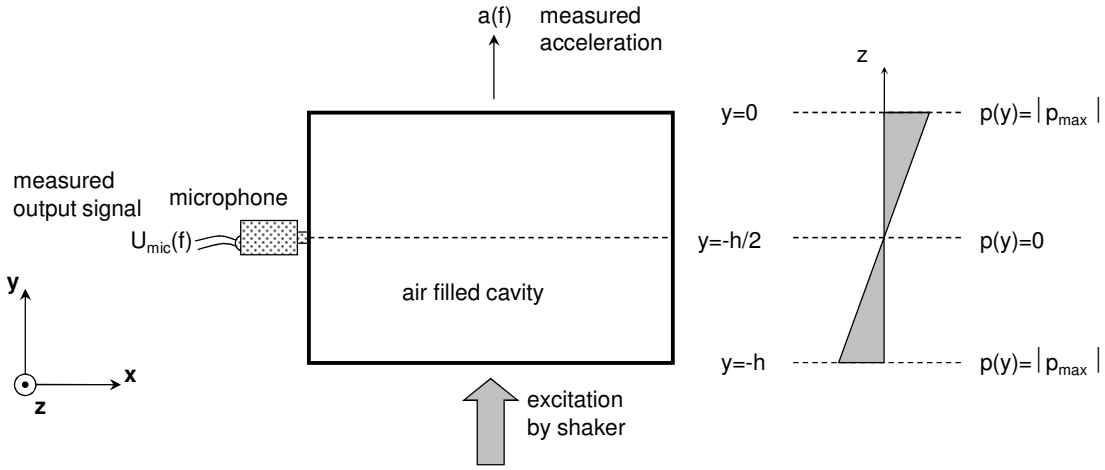

Figure 11.4. Sketch of the experimental setup for measuring the vibration sensitivity of miniature microphones.

As a check, the pressure field in the cavity can be determined by considering the cavity as a tube with the length h, which is driven with pistons at the ends, that is, the top and bottom walls. These pistons have the same vibration amplitude and phase. The general solution for the pressure $p(y)$ is of the form (Cremer *et al.*, 1988)

$$p(y) = p_+ e^{-iky} + p_- e^{iky} \tag{11.2}$$

where k is the acoustic wave number and p_+ and p_- are the complex pressure amplitudes of waves propagating in the positive and negative y-direction, respectively. Moreover it applies that the particle velocity $u(y)$ is given as

$$u(y) = \frac{p_+}{\rho c} e^{-iky} - \frac{p_-}{\rho c} e^{iky} . \tag{11.3}$$

If the pistons at the top and bottom plates have the velocity u_1 then the boundary conditions are

$$u(0) = u(-h) = u_1 . \tag{11.4}$$

Further, by combining eqs. (11.2)-(11.4) the pressure amplitudes p_+ and p_- can be derived and the pressure $p(y)$ hereby becomes

$$p(y) = \rho c \frac{u_1}{i2\sin kh} ((1 - e^{-iky}) e^{-iky} + (1 - e^{jky}) e^{iky}) . \tag{11.5}$$

By inserting $y = -h/2$ in eq. (11.5) it is seen that the pressure is zero in the middle of the cavity. Moreover, at frequencies where the acoustic wavelength is large compared to h the pressure variation with y is linear as shown in Fig 11.4.

The vibration sensitivity has been measured for three nominally identical miniature microphones of type EM-3346 from Knowles. Figure 11.5 shows the measured vibration sensitivities. For comparison, the average vibration sensitivity of the microphone of type EM-3046 from Knowles have been plotted. This sensitivity has been measured by Knowles using the same technique.

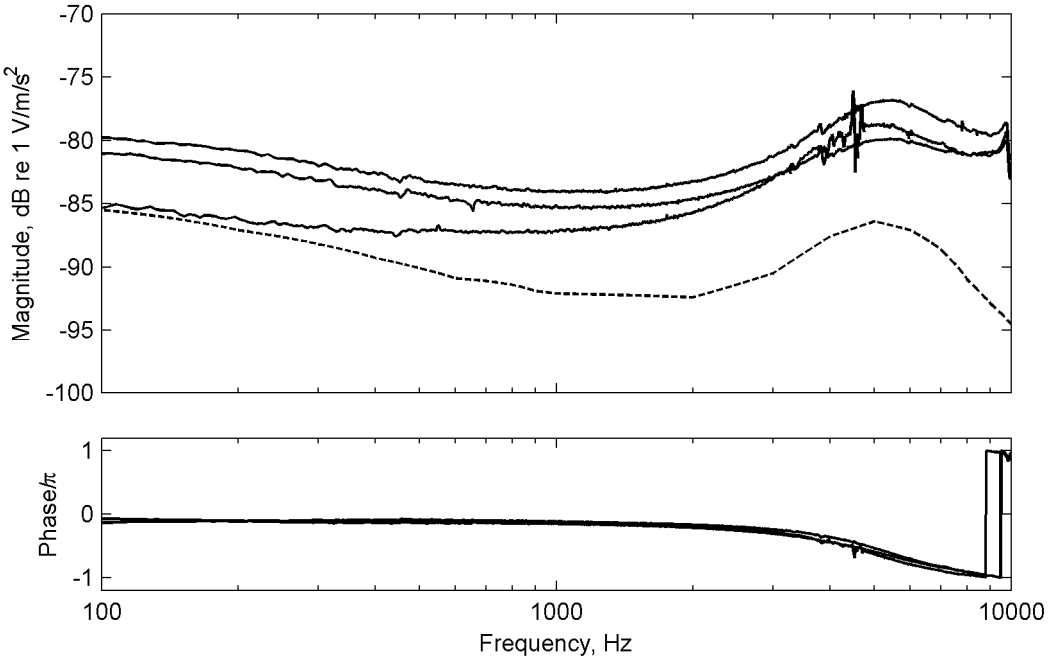

Figure 11.4. Measured vibration sensitivity for three EM-3346 microphones from Knowles (solid lines) and the average vibration sensitivity of a EM-3046 microphone from Knowles and measured by Knowles (dashed line).

It is seen that the sensitivities for the three EM-3346 microphones are relatively similar in size and shape. The largest difference between the measurements is about 5 dB at 100 Hz. Nonetheless, the difference becomes smaller with increasing frequency and at 10 kHz it is only about 2 dB. As expected the maximum vibration sensitivity coincide with the maximum pressure sensitivity around 5000 Hz, see fig. 11.2. It is furthermore observed that the electrical microphone output is in phase with the acceleration up to at least around 2500 Hz. The phase shifts according to the phase of the pressure sensitivity. In comparison, it is seen that the sensitivity of the EM-3046 microphone is generally lower. However, the difference in sensitivity between the two microphone types is only

about 5-10 dB in the considered frequency range. It should be noted that the EM-3046 microphone correspondingly has a lower pressure sensitivity than the EM-3346 microphone.

PART IV:

FULL 3D-MODEL AND CONCLUSIONS

12 Presentation of the full 3D-model

In this final part of the thesis all the individual acoustic and dynamic component properties, which were determined in Part II and III, are incorporated into a full 3D-model of the considered hearing aid. An illustration of the full model and details of the hearing aid are shown in figs. 12.1 and 12.2, respectively. The model has been developed using the finite element method (see Cook *et al.*, 2002) and it describes the vibroacoustics of the hearing aid in the frequency domain and assumes stationary harmonic excitation. Moreover, the model only applies for small signals and does not take any nonlinear effects into account. All main mechanical components as well as acoustics in the tube system, inside the shell and outside the hearing aid are included in the model. Furthermore, acoustics have been coupled to neighboring structures such that sound radiation and loading of the structures are incorporated in the 3D-model. The coupling between structural vibration and acoustics is achieved by using continuity and force equilibrium conditions.

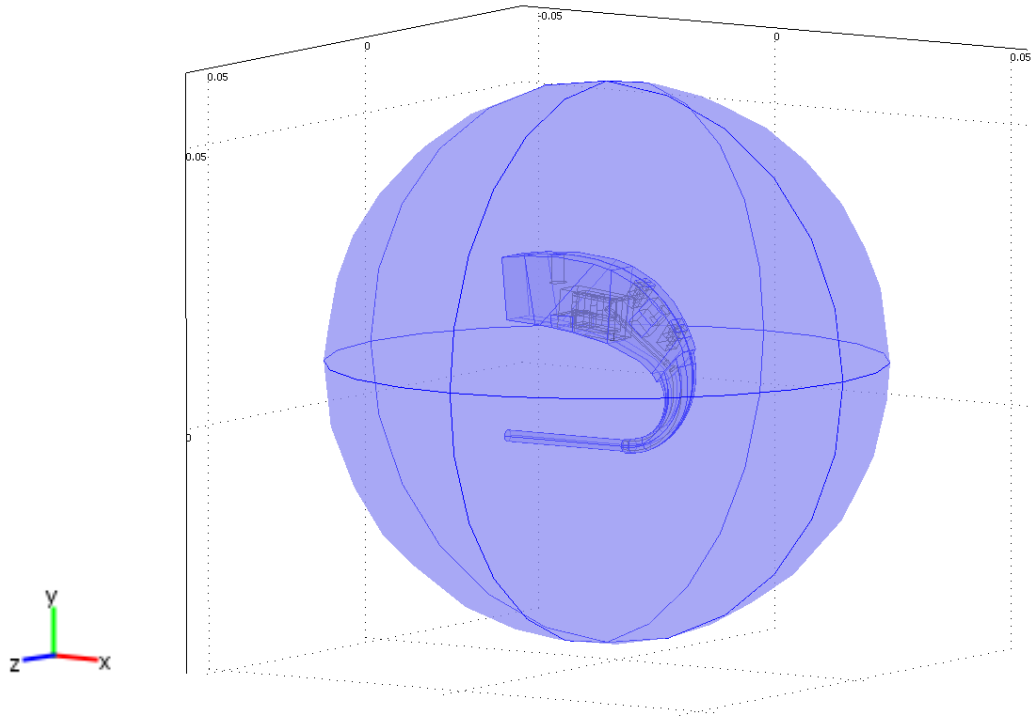

Figure 12.1. The full 3D-model of the considered hearing aid including all main mechanical parts as well as acoustics in the tube system, inside the shells and outside the hearing aid.

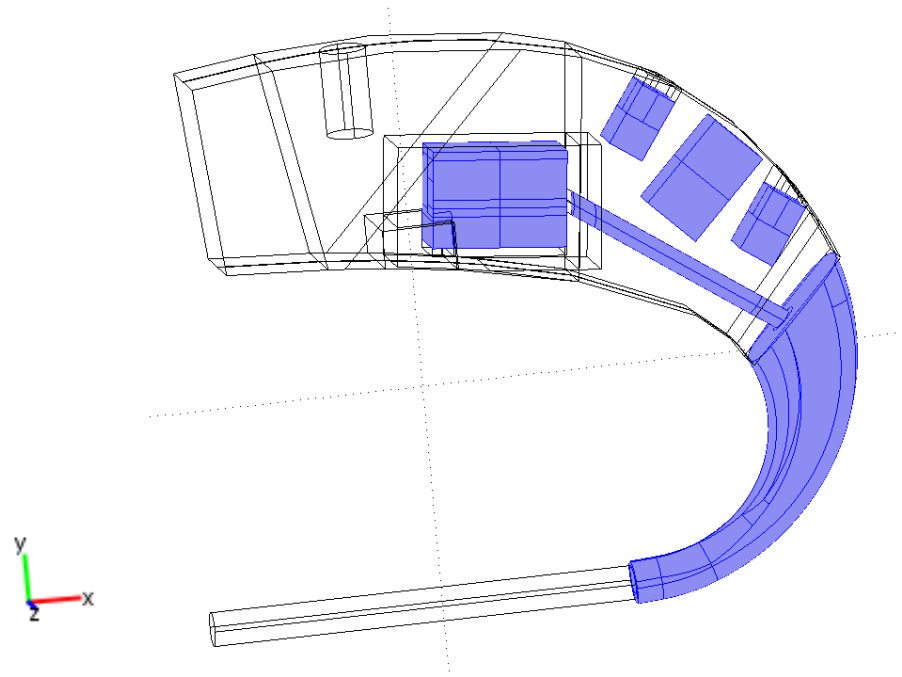

Figure 12.2. The 3D-model of the considered hearing aid without the outer acoustics.

Specifics concerning the modeling of the different structural and acoustic parts of the considered hearing aid are specified in table 12.1 and geometrical and material properties are listed in table 12.2. It should be noted that all weights, thicknesses, elastic properties etc used are in accordance with the actual properties of the considered hearing aid.

Solids, Lagrange quadratic elements	
Receiver	- Pure mass - The vibration force excitation per volt in the middle of the receiver was determined in section 10
Microphones	- Pure mass - The pressure sensitivity, which was determined in section 11, picks up the pressure outside the hearing aid in the positions where they are attached to the shell - The vibration sensitivity, which was determined experimentally in section 11, picks up the vibrations in the centre of the microphones
Tele coil	- Pure mass
Hook	- Standard solids
Shells, Argyris shell elements	

Shell	- Standard shells - The contact edge between the two half-shells has been modeled using a reduced thickness
Steel pipe	- Standard shells
Plastic tube	- Standard shells
Lossless acoustics, Lagrange quadratic elements	
Tube acoustics	- Viscous-thermal losses are modeled by introducing complex propagation speeds corresponding to each tube diameter. These propagation speeds, as well as the source strength per volt driving the receiver and the end impedance of the tube system, is found by using the two-port networks described in section 8
Acoustics inside the magnetic screen and inside the shell	- Standard lossless acoustics
Acoustics outside the hearing aid	- Standard lossless acoustics where the outer boundaries furthest away from the hearing aid are reflection-free
Custom definitions	
Coupling between acoustics and solids	- Continuity and force equilibrium
Coupling between acoustics and shells.	- Continuity and force equilibrium. When a shell has acoustics on both sides, the loading of the shell is given as the pressure difference between the pressure on each side
Attachment of structural fuzzy	- Impedance loading of the shell corresponding to a structural fuzzy with the parameters found in section 7
Receiver suspension	- Five mass-less springs with complex stiffnesses determined in section 9
Microphone suspensions	- Five mass-less springs with complex stiffnesses determined in section 9

Table 12.1. Modeling details for the individual parts of the 3D-model.

Component	Properties
Receiver	- Weight: 0.770 g
Microphones	- Weight: 0.098 g
Tele coil	- Weight: 0.160 g
Hook	- Weight: 0.267 g - Density: 1174 kg/m3 - Young's Modulus: Varying linearly from 2.5 GPa at 100 Hz to 2.2 GPa at 10000 Hz (material experiment) - Loss factor: 0.053 (material experiment)
Shell	- Weight: 1.233 g - Thickness: 0.85 mm in most places - Contact between half-shells, thickness: 0.002 mm - Density: 1050 kg/m3 - Young's Modulus: Varying linearly from 3.0 GPa at 100 Hz to 2.6 GPa at 10000 Hz (material experiment) - Loss factor: 0.019 (material experiment)
Steel pipe	- Weight: 0.009 g - Thickness: 0.22 mm - Density: 7850 kg/m^3 (see Cremer et al., 1988) - Young's Modulus: 200 GPa (see Cremer et al., 1988) - Loss factor: 0.005 (see Cremer et al., 1988)
Plastic tube	- Weight: 0.111 g - Thickness: 0.6 mm - Density: 1223 kg/m3 - Young's Modulus: 0.041 GPa (material experiment) - Loss factor: 0.1 (estimated)

Table 12.2. Geometrical and physical properties of the individual parts of the 3D-model.

As shell-like components are modeled with the low-order Argyris shell elements (see Argyris *et al.*, 1997 and Allman, 1988) it should be noted that proper coupling to the Lagrange quadratic elements used for modeling the acoustics requires a fine mesh. This is due to the so-called shape functions of the two element types being different.

Since a variety of modeling properties will be used for the simulations in the succeeding sections, simulations based on the properties listed in table 12.2 will be referred to as the "standard case". Also, simulation results for the considered hearing aid during operation are for a harmonically varying voltage with an amplitude of 1 V driving the receiver. The output voltages of the microphones thus correspond to the open-loop transfer functions of the hearing aid.

13 Experimental validation of numerical simulation results

The main purpose of the 3D-model is to simulate the open-loop transfer functions from the input voltage on the receiver to the output voltages from the microphones. In this section such simulations are presented and validated experimentally. The open-loop transfer functions has been measured on five nominally identical hearing aids of the considered type using the setup shown in fig. 13.1. This setup consists of four metal columns with attached elastic strings suspending the hearing aid. The plastic tube of the hearing aid is connected to a coupler that is rigidly mounted on a heavy block. This coupler simulates the acoustic properties of the ear canal and eardrum of the average human ear. Very thin cables are run through the shell and into the inside of the hearing aid in order to drive the receiver and to measure the output voltage from the microphones. A Pulse spectral analyzer from Brüel & Kjær (input output module type 3109 and communication controller module type 7536) was used to drive the receiver with white noise and for analyzing the electrical signals of the microphones.

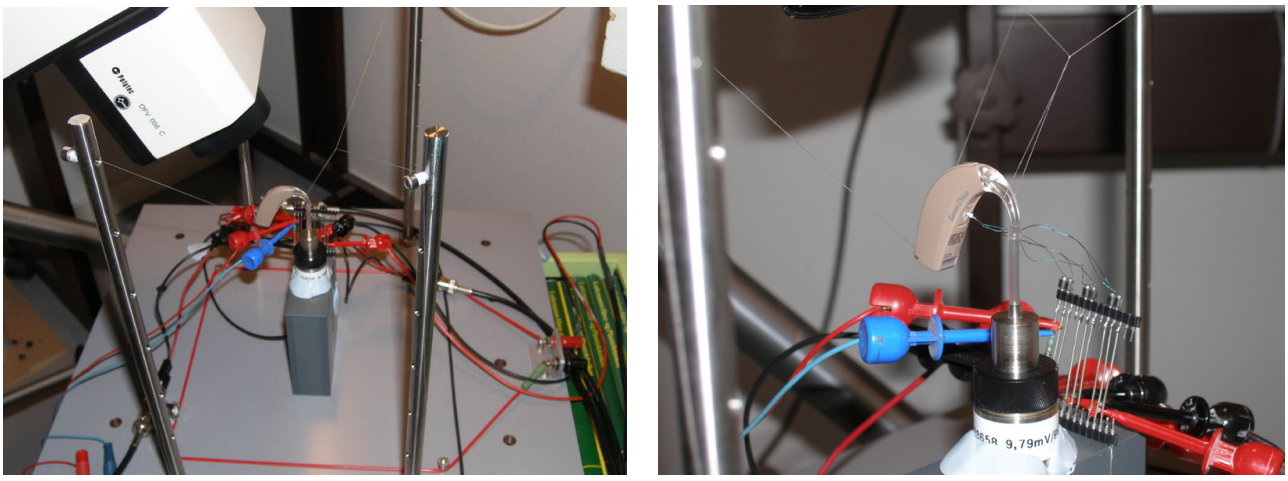

Figure 13.1. Experimental setup for measuring the open-loop transfer functions. The full setup is shown on the left and a close-up picture of a mounted hearing aid is shown on the right.

Experiments were carried out on five nominally identical hearing aids of the considered model. Furthermore, five measurements were conducted on each of these hearings aids. Between each measurement the concerned hearing aid was handled in a way as to emulate everyday use. The handling included squeezing the shell and shaking the device. Figure 13.2 shows the simulated and

measured open-loop transfer functions for the front microphone. The figure shows the span between the highest and lowest simulation using fuzzy parameters as well as the span between the highest and lowest of the five measurements on hearing aids 1 and 4. Gridlines are shown in order to ease the comparison of the transfer functions. Similarities between simulations and measurements are clearly displayed. Especially from the local maximum at approximately 1200 Hz and upwards, the shapes of the transfer functions are in good agreement. Despite of discrepancies in the level of the peaks up to about 10 dB, it is clear that the trends of the measurements on both hearing aids 1 and 4 are fully described by the simulations. Below 1200 Hz, both the simulated and measured transfer functions significantly decrease in amplitude, and it is seen that the agreement between the overall levels of these are satisfactory.

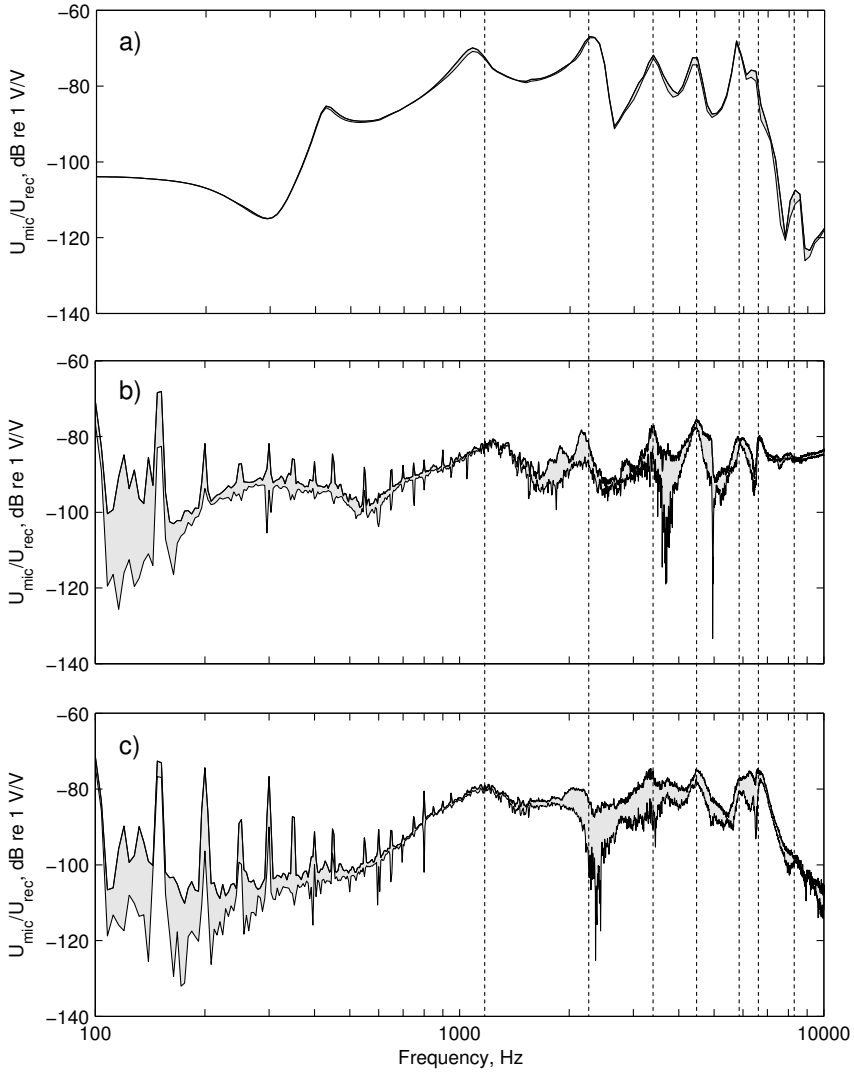

Figure 13.2. Open-loop transfer functions U_{mic}/U_{rec} for the front microphone. The figure shows the span between the highest and lowest transfer function for each frequency obtained from (a) simulations with fuzzy parameters and from five measurements conducted on (b) hearing aid 1 and (c) hearing aid 4.

It should be noted that the many peaks in the measurements below 1200 Hz are harmonics of the electrical supply oscillating at 50 Hz. Unfortunately, these harmonics are difficult to avoid as the output voltages from the microphones are very low. Considering the size of the spans in fig. 13.2 it is seen that the variation between the measurements on each hearing aid is somewhat larger than the simulated span caused by the structural fuzzy. One explanation for this discrepancy is that measurements conducted on actual hearing aids involve other uncertainties than those introduced by the structural fuzzy. An example of this could be the altering of the way suspensions are mounted due to handling of the hearing aid.

Figure 13.3 shows the simulated and measured open-loop transfer functions for the rear microphone.

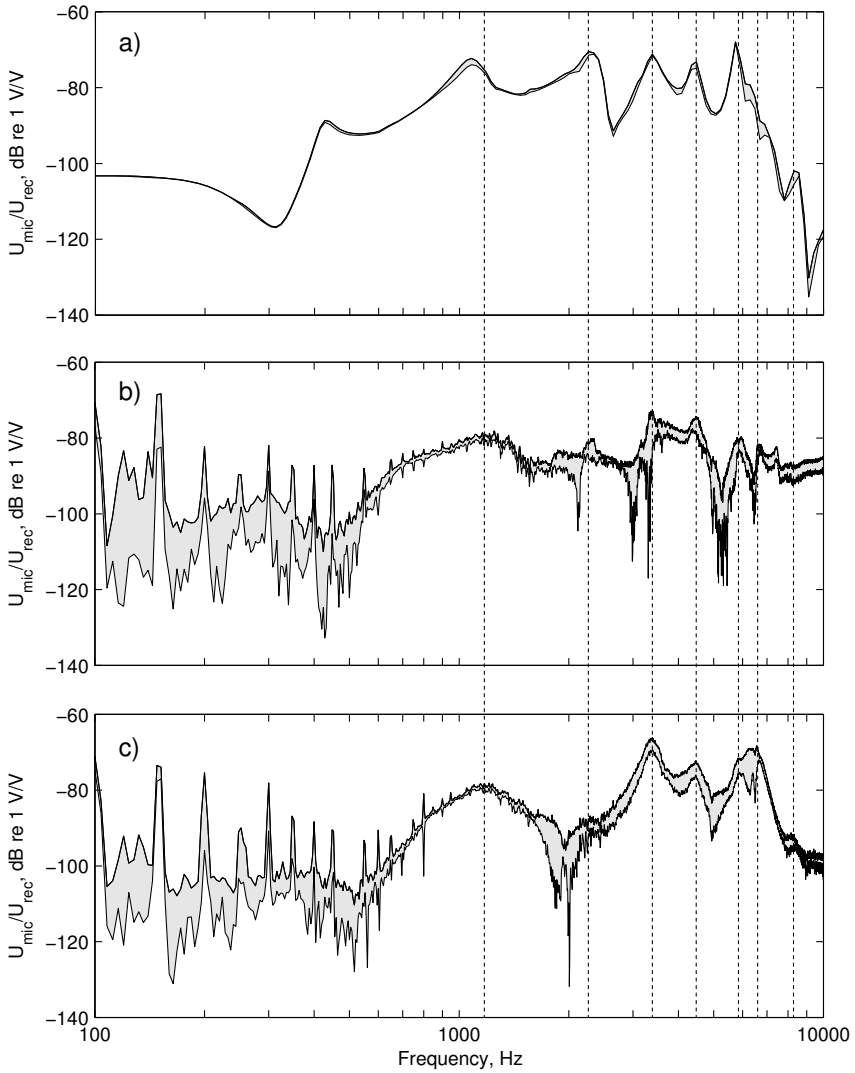

Figure 13.3. Similar to fig. 13.2 but for the rear microphone.

It is seen that the agreement between the levels of the peaks in the simulations and measurements are not as good as for the front microphone. The levels and balance between the peaks related to hearing aid 1 are acceptable, whereas the measurements on hearing aid 4, show a distinct maximum around 3500 Hz, which is not replicated by the simulations. Moreover, the simulations predict that the transfer functions for the front and rear microphones are very similar. This is in accordance with the measurements on hearing aid 1 that shows clear similarities for the output voltages of the two microphones. Nevertheless, the measurements on the rear and front microphone of hearing aid 4 are quite different in the frequency range from 1500 Hz up to, say, 4000 Hz. It appears that the rear microphone picks up sound or vibrations that are not predicted by the simulations. The signal that is picked up clearly resembles the sound pressure at the receiver outlet showing a distinct maximum at 3500 Hz as revealed in section 8. The reason for this resemblance may be leakage of sound pressure at the receiver outlet. The transmission path of the leaked sound, however, is not identified here. As the rear microphone is placed very close to the receiver, leakage of sound would surely explain why it produces the highest output signal.

The open-loop transfer functions for the front and rear microphones of the remainder hearing aids 2, 3 and 5 are shown in figs. 13.4 and 13.5, respectively. Surprisingly, it is observed that the maximum around 3500 Hz also appears in the transfer functions of the front microphone. In fact, this peak has the same level for the two microphones. Such an effect could be caused by sound pressure from the inside of the shell being leaked out through the microphone suspensions. Despite of the considered maximum around 3500 Hz the resemblance between simulations and measurement is acceptable especially outside the frequency range going from about 2500 Hz to 4000 Hz. In particular, the measurements on hearing aid 5 show many details that are clearly predicted by the simulations.

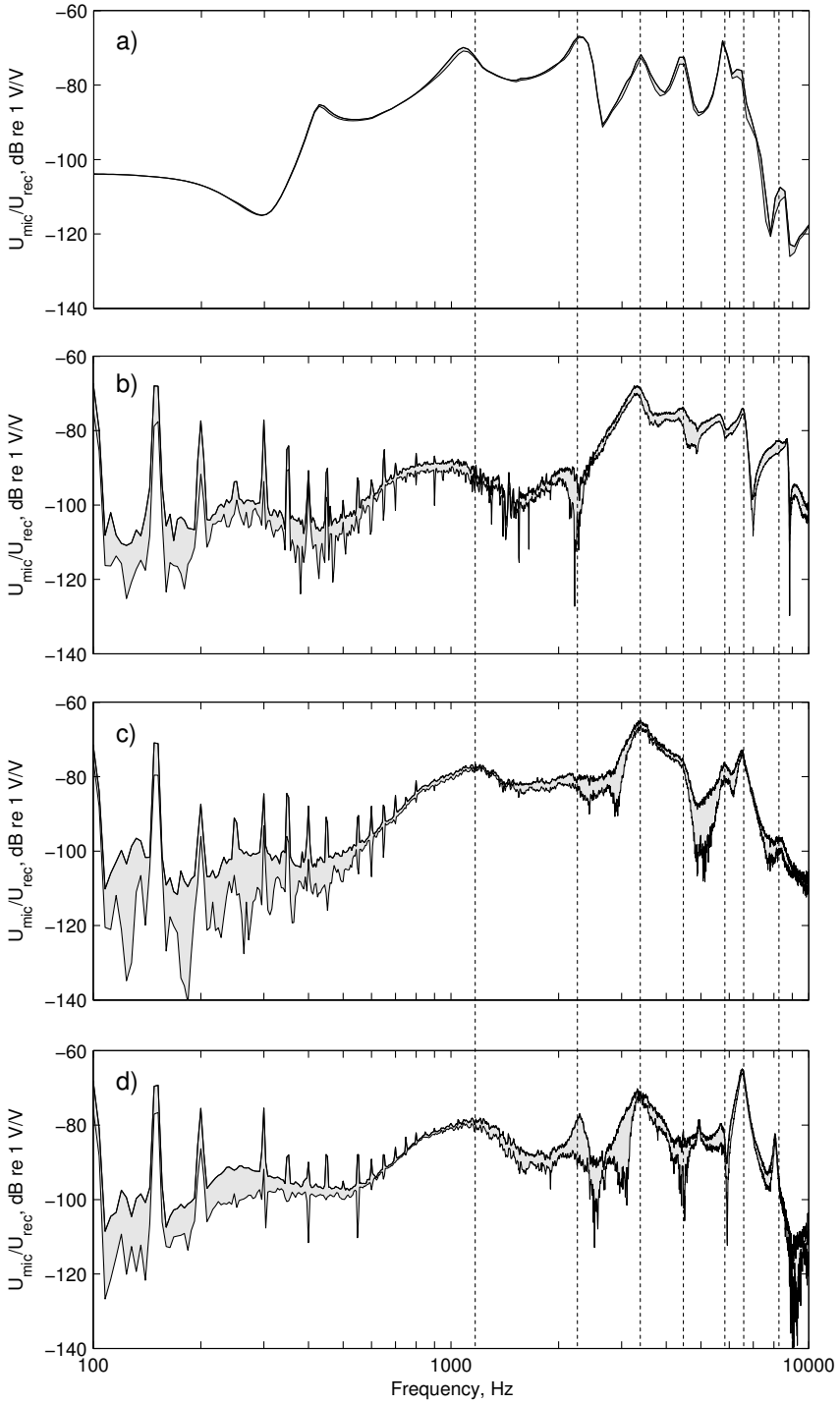

Figure 13.4. Open-loop transfer functions U_{mic}/U_{rec} for the front microphone. The figure shows the span between the highest and lowest transfer function for each frequency obtained from (a) simulations with fuzzy parameters and from five measurements on hearing aid (b) 2, (c) 3 and (d) 5.

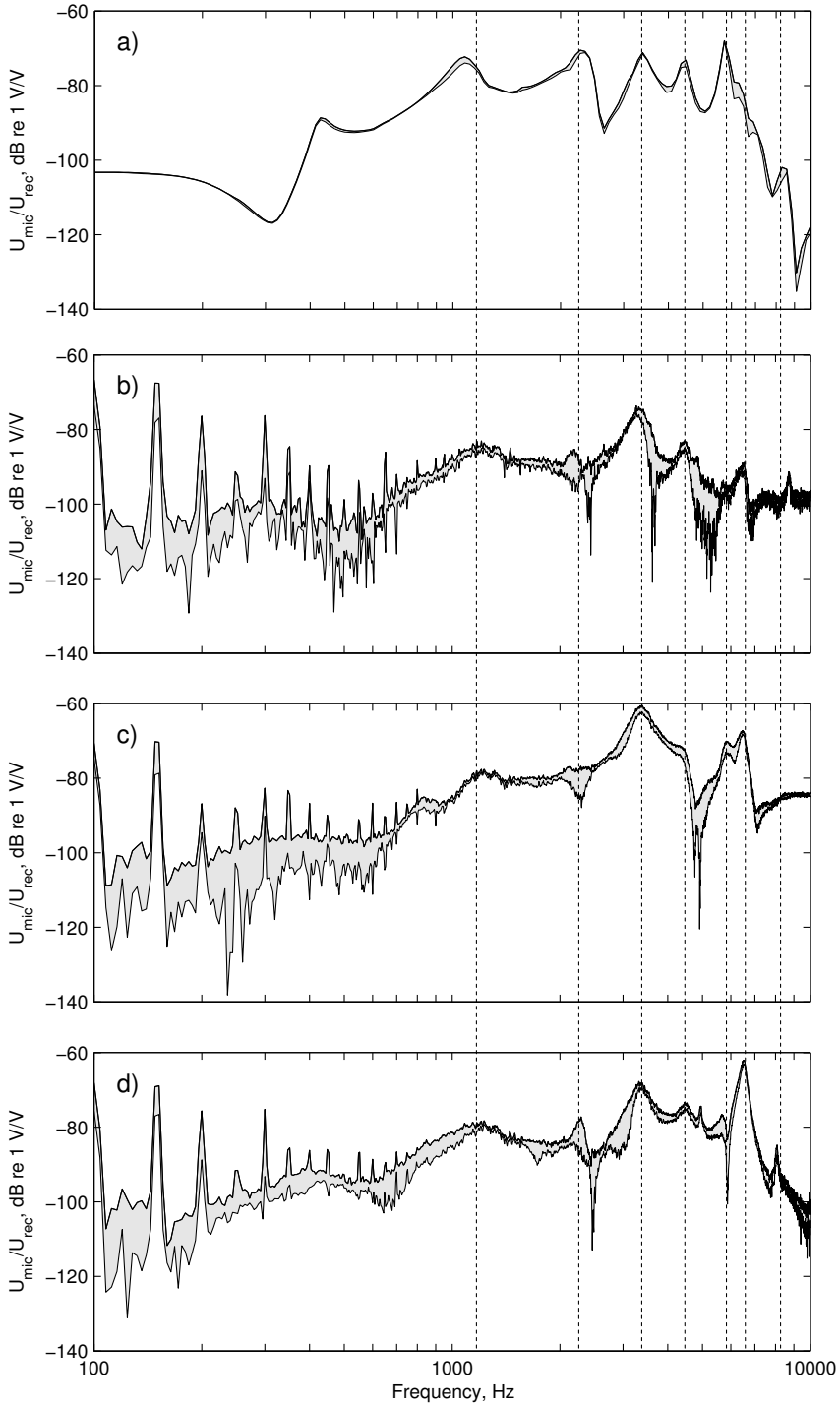

Figure 13.5. Similar to fig. 13.4 but for the rear microphone.

14 Analysis of simulation results

14.1 Separation of contributions from pressure and vibrations

The current section presents an analysis of the simulation results obtained from the 3D-model of the considered hearing aid. In fig. 14.1 and 14.2 the simulated open-loop transfer functions of the front and rear microphones, respectively, have each been split up into open-loop transfer functions due to pressure and vibrations. This has been achieved by considering the individual signals picked up by the microphones' pressure sensitivity and vibration sensitivity.

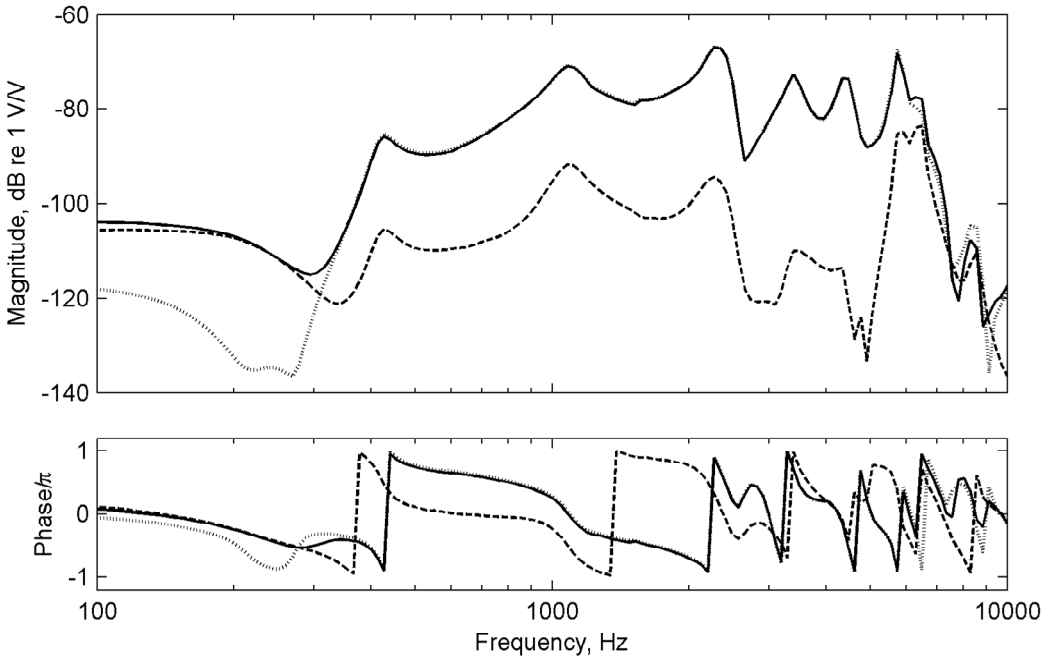

Figure 14.1. Open-loop transfer functions U_{mic}/U_{rec} for the front microphone. Total transfer function (solid line), the pressure transfer function (dotted line) and the vibration transfer function (dashed line).

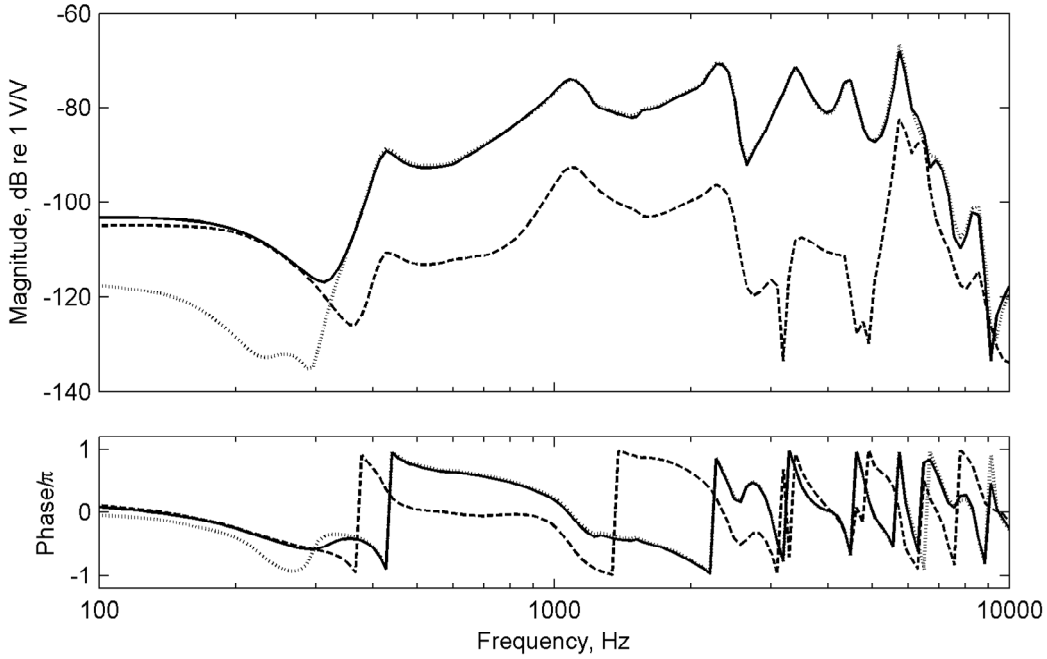

Figure 14.2. Like fig. 14.1 but for the rear microphone.

In both figs. 14.1 and 14.2 it is observed that the pressure at the microphone inlets dictates the electrical output from 350 Hz up to about 6000 Hz. At some frequencies the pressure transfer function is as much as 40 dB higher than the vibration transfer function. Above 6000 Hz the two contributions have approximately the same amplitude levels going from -80 dB and downwards. These levels, however, are relatively low compared to the critical peak levels in the frequency range below 6000 Hz. It can therefore be concluded that the vibrations of the microphones are not critical with regards to feedback for the present construction of the considered hearing aid. It is furthermore noted that the critical maxima at the frequencies 1080 Hz, 2268 Hz, 3390 Hz, 4470 Hz and 5733 Hz with levels between -74 dB and -68 dB somewhat resemble the peaks of the pressure at the eardrum discussed in section 8. This resemblance will be examined further in the following subsection.

To study the causes of the pressure picked up by the microphones, a slice plot of the sound pressure surrounding the hearing aid is shown in fig. 14.3. This plot is made for the frequency 1114 Hz where the total transfer functions in figs. 14.1 and 14.2 both have critical maxima.

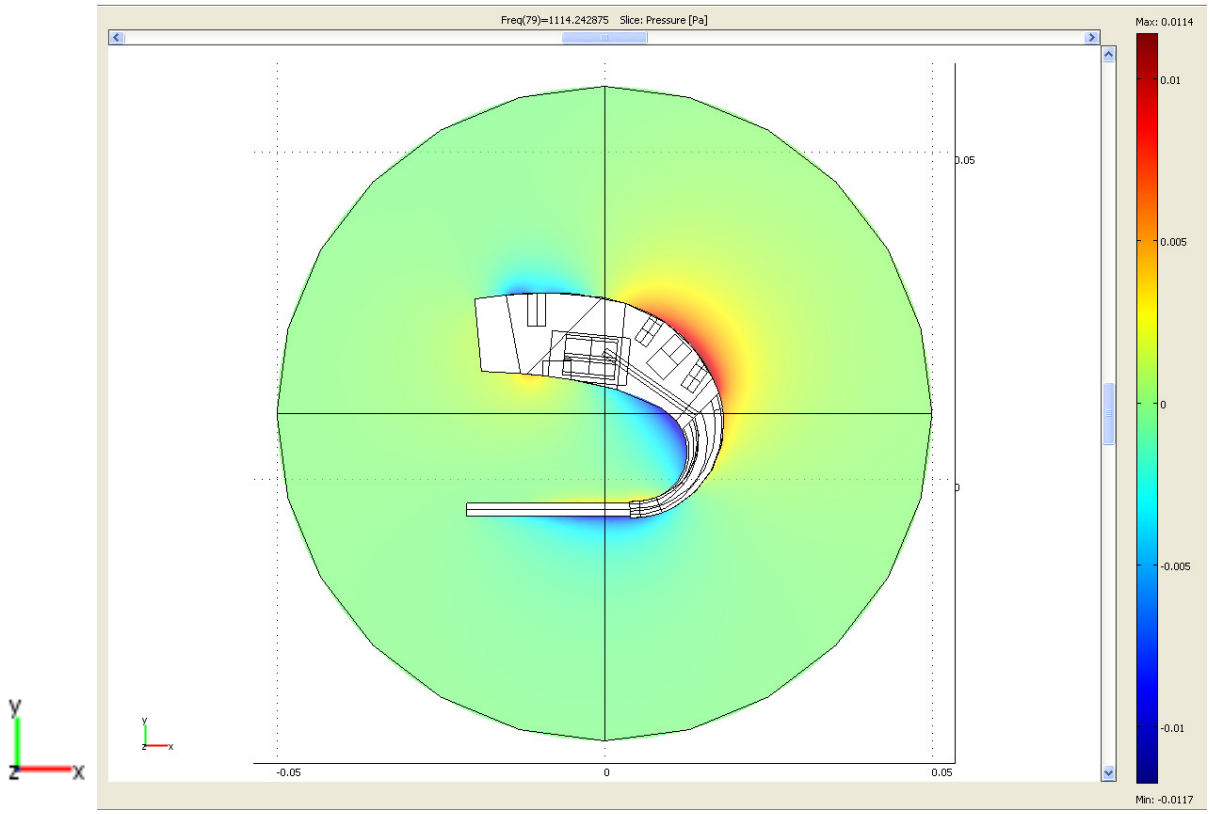

Figure 14.3. The simulated sound pressure generated outside the hearing aid at 1114 Hz.

The figure reveals that the critical sound pressure is generated locally by shell vibrations. This local pressure is generated mainly in the area of the two microphones and reaches a maximum value of 0.0114 Pa corresponding to 55.1 dB SPL. As seen in fig. 14.3 the considered hearing aid is radiating sound like a dipole source in the region close to the microphones. When the pressure is positive above the hearing aid at the microphone inlets, it is also negative beneath the hearing aid. Accordingly, the acoustic wavelength is about 31 cm at 1114 Hz. This length is relatively large compared to the actual dimensions of the hearing aid, as the total length of the shell is about 3.5 cm.

Figure 14.4 shows the displacements of the shell at 1114 Hz. This plot reveals that the shell vibrates mainly in the *xy*-plane parallel to the large surface of the shell. A vibration pattern like this naturally results in a surrounding pressure as shown in fig. 14.3.

Similar plots for the pressure at other important frequencies likewise indicate locally generated pressure as the main cause of the simulated vibroacoutic transmission from the receiver to the microphones. Figure 14.5 shows a 3D slice plot of the sound pressure surrounding the hearing aid at 5733 Hz. The position of the slice plot is chosen to be close to the rear microphone.

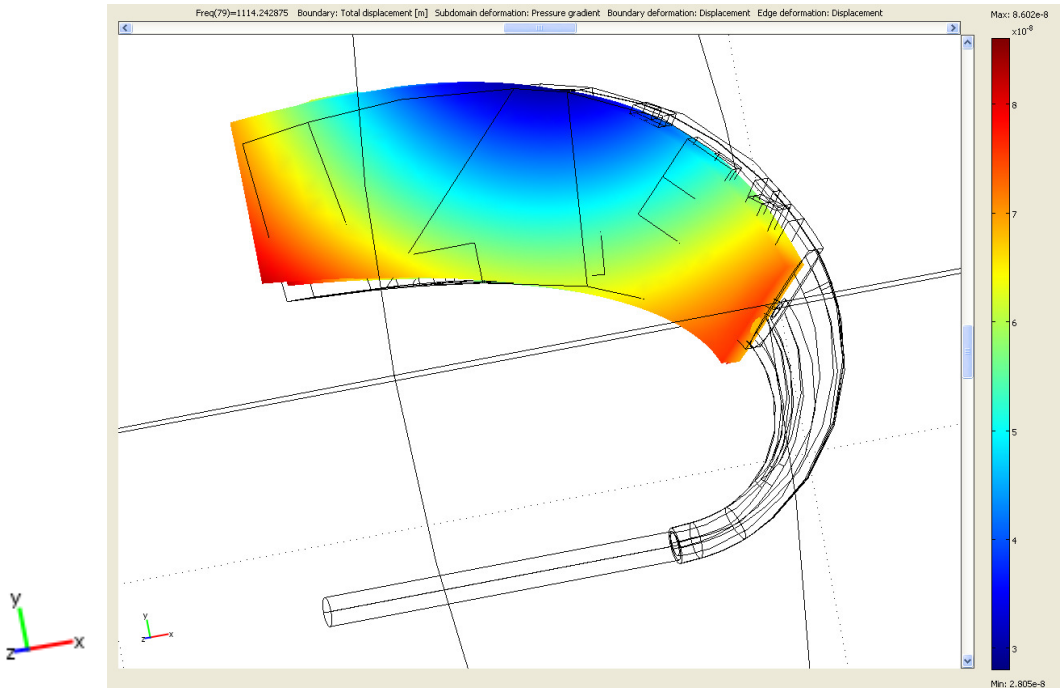

Figure 14.4. Displacements of the shell at 1114 Hz.

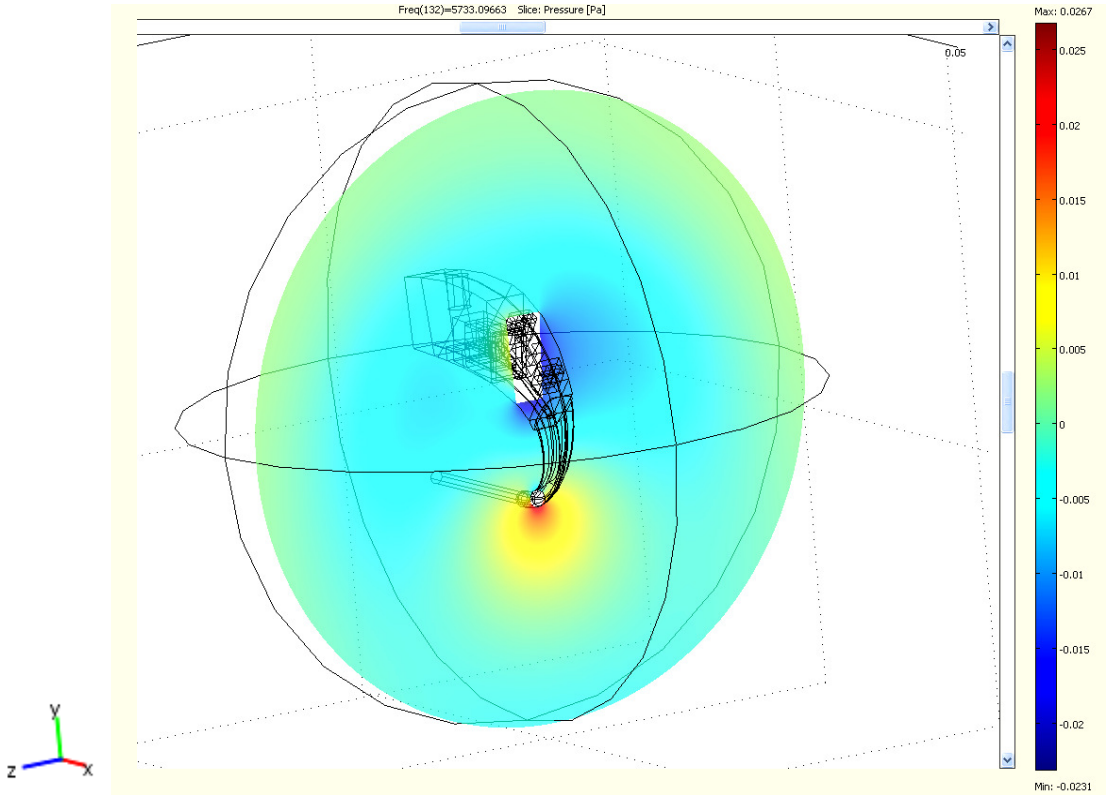

Figure 14.5. The simulated sound pressure generated outside the hearing aid close to the rear microphone at 5733 Hz.

As opposed to the pressure in fig. 14.3, the pressure is not symmetrically distributed with respect to the *yz*-plane. This imbalance is mainly due to the rather heavy telecoil located in the right side of the hearing aid. The pressure plots shown in figs. 14.3 and 14.5 illustrate that the pattern of the radiated pressure is highly dependent on frequency. Regarding the radiation from the shell, the critical frequency of an infinite plate with the same properties as the shell of the considered hearing aid is about 43000 Hz (see Cremer *et al.*, 1998). This very high frequency is due to the small thickness of the shell of 0.85 mm and the relatively low Young's modulus of the plastic material used. According to Cremer *et al.* (1998), only a nearfield is radiated for frequencies below the critical frequency. The reason for this is a mechanism called "hydrodynamical short-circuiting" where the air quickly cancels out fluctuations in pressure.

14.2 Separation of the excitation forces

It is important to identify the sources of both vibrations and sound pressure in order to minimize vibroacoustic feedback. These sources are different excitation forces originating from the receiver and they will be examined in the following. The vibration forces which were determined experimentally in section 10, represent some of these excitation forces. Moreover, the receiver generates a high sound pressure in the tube system carrying the sound to the eardrum of the user. The high sound pressure in the tube system loads the tube walls in the direction of their normal vectors pointing away from the acoustics. These loads are in equilibrium, but, due to the curvature of the hook, internal moments are introduced in the tube walls. Such internal moments causes the tube system to deflect. It should be noted that the internal pressure closely resembles the simulation results for the pressure presented in section 8, even though the tube system is not straight.

Figure 14.6 shows three of the most important excitation forces of the hearing aid as a function of frequency. The first excitation force is the resulting reaction force on the hook caused by the sound pressure in the tube system. The second excitation force is the acoustic "recoil", which is the reaction force to the sound pressure generated by the receiver. Finally, the third excitation force is the vibration force of the receiver acting in its local *y*-direction, see fig. 9.4c.

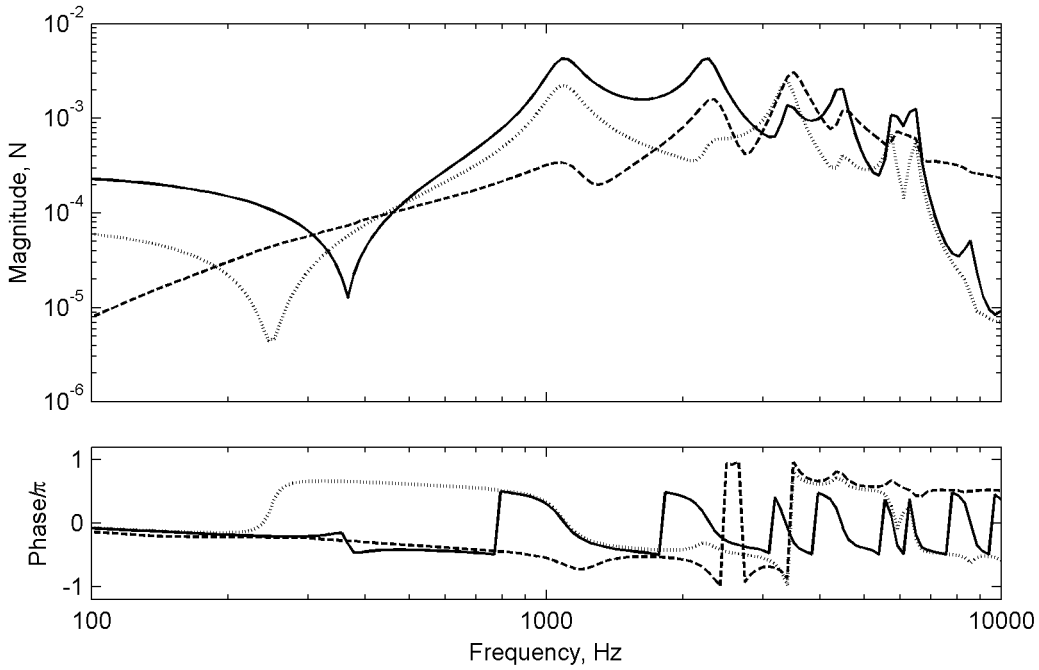

Figure 14.6. Three of the most important excitation forces of the hearing aid: Resulting force on the hook due to acoustic pressure from the tube system (solid line), force from the acoustic recoil at the receiver outlet (dotted line) and vibration force of the receiver as presented in section 10 (dashed line).

The total reaction force on the hook from the sound pressure in the tube system has been determined by integrating the product of the pressure and the normal vector components in the *x*-, *y*- and *z*-directions of the inner hook walls over the loaded wall surface. The excitation force shown in fig. 14.6 is the vector sum of the components in the *x*- and *y*-directions as the resulting force in the *z*-direction is zero due to symmetry. The recoil force has been estimated as the negative sound pressure at the outlet of the receiver times the cross-section area of the steel tube.

From fig. 14.6 it is clearly seen that the reaction force on the hook generally is the largest force. To some extent the shape of this reaction force resembles the shape of the sound pressure at the eardrum studied in section 8. The recoil force and the vibration force of the receiver both have maxima in the frequency range from 3000 Hz to 4000 Hz and they are therefore larger than the hook force at these frequencies. It should be noted that not only the magnitudes, but also the excitation positions of the excitation forces are important.

To fully understand the origin of the forces caused by the internal acoustics of the tube system, further study is needed. As previously mentioned, the internal pressure loads the tube walls in the direction of their normal vectors. Hence, the specific loading depends on the variation of the pressure with position in the tube system *and* the geometry of the tubes. Figure 14.7 shows a sketch of the resulting reaction forces loading the tube walls for an internal overpressure in the tube system.

Moreover, this pressure is considered to be constant with position. Resulting reaction forces occur in the positions where the cross-section changes or where the tube system changes shape. Note that the shown system of resulting reaction forces is in equilibrium.

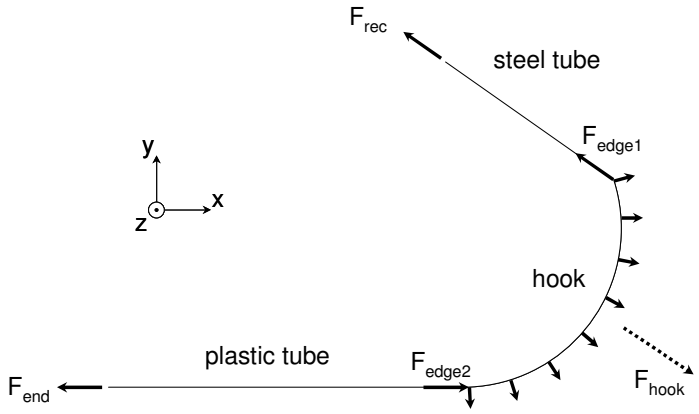

Figure 14.7. Sketch of the resulting forces acting on the tube walls of the considered hearing aid when the internal pressure is constant with position.

The relative sizes of the reaction forces are readily found by integrating the *x*-, *y*- and *z*-components of the tube walls' normal vectors pointing outwards over the surface of each component according to the coordinate system shown. Such integration yields projected areas for each direction. For a constant static internal pressure of 1 Pa, these areas in square meters represent the total resulting force acting in each direction on each component. The projected areas for the different components of the tube system have been calculated and they are listed in table 14.1. Note that the sum of the areas in the *x*- and *y*-directions, respectively, equals zero due to force equilibrium. As mentioned earlier the tube system is symmetrical with regards to the *xy*-plane and all projected areas for the *z*-direction are correspondingly zero. Even though the forces shown in fig. 14.7 are in equilibrium they introduce internal shear forces and moments in the tubes. So to speak, these internal forces "attempt to straighten out" the tube system and in return the tube system is deformed in weak places. Especially the relatively soft plastic tube is likely to deform. According to table 14.1, the largest area or "reaction force" is associated with the hook in the *x*-direction. As shown in fig. 14.7, the distributed force acting on the hook produces a resultant force acting in the middle of the hook with the magnitude as shown in table 14.1. The second largest force, occurs at the end of the tube system. This force, however, has no significant influence on the deformation of the tube system as the plastic tube is fixed for any motion at the end. In the other end of the tube system the receiver produces the third largest reaction force or recoil F_{rec}, which also was shown in fig. 14.6.

Component	Symbol	Projected area, mm^2		
		***x*-dir**	***y*-dir**	**total**
Hook	F_{hook}	3.66	-1.41	3.93
Plastic tube	$F_{plastic}$	0.00	-0.21	0.21
Steel tube	F_{steel}	0.47	0.67	0.81
Edge, hook/steel tube	F_{edge1}	-0.78	0.76	1.09
Edge, hook/plastic tube	F_{edge2}	1.06	0.07	1.07
Start, receiver recoil	F_{rec}	-1.27	0.12	1.28
End	F_{end}	-3.14	0.00	3.14

Table 14.1. Projected areas of the different components of the tube system.

As shown in fig. 14.7, many resulting reaction forces each with different directions occur in the tube system. The deflection shape of the tube system has therefore been simulated in the case of a constant static overpressure. Computed results for the deformed shape are shown in fig. 14.8. All tubes in the simulations, except for the soft plastic tube, are considered to be very stiff. The left side of fig. 14.8 shows the deflection shape for a case where the plastic tube is fixed for any motion at the end. It is clearly seen that mainly the plastic tube is deformed and as a result the rest of the tube system is rotated and displaced. The right side of fig. 14.8 shows the deformed shape for the case where the plastic tube is free at the end. Altering the boundary condition for the plastic tube does not change the deflection shape significantly as the tube system still is rotated and displaced.

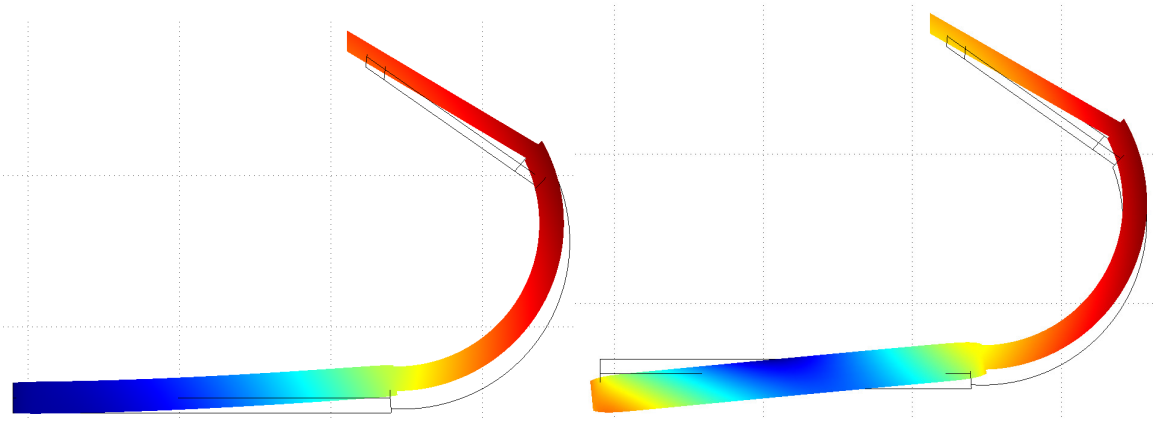

Figure 14.8. Deformed shape of the tube system having an internal constant and static overpressure. On the left, the end of the plastic tube is fixed for any motion and on the right the end is free.

In the actual tube system of the 3D-model, all the components will deflect when exposed to internal sound pressure. Moreover, according to the results presented in section 8, the internal pressure is varying with position in the tube system. Prediction of the influence of the pressure reaction forces is therefore a complex task. This is further illustrated in fig. 14.9, which shows the open-loop transfer function of the rear microphone for different cases of the standard case being altered. In one case the standard case has been altered such that pressure reaction forces of the tube system have been removed. The only excitation force left on the hearing aid is therefore the vibration forces of the receiver. Considering fig. 14.9 it is revealed that the removal of these reaction forces reduces the transfer function drastically. Below 1000 Hz, the transfer function is even less than -140 dB. Even though the receiver vibration forces reach considerable levels above 1 mN, they are effectively isolated by the receiver suspension. Moreover, the vibration forces are acting in the direction perpendicular to the microphone inlets. This implies that the pressure in front of the microphone inlets is very weak. Figure 14.9 also shows the open-loop function for a case where only the reaction forces on the hook have been removed. This result in a decrease of the transfer function magnitude up to frequencies of approximately 2500 Hz. Above this frequency, no general reduction in the magnitude of the transfer function is achieved. At some frequencies the transfer function even becomes higher than in the standard case. This is due to the complicated system of reaction forces in the tube system. At some frequencies these reaction forces “work against” one another and vice versa. In the third case shown in fig. 14.9, Young’s modulus of the plastic tube has been altered such that the tube is very stiff. Again a clear decrease in the open-loop transfer function is anticipated. This is also the case for frequencies below 3000 Hz. Above this frequency, however, all components of the tube system are flexible and the transfer function is therefore only reduced with approximately 5 dB.

The different cases of open-loop transfer functions shown in fig. 14.9, clearly illustrate the difficulties in reducing internal feedback. Surely, it is possible to find theoretical solutions to the problem. Practically viable solutions, however, are more difficult to find.

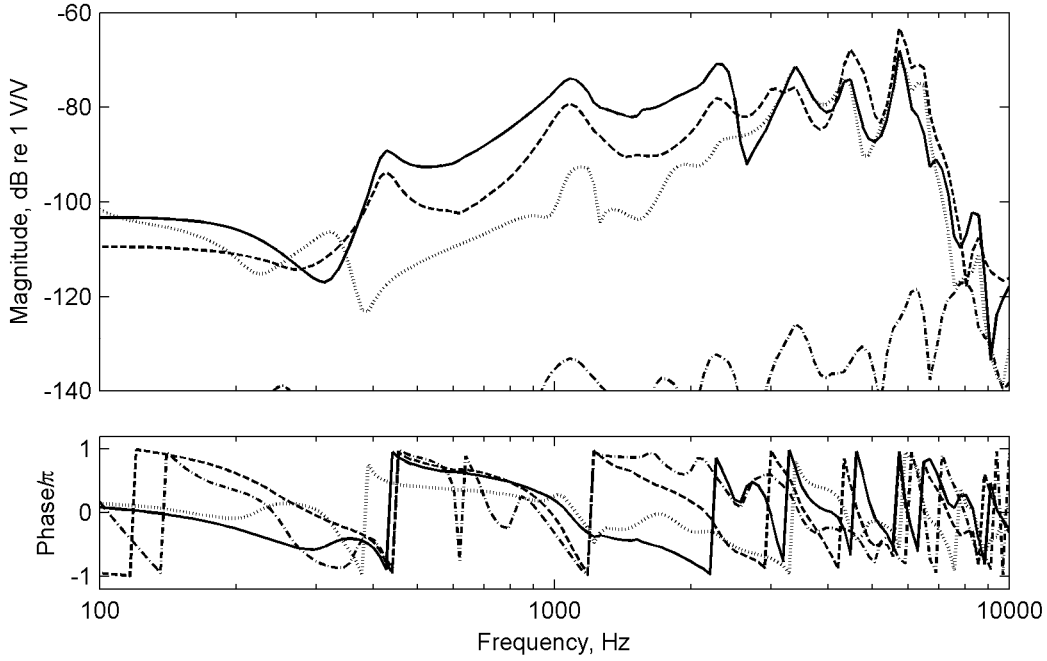

Figure 14.9. Simulated transfer functions U_{mic}/U_{rec} of the rear microphone for the following cases: Standard case (solid line), without pressure reaction forces in the whole tube system (dashdot line), without pressure reaction forces on the hook (dashed line) and with a stiff plastic tube (dotted line).

14.3 General properties of the hearing aid

In this subsection the general properties of the considered hearing aid are examined. First, the direct mobilities in selected positions on the hearing aid are presented and discussed. Second, the vibration velocities during operation of the considered hearing aid are studied for the same positions.

The considered positions on the hearing aid are indicated in fig. 14a. Position 1 is midways on the hook, position 2 is in the middle of the shell close to the telecoil and position 3 is in the centre of the receiver.

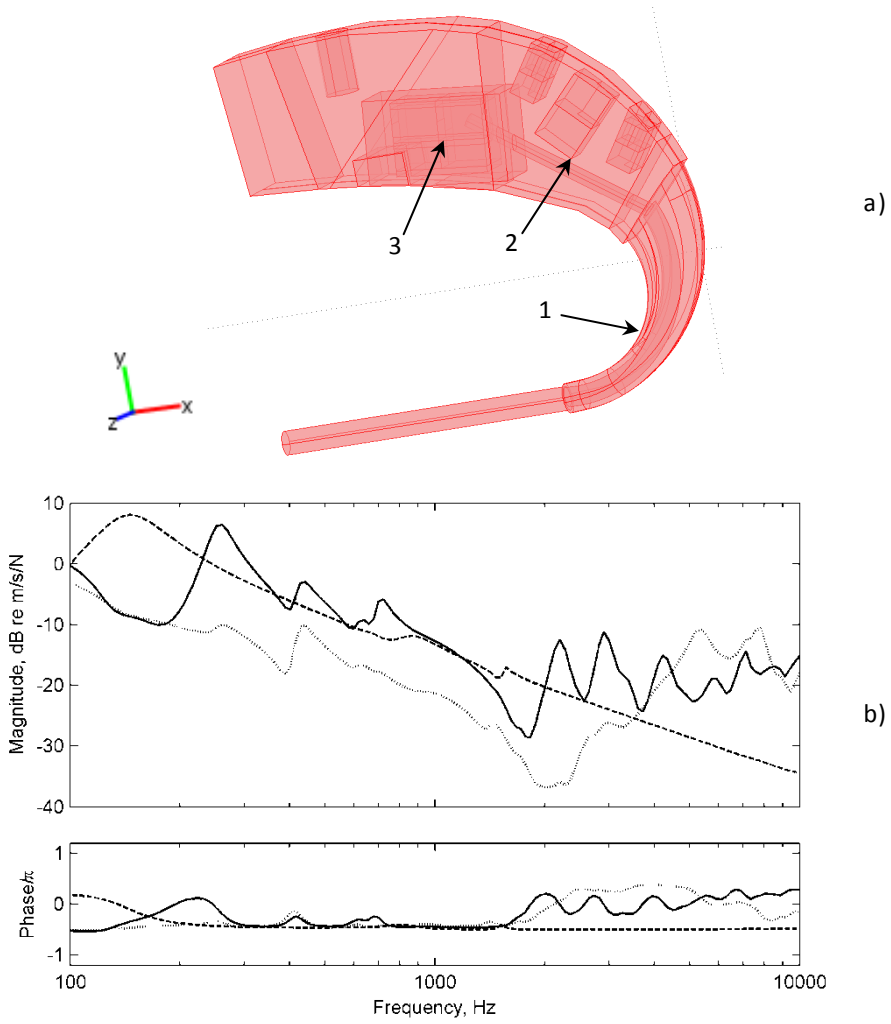

Figure 14.10. (a) Positions of point 1, 2 and 3. (b) Direct mobilities of the hearing aid in the three positions: Point 1 (solid line), point 2 (dotted line) and point 3 (dashed line).

Figure 14.10b shows the direct mobilities for the three positions. The input mobility in point 1 is in the direction with the normal vector $(n_x, n_y, n_z) = (0, \frac{1}{\sqrt{2}}, \frac{1}{\sqrt{2}})$. This mobility clearly illustrates the modal behaviour of the hearing aid. Well-separated modes are observed in the whole frequency range, even though the hook itself only has modes above 4000 Hz. As a check, it is seen that the mobility phase alternates between the extremes $-\pi/2$ and $\pi/2$, representing mass-like and spring-like dynamical behaviour, respectively. The direct mobility in point 2 is also in the direction with the normal vector $(n_x, n_y, n_z) = (0, \frac{1}{\sqrt{2}}, \frac{1}{\sqrt{2}})$. This mobility shows a modal behaviour with well separated modes starting from about 250 Hz. At the position considered, the hearing aid is driven close to its centre of gravity and the driving force therefore only introduces minor rotation of the hearing aid. Finally, the direct mobility in point 3 for the *z*-direction (the local *y*-direction of the receiver, see fig. 9.4c). Since the receiver is mounted in its soft suspension, the first resonance

occurs below 100 Hz. This is clearly revealed by the phase of the mobility that has a positive value. Such positive value indicates a spring-like behaviour. The loss factor of the suspension is very high and only weak resonance peaks are observed above 150 Hz.

For further insight, fig. 14.11 shows the vibration velocities during operation of the hearing aid for the three positions shown in fig. 14.10a. The three vibration velocities generally have the same amplitude levels. From about 100 Hz and up to 7000 Hz the amplitude levels are mostly between 90 dB and 110 dB and only after 7000 Hz they reduce significantly with increasing frequency. For comparison fig 14.12 shows the vibration velocities in the centre of the microphones. These velocities are in the local *y*-direction of the microphones considering the coordinate system shown in fig. 9.4b. Comparing the velocities in figs. 14.11 and 14.12, it is clearly seen that the vibration velocities of the microphones are about 15 to 20 dB lower than those of the rest of the hearing aid. Naturally this is because of the resilient microphone suspensions.

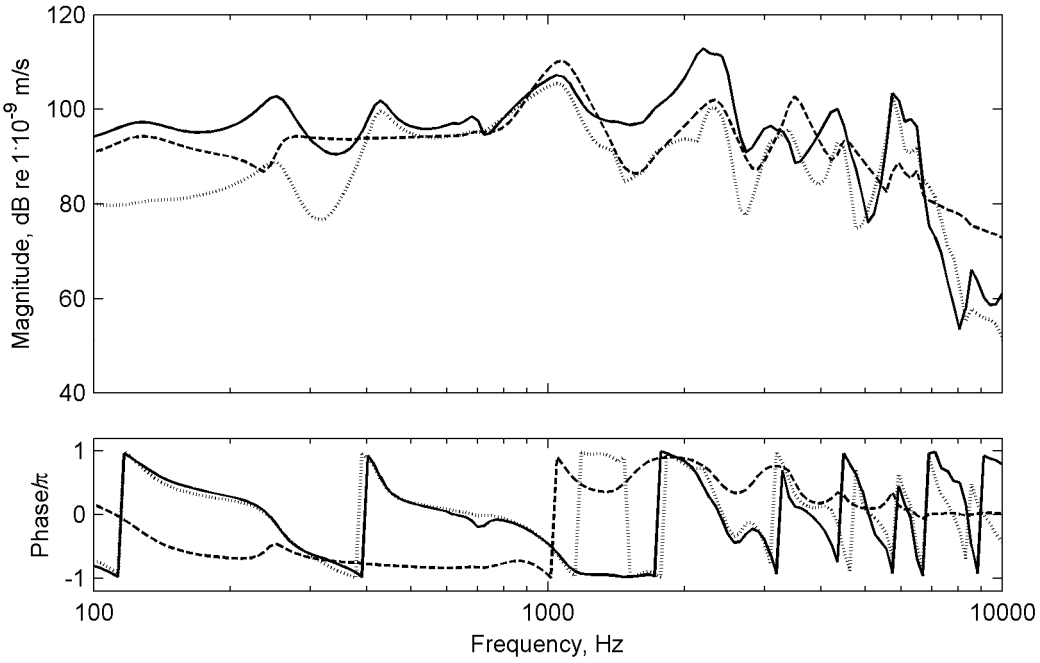

Figure 14.11. Vibration velocities of the hearing aid during operation for position 1 (solid line), 2 (dotted line) and 3 (dashed line) shown in fig. 14.10a.

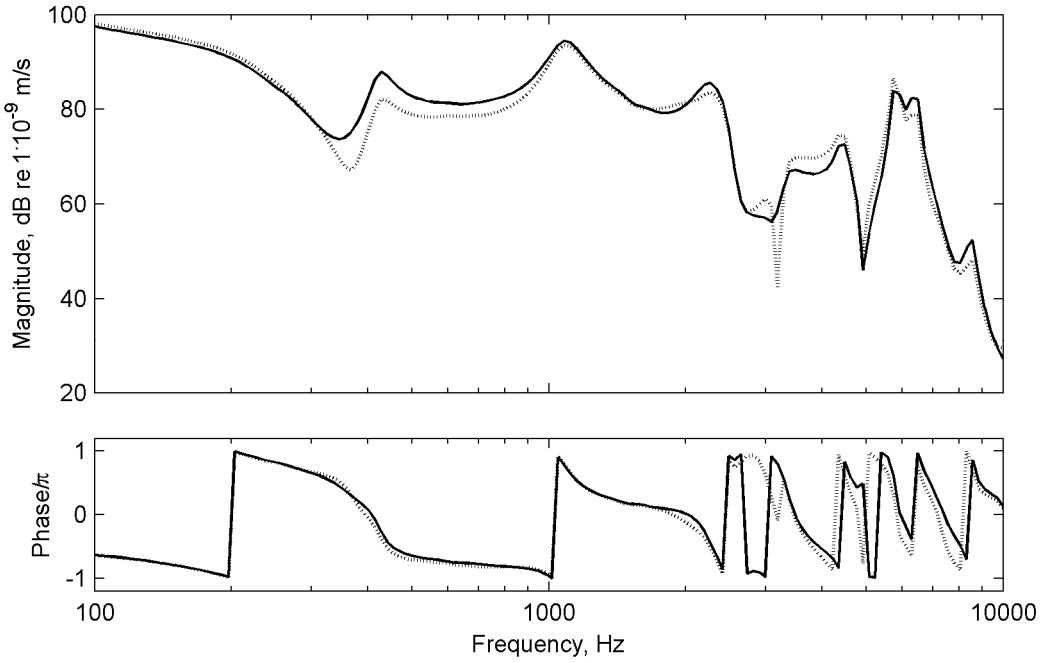

Figure 14.12. Vibration velocities in the centre of the front microphone (solid line) and the rear microphone (dotted line).

14.4 Acoustics inside the shell and magnetic screen

In the following the sound pressure inside the shell and the magnetic screen is examined. Figure 14.13 shows different cases of the frequency response of the sound pressure inside the shell and the magnetic screen. The first case shows the pressure inside the screen when only the receiver is vibrating in its suspension due to its vibration forces. This also means that the rest of the hearing aid is fixed for any motion. The purpose of this particular case is to investigate the pressure inside the magnetic screen solely caused by the receiver vibrations. The second, third and fourth cases show the sound pressure in different positions in the hearing aid for the standard case where all excitation forces are included. These positions in the cavity inside the shell are located; close to the microphone, close to the telecoil and close to the receiver end of the steel tube, respectively.

From the first case shown in fig. 14.13 it is clearly seen that the pressure generated inside the magnetic screen is closely related to the vibration forces of the receiver, which were determined in section 10. As expected the maximum sound pressure level of almost 70 dB SPL occurs around 3390 Hz where the vibration forces have their maximum. Figure 14.14a shows the simulated pressure generated by the receiver inside the screen at 3390 Hz. As anticipated the pressure is

almost anti-symmetrical with regards to the *xy*-plane going through the centre of the receiver. Hence, the pressure is close to zero in this plane. Since the magnetic screen also works as an acoustic screen, the sound pressure inside the screen does not propagate freely into the rest of the cavity between the shell. This cavity and the inner acoustics of the screen are only connected to one another through the narrow slit shown in fig. 14.14b. This slit is only about one millimeter wide and it therefore represents a high acoustic impedance. Simulations of the acoustics in the cavity inside the shell showed that the pressure solely generated by the receiver vibrations is neglegible small.

The sound pressure levels for the three other cases shown in fig 14.13 reach relatively high levels of almost 85 dB in the feedback-critical frequency range from 1 kHz to 10 kHz. These high levels in sound pressure are generated by the vibrations of the shell. As previously discussed in subsection 14.2, the vibrations of the shell are mainly caused by the pressure reaction forces in the tube system of the hearing aid. It is observed that the frequency dependent pressures are almost the same for the three positions chosen. The reason for this is revealed in fig. 14.15, which shows the pressure distribution in the cavity at 5733 Hz. For the phase angle considered, it is seen that the pressure is practically positive in all of the cavity. At 5733 Hz the free acoustic wavelength is about 60 mm, which is significantly larger than the largest dimension of the cavity having a diagonal length of about 12 mm.

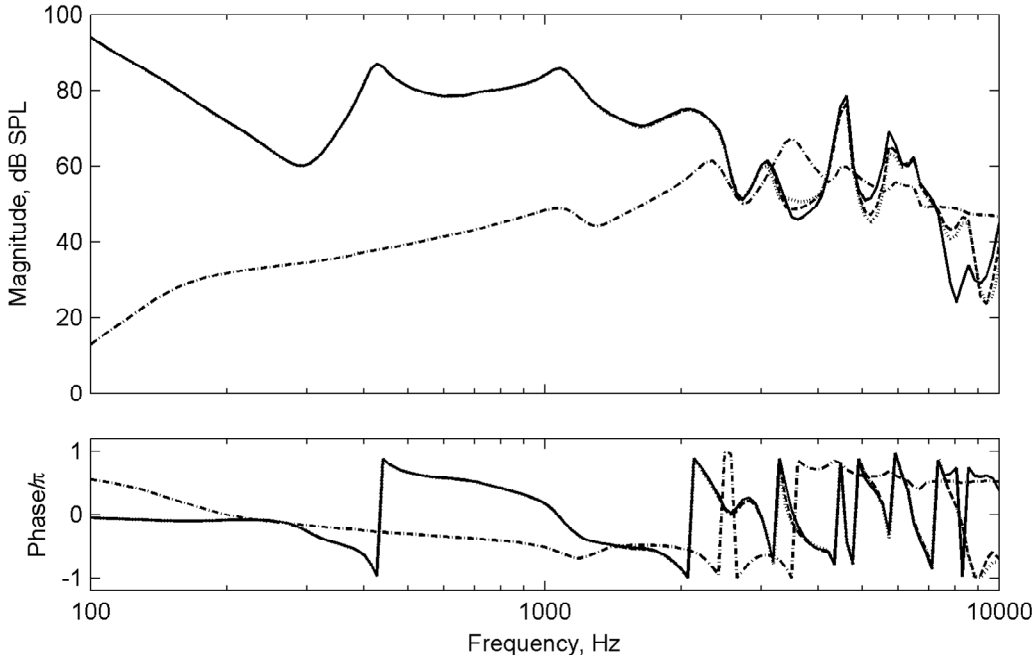

Figure 14.13. The sound pressure level for the following cases: Inside the screen when only the receiver is vibrating due to its vibration forces (dashdot line). The standard case for the following positions; Close to the front microphone (solid line), close to the telecoil (dotted line) and close to the receiver end of the steel tube (dashed line).

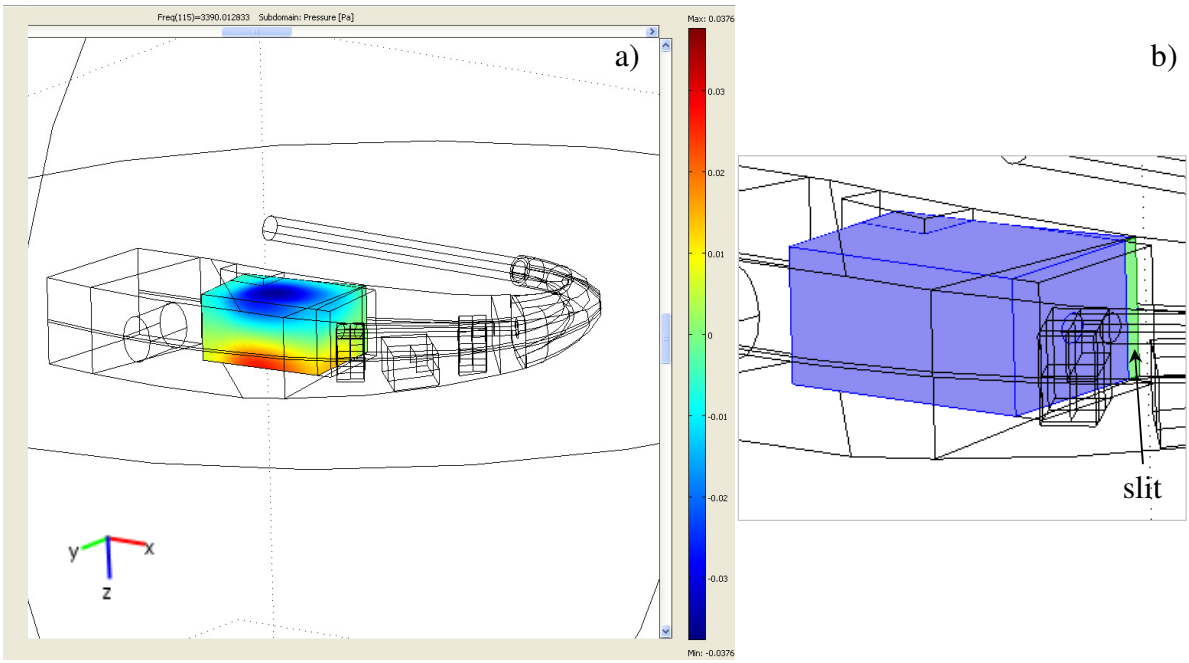

Figure 14.14. (a) The sound pressure inside the magnetic screen at 3390 Hz. (b) The slit connecting the acoustics inside the magnetic screen and the acoustics inside the shell.

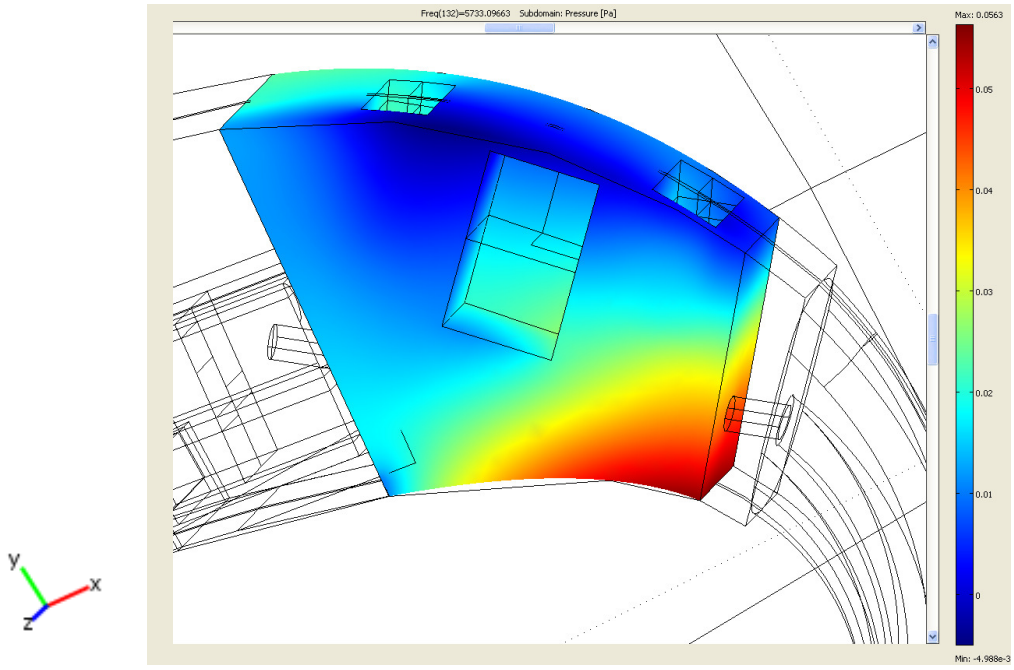

Figure 14.15. The sound pressure in the cavity inside the shell at 5733 Hz.

A study of the acoustic eigenmodes of the cavity shows that the first mode occurs around 11 kHz. This indicates that the sound pressure in the cavity is dictated by the shell vibrations and not by

acoustic modes. A problem with the high sound pressure inside the shell may be leakage of sound to the outer acoustics. In many cases, however, sound leaking through the connection of the half-shells or microphone suspensions will be attenuated drastically before reaching the microphone inlets. Hence, the sound leakage may not cause any feedback problems.

In regards to both the inner and outer acoustics, it was generally found from parameter studies that the pressure loading of the neighbouring mechanical parts was of negligeble influence. On the other hand, this does not apply for the very high pressure in the tube system as discussed in subsection 14.2.

14.5 Parameter studies

In this section further insight into the properties of the 3D-model and the feedback problem is provided by performing various parameter studies. First examined is the implications of placing the microphones in different positions in the shell.

Figure 14.16a shows the open-loop pressure transfer functions for the rear microphone placed with the inlet in three different positions in the shell. The locations of these three positions are shown in fig. 14.16b. The first case shown in fig. 14.16a is the standard case where the microphone inlet is placed in point 1. In the second and third cases the microphone inlet is placed in the z-direction in points 2 and 3, respectively. Compared to the standard case it is seen that the transfer functions in case 2 and 3 are reduced significantly up to about 2500 Hz. Above this frequency the transfer functions are very close. This is caused by the shell vibrating in all directions. Hence, it must be concluded that the microphone positions and their inlet directions should be considered carefully when designing hearing aids.

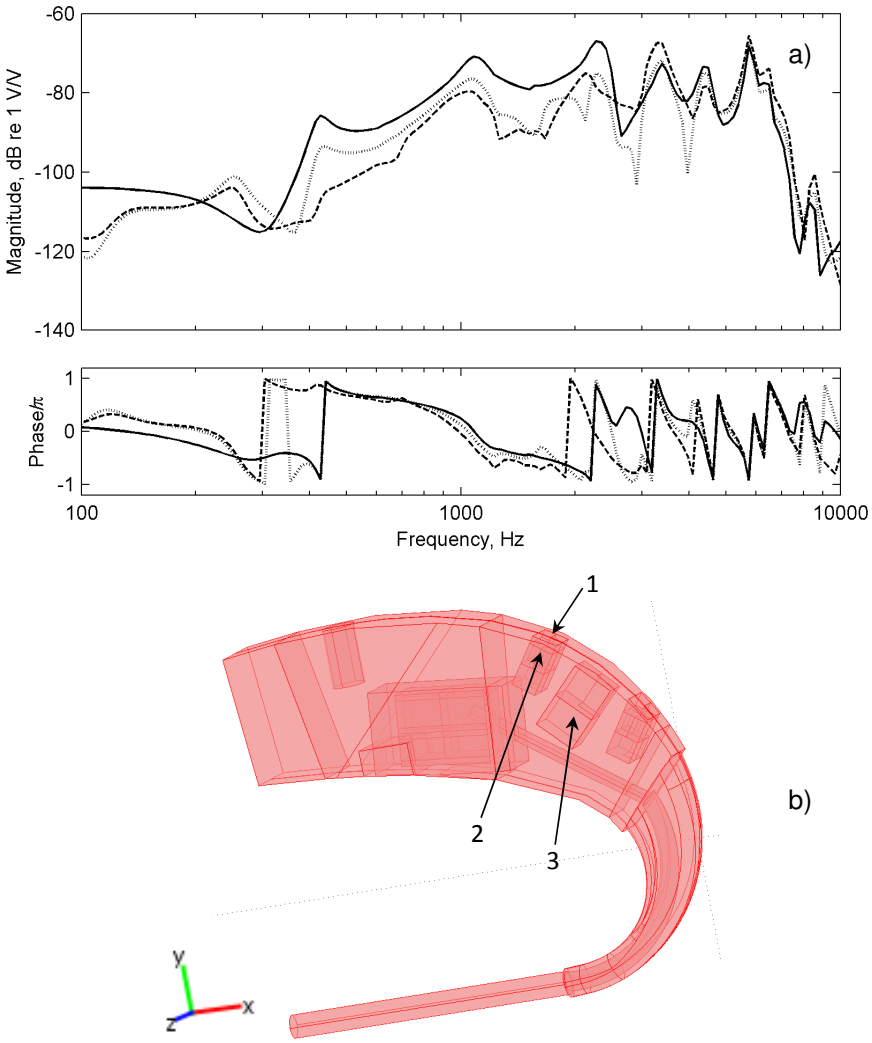

Figure 14.16. (a) Open-loop transfer functions U_{mic}/U_{rec} due to the microphone pressure sensitivity. Shown are the transfer function for the microphone inlet placed in point 1 (solid line), and in point 2 (dotted line) and point 3 (dashed line) in the z-direciton. (b) Positions on the hearing aid of point 1, 2, and 3.

Next, the effects of altering the properties of the receiver suspension are studied. Figure 14.17 shows the total open-loop transfer function for the rear microphone in the standard case and for two other cases where the receiver suspension properties have been changed. In the first case, spring contacts from the receiver suspension to the shell have been added. The purpose of these contacts is to simulate a condition where a part of the receiver vibrations is transmitted to the shell. The spring contacts have a stiffness of $S_{con} = S_{yy}$ where S_{yy} is the translational spring stiffness of the receiver suspension in its local *y*-direction (see section 9.2 and fig. 9.4b). In the second case, the receiver suspension is completely stiff, corresponding to a configuration where it is rigidly attached

to the steel tube. From fig. 14.17 it is seen that adding spring contacts from the receiver suspension to the shell hardly changes the open-loop transfer function. One reason is that the receiver is more likely to rotate around its attachment point than to transfer transversal forces to the shell. Moreover, the attachment positions of the spring to the shell are close to the centre of gravity of the hearing aid. This implies that the transmitted contact forces are not able to rotate the hearing aid significantly. In the case where the receiver suspension is completely stiff the open-loop transfer function is somewhat different from the one in the standard case. Nevertheless, the overall amplitude level of this transfer function is not more critical than the open-loop transfer function for the standard case. It should be kept in mind that the vibration forces being transferred directly to the steel tube, are acting in a direction perpendicular to the microphone inlets.

On the other hand, if the microphones are placed with the inlets in the *z*-direction, changing the properties of the receiver suspension is far more critical. This postulate is confirmed in fig. 14.18, which shows the pressure transfer function for the same cases as in fig. 14.17 but with the microphone inlets placed in the *z*-direction in point 3, see fig. 14.16b.

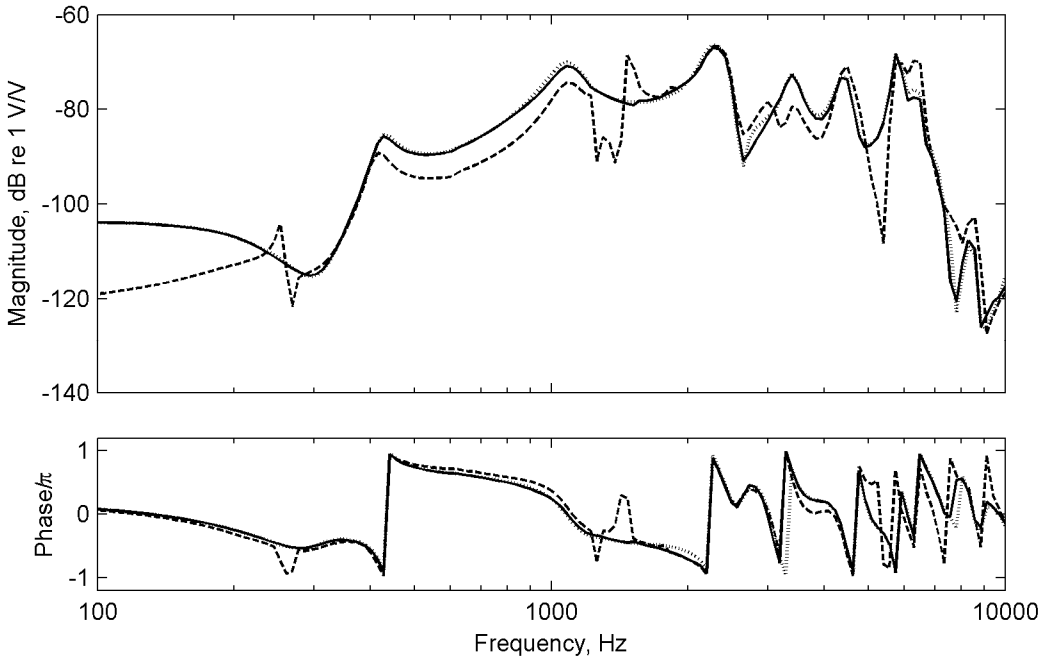

Figure 14.17. Open-loop transfer functions U_{mic}/U_{rec} for the rear microphone in the following cases: Standard (solid line), spring contact to the shell of $S_{con} = S_{yy}$ (dotted line) and completely stiff receiver suspension (dashed line).

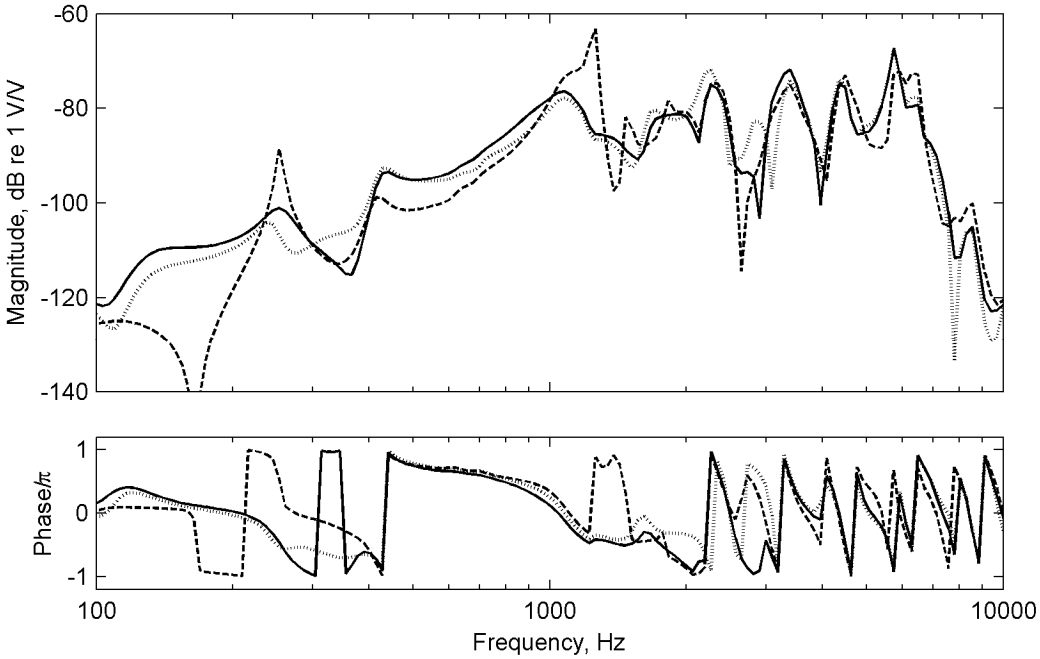

Figure 14.18. Open-loop transfer functions U_{mic}/U_{rec} for a microphone with the inlet placed in the z-direction in point 3 (see fig. 14.16b). Standard case (solid line), spring contact to the shell of $S_{con} = S_{yy}$ (dotted line) and completely stiff receiver suspension (dashed line).

In the case where spring contacts to the shell have been added, the transfer function is quite close to the standard case. For a stiff suspension, however, the transfer function is critically increased to a value of -63 dB at 1261 Hz. The cause of this distinct peak in the transfer function is the excitation of the vibration mode of the shell shown in fig. 14.19. The strong vibrations at 1261 Hz, generate critical sound pressure levels around the hearing aid. One might expect an increase at other frequencies as well, but it should be kept in mind that the strong forces in the tube system also play an important role. Moreover, imbalance caused mostly by the telecoil results in the whole hearing aid vibrating in all directions for frequencies above, say, 3000 Hz.

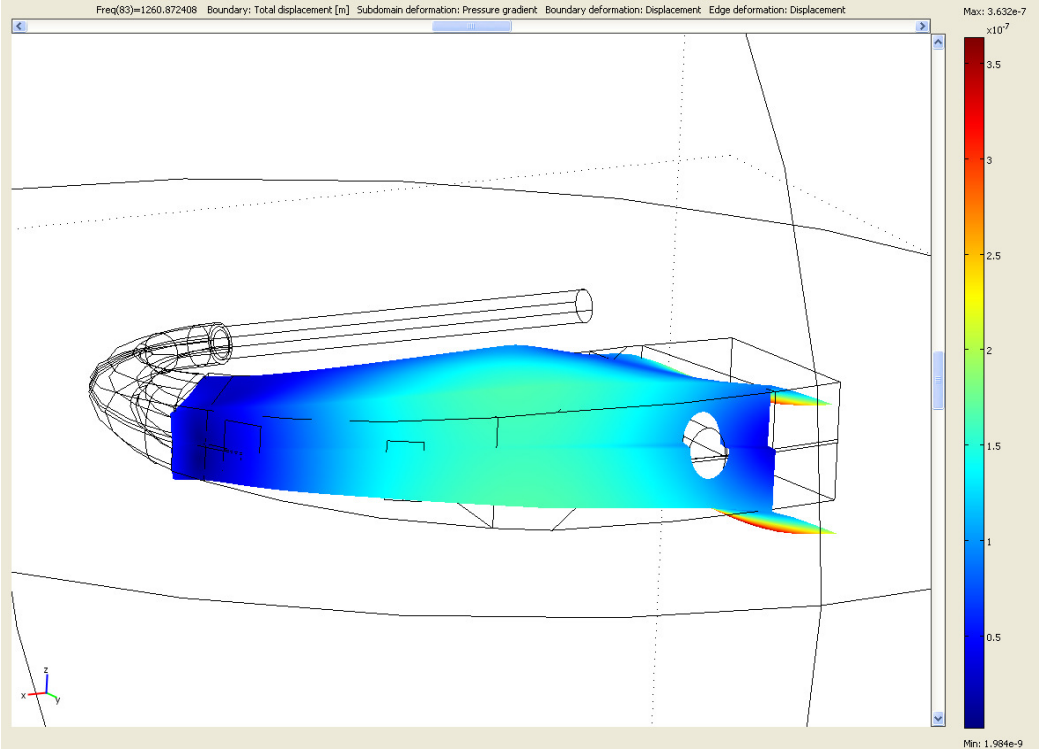

Figure 14.19. Displacements of the shell at 1260 Hz.

Finally, the effects of altering the microphone suspension properties are studied. Figure 14.20 shows the total open-loop transfer function for the rear microphone for the standard case and for a case of completely stiff microphone suspensions. Such a choice of properties corresponds to a configuration where the microphones are rigidly attached to the shell. Also plotted are the open-loop transfer functions divided into pressure and vibration contributions for the case of the stiff microphone suspensions.

Generally it is seen that the total open-loop function is only changed at certain frequencies when the suspension is altered. However, at some of these frequencies, say, 2340 Hz, 3090 Hz and 5733 Hz, the transfer function is increased to critical levels. Even though the pressure contribution still dominates the total transfer function, the vibration contribution becomes severe at certain frequencies. It must be concluded that one should be cautious when altering the properties of the microphone suspensions, as a critical increase at just a single frequency may lead to severe feedback problems.

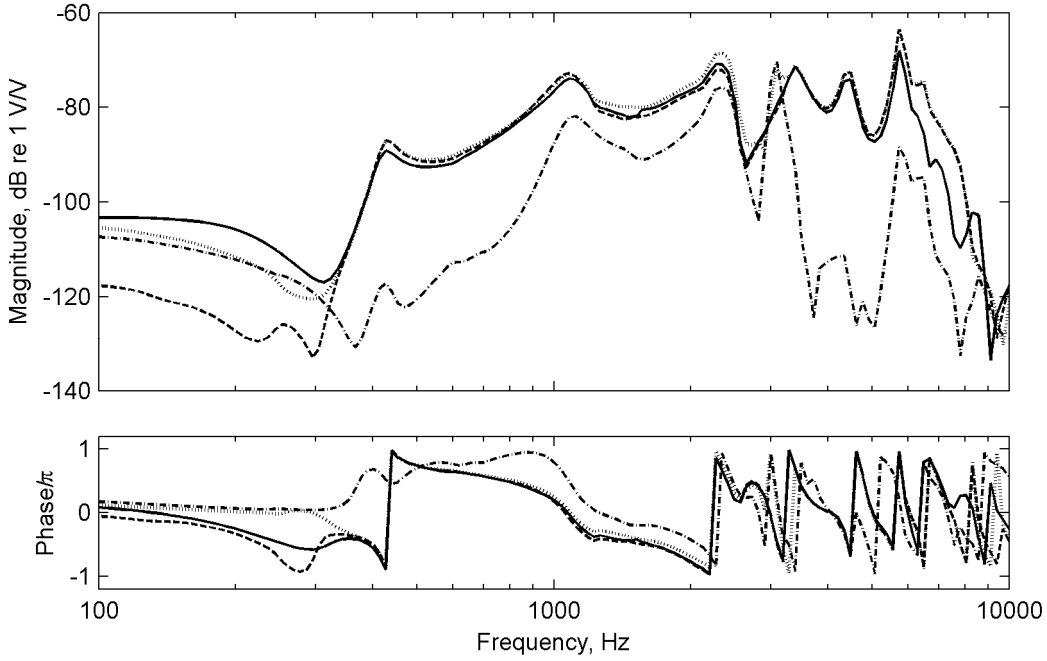

Figure 14.20. Open-loop transfer functions U_{mic}/U_{rec} for the rear microphone. The standard case (solid line) and the microphones directly attached to the shell: Total transfer function (dotted line), pressure transfer function (dashed line) and vibration transfer function (dashdot line).

15 Concluding remarks

15.1 Results obtained in the thesis

15.1.1 Structural fuzzy

Several results regarding the theory of fuzzy structures have been obtained in part II of the thesis. In paper II Soize's method of including spatial memory in structural fuzzy was thoroughly examined and reformulated in a more simple form. This implied a new derivation of the fuzzy boundary impedance including spatial memory by using a simple smoothing approach. Physical interpretations of Soize's so-called equivalent local oscillator and equivalent coupling factor were also given. These quantities are both used for transforming the non-local fuzzy boundary impedance with spatial memory into an equivalent local boundary impedance. It was suggested that the equivalent coupling factor should be determined as a function of the ratio between spatial memory and the free wavelength in the master structure. From numerical simulations of the response of a simply supported beam with structural fuzzy and different amounts of spatial memory, it was revealed that the spatial memory significantly reduces the damping introduced in the master structure.

The main objective of paper III was to extend the method of including spatial memory to two dimensions and to improve its usability. Expressions for the equivalent coupling factor as a function of the ratio suggested in paper II were derived for one- and two-dimensional wave motion in the master. For one-dimensional wave motion in the master structure this expression was evaluated analytically and it was shown that the solution is a sink-function to the power of four. Additionally, the validity of the method of including spatial memory was tested by comparing numerical simulations of the response of a master structure with structural fuzzy attached. Results, based on the use of spatial oscillators and equivalent local oscillators, respectively, showed a very good agreement for frequencies above $\Omega = 500$ where Ω is the non-dimensional frequency of the master structure.

In the following discussion presented in the thesis it was revealed that the apparent damping of a fuzzy substructure is proportional to both the resonating mass distribution and the equivalent coupling factor. This proportionality was utilized for developing a method for modeling structural fuzzy with spatial memory below the non-dimensional frequency $\Omega = 500$ of the master

structure. Using this method a fuzzy substructure with spatial coupling is modeled as structural fuzzy without spatial memory. To account for the reduction in apparent damping caused by spatial coupling, the resonating mass distribution is reduced. This, however, also results in the total resonating mass being less than the actual total mass of the fuzzy substructure. This is accounted for by modeling the residual mass as pure distributed mass.

After the discussion, a novel experimental method for estimating the fuzzy parameters of complex substructures was developed. This method requires a prototype of the master structure with the attached substructure. From vibration measurements, the power equilibrium for the master structure and complex substructure is set up, and using this equilibrium, the apparent damping of the structural fuzzy is extracted. Finally, the resonating mass distribution and the equivalent coupling factor are determined from the extracted apparent damping. Such determination opened the discussion of the uniqueness of the fuzzy parameters and it can be concluded that two different substructures may result in the exact same frequency dependent apparent damping.

The developed method was finally utilized for estimating the fuzzy parameters of the complex internals of the considered hearing aid. Six estimations of the fuzzy parameters were performed. It was revealed that the complex structures introduces relatively high damping in the master structure (the shell of the considered hearing aid) from about 2000 Hz and upwards in frequency. Despite of this high damping it must also be concluded that the impedance of the complex substructure has high spatial memory. This high spatial memory or coupling resulted in low values of the equivalent coupling factor between 0.15 and 0.29. The estimated fuzzy parameters were hereafter validated experimentally by vibration measurements on the shell with the complex internals inside.

15.1.2 Miniature components

Part III of the thesis concerned the determination of properties of miniature components used in the considered hearing aid. Results for the pressure in the tube system in the hearing aid were simulated using two-port network theory. The simulated results showed very good agreement with measurements of the pressure at the eardrum. Further, it was revealed that the pressure at the outlet of the receiver has strong peaks at 1170 Hz and 3421 Hz.

The complex stiffnesses of the resilient rubber suspensions were obtained experimentally. It was revealed that the transversal stiffnesses had the typical S-shape of highly damped rubber. Rotational stiffnesses were increasing almost proportionally to frequency. The loss factor of the butyl rubber used for the suspensions in the considered hearing aid was found to be extremely high with values of more than 1 at some frequencies.

Hereafter, the equivalent vibration forces of the receiver were determined from experiments involving the receiver placed in its suspension. These showed a maximum amplitude level of 3 mN at frequencies about 3500 Hz where the pressure at the receiver outlet has its maximum.

The pressure sensitivity of the microphones was determined using electrical analogue networks and results showed that the maximum sensitivity is found around 5000 Hz. The vibration sensitivity of the microphones was determined experimentally using a specially designed setup. Results for the vibration sensitivity correspondingly showed a maximum around 5000 Hz.

15.1.3 Full vibroacoustic 3D-model

The determined dynamic and acoustic properties of the different hearing aid components were collected in the present part of the thesis. The properties were incorporated into a full vibroacoustic 3D-model of the considered hearing aid. The 3D-model was developed using finite element analysis and it included all major mechanical parts as well as acoustics in the tube system of the hearing aid, inside the shell and outside the hearing aid.

Simulated results for the open-loop transfer function were validated experimentally by measurements. These measurements were performed on five nominally identical hearing aids suspended in elastic strings. Generally, the simulated and measured open-loop transfer functions showed good agreement. In particular the measured open-loop transfer function for the front microphone showed many details replicated in the simulations. For some of the hearing aids, the open-loop transfer functions of especially the rear microphone showed a significant peak around 3500 Hz. This peak, which resembles the shape of the sound pressure at the outlet of the receiver, was not predicted by the simulations. This implies that sound is leaked to the microphones through an unknown transmission path, and the nature of this transmission path needs to be investigated further.

By analyzing the simulation results, the excitation forces of the hearing aid were separated and compared. It was revealed that the high sound pressure generated in the tube system causes strong reaction forces exciting the tube walls. In most of the frequency range considered, these forces have higher amplitudes than the vibration excitation forces of the receiver. Moreover, the pressure reaction forces result in a rotation and thus displacements of the hearing aid. Local pressure at the microphone inlets is hereby generated and this critical pressure causes feedback problems. By means of parameter studies using the 3D-model, it was attempted to minimize the generated sound pressure theoretically. This succeeded below, say, 3000 Hz by making more or less practically realistic changes in the hearing aid. Above 3000 Hz, however, it was found that many factors have an influence on the generated sound pressure. It must therefore be concluded that

minimizing internal feedback is complicated. Nevertheless, the author believes that significant reductions in the open-loop transfer functions of 10 to 15 dB are achievable by making proper changes in the construction of the considered hearing aid.

15.2 Future work

In total six estimations of the fuzzy parameters of the complex hearing aid internals were obtained. The differences between these clearly illustrated the influence of everyday use on the open-loop transfer functions. Considering the size of the spans in the measured open-loop transfer functions, however, it was revealed that the variation between the measurements on each hearing aid was larger than the simulated span caused by the structural fuzzy. The explanation for this is that measurements on real hearing aids also involve other uncertainties than those introduced by the structural fuzzy. For example, the way suspensions are mounted may be altered during the handling of a hearing aid. Incorporation of such uncertainties in the full 3D-model would clearly improve the understanding of the observed variance of the open-loop transfer functions.

Simulation results for the open-loop transfer functions for the two microphones generally showed good agreement with the measurements. However, some details in the measured transfer functions were not included in the simulations. The most important of these details is the peak occurring in the some of the transfer functions around 3500 Hz. As previously mentioned, this peak clearly resembles the sound pressure at the receiver outlet and it is most likely caused by leakage of sound. The path of this leakage needs to be further investigated.

The thesis mostly concerns the theory of fuzzy structures, experimental determination of miniature component properties as well as modeling of the vibroacoustics in the considered hearing aid. All developments have been carried out with the goal of revealing the *main causes* of internal feedback. The next step in minimizing feedback is to find *practically viable solutions*. One strategy to reduce internal feedback is to isolate, balance and/or reduce critical excitation forces. Another strategy is to alter the geometry of the hearing aid to reduce the locally generated sound pressure in vicinity of the microphone inlets. Figuratively speaking these two strategies correspond to “avoiding a fire” and “putting out a fire”. Since neither of the two strategies can be carried out completely, it is the author’s opinion that the best chance of reducing internal feedback are obtained by pursuing both strategies in combination.

Appendix: Investigation of direct proportionality between the apparent damping and the equivalent coupling factor

In order to utilize the reduced-mass technique for modeling structural fuzzy it is necessary to investigate the general proportionality between the apparent damping and α. The apparent damping R_{app} introduced by a fuzzy substructure with the equivalent coupling factor α, is defined as the real part of the equivalent fuzzy boundary impedance $\underline{z}_{fuzzy,equ}$. This impedance is given in paper II eq. (25) and the frequency dependent apparent damping at position x_0 reads

$$\begin{aligned} \mathrm{R}_{\mathrm{app}}(x_0, f) &= \mathrm{Re}(\underline{z}_{fuzzy,equ}(x_0, f)) \\ &= \mathrm{Re}\left(-\frac{i2\pi f}{A} \int_{f_{r,lower}}^{f_{r,upper}} \left(\frac{f_r^2}{f^2} \right) (1+i\eta) m_{fuzzy}(f_r) \left(1 - \frac{f_r^2(1+i\eta)}{f_r^2(1+i\eta) - f^2} \alpha \right) df_r \right). \end{aligned} \tag{A.1}$$

If the expression integrated in eq. (A.1) is directly proportional to α for all values of f_r and f then R_{app} will also be directly proportional to α. This expression corresponds to the apparent damping effect of only one equivalent spatial oscillator. Each oscillator, however, only contributes significantly to the total impedance and the apparent damping in the vicinity of their individual natural frequencies. An investigation of proportionality around the natural frequencies is therefore adequate to prove general proportionality.

Consider a single equivalent oscillator with the natural frequency f_r, total mass M, equivalent coupling factor α and loss factor η. From eq. (A.1) the total apparent damping R_{app} of this oscillator is found as

$$R_{app}(f) = \mathrm{Re}\left(-i2\pi f_r \left(\frac{f_r^2}{f} \right) (1+i\eta) M \left(1 - \frac{f_r^2(1+i\eta)}{f_r^2(1+i\eta) - f} \alpha \right) \right). \tag{A.2}$$

Proportionality *at* and *around* its resonance is investigated by studying this total apparent damping as a function of α and for different frequencies. Such normalized results are shown in fig. A.1 for an oscillator with the high loss factor $\eta = 0.2$. The 3dB-bandwidth of this oscillator is given as $\Delta f_{3dB} = \eta f_r = 0.2 f_r$ and it is therefore sufficient to investigate proportionality for frequencies between, say, $0.8 f_r$ and $1.2 f_r$. From the results it is evident that the apparent damping can be regarded as being directly proportional to α in this frequency interval. Since oscillators with a lower lossfactor also have a smaller 3dB-bandwidth their apparent damping will also be

proportional to the equivalent coupling factor. It can therefore be concluded that the total apparent damping generally is directly proportional to α.

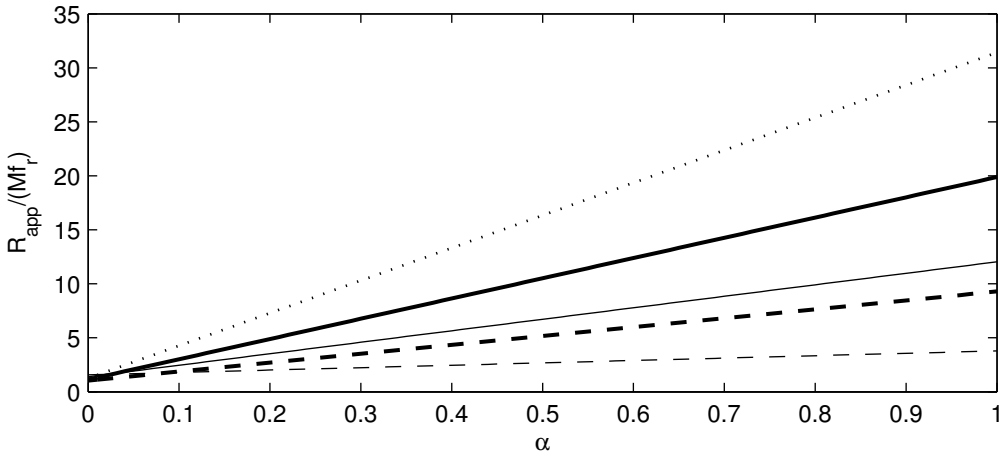

Figure A.1. The normalized apparent damping R_{app} / Mf_r of an oscillator with mass M, natural frequency f_r and loss factor $\eta = 0.2$. The apparent damping is shown as a function of α for the following normalized frequencies: $(f / f_r) = 0.8$ (thin dashed line), $(f / f_r) = 0.9$ (thin solid line), $(f / f_r) = 1$ (dotted line), $(f / f_r) = 1.1$ (thick solid line) and $(f / f_r) = 1.2$ (thick dashed line).

References

Akay, A., Xu, Z., Carcaterra, A., & Koc, I.M. (2005), "Experiments on vibration absorption using energy sinks", *J. Acoust. Soc. Am.*, **118**, 3043-3049.

Allman, D.J. (1988), "Evaluation of the constant strain triangle with drilling rotations", *Int. J. Numer. Meth. Eng.*, **26**, 2645-2655.

Argyris, J., Tenek, L., & Olofsson, L. (1997), "TRIC: A simple but sophisticated 3-node triangular element based on 6 rigid-body and 12 straining modes for fast computational simulations of arbitrary isotropic and laminated composite shells", *Comput. Methods Appl. Mech. Eng.*, **145**, 11-85.

Bishop, R.E.D., & Johnson, D.C. (1960), "The Mechanics of Vibration", Cambridge University Press, Cambridge.

Brennan, M.J. (1997), "Characteristics of a wideband vibration neutralizer", *Noise Control Eng. J.*, **45**, 201-207.

Bukhard, M.D. (1965), "Protection against shock and vibration", *Knowles Electronics*, www.knowles.com.

Carcaterra, A., & Akay, A. (2004), "Transient energy exchange between a primary structure and a set of oscillators: Return time and apparent damping", *J. Acoust. Soc. Am.*, **115**, 683-696.

Carcaterra, A., & Akay, A. (2007), "Theoretical foundations of apparent-damping phenomena and nearly irreversible energy exchange in linear conservative systems", *J. Acoust. Soc. Am.*, **121**, 1971-1982.

Carcaterra, A., Akay, A., & Lenti, F. (2007), "Pseudo-damping in undamped plates and shells", *J. Acoust. Soc. Am.*, **122**, 804-813.

Chabas, F., Desanti, A., & Soize, C. (1986), "Probabilistic structural modelling in linear dynamic analysis of complex mechanical systems, part II", *Rech. Aerosp.,* **5**, 49-67.

Cook, R., Malkus, D.S., Plesha, M.F., & Witt, R.J. (2002), *Concepts and applications of finite element analysis*, University of Wisconsin, John Wiley & Sons, Inc.

Cremer, L., Heckl, M., & Ungar, E.E. (1988), *Structure-Borne Sound*, Springer-Verlag, Berlin.

Dillon, H. (2001), "*Hearing aids*", Thieme Medical Pub.

Drexel, M.V., & Ginsberg, J.H. (2001), "Modal overlap and dissipation effects of a cantilever beam with multiple attached oscillators", *Journal of Vibration and Acoustics*, **123**, 181-187.

Egolf, D.P. (1977), "Mathematical modelling of a probe-tube microphone", *J. Acoust. Soc. Am.*,

61, 200-205.

Egolf, D.P., Haley, B.T., Bauer, K.M., Howell, H.C., & Larson, V.D. (1988a), "Experimental determination of cascade parameters of a hearing-aid microphone via the two-load method", *J. Acoust. Soc. Am.*, **83**, 2439-2446.

Egolf, D.P., Haley, B.T., Bauer, K.M., Howell, H.C., & Larson, V.D. (1988b), "A technique for simulating the amplifier-to-eardrum transfer function of an in situ hearing aid", *J. Acoust. Soc. Am.*, **84**, 1-10.

Egolf, D.P., Haley, B.T., Howell, H.C., Legowski, S., & Larson, V.D. (1989), "Simulating the open-lopp transfer function as a means for understanding the acoustic feedback in hearing aids", *J. Acoust. Soc. Am.*, **85**, 454-467.

Egolf, D.P., Haley, B.T., & Larson, V.D. (1986), "The constant-volume-velocity nature of hearing aids: Conclusion based on computer simulations", *J. Acoust. Soc. Am.*, **79**, 1592-1602.

Egolf, D.P., Howell, H.C., Weaver, K.A., & Barker, D.S. (1985), "The hearing aid feedback path: Mathematical simulations and experimental verification", *J. Acoust. Soc. Am.*, **78**, 1578-1587.

Egolf, D.P., & Leonard, R.G. (1977), "Experimental scheme for analysing the dynamic behavior of electroacoustic transducers", *J. Acoust. Soc. Am.*, **62**, 1013-1023.

Egolf, D.P., Tree, D.R., & Feth, L.L. (1978), "Mathematical predictions of electroacoustic frequency response of in situ hearing aids", *J. Acoust. Soc. Am.*, **63**, 264-271.

Garrelick, J., "The modelling of a continuous structure as fuzzy" (1997), *J. Acoust. Soc. Am.*, **101**, 613-615.

Harris, C.M., & Crede, C.E. (1976), "*Shock & vibration handbook*", McGraw-Hill book company, second edition.

Igusa, T., & Xu, K. (1994), "Vibration control using multiple tuned mass dampers", *J. Sound Vib.*, **175**, 491-503.

Killion, M.C. (1975), "Vibration sensitivity measurements on subminiature condenser microphones", *Journal of the Audio Engineering Society*, **23**, 123-127.

Knowles Electronics (1969), "Vibration isolation of the BL microphone", *Report no. 10373-2*, www.knowles.com.

Knowles Electronics (1981), "Vibration isolator design", *Report no. 10373-1*, www.knowles.com.

Koc, I.M., Carcaterra, A., Xu, Z., & Akay, A. (2005), "Energy sinks: Vibration absorption by an optimal set of undamped oscillators", *J. Acoust. Soc. Am.*, **118**, 3031-3042.

Langley, R.S. (1997), "Can an undamped oscillator dissipate energy?", *J. Sound. Vib.*, **206**, 624-

626.

Langley, R.S., & Bremner, P. (1999), "A hybrid method for the vibration analysis of complex structural-acoustic systems", *J. Acoust. Soc. Am.*, **105**, 1657-1671.

Laugesen, S., & Ohlrich, M. (1994), "The vibrational source strength descriptor using power input from equivalent forces: A simulation study", *Acta Acustica*, **2**, 449-459.

LoPresti, J.L. (2003), "Electrical analogs for Knowles Electronics, LLC. Transducers", *Knowles Electronics*, www.knowles.com.

Lyon, R.H. (1995), "Statistical energy analysis and structural fuzzy", *J. Acoust. Soc. Am.*, **97**, 2878-2881.

Maidanik, G. (1995), "Power dissipation in a sprung mass attached to a master structure", *J. Acoust. Soc. Am.*, **98**, 3527-3533.

Maidanik, G. (2001), "Induced damping by a nearly continuous distribution of nearly undamped oscillators: Linear analysis", **240**, 717-731.

Maidanik, G., & Becker, K.J. (1998a), "Various loss factors of a master harmonic oscillator coupled to a number of satellite harmonic oscillators", *J. Acoust. Soc. Am.*, **103**, 3184-3194.

Maidanik, G., & Becker, K.J. (1998b), "Noise control of a master harmonic oscillator coupled to a set of satellite harmonic oscillators", *J. Acoust. Soc. Am.*, **104**, 2628-2637.

Maidanik, G., & Becker, K.J. (1999a), "Characterization of multiple-sprung masses for wideband noise control", *J. Acoust. Soc. Am.*, **106**, 3109-3118.

Maidanik, G., & Becker, K.J. (1999b), "Criteria for designing multiple-sprung masses for wideband noise control", *J. Acoust. Soc. Am.*, **106**, 3119-3127.

Maidanik, G., & Becker, K.J. (2003a), "Dependence of the induced loss factor on the coupling forms and coupling strengths: linear analysis", *J. Sound. Vib.*, **266**, 15-32.

Maidanik, G., & Becker, K.J. (2003b), "Dependence of the induced loss factor on the coupling forms and coupling strengths: linear analysis", *J. Sound. Vib.*, **266**, 33-48.

Maidanik, G., Becker, K.J., & Maga, L.J. (2006), "Replacement of a summation by an integration in structural acoustics", *Journal of Sound and Vibration*, **291**, 323-348.

Maidanik, G., & Dickey, J. (1996), "Design criteria for the damping effectiveness of structural fuzzies", *J. Acoust. Soc. Am.*, **100**, 2029-2033.

Mead, D.J. (1998), "Passive vibration control", *Wiley*.

Mencik, J.-M., & Berry, A. (2005), "A theoretical formulation of the dynamical response of a master structure coupled with elastic continuous fuzzy subsystems with discrete attachments", *J. Sound Vib.*, **280**, 1031-1050.

Nagem, R.J., Stokes, A.W., & Selle, C.P. (1996), “Experimental analysis of fuzzy structures parameters”, *Proceedings of the ASME*, 47-51.

Ohlrich, M. (1998), ”A simple structural power method for determining the vibratory strength of machinery sources”, *Proc. Euronoise 98*, München, Germany, 383-388.

Ohlrich, M., & Friis, L. (2006), “Effect of cross-coupling on the injection of vibratory power from sets of point forces into a periodic support structure”, *Proceedings of the Thirteenth International Congress of Sound and Vibration*, Vienna, Austria, 1-8.

Ohlrich, M., Friis, L., Aatola, S., & Lehtovaara, A., Martikainen, M., & Nuutila, O. (2006), ”Round Robin Test of technique for characterizing the structure borne sound-source-strength of vibrating machines”, *Proc. Euronoise 06*, Tampere, Finland, 1-6.

Ormondroyd, J., & Den Hartog, J.P. (1928), “Theory of dynamic vibration absorber”, *Trans. ASME*, **50**, APM-241.

Pierce, A.D. (1997), “Resonant-frequency-distribution of internal mass inferred from mechanical impedance matrices, with application to fuzzy structure theory”, *Journal of Vibration and Acoustics*, **119,** 324-333.

Pierce, A.D., Sparrow, V.W., & Russell, D.A. (1995), “Fundamental structural-acoustic idealizations for structures with fuzzy internals”, *Journal of Vibration and Acoustics*, **117**, 339-348.

Rochat, J.L., & Sparrow, V.W. (1995), “Incorporating compressional and shear wave types into fuzzy structure models for plates”, *Design Engineering Technical Conferences*, **3**, 247-252.

Ruckman, C.E., & Feit, D. (1995), “A tutorial on Soize’s method for strachastic modelling in structural acoustics (fuzzy structures analysis)”, *Design Engineering Technical Conferences*, **3**, 241-246.

Russell, D.A. (1995), “The theory of fuzzy structures and its application to waves in plates and shells”, Ph.D. thesis, The Pennsylvania State University.

Smith, T.L., Rao, K., & Dyer, I. (1986), “Attenuation of plate flexural waves by a layer of dynamic absorbers”, *Noise Control Engineering Journal*, **26**, 56-60.

Snowdon, J.C. (1968), ”Vibration and shock in damped mechanical systems”, *John Wiley & Sons*.

Soize, C. (1986), “Probabilistic structural modeling in linear dynamic analysis of complex mechanical systems, part I”, *Rech. Aerosp.*, **5**, 23-48.

Soize, C. (1993), “A model and numerical method in the medium frequency range for vibroacoustic predictions using the theory of structural fuzzy”, *J. Acoust. Soc. Am.*, **94**, 849-865.

Soize, C. (1995), “Vibration damping in low-frequency range due to structural complexity. A model based on the theory of fuzzy structures and model parameters estimation”, *Computers*

& Structures, **58**, 901-915.

Soize, C. (1998), "Estimation of fuzzy substructure model parameters using the mean power flow equation of the fuzzy structure", *Journal of Vibration and Acoustics*, **120**, 279-286.

Soize, C., & Bjaoui, K. (2000), "Estimation of fuzzy structure parameters for continuous junctions", *J. Acoust. Soc. Am.*, **107**, 2011-2020.

Soize, C., Hutin, O.M., Desanti, A., David, J.M. and Chabas, F. (1986), "Linear dynamic analysis of mechanical systems in the medium frequency range", *Computer & Structures*, **23**, 605-637.

Sparrow (1994), V.W., Russell, D.A., & Rochat, J.L., "Implementation of discrete fuzzy structure models in Mathematica", *International Journal for Numerical Methods in Engineering*, **37**, 3005-3014.

Strasberg, M. (1997), "Is the dissipation induced by "fuzzy" substructures real or apparent?", *J. Acoust. Soc. Am.*, **102**, 3130.

Strasberg, M. (2000), "When is a "fuzzy" not a fuzzy", *J. Acoust. Soc. Am.*, **107**, 2885.

Strasberg, M., & Feit, D. (1996), "Vibration damping of large structures induced by attached small resonant structures", *J. Acoust. Soc. Am.*, **99**, 335-344.

Warren, D.M. (2001), "Two-Dimensional Vibration Modeling for Knowles Receivers", *Knowles Engineering Report # 138, Rev. B,* www.knowleselectronics.com.

Weaver, R.L. (1996), "The effect of an undamped finite degree of freedom "fuzzy" substructure: Numerical solutions and theoretical discussion", *J. Acoust. Soc. Am.*, **100**, 3159-3164.

Weaver, R.L. (1997a), "Mean and mean-square response of a prototypical master/fuzzy structure", *J. Acoust. Am.*, **101**, 1441-1449.

Weaver, R.L. (1997b), "Multiple-scattering theory for mean responses in a plate with sprung masses", *J Acoust. Soc. Am.*, **101**, 3466-3474.

Weaver, R.L. (1998), "Mean-square response in a plate with sprung masses, energy flow and diffusion", *J. Acoust. Soc. Am.*, **103**, 414-427.

Weaver, R.L. (2001), "Equipartition and mean-square response in large undamped structures", *J Acoust. Soc. Am.*, **110**, 894-903.

White, R.G., & Walker, J.G. (1982), "Noise and vibration", Chapter 25, *Ellis Horwood Ltd.*, Chichester, England.

Xu, K., & Igusa, T. (1992), "Dynamic Characteristics of Multiple Substructures with Closely Spaced Frequencies", *Earthquake Engineering and Structural Dynamics*, **21**, 1059-1070.